Residential heating using heat pumps and hot water storage tanks

Tank sizing to minimize environmental impact in a renewable energy context

Brecht Baeten

Residential heating using heat pumps and hot water storage tanks

Tank sizing to minimize environmental impact in a renewable energy context

Brecht BAETEN

Examination committee:
Prof. dr. Adhemar Bultheel, chair
Prof. dr. ir. Lieve Helsen, supervisor
Prof. dr. ir. Martine Baelmans
Prof. dr. ir.-arch. Dirk Saelens
Prof. dr. Alessia Arteconi
  (Università e-Campus)
Prof. dr. Wolfgang Streicher
  (Universität Innsbruck)

June 2017

Preface – Voorwoord

Toen ik begon aan dit doctoraat was dat uit een drang om de wereld te verbeteren. Als snel kom je echter tot de conclusie dat je slechts een zeer klein radertje bent van een heel ingewikkeld systeem en dat er over wat nu daadwerkelijk verbetering is, wel degelijk kan gediscussieerd worden. Zelfs als ik enkel naar mijn eigen werk kijk, en niet naar de plaats die het inneemt in de opeenvolging van nieuwigheden die wij vooruitgang noemen, besef ik dat ik ook hierin slechts de uitvoerder ben en dat ik me heb laten beïnvloeden, overtuigen, inspireren door de mensen om me heen. Het is dan ook gepast om hier iedereen die, al dan niet moedwillig, heeft bijgedragen aan dit werk te bedanken.

Als eerste wil ik graag Lieve Helsen, mijn promotor, bedanken voor alle steun en begeleiding tijdens de voorbije 6 jaar. Bedankt voor de vrijheid die je me gaf om mee de richting van het onderzoek te bepalen. Onze meetings waren niet zeer talrijk, maar bij elke bijeenkomst kon je mij de juiste input geven of me naar de juiste personen sturen en me motiveren om door te gaan.

I would also like to thank all members of the examination committee for their critical review of my work and the interesting discussion during and after the preliminary defense. The remarks made proved very useful and surely increase the value of the final text.

Verder wil ik Kris Henrioulle en Myriam Lynen van de opleiding industrieel ingenieur aan de technologiecampus Diepenbeek bedanken voor de ondersteuning, het vertrouwen en de ruimte die ik van hen kreeg om dit werk te kunnen combineren met mijn onderwijstaken.

Onderzoek aan een universiteit biedt niet alleen wetenschappelijke uitdagingen. Af en toe moet de strijd met de bureaucratie aangegaan worden. Gelukkig kon ik daarbij rekenen op de hulp van het secretariaat, in het bijzonder Valérie en Kathleen. Bedankt voor het vergelijken van agenda's om toch nog een vergadering te kunnen plannen, afhandelen van papierwerk, het bestellen van koffie als ik dit weeral vergeten was en de succeswensen voor elke presentatie.

Zonder jullie weet ik niet of dit gelukt was.

Furthermore, I would like to thank all my colleagues at TME for the interesting discussions I've had the privilege to be a part of over these past years. Geert, het is zeer nobel van je om te proberen je eetgewoontes aan te passen. En ook al lukt dit misschien niet altijd, het in de belangstelling zetten van zulke problemen, al is het maar onder collega's, zal zeker anderen bewustmaken en misschien zelfs doen volgen.

Verder wil ik iedereen uit de onderzoeksgroep, the Sysi's (thermal system simulators), bedanken voor de interessante presentaties en daaropvolgende discussies die ik heb mogen meemaken. De presentaties tijdens de sysi meetings en jullie opmerkingen op mijn presentaties zijn zeer nuttig gebleken bij de totstandkoming van dit werk.

In het bijzonder wil ik mijn TME part-time bureaugenoten Dieter en Damien bedanken. Damien, bedankt voor het delen van je nieuwe Python programmeertips en babbels over het opvoeden van kinderen of het maken van meubels. Dieter, bedankt voor de vele discussies over opslagtanks, demand response, en de klimaatsveranderingen en je eigen kijk op hoe we de wereld een betere plek kunnen maken.

Frederik, voor onze vele discussies over mijn en jouw werk, je verse kijk op onderzoeksresultaten en je steeds zéér kritische reviews van papers, bedankt. Voor je inzichten rond duurzaamheid, ecologisch speelgoed en het onderwijssysteem. Ik vond het een eer om een bureau met je te mogen delen.

Als laatste wil ik mijn prachtige vrouw Ellen en onze fantastische kinderen Egon en Gilan bedanken. Ellen, bedankt dat je tijdens stressvolle periodes zo'n goede vrouw voor me was, me op m'n gemak stelde en m'n taken in het huishouden overnam. Zonder jou was het niet gelukt. Als laatste, Egon en Gilan, bedankt dat ik met jullie kon spelen als ik m'n zinnen moest verzetten. Jullie blijven mijn bron van inspiratie en motivatie om te dromen over, en te werken aan een betere wereld.

Brecht Baeten
Mei 2017

Abstract

Global warming caused by anthropogenic greenhouse gas emissions is expected to have long lasting effects on the environment, ecosystems and human society unless emissions are decreased soon. In Europe, the building sector is a large energy user and has a huge potential for efficiency gains which can be accompanied by a significant reduction in CO_2 emissions. Electrifying residential heating loads through the use of heat pumps, can contribute to these efficiency gains and thereby reduce greenhouse gas emissions. However, the introduction of large numbers of heat pumps in the electricity system could disrupt the load diversity and require substantial investments in generation capacity and the electricity transport network.

Flexible operation of heat pumps in response to the needs of the electricity system, i.e. demand response, could mitigate this problem. Due to the thermal inertia present in most buildings, it is possible to shift the heat pump operation in time without jeopardizing the thermal comfort of the inhabitants. The addition of thermal energy storage in the form of a hot water storage tank can provide additional flexibility to the electricity generation system which can be used to further lower electricity generation related CO_2 emissions. However, the investment in a hot water storage tank also induces emissions related to its construction and end-of-life treatment which must be accounted for when evaluating the environmental impact of such systems.

In this thesis, the environmental impact of residential heating with heat pumps and hot water storage tanks is estimated through a life-cycle assessment, including the effects a large scale application has on the electricity generation side.

To this end, an integrated model predictive control simulation of a building in interaction with the electricity system is developed. As the hot water storage tank is an essential system component, additional attention is paid to its modeling and integration in optimal control problems. A one-dimensional

storage tank model is developed, amended with formulations for three dimensional flow phenomena such as inflow buoyancy. The resulting model is partially validated through experiments. Results of an integrated simulation of a set of buildings and the electricity generation park are used as inputs to a life-cycle assessment, delivering the environmental impact of residential heating as damage to human health, damage to ecosystems and resource depletion endpoint indicators, as well as several midpoint indicators among which focus is on climate change.

In a case study inspired by the Belgian electricity system, with a high share of renewable energy sources and a large number of heat pumps, the effect of varying control objectives and storage tank sizes on the electricity generation mix and the required electricity transport capacity is determined. Depending on the objective, demand response significantly reduces the required electricity transport capacity and allows a shift of electricity generation to more efficient power plants. The addition of hot water storage tanks further reduces the required additional electricity transport capacity.

The decrease in environmental impact of switching from gas boiler heating to heat pumps is significant even if the individual heat pump control systems do not take the electricity generation side into account. By switching to heat pump heating, greenhouse gas emissions are reduced from 3800 kg CO_2 equivalents per building per year to around 2600 kg CO_2 equivalents. If demand response is applied, the emissions are further reduced to around 2200 kg CO_2 equivalents per building per year. The addition of a 4 m^3 storage tank allows for only a small further reduction to around 2100 kg CO_2 equivalents per building per year. However, at current energy tariff structures, these environmental benefits come at a significant cost for participating home owners.

The observations lead to the conclusion that the addition of a hot water storage tank as a space heating energy buffer to a residential heat pump heating system is not recommended from an environmental viewpoint. Benefits are small and the large financial and environmental investments are probably better allocated elsewhere. However, the large scale application of demand response with heat pumps has a large potential for reducing the environmental impact associated with residential heating and presents an opportunity to reduce global warming.

Beknopte samenvatting

De opwarming van de aarde, veroorzaakt door antropogene emissies van broeikasgassen, wordt verwacht blijvende effecten te hebben op het milieu, ecosystemen en de samenleving tenzij de uitstoot snel wordt verlaagd. De gebouwensector in Europa is een grote energiegebruiker met een gigantisch potentieel voor efficiëntiewinsten die gepaard kunnen gaan met een significante daling van de CO_2 uitstoot. Het elektrificeren van residentiële verwarming door het gebruik van warmtepompen kan bijdragen tot deze efficiëntiewinsten en dus ook tot een reductie van broeikasgasemissies. De introductie van een groot aantal warmtepompen in het elektriciteitssysteem kan echter de diversiteit van de belasting verstoren en grote investeringen in generatiecapaciteit en het elektriciteitsnet met zich mee brengen.

Flexibele sturing van warmtepompen met het oog op de noden van het elektriciteitssysteem, vraagsturing, kan dit probleem verlichten. Door de aanwezigheid van thermische inertie in de meeste gebouwen is het mogelijk om de werking van een warmtepomp te verschuiven in de tijd zonder het thermisch comfort van de bewoners in het gedrang te brengen. Het toevoegen van thermische energieopslag in de vorm van een warmwateropslagtank kan extra flexibiliteit leveren aan het elektriciteitssysteem waardoor de CO_2 emissies gerelateerd aan de elektriciteitsopwekking verder kunnen worden verlaagd. De investering in een warmwateropslagtank veroorzaakt echter ook emissies, gerelateerd aan zijn productie en recyclage, die in rekening gebracht moeten worden om de milieu-impact van dit systeem te evalueren.

In deze thesis wordt de milieu-impact van residentiële verwarming met warmtepompen en warmwateropslagtanks geschat door middel van een levenscyclusanalyse. Hierbij wordt rekening gehouden met de effecten van een grootschalige integratie op het elektriciteitssysteem.

Hiertoe is een geïntegreerde modelpredictieveregelingssimulatie van de interactie tussen een gebouw en het elektriciteitssysteem ontwikkeld. Aangezien de

warmwateropslagtank een essentiële component van het systeem is, werd extra aandacht geschonken aan het modelleren ervan en aan de integratie ervan in optimalisatieproblemen. Een ééndimensionaal opslagtankmodel werd ontwikkeld, met de toevoeging van formuleringen voor driedimensionale stromingsfenomenen. Het resulterende model werd gedeeltelijk gevalideerd met behulp van experimenten. De resultaten van een geïntegreerde simulatie van een groep gebouwen en het elektriciteitsproductiepark zijn gebruikt als input voor een levenscyclusanalyse met als resultaat de milieu-impact van residentiële verwarming uitgedrukt als de eindpuntindicatoren: schade aan de menselijke gezondheid, schade aan ecosystemen en uitputting van grondstoffen. Dit leidt ook tot verscheidene midpuntindicatoren waar de nadruk ligt op klimaatsverandering.

In een casestudie geïnspireerd door het Belgische elektriciteitssysteem met een groot aandeel van hernieuwbare energiebronnen en een groot aantal warmtepompen werden de effecten van verschillende regelobjectieven en opslagtankgroottes op de elektriciteitsmix en de nodige elektriciteitstransportcapaciteit bepaald. Afhankelijk van de doelfunctie kan vraagsturing de elektriciteitstransportcapaciteit significant doen dalen en laat het toe de elektriciteitsproductie te verschuiven naar efficiëntere elektriciteitscentrales. Het toevoegen van een warmwateropslagtank laat de nodige elektriciteitstransportcapaciteit verder dalen.

De daling in milieu-impact van het omschakelen van verwarming met behulp van gasketels naar warmtepompen is significant zelfs wanneer de warmtepompregelaars geen rekening houden met het elektriciteitssysteem. Door om te schakelen naar verwarming met warmtepompen worden broeikasgasemissies verlaagd van 3800 kg CO_2 equivalenten per gebouw per jaar tot ongeveer 2600 kg CO_2 equivalenten. Wanneer vraagsturing wordt toegepast kunnen emissies verder gereduceerd worden tot ongeveer 2200 kg CO_2 equivalenten per gebouw per jaar. Het toevoegen van een 4 m^3 grote warmwateropslagtank laat slechts een kleine bijkomende daling toe tot ongeveer 2100 kg CO_2 equivalenten per gebouw per jaar. Op basis van de huidige energieprijzen leidt deze daling van milieu-impact echter tot een significante stijging van de kosten voor de gebouweigenaars die deelnemen aan de vraagsturing.

Deze waarnemingen leiden tot de conclusie dat het gebruik van warmwateropslagtanks als energiebuffer voor residentiële warmtepompsystemen niet is aangeraden vanuit een milieustandpunt. De voordelen zijn klein en de grote financiële en milieu-investeringen worden waarschijnlijk beter anders gebruikt. Desalniettemin heeft de toepassing van vraagsturing met warmtepompen een groot potentieel om de milieu-impact geassocieerd met residentiële verwarming te verminderen en biedt het een kans om de klimaatsveranderingen tegen te gaan.

Abbreviations

CCGT   combined cycle gas turbine

CFD   computational fluid dynamics

CHP   combined heat and power

COP   coefficient of performance

DHW   domestic hot water

DR   demand response

GWP   global warming potential

LCA   life-cycle assessment

LCIA   life-cycle impact assessment

LP   linear programming problem

MILP   mixed integer linear programming problem

MPC   model predictive control

NLP   non-linear programming problem

OCGT   open cycle gas turbine

OCP   optimal control problem

ODE   ordinary differential equation

PV   photovoltaic

QCQP   quadratically constrained quadratic programming problem

QP   quadratic programming problem

RANS   Reynolds-averaged Navier-Stokes

RCP   representative concentration pathway

RES   renewable energy source

RF   radiative forcing

RMSE   root mean squared error

Nomenclature

Roman symbols

A	area	$[\mathrm{m}^2]$
$\mathcal{C}$	coefficient	$[-]$
C	heat capacity	$[\mathrm{J/K}]$
c	specific heat	$[\mathrm{J/kg\ K}]$
COP	coefficient of performance	$[-]$
D	storage tank diameter	$[\mathrm{m}]$
d	pipe diameter	$[\mathrm{m}]$
$D_{>20\ \mathrm{kV}}$	distance of transmission lines at a voltage higher than 20 kV	$[\mathrm{km}]$
$D_{1-20\ \mathrm{kV}}$	distance of transmission lines and cables at a voltage between 1 and 20 kV	$[\mathrm{km}]$
$D_{<1\ \mathrm{kV}}$	distance of distribution cables at a voltage lower than 1 kV	$[\mathrm{km}]$
E	energy	$[\mathrm{J}]$
f	distribution factor	$[-]$
g	gravitational acceleration	$[\mathrm{m/s}^2]$
$\dot{H}$	enthalpy flow rate	$[\mathrm{W}]$
H	Heaviside function	
$\tilde{\mathrm{H}}$	smooth Heaviside function	
J	cost functional or cost function	

l_cap	relative capacity limit	$[-]$
M	number of buildings	$[-]$
m	mass	$[\mathrm{kg}]$
$\dot{m}$	mass flow rate	$[\mathrm{kg/s}]$
N	number of layers	$[-]$
Nu	Nusselt number	$[-]$
P	power	$[\mathrm{W}]$
$\dot{P}$	power rate of change	$[\mathrm{W/s}]$
$\boldsymbol{p}$	parameter vector	
p_el	electricity price	$[\mathrm{EUR/kWh}]$
p_d	discomfort price	$[\mathrm{EUR/K\ h}]$
$p_\mathrm{impact,ene}$	marginal impact of energy use	$[\mathrm{points/kWh}]$
p_cap	price of impact related to the required capacity	$[\mathrm{EUR/kW^2h}]$
Pr	Prandtl number	$[-]$
$\dot{Q}$	heat flow rate	$[\mathrm{W}]$
R	thermal resistance	$[\mathrm{K/W}]$
r	rate factor	$[-]$
Ra	Rayleigh number	$[-]$
Re	Reynolds number	$[-]$
S	shading solar gains fraction	$[-]$
T	temperature	$[\mathrm{K}]$ or $[\mathrm{^\circ C}]$
ΔT	temperature difference	$[\mathrm{K}]$
t	time	$[\mathrm{s}]$
Δt	time step	$[\mathrm{s}]$
U	overall heat transfer coefficient	$[\mathrm{W/m^2K}]$
$\boldsymbol{u}$	control input vector	

V	volume	$[\text{m}^3]$
w_{EIE}	environmental impact of energy use weight	$[\text{EUR/point}]$
$\boldsymbol{x}$	state vector	
z	height	$[\text{m}]$
Δz	height difference	$[\text{m}]$

Subscripts

0	initial
amb	ambient
aux	auxiliary
avg	average
b	boundary
bdl	boundary layer
buo	buoyancy
cap	capacity
cold	cold
d	discomfort
df	diffusion
down	downward
dw	domestic hot water storage tank
el	electricity
em	emission
ene	energy
ext	external
f	final
f1	interior side of the floor
f2	technical room side of the floor

fittings	fittings
fl	floor
gain	internal gains
gen	generation
gnd	ground
h	high
hl	heat loss
hp	heat pump
ht	high temperature
hx	hear exchanger
i	time index
impact	environmental impact
in	inflow
in	interior
int	internal
l	low
lin	linear
lt	low temperature
mix	mixing
mt	medium temperature
op	operative
out	outflow
overload	overload
qua	quadratic
rec	recirculation
ret	return

sh	space heating storage tank
sol	solar
sup	supply
tr	technical room
up	upward
ve	ventilation
vht	very high temperature
w1	interior side of the external walls
w2	ambient side of the external walls
warm	warm
we	external walls
wi	internal walls and furniture

Superscripts

dem	demand
j	generation unit index
j	layer index
k	layer index
max	maximum
min	minimum
nom	nominal

Greek symbols

α	discretization weighting factor	$[-]$
β	volumetric expansion coefficient	$[1/K]$
ε	effectiveness	$[-]$
ζ	heat pump performance fit coefficient	$[W/W]$ or $[W/W^2]$

η	efficiency	$[-]$
λ	thermal conductivity	$[\text{W/m K}]$
μ	dynamic viscosity	$[\text{Pa s}]$
ν	kinematic viscosity	$[\text{m}^2/\text{s}]$
ρ	density	$[\text{kg/m}^3]$

Contents

Chapter 1

Introduction

1.1 Context and motivation

In 2015 the United Nations General Assembly agreed on 17 sustainable development goals for the next 15 years. These goals are set to end poverty, ensure prosperity for all and protect the planet from degradation through sustainable consumption and production and the management of natural resources so Earth can support the needs of the present and of future generations [180]. Combating climate change is a major duty in this framework.

Global warming caused by anthropogenic greenhouse gas emission is expected to have long lasting effects on the environment, ecosystems and human society in the near future unless emissions are decreased [94]. If global warming would exceed 4°C above pre-industrial levels by 2100, food insecurity, substantial species extinction and a limited potential for human adaptation are very likely. When the temperature increase can be limited to 2°C above pre-industrial levels, the risk of substantial changes is decreased although some unique systems remain threatened and risks associated with extreme weather events remain. To limit the temperature increase to 2°C, total cumulative anthropogenic emissions since 1870 must remain below 2900 Gt CO_2 while up to 2011 already 1900 Gt CO_2 was emitted [93] and global per capita emissions continued to increase from 4.2 t CO_2/capita in 1990 up to 4.8 t CO_2/capita in 2008 [20]. If global CO_2 emissions are decreased by 65% by 2050 and 100% by 2100 relative to 2010 levels, the probability that the temperature increase in the long term remains below 2°C is around 78% [33]. Higher emissions will result in atmospheric CO_2 concentrations higher than 450 ppm in 2100, which could lead to dangerous

anthropogenic interference with the climate system [93].

The European Union has set targets for increasing renewable energy use, increasing energy efficiency and reducing greenhouse gas emissions which aid in tackling global warming [54, 58]. In Europe, the building sector is a large energy consumer and has a huge potential for efficiency gains [60]. Electrifying residential heating loads through the use of heat pumps, can contribute to these efficiency gains and thus reduce residential greenhouse gas emissions.

Moreover, this electrification increases the viability of large scale deployment of non-dispatchable renewable energy conversion by increasing the load factor [90, 188, 199]. However, the introduction of large numbers of heat pumps in the electricity system could disrupt the load diversity [126].

In an electricity system, load diversity lowers the required generation and transportation capacity [166]. Unfortunately, space heating is a highly simultaneous load as it is predominantly ambient temperature dependent and deploying heat pumps for space heating on a large scale could induce large peak loads in winter times [184]. However, due to the thermal inertia present in most buildings, it is possible to decouple the heat demand and heat generation in time to some extent. This allows for a flexible operation of the heat pump to support the operation of the electricity system. The time scale of this flexibility is in the order of a few hours to a day, depending on the building type, materials and insulation level [148]. The addition of a dedicated thermal energy storage tank can provide additional flexibility to the electricity generation system which can be used to lower electricity generation related CO_2 emissions. For residential applications, hot water storage tanks are a cost effective thermal energy storage technology as the required temperatures are in the range of 20-80°C [9].

This work investigates the total environmental impact of residential heating with heat pumps and hot water storage tanks. To evaluate the total environmental impact, the emissions (broader than CO_2 alone) related to the construction and waste treatment of the heat pump and the additional thermal energy storage tank must be taken into account alongside with emissions in the electricity sector. Furthermore, resources used for the construction of these systems have an impact on the availability of resources for future generations which must be taken into account in a sustainability evaluation.

1.2   Research objective

The main objective of this work is to assess the environmental impact of residential heating systems with heat pumps and hot water storage tanks in

an electricity system with renewable energy sources. From this objective, the following research questions can be distilled:

- How can the total environmental impact of residential heating with heat pumps and hot water storage tanks be estimated, accounting for the effects a large scale integration of heat pumps has on the electricity system?

- What is the optimal storage tank size to minimize the total environmental impact of residential heating with heat pumps?

- What is the trade-off between total environmental impact and financial cost of such a system?

1.3   System and boundaries

Residential buildings are heated or cooled to provide a certain level of thermal comfort to the building occupants. The environmental impact of this heating or cooling can be allocated to the life-cycles of the required systems and components.

The construction of the heating system requires the extraction of raw materials from the environment and energy to transform these materials into the finished products.

Heating systems with electricity as energy vector, such as heat pumps, extract electrical energy from the electricity grid during their operation. The required electricity is generated in classic, fossil fuel or uranium powered, power plants, or by renewable energy sources (RES), e.g. wind turbines or photovoltaic panels. The former use fuels which need to be extracted and refined. Moreover, burning fossil fuels emits CO_2 among other substances into the atmosphere. Both classical power plants and RES require materials and energy for the construction of the generating facility. Furthermore, the electrical energy must be transported from the generation facilities to the end users. This requires a significant amount of infrastructure, e.g. transmission grid lines, electricity distribution networks, transformers, ... , which carries certain environmental burdens. If heating systems with electricity as energy vector are deployed on a large scale, they will affect the required generation and transportation capacity and use.

Finally, at the end of the heating system's service life, it is disassembled and recycled or disposed of which again requires energy and releases harmful substances to the environment.

This work focuses on the environmental impact of residential heating with heat pumps, and whether and how hot water storage tanks can reduce the impact. By introducing a hot water storage tank to a heating system with a heat pump, additional operational flexibility is added. This flexibility can be used to shift heat pump energy use in time to limit the required generation capacity and to reduce overall emissions in the electricity system, reducing the environmental impact of space heating.

In this work, the environmental impact of the construction and waste treatment of the building is not accounted for. As the same building can use several heating systems to provide similar levels of thermal comfort to the occupants, a reference building is chosen for comparing the effect of different heating systems and strategies. Therefore, optimization of the building itself to reduce the environmental impact is outside the scope of this work. Moreover, cooling of the buildings is not considered. In a Belgian, residential context, building overheating can be avoided throughout most of the year by adequate building design and the use of window shading. Furthermore, effects of the number of participating buildings fall outside the scope of this analysis.

On the electricity generation side, the available capacity of renewable electricity sources is assumed fixed throughout the work. Although the installed renewable generating capacity will affect the benefits of additional flexibility, the optimum capacities are influenced by many other parameters and systems such as investment costs, land availability, visual impacts and power quality. Therefore, in this work, the installed capacity is considered a boundary condition and remains fixed.

The above described system is schematically represented in figure 1.1. The next section presents a top-down analysis of the approach to achieve the research objective for the system.

1.4   Top-down system analysis

In the above described system, three levels can be distinguished. In figure 1.1 the system under consideration is presented schematically along with these three levels.

The highest level consists of the electricity system with electricity generation plants, buildings using electricity for space heating and domestic hot water production (DHW) and the electricity transport infrastructure. The environmental impact of each of these systems can be quantified with a life-cycle assessment (LCA) method. To accomplish this, the heating system components
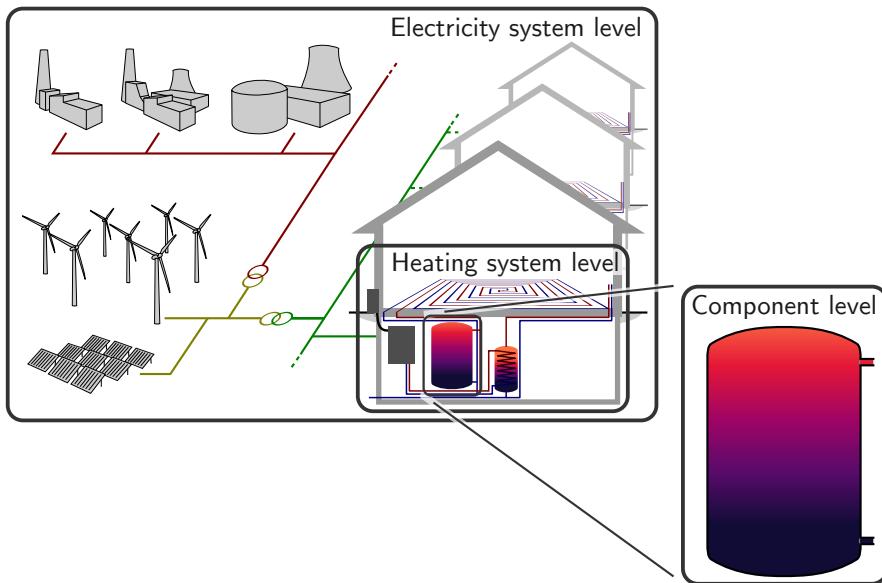
Figure 1.1: Schematic representation of the system under consideration with the three levels of modeling

must be specified and the amount of electricity generated by each type of power plant and the required generation and transportation capacity must be computed. Electricity generation is scheduled to minimize environmental impact while the balance between supply and demand must be met at all times. By introducing additional flexibility on the demand side in the form of hot water storage tanks in heating systems, energy use can be shifted in time to increase the share of the most efficient or environmentally friendly power plants [9] or to reduce the required peak generation or electricity transport capacity. In the literature, this is referred to as demand response (DR) [190]. The time scales of load shifting considered in this work are in the order of hours to a few days. Several authors have identified DR as a means to reduce peak loads generated by heat pump operation [11, 34, 184]. This lowers the environmental impact of electricity used by a heating system. However, larger storage tanks require more material extraction for storage tank construction and thus increase the environmental impact. This suggests that an optimum storage tank size, with minimum total environmental impact of space heating exists. Furthermore, larger storage tanks, present larger investments made by individual home owners. A trade-off curve balancing costs and environmental impact of residential heating with heat pumps is constructed.

If heat pump heating systems are deployed on a large scale, heat pump operation affects the scheduling of different power plants. Thus, to determine the electricity generated by different power plants, an integrated simulation of the building and electricity system is required. In these simulations, the heat pump control must take into account the current state of the building, storage tank and electricity system but must also make predictions of the effect of current actions on the future state of the involved systems. This can be achieved through the use of model predictive control (MPC). MPC employs a reduced order system model to compute the future states of the system and generates control signals that minimize an objective function over a certain prediction horizon while ensuring the system remains within the allowed boundaries. Only the first elements of the control signals are then applied to the real system. The next time step, the process is repeated [2]. This process is often referred to as moving horizon optimal control as it requires the solution of an optimal control problem (OCP) in each time step with a prediction horizon slightly shifted. In the OCP, the objective function must reflect the overall DR goals of shifting energy use or limiting peak capacity.

At a lower level, in a heating system, the heat pump and emission system and their control must be tailored to the presence of a hot water storage tank so that maximum flexibility can be offered to the electricity grid. The control of the heating system in a building forms an essential part in enabling DR through heat pumps and hot water storage tanks. The OCP requires a model of the heating system including the storage tank and the building. Depending on the heating system configuration and storage tank charging and discharging strategy, several mathematical representations of the heating system behavior can be formulated. Approximations are made in each of these formulations leading to a model mismatch which can lead to undesirable control actions.

The choice of optimal control formulation also depends on the integration of the storage tank in the heating system and the chosen strategy for charging and discharging the storage tank. Furthermore, these aspects influence the ability of the heating system to provide certain DR services to the electricity system as the effective available storage capacity and the efficiency of energy recovery from a storage tank change.

At the component level, flow phenomena in the storage tank must be accounted for in a sufficiently accurate manner, to ensure a correct representation of the benefits of adding a hot water storage tank to the heating system. As this storage tank model is used in the integrated simulation of the buildings and electricity system, a low-order model is needed for the storage tank, so long time span simulations have a limited computation time.

This system analysis reveals the subproblems encountered in solving the research questions.

- A hot water storage tank model is required for including the storage tank dynamics in building simulations.

- The effects of different integration methods of the storage tank in the heating system as well as the benefits of different charging and discharging strategies must be investigated.

- When an integration method and charging/discharging strategy are chosen, an OCP formulation which results in good system performance is required.

- An MPC simulation of the integrated system of buildings and electricity generation, capable of quantifying the effects of the storage tank on the electricity generation system must be developed. The developed storage tank model and OCP formulation are used here.

- An LCA framework delivering the environmental impact of residential heating with heat pumps and storage tanks from the previously obtained results must be developed. This framework is used to compute optimal storage tank sizes and trade-off curves.

1.5   Scientific challenges

Each of the subproblems defined in section 1.4 poses its own scientific challenges which this work will address.

First, the hot water storage tank model required in the building simulation must be sufficiently accurate for a range of storage tank sizes. This requires the development of a model structure, suitable to incorporate the effects of complex flow phenomena. Furthermore, a validation campaign, comparing simulated quantities to values obtained through independent experiments, is required to obtain a certain level of confidence in the model outcome.

Second, the merits of different charging and discharging strategies in a DR context must be investigated. To this end, a methodology capable of capturing the benefits of a storage tank in a DR context is needed. Connected to this methodology, performance indicators are required for comparing different set-ups. With this methodology, the benefits and disadvantages of charging and discharging strategies are investigated.

Third, an MPC control strategy requires a hot water storage tank model suitable for integration in an OCP. This model must be significantly more simplified

than the model used in the building simulations as this would lead to a too complex optimization problem which takes too long to solve or results in local optima. Nevertheless, the model needs to capture the general behavior of a real hot water storage tank. A methodology for comparing OCP formulations in an open-loop setting and an MPC setting must be developed. With this methodology OCP formulations commonly found in the literature and novel formulations can be evaluated.

Fourth, an integrated MPC simulation of a set of buildings and the electricity generation system needs to be developed. An MPC is preferred over an open-loop OCP approach as state-of-the-art controller models for hot water storage tanks show a significant mismatch with respect to the behavior of a real hot water storage tank. An integrated approach is required to take the feedback of a large number of heat pumps on the electricity system into account.

Fifth, a framework for executing LCAs for the integrated system of buildings and the electricity generation system is required. Here the impact of changing generating unit load factors and the required electricity transport capacity caused by peak load changes due to flexible heat pump operation must be taken into account. In current LCA studies and databases, historical average load factors or even historical electricity generation mixes are used. This is inappropriate in the current framework as the purpose of the control system is to reduce the total environmental impact through changing the electricity generation mix and thus changing generating unit load factors. Therefore, electricity generation unit-processes split in an energy related and a capacity related part are required.

Finally, the solvability of the developed methodology must be shown. This is done in a case study of a system inspired by the Belgian electricity system with a large number of renewable energy sources. Based on the case study results, the second and third research questions presented in section 1.2 are answered.
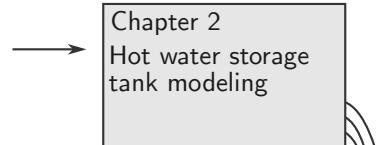
Each challenge is addressed in a different chapter of this thesis and leads to a contribution. The methodological developments and scientific contributions of this work are schematically presented in figure 1.2. Within each chapter, the current state-of-the-art related to that chapter will be discussed in detail resulting in a clear description of where this work contributes.

1.6 Outline
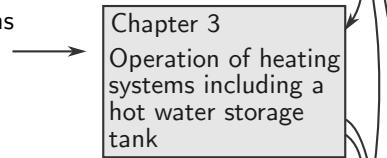
The problem analysis discussed in section 1.4 leads to subproblems and scientific challenges at the different levels which structure this thesis, as schematically

Component level
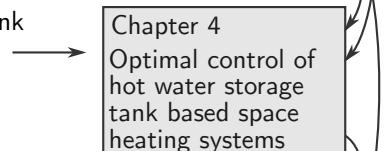
Validated hot water storage tank emulator
capable of representing the results on the   ⟶   Chapter 2
temperature profile of 3D flow phenomena   Hot water storage
                                                      tank modeling
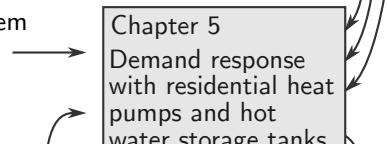
Heating system level

Methodology for comparing heating systems
including a hot water storage tank in   ⟶   Chapter 3
a DR context   Operation of heating
                                                      systems including a
                                                      hot water storage
                                                      tank
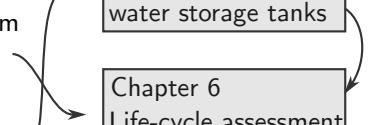
OCP formulation of a hot water storage tank
combined with a heat emission system and   ⟶   Chapter 4
a heat pump   Optimal control of
                                                      hot water storage
                                                      tank based space
                                                      heating systems

Electricity system level

Framework for MPC of the integrated system
including a set of buildings and the   ⟶   Chapter 5
electicity generation system   Demand response
                                                      with residential heat
Framework for LCA of the integrated system   pumps and hot
including a set of buildings and the   water storage tanks
electicity generation system
                                                      Chapter 6
                                                      Life-cycle assessment
Case study to show the solvability and   of residential heating
to answer research questions 2 and 3
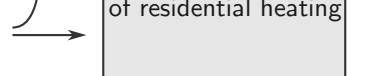
Figure 1.2: Schematic overview of scientific contributions and interdependencies of the solved
subproblems presented in this work.

presented in figure 1.2.

Chapter 2 provides an overview and discussion of modeling approaches for hot water storage tanks found in the literature. A reduced order mathematical model for simulating the behavior of a hot water storage tank is presented. The model is partly validated and simulation results are compared with experiments.

Chapter 3 proposes a methodology for comparing heating systems including a hot water storage tank in a demand response context. Several configurations of a hot water storage tank in a residential heating system are analyzed and their benefits and disadvantages are quantified and discussed.

Chapter 4 explores different model predictive control options. A novel optimal control formulation for a heating system with a hot water storage tank and heat pump is developed. Optimal control formulations are evaluated based on their energetic performance when integrated in an MPC.

Chapter 5 presents the used MPC approach for residential heating integrated in an electricity system. Different control objectives are formulated and combined into a single multi-objective optimization. Furthermore, the effects on the electricity generation mix and peak loads of introducing heat pumps and storage tanks in the electricity system are quantified in a case study inspired by the Belgian electricity system.

Chapter 6 provides an introduction to important aspects of sustainability and the environmental impact of products or product systems. A methodology for quantifying the environmental impact of residential heating, including the impact of changes in the electricity system, is developed. Results for the the Belgian case study are presented to answer the research questions posed in section 1.2.

Finally, chapter 7 summarizes the main results and conclusions of this PhD work and provides an outlook to future research.

Chapter 2

Hot water storage tank modeling

Parts of this chapter are based on a paper that was previously published as: Baeten, B., Confrey, T., Pecue, S., Rogiers, F., and Helsen, L. "A validated model for mixing and buoyancy in stratified hot water storage tanks for use in building energy simulations". In: *Applied Energy* 172 (2016), pp. 217–229.

2.1 Introduction

In this chapter, a model for a hot water storage tank, suitable for use in large time span building simulations is developed. The model is subsequently used in the next chapters to assess the value of different integration methods of a storage tank in a building heating system and to compare different charging strategies. Furthermore, the model is required to evaluate the merit of different OCP formulations. Finally, the model is used in the integrated simulations of the electricity system and buildings.

For design or component sizing of building heating systems including hot water storage tanks, integrated dynamic system simulations are essential. Campos Celador et al. [28] showed that in a combined heat and power system, the storage tank model used in such simulations can have major effects on calculated annual savings (an underestimation of up to 9%) and design decisions. With heat pump systems, the model influence is likely to increase due to the lower temperature

differences involved. When simulations are used for component sizing, the model order must remain low to allow running multiple simulations in a limited time span. An accurate, but low order model for a stratified hot water storage tank is thus required.

The goal of this chapter is to develop a low order hot water storage tank model, estimate model parameters and validate the model to attain some certainty on the accuracy of the model.

The chapter is structured as follows: In section 2.2, an overview of processes and systems relevant to hot water storage tanks is presented. Next, in section 2.3, these processes are further investigated and modeling attempts found in the literature are discussed. In section 2.4, the hot water storage tank model used throughout this thesis is presented. Subsequently, section 2.5 presents parameter estimations, a model validation and comparisons with experiments. Finally, in section 2.6, concluding remarks are formulated.

2.2   Hot water storage tanks

When considering thermal energy storage, three processes can be identified. During the charging process the thermal energy in the storage is increased. Energy flows from the heat generation system to the storage. Subsequently during the standby process, no energy transfers to or from the storage are imposed. However, heat losses can occur causing the energy content of the storage to decrease. Finally during the discharge process, energy is drawn from the storage and transferred to a load.

Active thermal energy storage in a residential context is achieved most economically using a hot water storage tank [146]. Most commercial hot water storage tanks are pressurized steel vessels with an insulation mantle to reduce heat losses to the surroundings. The steel vessels have rounded heads and several fittings to enable in- and outflow or instrumentation. Storage tanks are often directly connected to the heating system or domestic water supply. As the temperature variation in the large mass of water causes substantial changes in volume, adequate pressure controlling measures must be taken. To prevent contamination of potable water by corrosion, domestic hot water tanks are made of stainless steel or the interior is finished with a polymer or ceramic coating. For ceramic coated tanks a cathodic protection is often added to prevent corrosion at fittings where the coating might be insufficient [61].

Due to the density difference between warm and cold water, stratification inside the water tank can occur. When charging a hot water storage tank, warmer
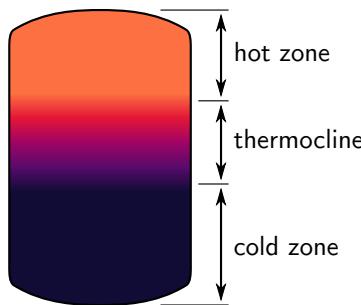
Figure 2.1: Stratification inside a hot water storage tank

water tends to gather at the top while colder water drops to the bottom. In-between a zone of varying temperature exists called the thermocline (figure 2.1). Depending on the thickness of the thermocline zone one can characterize a temperature profile inside a storage tank as highly or moderately stratified [37]. When no temperature differences are present in the storage tank, it is said to be fully mixed.

For many thermal energy applications, the temperature at which the thermal energy is demanded is important. When integrating thermal energy storage in such processes, stratification can greatly affect the performance of the integrated system [152, 153]. Some authors have investigated the effect of stratification on global system efficiency for a variety of systems. Rosen et al. [153] identified stratification as advantageous for the amount of energy that can be recovered from a storage process. In solar domestic hot water systems, thermal performance in tanks with more stratification is higher [110].

An important factor in creating stratification in a storage tank is the charging method. Charging and discharging of a storage tank can be achieved in several ways depending on the application [144]. Different charging methods are visualized schematically in figure 2.2. Charging by direct inflow, replacing cold water inside the storage tank with hot water from the heat generation system can be used if the fluids in the storage tank and heat generation system can be mixed (figure 2.2a). If the fluids in the storage tank and the heat generation system should remain separated, a heat exchanger must be used. Several methods are found in the literature. The most common method is charging the storage tank through an immersed coil heat exchanger (figure 2.2c). Here, the heat transfer fluid flows through a coiled pipe often located at the bottom of the storage tank. Heat exchangers are often placed on the bottom of the storage tank to take advantage of lower temperatures near the bottom of the tank to increase heat transfer. A mantle heat exchanger (figure 2.2d) consists of a double walled

storage tank, where the heat transfer fluid flows in the cavity between both walls. Several authors investigated the performance of these storage tanks both experimentally and numerically [15, 110, 160]. A last option for storage charging is using an external (or side arm) heat exchanger (figure 2.2b). Here the heat transfer between the heat transfer fluid and the storage fluid occurs outside the storage tank in an external heat exchanger. For some applications it is possible to eliminate the use of an additional circulation pump by utilizing natural convection in the side arm, also called the thermosyphon effect.

The charging methods can be categorized based on the mixing of heat transfer fluid and storage fluid, as done above, or based on the main principle of energy transfer. When charging a storage tank via an immersed or mantle heat exchanger, the energy is transferred to the storage tank mainly through natural convection. This method of energy transfer requires vertical flows inside the storage tank which impede thermal stratification [144]. If a storage tank is charged directly, the heat transfer fluid flows directly into the storage tank. Under the right conditions, mixing of fluid at different temperatures can be minimized which results in good thermal stratification. If an external heat exchanger is properly sized and controlled, similar results can be obtained.

2.3 Hot water storage tank modeling: literature review

The three phases in a storage cycle, charging, standby and discharging, can be represented by the physical phenomena which occur during these phases. In this perspective the charging and discharging processes consist of the same phenomena, as long as the same charging or discharging method is used. The distinction between the two lies solely in the temperature levels of supply and return fluid. When the supply temperature is higher than the return temperature, the storage is charged, when the return temperature is higher than the supply temperature, storage discharging occurs.

Storage tank models can be categorized based on their complexity. Computational fluid dynamics (CFD) models are mostly used for investigating effects of varying geometry on the storage processes. Simplified algebraic or low order models are mainly used in an optimization context. Finally, one-dimensional models are suitable for dynamic system simulations, stated that their accuracy is checked.

In the following sections an overview of the physics involved in the different storage processes is presented. Furthermore, attempts to model these processes

(a) direct charging

(b) external heat exchanger charging

(c) immersed heat exchanger charging

(d) mantle heat exchanger charging
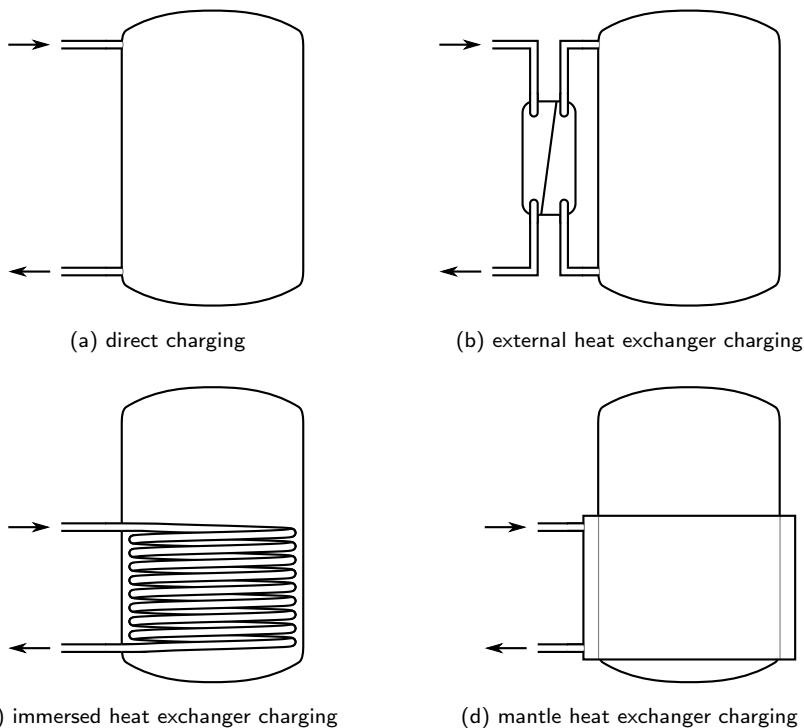
Figure 2.2: Charging methods for a hot water storage tank

found in the literature are discussed.

2.3.1 Direct inflow charging

When discussing the physics involved in the charging or discharging process of a hot water storage tank, a clear distinction should be made between direct charging and charging using an immersed or mantle heat exchanger. With direct charging or discharging, an attempt is made to replace the fluid in the storage tank with fluid at a different temperature. In an idealized situation plug flow occurs and there is no mixing between the entering fluid and the fluid in the storage tank. During charging, a stratification front arises where the temperature suddenly changes from the supply temperature to the temperature of the fluid originally in the storage tank. The thermocline is thus infinitely small. This can be described as ideal stratification and is schematically represented in figure 2.3a.

(a) ideal stratification

(b) a more realistic charging process with inflow and outflow mixing
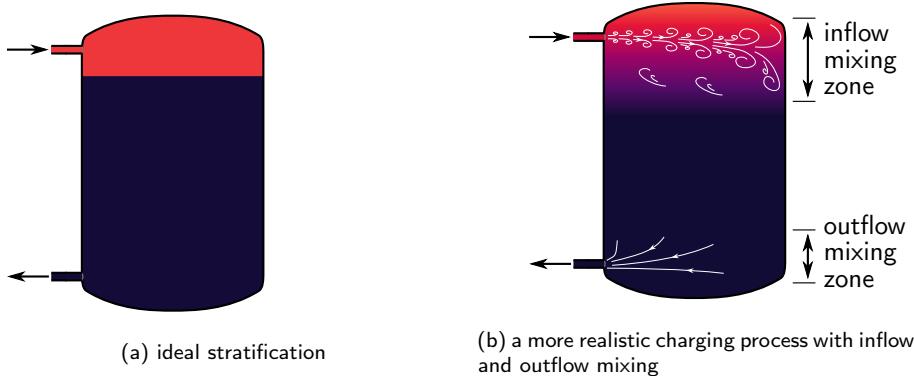
Figure 2.3: Schematic representation of the flow and mixing phenomena when charging or discharging a storage tank through direct inflow and outflow ports under idealized and real circumstances

When a real storage tank is charged or discharged, the occurring phenomena become more complex. At the inflow port, a jet is formed. As the entering water is flowing at a higher velocity than the water inside the storage tank, a free shear layer is formed causing turbulent mixing and entrainment of surrounding water. If the jet reaches the far wall of the storage tank before its velocity is sufficiently diminished, the affected region increases. Furthermore, if the temperature of the entering fluid does not match the temperature of the storage fluid near the inflow port, buoyancy will force the jet upward or downward, expanding the mixing zone. These phenomena result in significant mixing in the entrance region of the storage tank [165, 173]. Because of this mixing a thermocline of finite height forms. When the charging process continues the thermocline will shift downward and if the inflow temperature remains constant, the mixing zone near the inflow port will contain only fluid at the inflow temperature. Buoyancy effects will then no longer occur and the mixing of supply fluid and storage fluid no longer has an effect on the temperature distribution inside the storage tank. The thermocline will then only be affected by diffusion in the storage fluid, heat conduction through the tank walls and natural convection flows caused by heat losses.

Near the outflow port, fluid in the storage tank will be drawn to the outflow port causing the outflow to be a mix of fluid from different levels. Furthermore, these three-dimensional flows cause some mixing inside the storage tank near the outflow port. The above described phenomena are schematically represented in figure 2.3b.

Direct storage charging of a thermal storage tank can be modeled using various methods, each with some benefits and disadvantages, fit for a specific application.

Several authors presented two-dimensional or three-dimensional finite volume numerical solutions of the governing equations when studying thermocline dynamics or inflow geometry dependency. 2D models have been shown to correlate well with experiments in both rectangular enclosures [181, 182] and axisymmetric setups [83, 161]. El-Amin et al. [6], Eames and Norton [50], Ievers and Lin [91], and Kaloudis et al. [102] investigated storage temperature distributions during charging or discharging situations with different inflow positions using a three-dimensional finite volume model. They showed the formation of a buoyant jet or plume at the inflow which causes mixing around and above the inflow port of the storage tank. Eames and Norton [50] also showed that under varying inflow temperature conditions, an inflow at the top of the storage tank could perform worse than an inflow located elsewhere. The effects of inflow stratifiers or diffusers on thermocline formation were also investigated using 3D finite volume models [31, 159]. Although the accuracy reached using the above mentioned CFD techniques is very high, these models are inappropriate for use in building energy system simulations due to the long calculation and development times.

In storage tank sizing problems, perfectly stratified storage tank models are predominant [11, 44, 65, 82, 89, 147, 167]. Such a model can be seen as a state-of-charge model, where the average storage tank temperature is influenced by the energy transfers to and from the storage tank. Furthermore, the possible energy transfers are independent of the temperature distribution inside the storage tank as long as the storage tank is not fully charged or fully discharged. In analyzing large systems over long periods, perfectly stratified [65, 82, 167] or mixed [3, 68, 133] storage tank models are found regularly in the literature. Steen et al. [164] proposed to split the storage tank model in a low and high temperature section to increase the accuracy of modeled heat losses. However, this approach does not increase the accuracy of modeling mixing or buoyancy effects.

These state-of-charge models are used because of their simplicity and are therefore well suited for large scale simulations. However, attention must be paid to the range of applicability of these models. When the temperature at which energy is drawn from the storage tank is important, using a perfectly stratified storage tank model will result in an overestimation of effective storage capacity while using a fully mixed storage tank model will result in an underestimation of deliverable power (see section 4.4).

In building energy simulations, the most encountered stratified storage tank models are one-dimensional finite volume discretizations [35, 42, 63, 66, 124, 128,

151, 162, 193, 201]. As in a 1D, incompressible approach, the momentum and mass balance become trivial, only the energy balance remains. This approach greatly reduces model complexity but implies that modeling three-dimensional effects, like jet mixing and buoyancy, requires model adaptations or correlations [86]. However, dynamic simulations of energy systems using one-dimensional temperature distributions, omitting buoyancy and mixing effects are common in the literature [35, 124, 128, 151, 162, 201]. In some applications, these simplifications can be justified, as specific boundary conditions prevent three-dimensional effects from occurring. In one-dimensional models, an adequate representation of the temperature distribution is required to enable a good estimate of the outflow temperature in storage charging-discharging cycles.

Several authors have compared 1D models using different mixing formulations with experiments or CFD simulations for a variety of situations [42, 101, 109, 128, 130, 151, 162, 193]. Without using any modifications for inflow mixing, Nelson et al. [128] and Spur et al. [162] found good accordance for storage charging at constant temperature. This behavior is expected, as if the inflow velocity is low enough, no mixing or buoyancy will occur if the inflow ports are positioned at the top and bottom of the storage tank. Rodríguez-Hidalgo et al. [151] reported excellent correspondence of simulated and measured energy extracted from a solar domestic hot water tank with a constant draw flow rate. This result is expected as the draw flow dominates the fluid motion inside the storage tank, avoiding mixing or buoyancy. Kleinbach et al. [109] compared two mixing formulations with experiments and reported varying correspondence. Jordan and Furbo [101] adapted an often used storage tank model [49] by including a fully mixed zone near the inflow with a height dependent on the local densimetric Froude number. The formulation could be fitted to correspond well with experiments of domestic hot water draws but no validation was performed. Wetter [193] and De Coninck et al. [42] used a directional diffusion approach to model buoyancy effects with a diffusion time constant and a node number dependent conduction coefficient respectively. However, when applying directional diffusivity, buoyancy occurs only when an adverse average temperature gradient is present. In real hot water storage tanks, this temperature reversal is never seen [83, 101, 130, 134, 161, 181, 182], leading to a mismatch in storage temperature profile. Nizami et al. [130] modeled the jet mixing created by a vertical inflow by adding a mixed jet node in which the inflow is discharged and to which entrainment from the neighboring layers occurs. The mixing height and the entrainment mass flow rates were correlated with the Richardson number and inflow diameter based on a parametric CFD study. The model shows good accordance with experiments. However, it can not easily be extrapolated to a case with horizontal inflows, which is more common in hot water storage applications as it causes less jet mixing. Steinert et al. [165] used a self-similar buoyant jet solution to determine the distribution

and temperature of the entering fluid. Comparison with experiments showed good results for storage tanks with a small height over diameter ratio. However, in more realistic hot water storage tanks the entering jet often reaches the far side of the storage tank. In such a situation the self-similar buoyant jet solution is no longer valid and mixing will be underestimated. The solution of the model also requires the solution of a system of differential equations that govern the buoyant jet flow, separate from a time stepping procedure. This solution method makes the model computationally intensive. Palacios et al. [134] and Toyoshima and Okawa [173] experimentally correlated a mixing zone due to a horizontal buoyant jet with the ratio of specific momentum and buoyancy flux. Using this mixing zone Palacios et al. [134] constructed a two layer storage tank model with an intermediate thermocline that shows good outflow temperature prediction capabilities when the temperature variation inside the storage tank is small. However, this model is unable to represent the more complex temperature profiles encountered when storing energy at different temperature levels. Toyoshima and Okawa [173] constructed a multi-layer model with uniform inflow distribution that neglects internal mixing occurring when the inflow is near the thermocline.

In the literature, no model for direct charging of a hot water storage tank, valid over a range of storage tank sizes and inflow conditions was found. As such a model is required for the remainder of this work, a model for inflow buoyancy and mixing is described in section 2.4.1 and validated against experiments in section 2.5.2.

2.3.2   Immersed heat exchanger charging

The charging or discharging of a hot water storage tank through an immersed heat exchanger creates natural convection flows inside the storage tank. The storage fluid near the heat exchanger heats up and rises as energy is transferred from the heat exchanger fluid. While rising, the fluid can extract more energy from the heat exchanger and entrain adjacent fluid forming a thermal and momentum boundary layer along the heat exchanger. When the heated fluid reaches the top of the heat exchanger a buoyant plume sheet is formed, further rising and entraining storage fluid until the plume temperature matches the average temperature in the storage tank or the top of the storage tank is reached [64]. Here the heated fluid gathers, pushing colder fluid down to complete the natural convection loop [168]. The afore mentioned processes are schematically represented in figure 2.4.

Several authors presented models for the heat transfer from an immersed heat exchanger in a hot water storage tank of various complexities. 3D finite volume
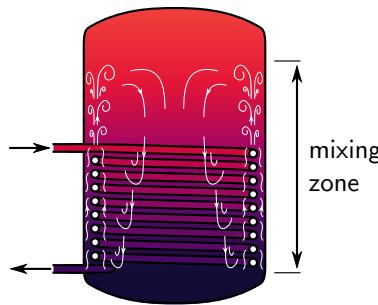
Figure 2.4: Schematic representation of the natural convection process when charging or discharging a storage tank through an immersed coil heat exchanger

models are mainly used to investigate the effects of changing heat exchanger geometry or inserting baffles in the storage tank on the heat transfer process. Su and Davidson [168] described a CFD study where the effects of adding baffles to a storage tank were investigated. They concluded that introducing straight vertical baffles in a storage tank increases the velocity along the heat exchanger. This results in an increased heat transfer rate but is detrimental for the stratification inside the storage tank. Differently designed baffles can increase the flow resistance and promote stratification. However, these baffles reduce the heat transfer rate. Similar results, describing an increased heat transfer rate when introducing baffles of different geometries for storage discharging have been presented by Boetcher et al. [21, 22]. These models, although very accurate, are not suitable for use in system simulations due to their complexity.

In simplified situations, correlations describing the heat transfer from an immersed heat exchanger can be derived and used to represent the storage tank dynamics. Su and Davidson [169] proposed a Nusselt number correlation for transient heat transfer from a heat exchanger to a perfectly mixed storage tank. They derived an analytical expression which requires two empirical constants for each heat exchanger - storage tank combination. The limitation of perfectly mixed storage tanks is however a very strong disadvantage. Kulacki et al. [115] used analytical heat transfer correlations and expressions for a negatively buoyant plume origination from a shroud and baffle heat exchanger. The used heat exchanger geometry in this work is significantly simplified in comparison to real heat exchangers and the expressions are strongly geometry dependent, making extrapolation to different, more realistic geometries difficult.

One-dimensional storage tank models are interesting for use in building energy simulations as the required computational effort is limited. The addition of an immersed heat exchanger in such a model is however not straight forward.

Spur et al. [162], Klein et al. [108] and Cadafalch et al. [26] described a 1D model where the local heat transfer from a portion of the heat exchanger to the storage tank layer it resides in is calculated iteratively using known natural convection correlations. This modeling approach however causes the storage fluid temperature to increase only in the proximity of the heat exchanger, it generates temperature inversions (zones of fluid at a high temperature, located below fluid at a lower temperature) which are not observed in experiments. To avoid this, they artificially mix layers where temperature inversion occurs at the end of each time step. As a result, the formation of a thermocline is inhibited and a fully mixed temperature profile is generated around the heat exchanger while in experiments and CFD simulations a thermocline is observed along the height of the heat exchanger. Furthermore, such a procedure is not suited for variable time step solvers as it would result in variations in the output depending on the time step. A comparison of simulations and experiments was performed by Cadafalch et al. [26]. They presented good accordance of heat transfer and heat exchanger return temperature, however, no storage tank temperature profiles were presented.

In the literature, low-order models for charging a hot water storage tank through an immersed heat exchanger, applicable for building energy system simulations, are scarce. Most authors compute the heat transfer localized to the position of the heat exchanger and use a heuristic to minimize temperature inversions. However, no models capable of predicting the storage tank temperature distribution, suitable for use in building energy system simulations were found. In section 2.4.2 such a model, suitable for use with efficient variable time-step solvers, is presented and model parameters are fitted to experiments in section 2.5.3.

2.3.3 Heat loss

As the temperature of the storage fluid is higher than the ambient air temperature surrounding the storage tank, the energy content of the storage tank will diminish as heat is transferred to the ambient. To reduce heat losses, hot water storage tanks are usually enclosed in an insulation mantle, often made of flexible polyurethane foam. Nevertheless, heat losses can not be avoided and if left undisturbed for a sufficient amount of time, the storage tank will converge to a state of thermal equilibrium with its surroundings. In the storage fluid, heat is transferred to the storage tank wall by means of natural convection. Fluid near the wall cools and, due to density differences, drops to a layer with corresponding temperature. The layer at the top is simultaneously replenished with fluid from the cooler layers located below. Conduction in the storage fluid

results in heat diffusion in the storage tank and an increase in the thermocline height.

In the storage tank wall, heat is transferred to the insulation layer by conduction and axial conduction causes an increase in axial heat diffusion of the storage fluid. The heat transfer from the outside surface of the insulation to the ambient air is governed by natural convection and radiation.

Cruickshank and Harrison [36] presented standby experiments on a vertical cylindrical storage tank while measuring the temperature distribution in the vertical and horizontal direction. No variations in the horizontal temperature distribution were observed, and the vertical temperature measurements show a faster cooling of the storage fluid near the bottom of the tank. The upper section of the storage tank was shown to cool more or less uniform. Wood et al. [195] and Walmsley et al. [189] performed experiments to investigate the decay of stratification. Their results were similar and showed the thermocline moving upward while its height increases. Only a slight decrease in temperature of the upper section of the storage tank was observed. Gasque et al. [76] computed a partial charging and standby process for a rectangular storage tank using a three-dimensional CFD method. Results showed the natural convection loops originating from heat loss. While cooling, fluid drops near the sides of the storage tank to a layer of similar temperature. This causes the thermocline to increase in height during the standby phase, while the temperature at the top of the storage tank is maintained.

Steen et al. [164] presented a model for use in a large scale system optimization context. They showed the difference in heat loss from an ideally stratified and a completely mixed storage tank as calculated by using a uniform heat transfer coefficient. The mixed tank showed a variation of heat loss rate with charge fraction due to a changing temperature at top and bottom of the storage tank while under the stratified assumptions, these temperatures were fixed.

Nelson et al. [128] presented a one dimensional model with separate modeling of the tank wall temperature and axial conduction. Simulation results compared very well with destratification experiments. In these experiments, the bottom half of the storage tank is at a temperature only slightly higher than the surrounding temperature. Using this modeling approach does not result in a more rapid cooling of the lower parts of a storage tank as seen in the experiments and detailed simulations presented above. A similar approach was used by Klein et al. [108]. They however used an additional conductivity in the storage fluid to model the axial tank wall conduction, which showed good results.

In the literature, some models for the temperature decay in a hot water storage tank suitable for building energy system simulations were found [108, 128].

These models compare well to experiments. However, not all experiments are representative for situations occurring in a hot water storage tank used for space heating. In a space heating system, the heating system return temperature is most likely higher than the temperature of the surroundings of the storage tank. If the storage tank is partially discharged, the temperature in the lower part of a storage tank will thus still be higher than the surrounding temperature, affecting the heat losses from this part of the storage tank. Furthermore, the necessity of modeling axial conduction in the storage tank walls is unclear.

In section 2.4.3 a model taking these effects into account and a model more similar to those used in the literature are presented. In section 2.5.4 model parameters are estimated, and simulation results are compared to experiments.

From the literature review presented above it is clear that the available models for hot water storage tanks useful for building energy simulations are limited in their applicability to the specific scenarios they were designed for. Most often, one dimensional models are used. However, in such models the effects of three-dimensional flow phenomena such as inflow buoyancy, mixing and natural convection from immersed heat exchangers or heat losses must be added through separate formulations. As these phenomena affect the temperature distribution inside the storage tank, they affect the operation of the storage tank in a heating system and must be accounted for. In this work methods are developed to incorporate several three-dimensional flow phenomena in a one dimensional model.

In the following section, models for the different physical phenomena occurring during the charging, discharging or the storage phase in hot water storage tanks are described. All models aim at giving an accurate representation of the temperature profile inside the storage tank, while the model order must remain sufficiently low. This allows the models to be used in building energy simulations.

2.4 Model description

The storage tank modeling approach used in this work consists of a spatial one-dimensional finite volume discretization of the energy equation. To achieve a sufficient spatial resolution the storage tank is divided vertically into N layers of equal height. The number of layers used in this work is determined from a sensitivity analysis of a direct inflow storage tank charging simulation with a storage tank model without buoyancy or mixing formulations and a hybrid QUICK-upwind discretization scheme. Simulations with the number of layers between 5 and 90 and storage tank heights between 1.5 m and 2.5 m were

performed. Increasing the number of layers above 50 does not significantly affect the simulated temperature profiles. With values below 50, simulated temperature differences due to the increasing discretization error are observable. This is in line with values reported in the literature [37]. Therefore, in this study the number of layers is always 50.

The modeling of the storage tank heads is an important aspect which is often overlooked in models found in the literature. When assigning inflow ports or heat exchangers at a certain height to a storage layer or a set of layers, it is not the actual height of the inflow port which is important but the division of mass above and below the port. When the storage heads are assumed flat while they are curved in reality, the storage tank volume above a certain height can differ up to 3% for common storage tank geometries resulting in noticeable errors. For instance, in idealized direct storage tank charging, with the assumption of plug flow between in and outflow port, only the storage fluid between the in- and outflow ports is considered. When the tank heads are modeled incorrectly, the fluid mass between in- and outflow port is overestimated with twice the error cited above, depending on the in and outflow port height. This leads to an error in storage capacity of the same magnitude.

In the present approach the radius at the top and bottom of each layer is computed according to the specification for tori-spherical heads as defined in DIN-28011 [45]. A linear variation between these radii is assumed to compute the layer volume. As an illustration, the relative difference in volume between the above described approach, incorporating the shape of the storage tank heads in the volume computation, and a linear assumption with varying height in the storage tank is presented in figure 2.5 for several storage tank height over diameter ratios. In this figure it can be seen that depending on the height over diameter ratio, the error in volume above a certain height can be as much as 6% if the volume is assumed to be linear with height. The errors are largest in a zone between 5% and 15% from the top and bottom, the zone where the in- and outflow ports are placed most often. This leads to a significant overestimation of the storage fluid volume above and below the inflow and outflow port which affects phenomenon such as inflow buoyancy.

For each layer an energy balance is made similar to the models proposed by [42, 49, 165, 173, 193]. Mass and energy flows to layer j are schematically represented in figure 2.6 and are treated as positive when the flow is directed along the arrow indicated in the figure. Throughout this work, the storage fluid is considered incompressible. The effects of buoyancy driven flows are accounted for through specific formulations and correlations. This implies the specific heat at constant volume and specific heat at constant pressure are equal and are designated c throughout this work. Furthermore, the fluid specific heat c is assumed to be constant. This results in the following equations for the energy
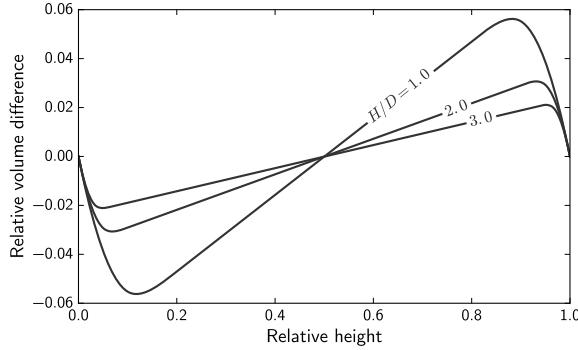
Figure 2.5: Relative difference in volume above a certain location when computing the storage tank volume using the actual geometry or when assuming a linear variation with height. Curves for different height (H) over diameter (D) ratio are presented.
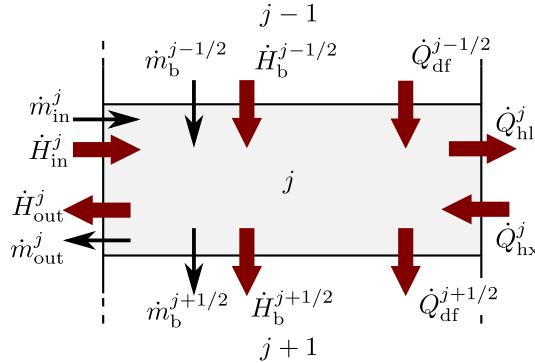
Figure 2.6: Schematic representation of mass and energy flow rates to a storage tank layer.

balance of layer j:

$$m^j c \frac{\mathrm{d}T^j}{\mathrm{d}t} = \dot{Q}^j_{\mathrm{df}} - \dot{Q}^j_{\mathrm{hl}} + \dot{Q}^j_{\mathrm{hx}} + \dot{H}^j \tag{2.1}$$

$$\dot{Q}^j_{\mathrm{df}} = \dot{Q}^{j-1/2}_{\mathrm{df}} - \dot{Q}^{j+1/2}_{\mathrm{df}} \tag{2.2}$$

$$\dot{H}^j = \dot{H}^{j-1/2}_{\mathrm{b}} - \dot{H}^{j+1/2}_{\mathrm{b}} + \dot{H}^j_{\mathrm{in}} - \dot{H}^j_{\mathrm{out}} \tag{2.3}$$

With m^j the layer mass, c the fluid specific heat, T^j the average layer temperature, $\dot{Q}^j_{\mathrm{df}}$ the heat flow rate due to diffusion, $\dot{Q}^j_{\mathrm{hl}}$ the heat loss through the storage tank walls to the surroundings and $\dot{Q}^j_{\mathrm{hx}}$ the heat transfer from

an immersed heat exchanger. These heat flows will be discussed in section 2.4.2 and 2.4.3. $\dot{m}_\mathrm{b}$ and $\dot{H}_\mathrm{b}$ respectively represent the mass flow rate and accompanying enthalpy flow rate through the boundary between layers, where $j - 1/2$ represents the boundary with the above layer and $j + 1/2$ the boundary with the layer below. $\dot{H}_\mathrm{in}^j$ and $\dot{H}_\mathrm{out}^j$ represent the enthalpy flows accompanying mass flows $\dot{m}_\mathrm{in}^j$ and $\dot{m}_\mathrm{out}^j$ caused by in- and outflows respectively and will be discussed in section 2.4.1.

The convective energy transfer between layers is computed similar to [193] with adjustments to allow for variable height in- and outflow ports and multiple port pairs. To achieve this, the mass flow rate through each layer surface is computed from a set of mass balances. To compute enthalpy flow rates across each layer boundary an estimate of the temperature at the layer boundary is required. A hybrid QUICK-upwind discretization scheme [117] is used to obtain these from the average layer temperatures. As the higher order QUICK discretization scheme introduces spatial oscillations when sharp gradients are present, a weighted average with an upwind discretization is computed [193]. During all simulations, the weighting factor α was set to 0.7 as this reduced numerical diffusion from the upwind discretization and reduced oscillations. The enthalpy flow rate through the upper boundary of a layer can then be computed as:

$$
\begin{aligned}
\dot{H}_\mathrm{b}^{j-1/2} = \quad & \alpha \left(\dot{m}_\mathrm{b}^{j-1/2} \right)^+ c \left(\frac{3}{8} T^j + \frac{6}{8} T^{j-1} - \frac{1}{8} T^{j-2} \right) \\
& + (1-\alpha) \left(\dot{m}_\mathrm{b}^{j-1/2} \right)^+ c \, T^{j-1} \\
& + \alpha \left(\dot{m}_\mathrm{b}^{j-1/2} \right)^- c \left(\frac{3}{8} T^{j-1} + \frac{6}{8} T^j - \frac{1}{8} T^{j+1} \right) \\
& + (1-\alpha) \left(\dot{m}_\mathrm{b}^{j-1/2} \right)^- c \, T^j
\end{aligned}
\tag{2.4}
$$

With $\left(\dot{m}_\mathrm{b}^{j-1/2} \right)^+$ representing the mass flow rate through the upper boundary when it is larger than zero and zero otherwise and $\left(\dot{m}_\mathrm{b}^{j-1/2} \right)^-$ representing the mass flow rate when it is less than zero and zero otherwise. At the upper and lower end of the storage tank, required temperatures with index less than 1 or larger than N are assumed equal to respectively the first and last layer average temperature. The heat losses occurring here will be discussed in section 2.4.3.

2.4.1 Direct inflow charging

When a hot water storage tank is charged with hot water through a direct inflow port, a buoyant jet is formed. Entrainment of water in this jet and the possible collision of the jet with the opposing tank wall result in significant mixing in the entrance region of the storage tank. In a semi-infinite, quiescent, uniform temperature fluid the shape of a buoyant jet is solely dependent on the jet densimetric Froude number with respect to the inflow port diameter ($\mathrm{Fr}_d = v/\sqrt{g\beta\Delta T d_{\mathrm{in}}}$) with v the inflow velocity, β the fluid coefficient of volumetric expansion, ΔT the temperature difference between the inflow and surrounding fluid and d_{in} the diameter of the inflow port.

In the present approach, the energy flow rate caused by natural convection and mixing at the inflow is modeled by distributing a mixing flow across several storage layers (figure 2.7). The final inflow distribution (f_{in}) is composed of two parts: f_{buo} and f_{mix}. The buoyancy distribution (f_{buo}) is based on the difference between the mixing temperature and the average layer temperature and the position of the layer relative to the inflow port, respecting the logical directions of buoyant flows. This distribution can be written as in equation (2.5) with j the layer number, z the height measured from the top of the storage tank and H representing the Heaviside function. In addition, a mixing zone, with half height $\Delta z_{\mathrm{mix,in}}$, is defined around the inflow where fluid is injected with a distribution f_{mix}, related to the distance between the layer and the inflow port to the fourth power (equation (2.6)). This zone is added to take into account the effects of the widening of a horizontal jet and possibly the increased mixing when the jet reaches the far side of the storage tank. The height of the mixing zone will be dependent on several quantities and can vary in time. The final distribution is created by summing f_{buo} and f_{mix}, limiting the result to one and scaling the result with the layer mass m^j (equation (2.7)). The scaling by the layer mass is necessary as the fluid layers at the top and bottom will contain significantly less mass than the layers near the center of the storage tank. Without scaling, these layers would receive an equal amount of energy as the layers with more mass, which leads to a faster temperature change in these layers, not the uniform temperature change as intended by the model. An example of the mass flow distribution and its contributions is shown in figure 2.8.
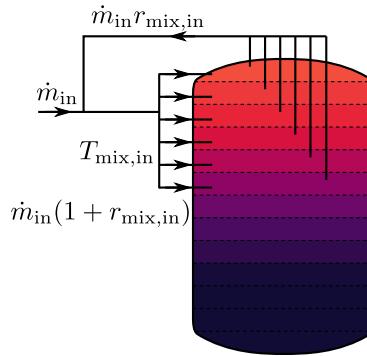
Figure 2.7: Schematic representation of the inflow buoyancy and mixing model.
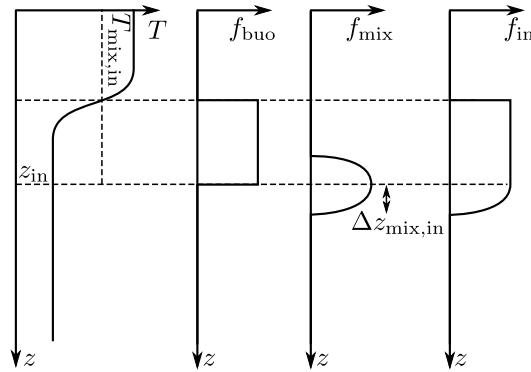
Figure 2.8: Schematic representation of the direct inflow rate distribution for a storage tank charging situation starting from a known storage tank temperature distribution, inflow mixing temperature and inflow height.

$$f_{\text{buo}}^j = \text{H}\left(z^j - z_{\text{in}}\right) \ \text{H}\left(T^j - T_{\text{mix,in}}\right)$$
$$+ \ \text{H}\left(z_{\text{in}} - z^j\right) \ \text{H}\left(T_{\text{mix,in}} - T^j\right) \tag{2.5}$$

$$f_{\text{mix}}^j = \max\left[0, 1 - \left(\frac{z^j - z_{\text{in}}}{\Delta z_{\text{mix,in}}}\right)^4\right] \tag{2.6}$$

$$f_{\text{in}}^j = m^j \ \min\left[1, f_{\text{buo}}^j + f_{\text{mix}}^j\right] \tag{2.7}$$

The net mass flow rate to each layer can be computed as:

$$\dot{m}_{\text{in}}^j = \frac{f_{\text{in}}^j}{\sum_k f_{\text{in}}^k} \dot{m}_{\text{in}} \tag{2.8}$$

To include cross layer mixing phenomena caused by entrainment of fluid in the buoyant jet, the temperature of the mixing flow is determined by extracting fluid from each layer according to the above described distribution and perfectly mixing it with the inflow (figure 2.7). A mixing rate ($r_{\text{mix,in}}$) is defined as the ratio of extraction flow rate to the inflow rate. The inflow mixing temperature ($T_{\text{mix,in}}$) can then be determined from:

$$\dot{m}_{\text{in}} \left(1 + r_{\text{mix,in}}\right) T_{\text{mix,in}} = \dot{m}_{\text{in}} T_{\text{in}} + r_{\text{mix,in}} \dot{m}_{\text{in}} \frac{\sum_k T^k f_{\text{in}}^k}{\sum_k f_{\text{in}}^k} \tag{2.9}$$

The energy flow to layer j, resulting from inflow mixing and buoyancy, can then be computed as:

$$\dot{H}_{\text{in}}^j = \frac{f_{\text{in}}^j}{\sum_k f_{\text{in}}^k} \dot{m}_{\text{in}} c \left[(1 + r_{\text{mix,in}}) T_{\text{mix,in}} - r_{\text{mix,in}} T^j\right] \tag{2.10}$$

At the outflow port, a Gaussian distribution of outflow (f_{out}) is assumed with a standard deviation related to the outflow mixing zone $\Delta z_{\text{mix,out}}$. Cross layer mixing is modeled using the above described approach.

$$f_{\text{out}}^j = m^j \exp \left[-6 \left(\frac{z^j - z_{\text{out}}}{\Delta z_{\text{mix,out}}}\right)^2\right] \tag{2.11}$$

As the exiting mass flow must equal the entering mass flow at all times, mass flow from each layer ($\dot{m}_{\text{out}}^j$) can be computed as:

$$\dot{m}_{\text{out}}^j = \frac{f_{\text{out}}^j}{\sum_k f_{\text{out}}^k} \dot{m}_{\text{in}} \tag{2.12}$$

The outflow temperature (T_{out}) is computed from an energy balance:

$$T_{\text{out}} = \frac{\sum_k T^k f_{\text{out}}^k}{\sum_k f_{\text{out}}^k} \tag{2.13}$$

With $r_{\text{mix,out}}$ the outflow mixing rate, the energy flow resulting from outflow becomes:

$$\dot{H}_{\text{out}}^j = \frac{f_{\text{out}}^j}{\sum_k f_{\text{out}}^k} \dot{m}_{\text{in}} c \left[(1 + r_{\text{mix,out}}) T^j - r_{\text{mix,out}} T_{\text{out}}\right] \tag{2.14}$$

From the presented model we can construct two unknown non-dimensional parameters for both inflow and outflow: $\Delta z_{\mathrm{mix}}/D$ and r_{mix}. It is important to note these parameters will depend on other quantities such as mass flow rates and temperatures and thus can vary in time. A correlation for these parameters will be presented in section 2.5.2.

2.4.2 Immersed heat exchanger charging

When a storage tank is charged through an immersed heat exchanger, heat is transferred from the heat exchanger surface to the storage fluid through natural convection. Heat is transferred to a thin boundary layer surrounding the heat exchanger. Fluid is entrained in this boundary layer which thickens along the height of the heat exchanger. At the top, a buoyant plume is formed which mixes with the surrounding storage fluid. The plume rises until its temperature matches the storage fluid temperature. These phenomena cause a rather uniform storage temperature above the heat exchanger and the formation of a thermocline of approximately the height of the heat exchanger at the location of the heat exchanger.

To model the natural convection heat transfer, a separate mass representing the boundary layer (bdl) is added to each layer. The heat exchanger (hx) is modeled by dividing it into layers corresponding to the storage tank model layers. In doing this, the actual geometry of the heat exchanger is abstracted. Each heat exchanger layer is assigned a mass corresponding to the actual mass of heat exchanger fluid in the heat exchanger between the layer lower and upper boundaries. The total mass in each heat exchanger layer and boundary layer element are subtracted from the corresponding storage tank layer to maintain an equal total amount of mass in the storage tank. Heat is transferred between the heat exchanger layers and the corresponding boundary layer elements. At the locations of the heat exchanger, the boundary layer will grow in thickness, meaning that fluid is entrained in the boundary layer. This is modeled as a mass flow rate entering the boundary layer. Throughout the boundary layer, mixing occurs with the adjacent fluid. This is modeled as mass flowing from a boundary layer element to the adjacent storage layer. The additional heat exchanger and boundary layer elements and the possible mass flows to and from these layers are schematically presented in figure 2.9

The amount of heat transfer between a heat exchanger layer and a boundary layer element is computed based on heat transfer correlations for the internal and external heat transfer. The heat transfer resistance of the heat exchanger wall is neglected as for immersed heat exchangers used in hot water storage
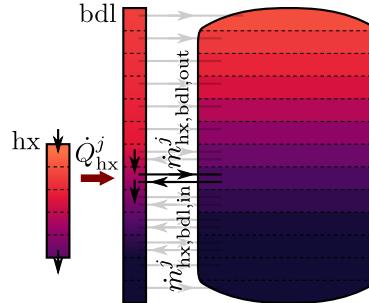
Figure 2.9: Schematic representation of the immersed heat exchanger charging model.

tanks it is typically an order of magnitude smaller than the resistances stemming from the convective heat transfers.

For laminar internal flows in circular pipes, the Nusselt number can be computed to be 3.66 and 4.36 under the assumption of constant wall temperature and constant heat flux respectively [16]. For turbulent flow, the well known Dittus-Boelter correlation [48] can be used. In the current model, the heat transfer is simplified by assuming a Nusselt number for the heat transfer inside the heat exchanger according to Dittus-Boelter with a minimum of 3.66:

$$\mathrm{Nu_{hx,int}} = \max\left(3.66 \ , \ 0.023 \ \mathrm{Re_{hx}^{0.8}} \ \mathrm{Pr_{hx}^{0.3}}\right) \tag{2.15}$$

With $\mathrm{Re_{hx}}$ the Reynolds number with respect to the internal heat exchanger diameter, $d_{\mathrm{hx,int}}$ and $\mathrm{Pr_{hx}}$ the heat exchanger fluid Prandtl number.

The external heat transfer is governed by natural convection and the formation of a boundary layer around the individual coils of the heat exchanger. Kitamura et al. [107] experimentally investigated the natural convection heat transfer from a vertical row of cylinders. They presented a correlation between Nusselt numbers for each cylinder in the row and the Rayleigh number. However, the investigated Rayleigh numbers are significantly lower than the ones expected to occur during immersed coil charging of a hot water storage tank. Therefore, in the current work the external Nusselt number ($\mathrm{Nu_{hx,ext}}$) is assumed constant and is fitted to the measurements. The overall heat transfer from the heat exchanger fluid to the boundary layer fluid is computed as:

$$\dot{Q}_{\mathrm{hx,bdl}}^{j} = A_{\mathrm{hx}}^{j} U_{\mathrm{hx,bdl}}^{j} (T_{\mathrm{hx}}^{j} - T_{\mathrm{bdl}}^{j}) \tag{2.16}$$

With A_{hx}^{j} the area of the heat exchanger within layer j and $U_{\mathrm{hx,bdl}}^{j}$ the overall heat transfer coefficient computed as:

$$U_{\text{hx,bdl}} = \left(\frac{d_{\text{hx,int}}}{\text{Nu}_{\text{hx,int}}\lambda_{\text{hx}}} + \frac{d_{\text{hx,ext}}}{\text{Nu}_{\text{hx,ext}}\lambda} \right)^{-1} \tag{2.17}$$

Here λ_{hx} is the heat exchanger fluid thermal conductivity, λ is the storage fluid thermal conductivity and $d_{\text{hx,ext}}$ the heat exchanger external diameter.

At the height of the heat exchanger, mass is entrained in the boundary layer, causing the boundary layer to grow. The amount of entrainment is difficult to compute due to the complex geometry of the heat exchanger, therefore a correlation is suggested. In the model, the mass flow rate of fluid entering the boundary layer in a certain storage tank layer is computed as if the Reynolds number with respect to the heat exchanger surface area in that layer is proportional to the local Rayleigh number.

$$\text{Re}_{\text{hx,bdl}}^{j} = \mathcal{C}_{\text{hx,bdl,in}}\text{Ra}_{\text{hx,bdl}}^{j} \tag{2.18}$$

The Reynolds and Rayleigh number are evaluated as:

$$\text{Re}_{\text{hx,bdl}}^{j} = \frac{\dot{m}_{\text{hx,bdl,in}}^{j}}{\rho\nu\sqrt{A_{\text{hx}}^{j}}} \tag{2.19}$$

$$\text{Ra}_{\text{hx,bdl}}^{j} = \frac{g\rho c\beta|T_{\text{hx}}^{j} - T^{j}|d_{\text{hx,ext}}^{3}}{\nu\lambda} \tag{2.20}$$

Here, $\dot{m}_{\text{hx,bdl,in}}^{j}$ represents the mass flow into the boundary layer at a given storage layer j, A_{hx}^{j} represents the area of the heat exchanger in that layer, $d_{\text{hx,ext}}$ the external diameter of the heat exchanger and T_{hx}^{j} the temperature of the heat exchanger fluid in element j. The mass flow rate to the boundary layer can then be expressed as:

$$\dot{m}_{\text{hx,bdl,in}}^{j} = \mathcal{C}_{\text{hx,bdl,in}}\sqrt{A_{\text{hx}}^{j}}\frac{g\rho^{2}c\beta|T_{\text{hx}}^{j} - T^{j}|d_{\text{hx,ext}}^{3}}{\lambda} \tag{2.21}$$

The value of the coefficient $\mathcal{C}_{\text{hx,bdl,in}}$ can be determined through experiments. As the coefficient will be geometry dependent, this exercise must be done for every heat exchanger of interest. During all parameter estimations and simulations, fluid properties at standard conditions are used in the presented correlations except for the thermal expansion coefficient β, for which a quadratic fit is used to relate the coefficient to the mean storage tank temperature around the heat exchanger. In the range of temperatures seen in the experiments, the thermal expansion coefficient of water shows substantial variation (20°C: $\beta = 0.207 \times 10^{-3}$ 1/K, 60°C: $\beta = 0.523 \times 10^{-3}$ 1/K). This variation has a

significant effect on the Rayleigh number and thus on the mass flow entering the boundary layer.

At the top of the heat exchanger, a buoyant plume is formed. As the plume rises, it is mixed with the surrounding fluid. This phenomenon is very similar to the buoyant jet formation at a direct inflow port. The approach used to model it is also similar. An exit mass flow rate distribution is computed based in the average outflow temperature ($T_{\mathrm{bdl,out}}$), the position ($z_{\mathrm{hx,cen}}$) and height (Δz_{hx}) of the heat exchanger and the storage tank temperature according to:

$$f_{\mathrm{hx,bdl}}^{j} = m^{j} \, \tilde{\mathrm{H}}_{\frac{\Delta z_{\mathrm{hx}}}{2}}(z^{j} - z_{\mathrm{hx,cen}}) \, \tilde{\mathrm{H}}_{\Delta \mathrm{T}_0}(T^{j} - T_{\mathrm{hx,bdl,out}}) \tag{2.22}$$

$$+ \, m^{j} \, \tilde{\mathrm{H}}_{\frac{\Delta z_{\mathrm{hx}}}{2}}(z_{\mathrm{hx,cen}} - z^{j}) \, \tilde{\mathrm{H}}_{\Delta \mathrm{T}_0}(T_{\mathrm{hx,bdl,out}} - T^{j})$$

Here, $\tilde{\mathrm{H}}_{\Delta x}(x)$ represents a smooth Heaviside function which varies gradually from 0 if $x \leq -\Delta x$ to 1 if $x \geq \Delta x$. ΔT_0 is a parameter determining how much an already present thermocline is affected by the buoyant plume. It is taken 1 K throughout this work as this corresponded well with the zone of thermocline widening seen in experiment hex_10 (see section 2.5.3). The distribution is multiplied with the layer mass m^{j} to ensure layers containing less fluid receive less energy. If this is omitted, unrealistic temperature fluctuations are seen in the top and bottom nodes. The average boundary layer outflow temperature is computed from an energy balance as:

$$\sum_{j} \dot{m}_{\mathrm{hx,bdl,out}}^{j} T_{\mathrm{hx,bdl,out}} = \sum_{j} \dot{m}_{\mathrm{hx,bdl,out}}^{j} T_{\mathrm{hx,bdl}}^{j} \tag{2.23}$$

An example of the mass flow distribution is shown in figure 2.10. From this distribution and the total mass flow rate entering the boundary layer, the exiting mass flow from each boundary layer element is computed:

$$\dot{m}_{\mathrm{hx,bdl,out}}^{j} = \frac{f_{\mathrm{hx,bdl}}^{j}}{\sum_{k} f_{\mathrm{hx,bdl}}^{k}} \sum_{k} \dot{m}_{\mathrm{hx,bdl,in}}^{k} \tag{2.24}$$

From the boundary layer in- and outflow rate, a mass balance can be set up for each boundary layer element to compute the mass flow rate to the neighboring elements. The positive direction of mass flows between layers in the heat exchanger and boundary layer is chosen from top to bottom, consistent with figure 2.6. At the 1st and last boundary layer element, the top and bottom mass flow rate are set to zero respectively.

$$\dot{m}_{\mathrm{hx,bdl,b}}^{j-1/2} + \dot{m}_{\mathrm{hx,bdl,in}}^{j} = \dot{m}_{\mathrm{hx,bdl,b}}^{j+1/2} + \dot{m}_{\mathrm{hx,bdl,out}}^{j} \tag{2.25}$$
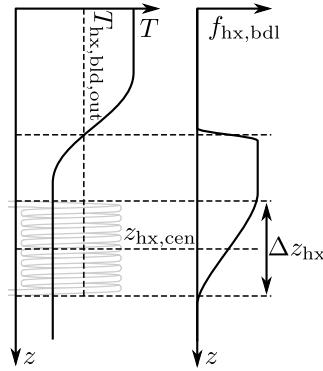
Figure 2.10: Schematic representation of the flow rate distribution exiting the boundary layer around an immersed heat exchanger

The energy balance for a boundary layer element is written as:

$$m_{\text{hx,bdl}}^{j} c \frac{\mathrm{d}T_{\text{hx,bdl}}^{j}}{\mathrm{d}t} = \dot{H}_{\text{hx,bdl,b}}^{j-1/2} - \dot{H}_{\text{hx,bdl,b}}^{j+1/2} + \dot{H}_{\text{hx,bdl,in}}^{j} - \dot{H}_{\text{hx,bdl,out}}^{j} \qquad (2.26)$$

$$+ \dot{Q}_{\text{hx,bdl}}^{j}$$

To model the convective energy transfer between layers in the boundary layer and heat exchanger, a 1st order upwind discretization is used. This results in an enthalpy flow across a boundary and in and out of a boundary layer element:

$$\dot{H}_{\text{hx,bdl,b}}^{j-1/2} = \left(\dot{m}_{\text{hx,bdl,b}}^{j-1/2} \right)^{+} c \, T_{\text{hx,bdl}}^{j-1} + \left(\dot{m}_{\text{hx,bdl,b}}^{j-1/2} \right)^{-} c \, T_{\text{hx,bdl}}^{j} \qquad (2.27)$$

$$\dot{H}_{\text{hx,bdl,in}}^{j} = \dot{m}_{\text{hx,bdl,in}}^{j} c \, T^{j} \qquad (2.28)$$

$$\dot{H}_{\text{hx,bdl,out}}^{j} = \dot{m}_{\text{hx,bdl,out}}^{j} c \, T_{\text{hx,bdl}}^{j} \qquad (2.29)$$

The boundary layer mass $m_{\text{hx,bdl}}^{j}$ is assumed equal for all boundary layer elements. In reality the boundary layer will grow in thickness along the height of the heat exchanger. Taking this into account will however introduce a lot of computational complexity as the starting point of the boundary layer is variable and the direction of boundary layer growth changes when the heat exchanger is used for heating or cooling the storage tank. The total boundary layer mass is estimated from the thickness of a turbulent boundary layer along a

flat plate. For heat exchanger dimensions which are common in large residential hot water storage tanks this results in an average boundary layer thickness $t_{\mathrm{hx,bdl}} = 0.005$ m, which was computed in accordance with [175]. The heat exchanger boundary layer mass contained in layer j with height Δz^j is then computed as:

$$m^j_{\mathrm{hx,bdl}} = \rho \frac{A_{\mathrm{hx}}}{\Delta z_{\mathrm{hx}}} \Delta z^j t_{\mathrm{hx,bdl}} \tag{2.30}$$

The in- and outflow to the boundary layer elements cause a recirculation flow in the storage tank. The mass flow rates across each layer boundary ($\dot{m}_{\mathrm{hx,rec,b}}$) can be computed from another set of mass balances in the form of:

$$\dot{m}^{j+1/2}_{\mathrm{hx,rec,b}} + \dot{m}^j_{\mathrm{hx,bdl,out}} = \dot{m}^{j-1/2}_{\mathrm{hx,rec,b}} + \dot{m}^j_{\mathrm{hx,bdl,in}} \tag{2.31}$$

To compute the accompanying enthalpy flow across a layer boundary, an estimate of the temperature at the layer boundary is required. An upwind convection discretization is used, leading to

$$\dot{H}^{j-1/2}_{\mathrm{hx,rec,b}} = \left(\dot{m}^{j-1/2}_{\mathrm{hx,rec}}\right)^+ c\, T^{j-1} + \left(\dot{m}^{j-1/2}_{\mathrm{hx,rec}}\right)^- c\, T^j \tag{2.32}$$

The actual energy transfer to each storage tank layer is then written as:

$$\dot{Q}^j_{\mathrm{hx}} = \dot{H}^{j-1/2}_{\mathrm{hx,rec,b}} - \dot{H}^{j+1/2}_{\mathrm{hx,rec,b}} + \dot{H}^j_{\mathrm{hx,bdl,out}} - \dot{H}^j_{\mathrm{hx,bdl,in}}$$

In this work, the heat exchanger fluid is also considered incompressible with constant specific heat c_{hx}. As the mass flow rate across the boundary of each heat exchanger element is equal, the enthalpy flow rate across a heat exchanger element boundary is:

$$\dot{H}^{j-1/2}_{\mathrm{hx,b}} = (\dot{m}_{\mathrm{hx}})^+ c_{\mathrm{hx}} T^{j-1}_{\mathrm{hx}} + (\dot{m}_{\mathrm{hx}})^- c_{\mathrm{hx}} T^j_{\mathrm{hx}} \tag{2.33}$$

Where at the 1$^{\mathrm{st}}$ heat exchanger node, the temperature T^{j-1}_{hx} must be replaced with the heat exchanger inflow temperature ($T_{\mathrm{hx,in}}$). The energy balance becomes:

$$m^j_{\mathrm{hx}} c_{\mathrm{hx}} \frac{\mathrm{d}T^j_{\mathrm{hx}}}{\mathrm{d}t} = \dot{H}^{j-1/2}_{\mathrm{hx,b}} - \dot{H}^{j+1/2}_{\mathrm{hx,b}} - \dot{Q}^j_{\mathrm{hx,bdl}} \tag{2.34}$$

The heat exchanger outflow temperature ($T_{\mathrm{hx,out}}$) is assumed equal to the last heat exchanger layer temperature, consistent with the upwind discretization.

The presented model requires the estimation of 2 heat exchanger dependent parameters: $\mathrm{Nu}_{\mathrm{hx,ext}}$, determining the heat transfer from the heat exchanger

to the boundary layer elements and $\mathcal{C}_{\mathrm{hx,bdl,in}}$, determining the inflow into the boundary layer elements. These parameters are determined from a limited set of experiments in section 2.5.3.

2.4.3 Heat loss

During all phases of the storage cycle, energy transfers can occur between a hot water storage tank and its surroundings. As during operation, the surroundings are usually at a temperature lower than the storage temperature, this energy transfer is termed a heat loss. The heat loss model is presented under the above assumption that the surroundings are at a lower temperature. The model is however also applicable when the surroundings are at a higher temperature than the storage tank.

The process of transferring energy from a hot water storage tank to its surroundings is composed of several sub-processes. On the outside interface between the surrounding air and the storage tank covering material, natural convection and radiation heat transfer occur. In the insulation layer, heat conduction takes place. Fittings for inflow ports, heat exchangers or instrumentation penetrating the insulation mantle, increase the rate of conduction locally. Finally, on the interface between the storage tank wall and the storage fluid, heat is transferred by natural convection. Furthermore, the natural convection loops in the storage fluid cause a redistribution of energy inside the storage tank. Diffusion of the temperature profile as a result of axial conduction in the storage tank wall will be taken into account by introducing an additional thermal conductivity in the storage fluid in accordance with Klein et al. [108]. The heat loss and redistribution of energy can be modeled as flows exiting a layer, cooling down and re-entering in the layer of matching average temperature. This is schematically represented in figure 2.11.

The re-injected fluid is cooled down to a certain boundary layer temperature $T_{\mathrm{hl,bdl}}^{j}$ larger than the temperature of the storage tank surroundings T_{hl} and less than the layer mean temperature T^{j}. The value is determined using a boundary layer parameter $\mathcal{C}_{\mathrm{hl,bdl}}$ according to:

$$\frac{T^{j} - T_{\mathrm{hl}}}{T^{j} - T_{\mathrm{hl,bdl}}^{j}} = \mathcal{C}_{\mathrm{hl,bdl}} \tag{2.35}$$

The heat flow rate from a given layer is computed using an overall heat transfer coefficient U and area A_{hl}^{j} which can be augmented with a heat loss caused by fittings penetrating the insulation mantle, accounted for as a thermal conductance $UA_{\mathrm{fittings}}^{j}$. As this heat flow rate is modeled as a mass flow from a
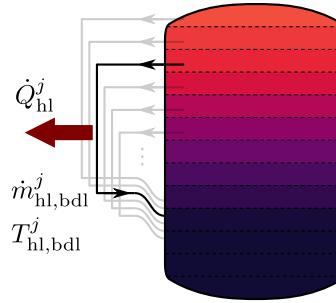
Figure 2.11: Schematic representation of the heat loss model which transfers energy to the surroundings and redistribute the energy inside the storage tank.

layer at the average layer temperature to the boundary layer temperature, the mass flow rate must be computed to match the heat loss:

$$\dot{m}_{\text{hl,bdl,in}}^j c(T^j - T_{\text{hl,bdl}}^j) = (UA_{\text{hl}}^j + UA_{\text{fittings}}^j)(T^j - T_{\text{hl}}) \tag{2.36}$$

or:

$$\dot{m}_{\text{hl,bdl,in}}^j c = (UA_{\text{hl}}^j + UA_{\text{fittings}}^j)\mathcal{C}_{\text{hl,bdl}} \tag{2.37}$$

The boundary layer flow from each layer is injected in the layer with matching average temperature. This causes a recirculation flow to the upper layers. The recirculation mass flow rate at each layer interface ($\dot{m}_{\text{hl,rec}}$) can be computed from a set of mass balances:

$$\dot{m}_{\text{hl,rec}}^{j-1/2} + \dot{m}_{\text{hl,bdl,in}}^j = \dot{m}_{\text{hl,rec}}^{j+1/2} + \sum_k \frac{f_{\text{hl}}^{k,j}}{\sum_i f_{\text{hl}}^{k,i}} \dot{m}_{\text{hl,bdl,in}}^k \tag{2.38}$$

The sign conventions for the mass flow rate across a boundary is chosen consistent with the convention used for convective energy transfer depicted in figure 2.6. A heat loss distribution function f_{hl} was used in the previous expression to determine the layer in which the boundary layer flow is re-injected. The value $f_{\text{hl}}^{k,j}$ is proportional to the modeled heat loss mass flow from layer k to layer j. As the boundary layer temperature should match the average layer temperature, this function can be expressed as:

$$f_{\text{hl}}^{k,j} = m^j \text{H}\left(z^j - z^k\right) \text{ H}\left(T^j - T_{\text{hl,bdl}}^k\right) \text{ H}\left(T_{\text{hl,bdl}}^k - T^{j+1}\right) \tag{2.39}$$

$$+ m^j \text{H}\left(z^k - z^j\right) \text{ H}\left(T_{\text{hl,bdl}}^k - T^j\right) \text{ H}\left(T^{j-1} - T_{\text{hl,bdl}}^k\right)$$

With H the Heaviside function. The distribution is scaled with the layer mass m^j to ensure layers containing less fluid receive less energy.

The enthalpy transfer across a layer boundary resulting from the recirculation flow and enthalpy transfers into and out of the boundary layer are calculated using an upwind convection discretization:

$$\dot{H}_{\text{hl,rec,b}}^{j-1/2} = \left(\dot{m}_{\text{hl,rec}}^{j-1/2}\right)^{+} c \, T^{j-1} + \left(\dot{m}_{\text{hl,rec}}^{j-1/2}\right)^{-} c \, T^{j} \tag{2.40}$$

$$\dot{H}_{\text{hl,bdl,in}}^{j} = \dot{m}_{\text{hl,bdl,in}}^{j} c \, T^{j} \tag{2.41}$$

$$\dot{H}_{\text{hl,bdl,out}}^{j} = \sum_{k} \dot{m}_{\text{hl,bdl,in}}^{k} f_{\text{hl}}^{k,j} c \, T_{\text{hl,bdl}}^{k} \tag{2.42}$$

The actual energy transfer from each layer is then computed as follows:

$$\dot{Q}_{\text{hl}}^{j} = \dot{H}_{\text{hl,rec,b}}^{j+1/2} - \dot{H}_{\text{hl,rec,b}}^{j-1/2} + \dot{H}_{\text{hl,bdl,out}}^{j} - \dot{H}_{\text{hl,bdl,in}}^{j} \tag{2.43}$$

The resulting heat loss model contains three unknown parameters: U, the overall heat transfer coefficient from the storage tank to the surroundings, UA_{fittings}, the thermal conductance of fittings which can be distributed accross several layers, and the boundary layer parameter $\mathcal{C}_{\text{hl,bdl}}$ which determines the boundary layer temperature and the resulting energy redistribution. To determine U and UA_{fittings}, correlations describing the heat transfer at the different interfaces can be used. To determine the boundary layer temperature, an electric analog of the heat transfer could be used to estimate the boundary layer temperature. However, in this work the heat loss boundary layer parameter ($\mathcal{C}_{\text{hl,bdl}}$) will be determined from experiments as described in section 2.5.4.

When the heat loss boundary layer parameter is at its minimum value 1, the boundary layer temperature is equal to the surrounding temperature. This will result in minimum boundary layer mass flow rates and maximum heat loss stratification. When an initially mixed storage tank cools down, the heat loss will be concentrated in the bottom of the tank. The upper layers will remain at the initial temperature leading to stratification. Increasing the heat loss boundary layer parameter will cause an increase in boundary layer temperature and thus an increase in boundary layer mass flow rate. These larger mass flow rates lead to more mixing in the storage tank caused by the heat loss. In the limit, when the boundary layer parameter goes to infinity, the storage tank will cool down completely mixed.

In the above described model the layer where the boundary layer flow is re-injected must be computed for all nodes and is dependent on the current state

of the storage tank. This makes the model rather computationally intensive. Therefore, a more simplified model is presented below.

When the heat loss from each layer is calculated with the local layer surface area and the local coefficients of heat transfer, unrealistic temperature distributions arise. As the top layer has a surface area which is much larger than the layer just below, the rate of heat transfer from this layer will be substantially larger. Thus, the upper layer will cool down faster than the layers just below which leads to a temperature inversion which is not observed during experiments. A pragmatic solution to avoid this temperature inversion is to compute the total overall heat transfer coefficient from all layers of the storage tank and redistribute this total overall heat transfer coefficient across all layers based on the layer mass (m^j). This results in an expression for the heat transfer from layer j:

$$\dot{Q}_{\mathrm{hl}}^j = \frac{m^j}{\sum_k m^k} \left(\sum_k UA_{\mathrm{hl}}^k + \sum_k UA_{\mathrm{fittings}}^k \right) (T^j - T_{\mathrm{hl}}) \qquad (2.44)$$

In section section 2.5.4 both models are compared with experiments.

2.4.4   Implementation

The above described general hot water storage tank model combined with the formulations for energy transfers through direct charging, heat exchanger charging and heat loss are implemented in the Modelica physical modeling language [123]. In all subsequent results, the presented equations are solved numerically using a variable time step differential-algebraic equation solver implemented in Dymola 2016.

2.5   Parameter estimation and validation of the presented models

The above presented models for direct storage charging, immersed heat exchanger charging and heat losses all require some parameters to be determined from experimental data or higher order models. To obtain estimates for these parameters an experimental measurement campaign and a numerical simulation campaign were set up. As direct charging of a storage tank has benefits toward stratification relative to immersed heat exchanger charging, the former was investigated most thoroughly.

(a) Storage tank dimensions
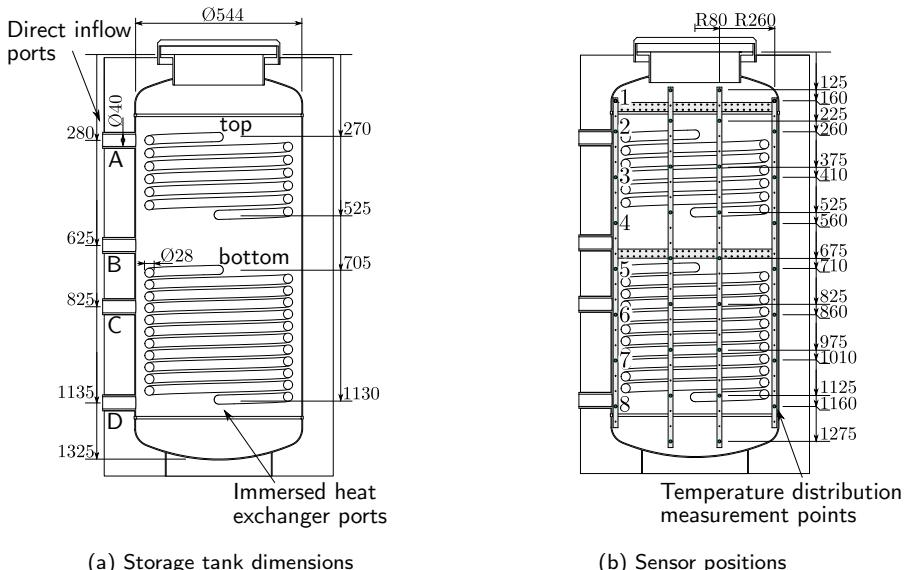
(b) Sensor positions

Figure 2.12: Hot water storage tank used in the experiments with dimensions, port labels and heat exchanger labels (left) and temperature distribution sensor positions (right). Sensors used during the CFD model validation are numbered 1 to 8. All dimensions are in mm.

For the direct inflow charging model, correlations for the model parameters with respect to the storage tank geometry and inflow properties were obtained based on a parametric CFD study. The correlations were then validated using independent experimental data. For the heat exchanger charging and heat loss model, parameters were estimated based on experimental data but not independently validated.

2.5.1 Experimental set-up

An experimental setup was designed to measure the temperature distributions inside a hot water storage tank and to investigate the effects on the temperature distribution of different storage tank charging and discharging methods. A series of charging, discharging and standby experiments was performed on a commercial 0.300 m^3 storage tank (Fiorinni Combi CMC300). The dimensions of the storage tank are given in table 2.1 and figure 2.12a. Direct charging of the storage tank can be done through 4 direct inflow ports labeled A to D. The storage tank includes two immersed coil heat exchangers which are designated top and bottom, as shown in figure 2.12a.

Storage tank data	
Inner diameter (m)	0.544
Height (m)	1.325
Tank volume (m^3)	0.300
Insulation thickness (m)	0.070
Insulation material	flexible polyurethane
inflow port inner diameter (m)	0.040
heat exchanger tube outer diameter (m)	0.028
heat exchanger tube wall thickness (m)	0.003
heat exchanger pitch diameter (m)	0.454
top heat exchanger outer surface area (m^2)	0.75
top heat exchanger height (m)	0.225
top heat exchanger revolutions (-)	6
bottom heat exchanger outer surface area (m^2)	1.40
bottom heat exchanger height (m)	0.425
bottom heat exchanger revolutions (-)	11

Table 2.1: Storage tank parameters.

To measure the spatial temperature distribution inside the storage tank, 34 T-type thermocouples were inserted through the open top of the storage tank, divided into 4 vertical arrays. Two central sensor arrays each contain 9 thermocouples, two arrays near the side each contain 8 thermocouples. The sensor arrays are placed in a vertical plane positioned in line with the direct inflow ports. All thermocouples are positioned with an accuracy of ± 10 mm in all directions. A drawing of the sensor placement is presented in figure 2.12b. The thermocouples were calibrated and have an accuracy of $\pm\ 0.2°$C. As the thermocouples are inserted in the tank through the open top, the tank is not pressurized and not completely full. The water level is always 100 mm below the top of the tank. The primary storage tank always contains 0.267 m^3 water.

A second hot water storage tank with a volume of 0.300 m^3 is used to supply a nearly constant temperature flow of water to the instrumented storage tank (figure 2.13). The volumetric flow rate is measured using an ultrasonic flow rate sensor and converted to a mass flow rate using the density of water at the measured temperature. This results in a mass flow rate measurement with an accuracy of $\pm\ 0.003$ kg/s.

Figure 2.13: Experimental set up.

2.5.2 Direct inflow charging

An experimental and computational measurement campaign were set up to validate the low-order direct inflow charging model. The methodology is schematically depicted in figure 2.14. Transient CFD simulations were carried out to analyze the evolution of the temperature stratification within the tank. The turbulence and buoyancy models in the CFD simulations were validated using a limited set of experiments. A series of 8 CFD storage charging simulations for different tank geometries was used to obtain correlations for the in- and outflow mixing zone and mixing rate. The low-order model including correlations was validated with an independent cross-validation set of charging and discharging experiments.

CFD validation

Before a parametric analysis was executed, the CFD model was assessed against experimental results in order to determine the best numerical parameters, giving an accurate solution within an acceptable time. The used CFD software was ANSYS Fluent v14.0.

A CAD model of the experimental geometry presented in section 2.5.1 was built, including the coil heat-exchangers (physically present, even if not used in the experiments and simulations). The water level was set constant. The geometry
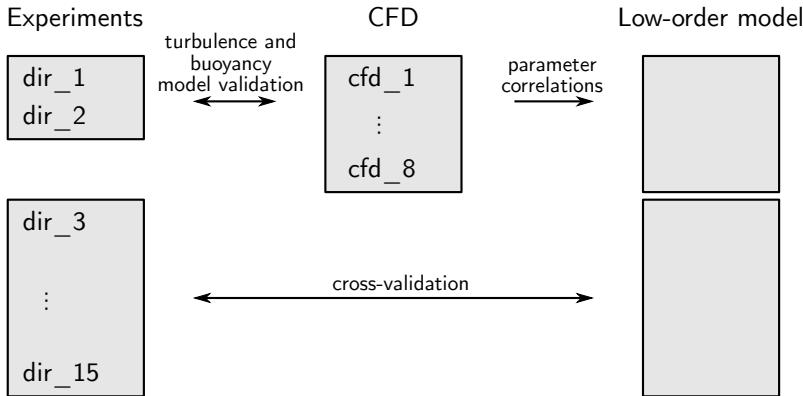
Figure 2.14: Schematic representation of the different steps undertaken to calibrate and validate the low-order direct inflow charging model.

was meshed with the CutCell algorithm in ANSYS Meshing which is an octree method, leading to fast mesh generation, creating a mesh with mainly high quality hexahedral elements. A grid refinement analysis was performed. The final mesh retained for the CFD validation experiments had about 1×10^6 cells.

Turbulence was modeled using a RANS approach. Both standard k-ε and k-ω-SST models were considered. It appeared that k-ε gives the best correspondence to local temperature measurements in the validation experiments and this approach was retained for the parametric analysis. The near-wall region is modeled using the standard wall functions implemented in ANSYS Fluent. The use of the k-ε turbulence model is in accordance with several studies found in the literature [6, 76, 160]. Buoyancy is modeled using the Boussinesq approximation in accordance with [6]. Physical properties of water (density, viscosity) were defined as polynomial functions of the temperature. Coefficients were fitted to match tabulated values between 20°C and 70°C:

$$\rho = -3.784 \times 10^{-3} \ T^2 + 2.010 \ T + 733.5 \qquad (2.45)$$

$$\mu = 0.2271 \times 10^{-6} \ T^2 - 0.1567 \times 10^{-3} \ T + 0.02743 \qquad (2.46)$$

With ρ the fluid density in kg/m^3, μ the dynamic viscosity in Pa s and T the temperature in K.

Turbulence variables were set to values representative of a fully developed flow in a circular pipe of the same diameter as the inflow port. Numerical schemes

run	inflow port	outflow port	$\dot{m}_{\text{in,avg}}$ (kg/s)	$T_{\text{in,avg}}$ (°C)
dir_1	A	D	0.085	57.0
dir_2	B	D	0.034	36.0

Table 2.2: Inflow conditions used for the validation of the CFD turbulence and buoyancy model. Port locations are shown in figure 2.12a.

were all second order in space. The time discretization was first-order implicit, with a time-step of 0.2 s.

Two charging experiments (dir_1 and dir_2) were performed to validate the CFD approach. Experiment details are presented in table 2.2.

As the inflow flow rate and temperature were nearly constant during the experiments, they were considered constant in the simulations. Moreover, in the simulations, the initial storage tank temperature was assumed constant throughout the storage tank, although there was a temperature difference of up to 2.5 K in dir_1 and 1.2 K in dir_2. For dir_1 the simulation was stopped when the experimental inflow temperature started decreasing as this was not included in the CFD model. For dir_2 the simulation was stopped when the experiment mass flow rate dropped.

The compared results are local measurements on a vertical line at R=260 mm from the centerline of the tank, just in front of the in- and outflows. Measurement points are numbered 1 to 8 from top to bottom (figure 2.12b). Comparison of the CFD and experimental data is illustrated in figure 2.15. The agreement is qualitatively good and relative root mean squared errors of simulated values are always below 8%, except at the measurement points close to the inflow port. The most significant out-lier is sensor 2 in dir_1. This sensor was very close to the inflow, and a small difference in the flow pattern or in the sensor position, or even numerical diffusion could result in a significant difference in the temperature that is seen by this sensor. For all other sensors, one sometimes observes a small shift in time. This shift could be caused by a difference in actual and simulated flow rate within the uncertainty of the flow measurement. In all measurement points it is seen that the simulated change in slope is more smooth than the experimentally observed change. This could mean that the used numerical scheme or turbulence model are slightly over-diffusive. The initial spike in simulated temperature for points above the inlet in dir_2 does not occur in the measurements as during the initial stage of the experiment there is a smooth increase in inflow temperature during the first 45 s of the experiment. In the simulations however the inflow temperature is constant causing warm fluid to pass the sensors during the jet

(a) dir_1

(b) dir_2
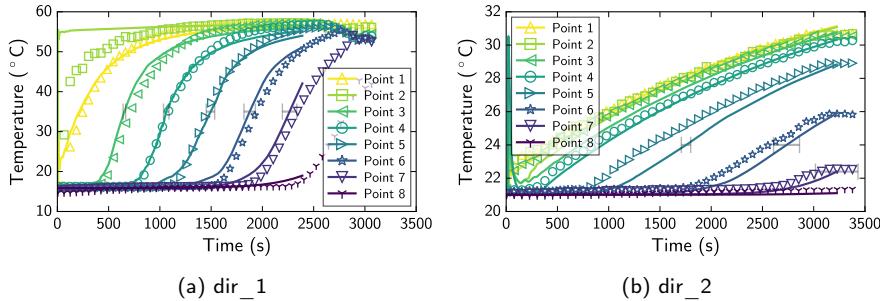
Figure 2.15: Validation of the CFD model. Experimental measurements are represented by markers while the CFD results are represented by solid lines. The horizontal error bars represent an estimate of the uncertainty in the simulated thermocline passage time caused by the flow rate measurement uncertainty. As these error bars assume plug flow in the storage tank section between the in- an outflow port, they are proportional to the distance between inflow port and the measurement point. The uncertainty of the temperature measurements is $\pm 0.2°$C.

formation phase. The differences in temperature immediately after this initial phase are caused by the assumption of uniform initial conditions as opposed to the small initial temperature gradient present in the experiments. Other differences between measured and simulated temperatures could be attributed to an imperfect geometric modeling, for instance, welds and heat exchanger supports were present in the experimental storage tank but omitted in the simulation model due to their complexity. These details could however have an effect on temperatures at points near these structures such as point 3 and 5. Considering this good agreement in local variables, one can expect an excellent agreement in integral variables (like layer averaged temperatures).

The simulation time was about 2000 cpu h for each case (respectively 16h and 18h on 128 processors).

Parameter estimation and correlation

To develop the correlation of the mixing parameters a series of 8 CFD storage charging simulations with different tank geometries was performed. In all simulations the storage height was equal to 1.25 m, the storage inflow and outflow port diameter was 0.025 m and the outflow port was positioned at 1.125 m from the top of the storage tank. The storage tank diameter (D), inflow height (z_{in}), mass flow rate ($\dot{m}_{in}$) and inflow temperature (T_{in}) were varied. Details are presented in table 2.3. The simulations were performed using the same methodology as for the CFD model validation. Note that, contrary to the CFD validation model, the CFD model used to develop mixing correlations did

run	D	z_{in}	$\dot{m}_{in}$	T_{in}
	(m)	(m)	(kg/s)	(°C)
cfd_1	0.294	0.050	0.149	32.3
cfd_2	1.333	0.050	0.222	32.3
cfd_3	0.793	0.050	0.089	32.3
cfd_4	0.381	0.150	0.208	69.2
cfd_5	1.123	0.150	0.301	69.2
cfd_6	0.587	0.050	0.182	52.8
cfd_7	0.830	0.050	0.269	32.3
cfd_8	0.500	0.150	0.062	69.2

Table 2.3: Geometry and inflow condition details used in the CFD charging simulations.

not include coil heat exchangers. The simulations were run until the difference between the outflow temperature and the average initial temperature reached 90% of the difference between the inflow temperature and the initial average temperature.

The CFD simulations used for the mixing parameter correlations were chosen to contain cases with strong jet flow, reaching the opposite side of the storage tank, and with a more plume like inflow behavior, which both can occur in storage operation (figure 2.16).

To estimate the in- and outflow mixing parameters, CFD simulated average temperature distributions inside the storage tank are compared with the temperature distribution obtained with the presented low order model (section 2.4.1). The comparison is made with a time step of 30 s to 120 s and averaged over all times. This results in a single temperature distribution root mean squared error (RMSE) value for every run. It is primordial to compare temperature distributions during charging experiments as comparing outflow temperatures only ensures an overall energy balance and obscures the distribution of energy inside the storage tank. Information about this temperature distribution is required to asses the discharge phase which follows the charging phase.

As the formation of the buoyant jet is dependent on the storage temperature distribution, each CFD simulation was split up in 5 parts over time (a - e). A minimization of temperature distribution RMSE for each 5 parts of the 8 CFD simulations with all mixing parameters free to vary first led to the observation of nearly linear dependence of the mixing rates to the inflow or outflow Reynolds number:

(a) cfd_1 velocity magnitude ($t = 180$ s)

(b) cfd_1 temperature ($t = 180$ s)

(c) cfd_8 velocity magnitude ($t = 120$ s)

(d) cfd_8 temperature ($t = 120$ s)
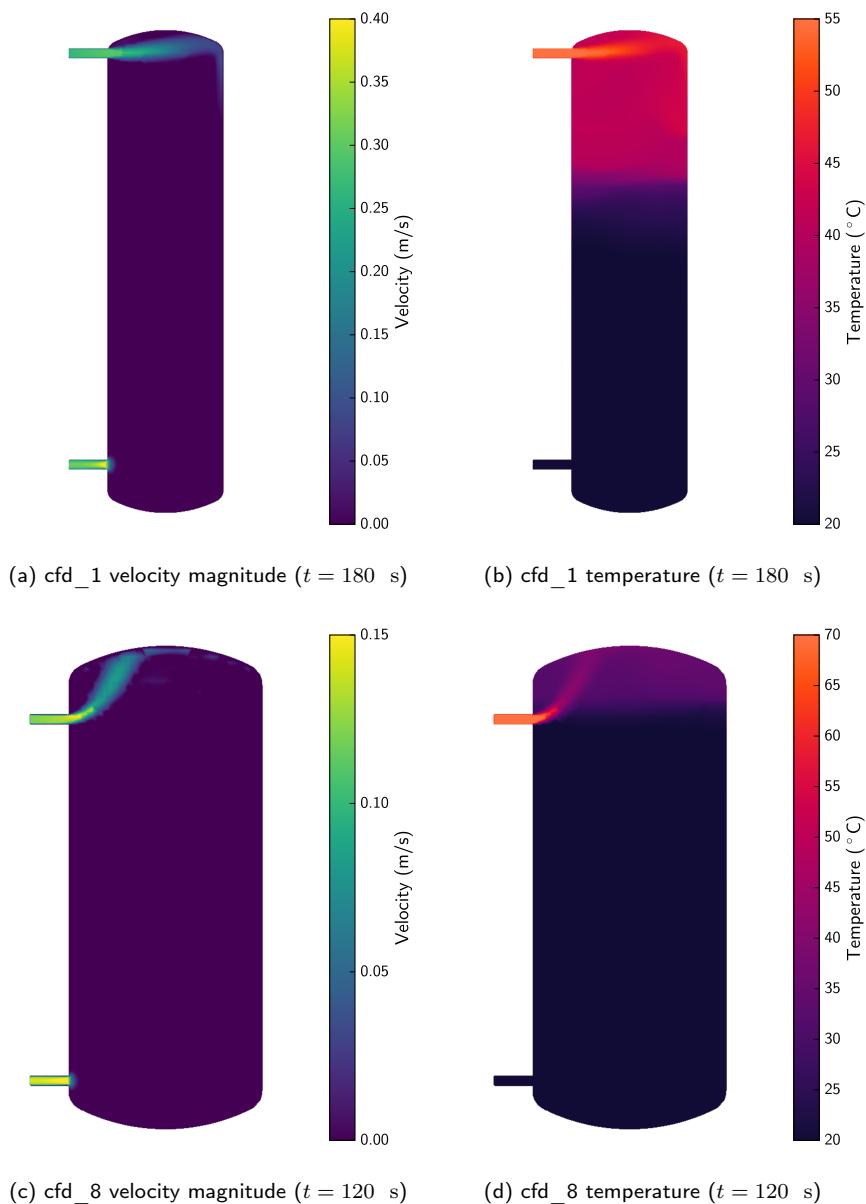
Figure 2.16: Examples of resulting CFD velocity and temperature distribution for a strong jet case cfd_1 (top), and a plume case cfd_8 (bottom).
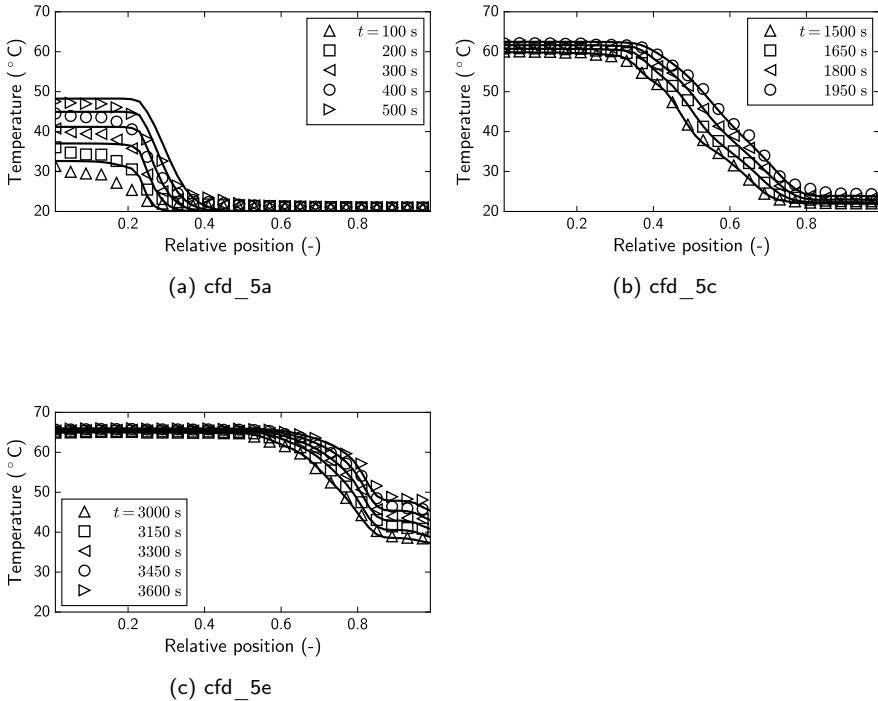
Figure 2.17: Accordance of CFD (markers) and the direct inflow charging model (lines) temperature distribution examples for run cfd_5a, cfd_5c and cfd_5e.

$$r_{\mathrm{mix,in}} = 0.0007 \ \mathrm{Re_{in}} \tag{2.47}$$

$$r_{\mathrm{mix,out}} = 0.0004 \ \mathrm{Re_{out}} \tag{2.48}$$

In a subsequent minimization the in- and outflow mixing rates were determined by this linear dependence and only the mixing zones were free to vary. Resulting temperature profiles showed good accordance with CFD simulations, examples for run cfd_5a, cfd_5c and cfd_5e are shown in figure 2.17. In the initial phase of the simulation, the low order model sometimes shows a too flat temperature profile above the inflow port (figure 2.17a). This is caused by the assumed inflow distribution, which is constant above the inflow port.

A dimensional analysis was conducted and revealed the following non-dimensional parameters to which the mixing parameters are correlated: the densimetric Froude number with respect to the storage tank diameter ($\mathrm{Fr} =$

$v/\sqrt{g\beta\Delta TD}$), the inflow Reynolds number ($\mathrm{Re_{in}} = vd_{in}/\nu$) with ν the fluid kinematic viscosity and the ratio of inflow port diameter over storage tank diameter, d_{in}/D. The storage tank diameter was chosen over the inflow port diameter for the length scale in the Froude number as this is more relevant for a buoyant jet in a confined space.

Weights were assigned to the different minimization runs based on the mixing parameter confidence intervals. A correlation for the inflow mixing zone was obtained which relates the relative mixing zone to the inflow densimetric Froude number, the inflow Reynolds number and the ratio of storage tank diameter to inflow port diameter (equation (2.49)). No significant correlation to the ratio of inflow port height to storage tank diameter could be determined. As the inflow distribution used in the model depends on this parameter, the effects of inflow port position are already included here. The values obtained through the CFD parameter estimation together with the confidence intervals and the correlation are shown in figure 2.18.

$$\frac{\Delta z_{\mathrm{mix,in}}}{D} = A\ \mathrm{Re_{in}}\ (D/d_{in})^{0.5}\ \mathrm{Fr}^{n}\ \exp\left[-B\ \mathrm{Re_{in}}\ (D/d_{in})^{0.5}\right] \qquad (2.49)$$

$$A = 7.090 \times 10^{-6}$$

$$B = 2.026 \times 10^{-5}$$

$$n = 1.343$$

The outflow mixing zone had considerably larger confidence intervals and no clear correlation was visible. Thus a constant ratio of outflow mixing zone to storage tank diameter was chosen as presented in equation (2.50) and figure 2.19.

$$\frac{\Delta z_{\mathrm{mix,out}}}{D} = 0.23 \qquad (2.50)$$

Low-order model validation

Seven charging experiments (dir_3 - dir_9) and six discharging experiments (dir_10 - dir_15) were performed to validate the storage tank direct inflow charging model. Experiment details are presented in table 2.4. The experimental conditions were simulated with the found mixing parameter correlations. Experiments and simulations are compared based on the temperature distribution RMSE at all experiment time steps and RMSE of outflow temperature at all experiment time steps. A qualitative assessment of
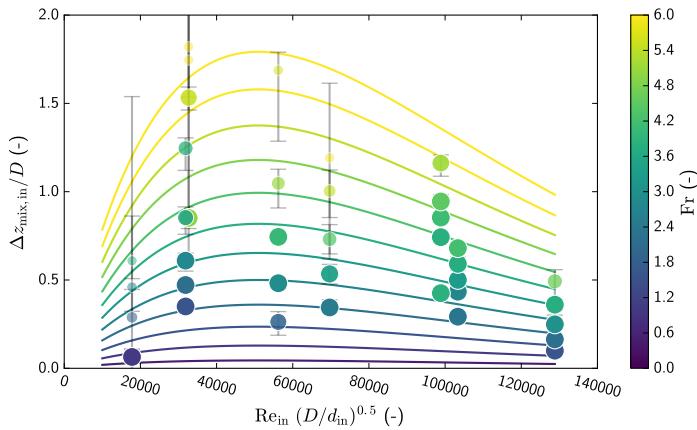
Figure 2.18: Inflow mixing zone correlation. Each circle shows the estimated inflow mixing zone of a partial CFD run. Smaller and transparent points had only a small weight in the correlation estimation as the parameter confidence interval was too large.
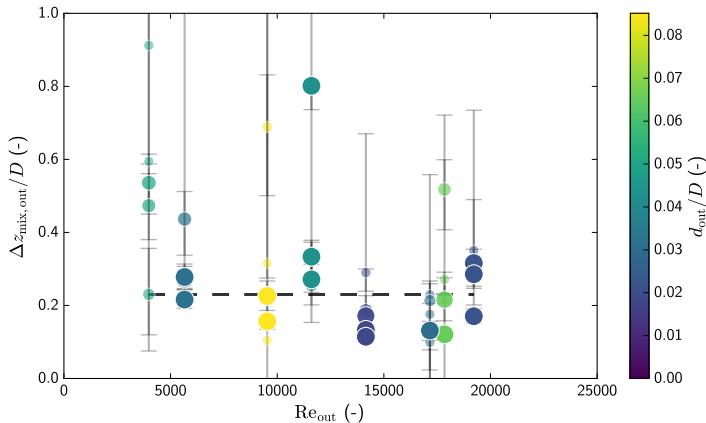

Figure 2.19: Outflow mixing zone correlation. Each circle shows the estimated outflow mixing zone of a partial CFD run. Smaller and transparent points had only a small weight in the correlation estimation as the parameter confidence interval was too large.

run	inflow port	outflow port	$\dot{m}_{in,avg}$ (kg/s)	$T_{in,avg}$ (°C)
dir_3	A	B	0.082	58.3
dir_4	A	D	0.211-0.324	45.1-54.2
dir_5	A	D	0.095	31.9-43.5
dir_6	B	D	0.035-0.047	59.0
dir_7	B	D	0.120	58.6
dir_8	B	D	0.113	37.2
dir_9	B	D	0.077	54.8
dir_10	D	A	0.090	27.6-39.2
dir_11	D	A	0.072	16.2-39.1
dir_12	D	A	0.054	14.9
dir_13	D	A	0.126	17.6-29.3
dir_14	D	B	0.120-0.200	6.5-50.4
dir_15	A	D	0.165-0.298	12.8-30.1

Table 2.4: Inflow conditions used for the direct inflow charging model validation. Port locations are shown in figure 2.12a. Some experiments are characterized by variable inflow rate and/or inflow temperature.

the storage tank temperature profile is also performed. To assess the model robustness, an inverted discharging experiment (dir_15), where cold fluid is injected at the top, is also performed, even though such a situation is unlikely to occur in a space heating hot water storage situation.

Examples of the agreement between the low order model under consideration and the experimental data are shown in figure 2.20. Both the storage temperature profile at different time steps and the outflow temperature are shown. As heat loss is negligible in the time span of the experiments, the latter can be used to evaluate the energy content of the storage tank during experiments and simulations. Good overall agreement is seen even with varying inflow temperature.

From figure 2.20a and figure 2.20e the mixing caused by buoyant flows when the inflow temperature changes is clearly visible. As the temperature drops/rises over time the zone below/above the inflow port at a higher/lower temperature than the inflow is mixed ($z/H > 0.147$ in figure 2.20a and $z/H < 0.845$ in figure 2.20e).

When in a charging experiment the inflow port is located away from the top of the storage tank (dir_6 - dir_9), the model underestimates the maximum storage tank temperature slightly. This effect is more pronounced when the inflow temperature is much higher than the average storage tank temperature. Due to buoyant forces warmer water will gather at the top of the storage tank.

Parameter	Range
Re_{in} (-)	3200 - 15000
Fr (-)	0 - 8
D/d_{in} (-)	12 - 53
z_{in}/D (-)	0.04 - 0.40

Table 2.5: Range of non-dimensional parameters for which the mixing and buoyancy correlations were identified.

In this situation, the assumed uniform mass flow distribution profile is too flat above the inflow. This causes a uniform modeled temperature, while in the experimental results, a temperature gradient is still present.

Figure 2.20g and figure 2.20h show the results of an inverted discharging experiment where cold water is injected at the top of the storage tank. The experiment shows almost uniform temperature profiles at all time steps, indicating severe mixing due to buoyant jet formation. The overall response of the model is in accordance with the experimental observations although the temperature in the center of the storage tank is slightly overestimated by the model and the temperature below the outflow is underestimated.

The RMSE values of storage temperature distribution and outflow temperature over all time steps are shown in figure 2.21. Both values are normalized with respect to the difference of maximum and minimum temperature in the experiment. A maximum difference in storage temperature RMSE of only 8% is seen. While the RMSE of storage outflow temperature is mostly below 6%, dir_9 shows an error of 8% (figure 2.21 and figure 2.20d). For dir_9, figure 2.20c shows that the thermocline in the storage tank model is less steep than the experimentally observed thermocline. This is caused by an overestimation of the mixing zone at the start of the simulation causing cold water below the inflow to mix with hot water above the inflow, creating a wider thermocline.

As correlations which were derived from a limited dataset are used for mixing and buoyancy parameters, the accuracy of the presented model is only guaranteed within the non-dimensional parameter range presented in table 2.5. However, during the validation experiments Reynolds numbers as low as 1100 showed accurate results.

It should be noted that when multiple inflows are present simultaneously, the formed buoyant jets can influence each other. The model and correlations presented above do not take such an influence into account. The situation of simultaneous charging and discharging occasionally occurs in solar buffer tanks with a direct inflow configuration. However, in such a situation the charging inflow jet is located near the top of the storage tank while the discharging inflow

(a) dir_5 storage temperature

(b) dir_5 outflow temperature

(c) dir_9 storage temperature

(d) dir_9 outflow temperature

(e) dir_13 storage temperature

(f) dir_13 outflow temperature

(g) dir_15 storage temperature

(h) dir_15 outflow temperature
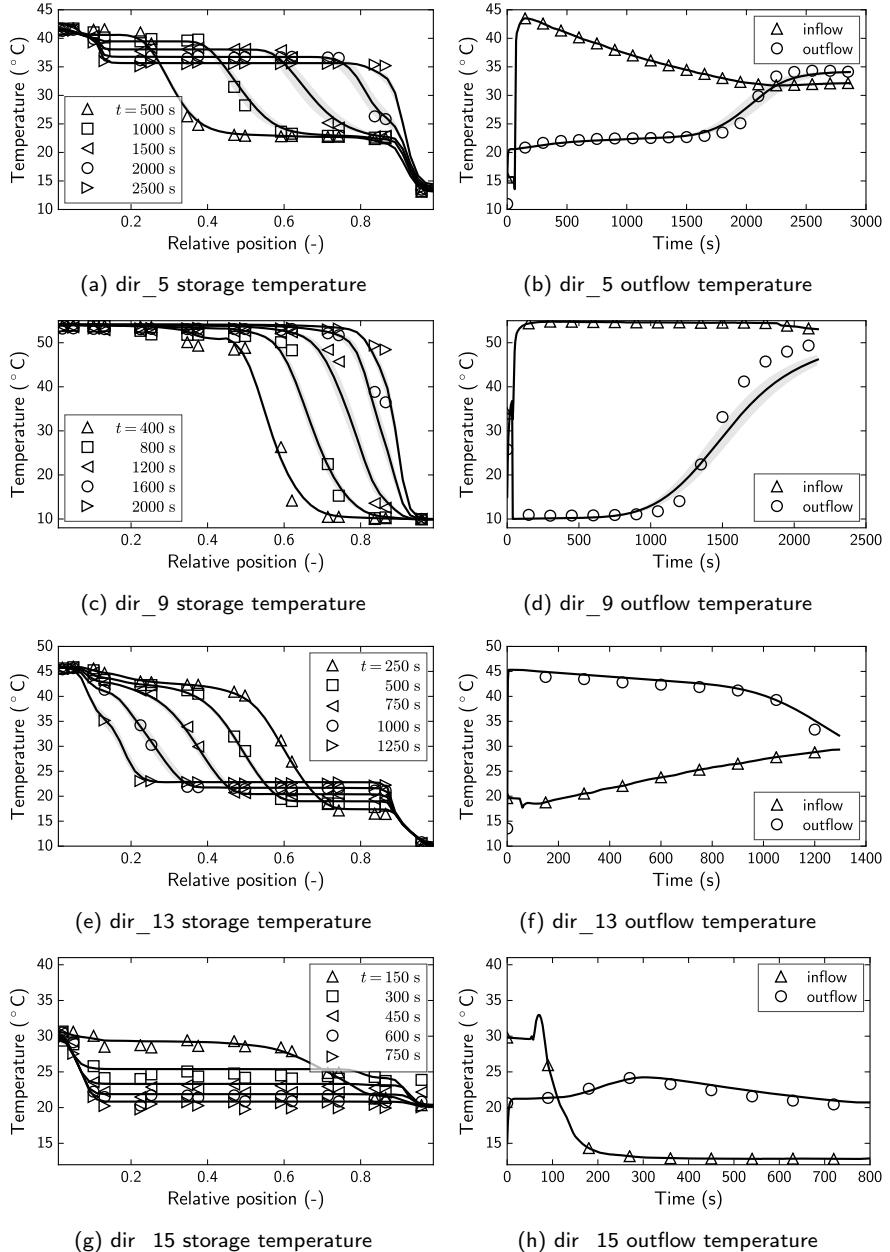
Figure 2.20: Comparison of experimental and simulated storage temperature profiles at different times (left) and experimental and simulated in- and outflow temperature (right) for dir_5, dir_9, dir_13 and dir_15. Markers represent the experimental observations, solid lines are the corresponding model results. The inflow temperature is equal for simulations and experiments. For clarity, not all measurement times are presented. The shaded region surrounding the simulated values represents simulations with flow rates within the uncertainty of the flow rate measurement. The uncertainty on temperature measurements is $\pm 0.2°$C, the uncertainty on relative measurement positions is ± 0.008.

(a) storage temperature RMSE (b) outflow temperature RMSE
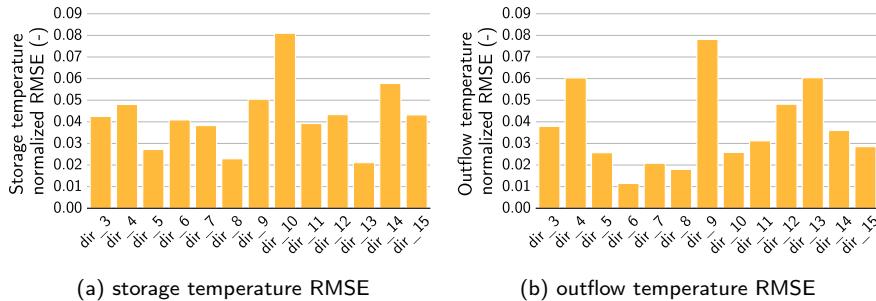
Figure 2.21: Temperature RMSE between experiments and simulations normalized with the maximum occurring temperature difference for the storage tank temperature distribution (left) and outflow temperature (right).

jet is located near the bottom, potentially reducing the interaction. Nevertheless, the presented model should be used carefully when simultaneous charging and discharging can occur.

In a DR context, when the storage tank serves as an energy buffer, this situation is not common as both charging and discharging can be controlled. As the model is intended to be used in DR simulations, no experiments or simulations were performed to investigate the phenomenon of simultaneous charging and discharging.

Comparison with models from the literature

For comparison, the same validation procedure was applied using a storage tank model often used in the literature, which uses a directional diffusivity approach to model buoyancy [193]. Resulting temperature profiles are presented in figure 2.22. As this model is only capable to model storage tanks with the in- and outflow ports located at the top and bottom of the storage tank, experiment dir_9, which uses an inflow port near the middle of the storage tank, is omitted. From this figure the improvements brought by the novel model with respect to the models from the literature are clear. The directional diffusivity approach is not able to represent buoyancy occurring when the inflow temperature changes and thus results in unrealistic storage tank temperature profiles. If the storage tank is integrated in a heating system, inflow temperature changes will occur during storage tank discharging, as in this situation the temperature is influenced by the building heat demand and temperature. These simulations also illustrate the need for comparing the storage tank temperature distribution in a charging experiment as the outflow temperature estimates can be relatively good (figure 2.22d).
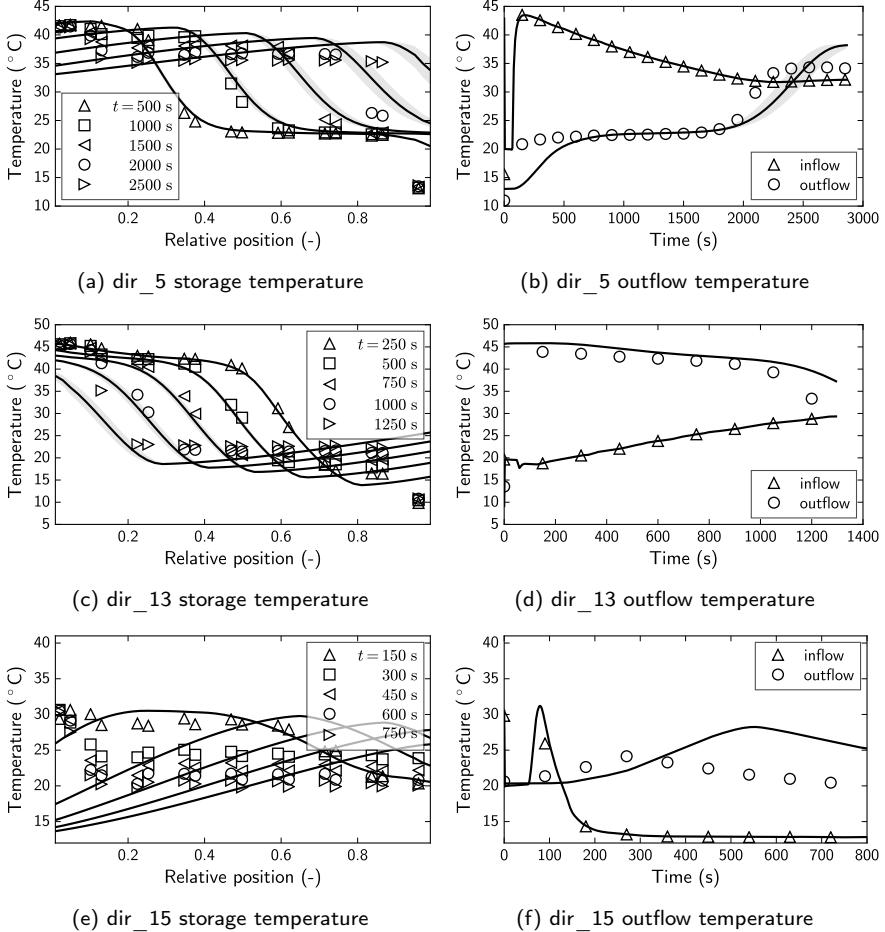
Figure 2.22: Comparison of experimental and simulated storage temperature profiles at different times (left) and experimental and simulated in- and outflow temperature (right) for dir_5, dir_13 and dir_15. Simulations were performed using the storage tank model developed in [193]. The directional diffusivity approach to modeling buoyancy is seen to cause unrealistic temperature profiles. Markers represent the experimental observations, solid lines are the corresponding model results. The inflow temperature is equal for simulations and experiments. For clarity, not all measurement times are presented. The uncertainty on temperature measurements is $\pm 0.2°$C, the uncertainty on the relative measurement positions is ± 0.008.

run	heat exchanger	$T_{0,\text{avg}}$ (°C)	$\dot{m}_{\text{hx,avg}}$ (kg/s)	$T_{\text{hx,in,avg}}$ (°C)
hex_1	bottom	18.2	0.017	35
hex_2	bottom	18.2	0.036	36
hex_3	bottom	13.3	0.085	35
hex_4	bottom	22.7	0.084	35
hex_5	bottom	19.6	0.018	57
hex_6	bottom	17.5	0.033	57
hex_7	bottom	33.1	0.034	59
hex_8	bottom	21.0	0.052	59
hex_9	bottom	22.5	0.080	60
hex_10	bottom	31.5	0.082	54
hex_11	top	8.4	0.083	38

Table 2.6: General data on the immersed heat exchanger charging experiments.

2.5.3 Immersed heat exchanger charging

To estimate the heat exchanger charging model parameters, 11 charging experiments (hex_1 to hex_11) are carried out. During all experiments, the heat exchangers are supplied with hot water at the top inlet. Used average initial storage tank temperatures, mass flow rates and average supply temperatures are listed in table 2.6.

The immersed heat exchanger charging model requires two parameters to be determined through experiments: $\text{Nu}_{\text{hx,ext}}$ and $\mathcal{C}_{\text{hx,bdl,in}}$. Values for $\text{Nu}_{\text{hx,ext}}$ and $\mathcal{C}_{\text{hx,bdl,in}}$ are obtained for each experiment by minimizing the RMSE of measured and simulated temperatures at all measurement heights and time steps. The resulting values are presented in figure 2.23. The error bars in this figure represent the variations in the parameter which cause an increase in the fit objective function of 5% of the optimal value. When a parameter value within this range is selected, the agreement between experiments and simulations remains qualitatively good. Figure 2.23 shows reasonable accordance between different experiments, however, an inverse correlation between $\text{Nu}_{\text{hx,ext}}$ and $\mathcal{C}_{\text{hx,bdl,in}}$ is clear. Both parameters affect the agreement of the model results with experiments and counteract each other.

To resolve this, the value of $\text{Nu}_{\text{hx,ext}}$ is fixed to the value corresponding best to the above experiments and the parameter $\mathcal{C}_{\text{hx,bdl,in}}$ is re-fitted. The resulting parameter values are presented in figure 2.24.

From this, parameter values corresponding relatively well to all experiments are selected and are used in the remainder of this work. The value of $\mathcal{C}_{\text{hx,bdl,in}}$

(a) $\mathrm{Nu_{hx,ext}}$
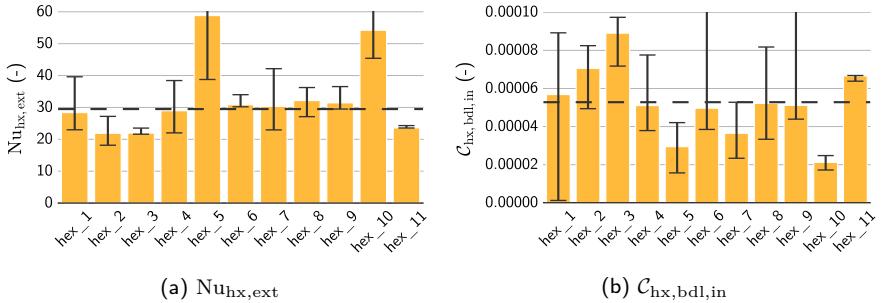
(b) $\mathcal{C}_{\mathrm{hx,bdl,in}}$

Figure 2.23: Optimal parameter values ($\mathrm{Nu_{hx,ext}}$ and $\mathcal{C}_{\mathrm{hx,bdl,in}}$) and ranges of good fit quality for all experiments. The overall best fitting value is depicted with a dashed line.
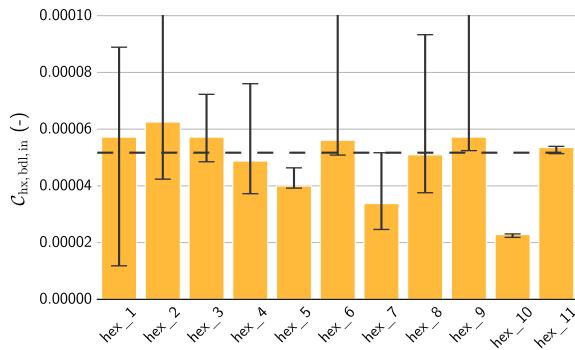
Figure 2.24: Optimal parameter values ($\mathcal{C}_{\mathrm{hx,bdl,in}}$) and ranges of good fit quality for all experiments after fixing $\mathrm{Nu_{hx,ext}}$ to the value determined above. The overall best fitting value is depicted with a dashed line.

selected from the parameter fit with fixed $\mathrm{Nu_{hx,ext}}$ is only slightly less than the one obtained with the initial parameter fit. As only one data set was available for the top heat exchanger, no value could be obtained and parameters for the bottom heat exchanger are applied to the top heat exchanger as well in the remainder of this section.

$$\mathrm{Nu_{hx,ext}} = 29.5 \tag{2.51}$$

$$\mathcal{C}_{\mathrm{hx,bdl,in}} = 53 \times 10^{-6} \tag{2.52}$$

To verify the obtained overall parameter values, all experiments were simulated with these parameters. As the same experiments are used to fit the parameters and to verify the model, this is not a model cross-validation. Resulting temperature distributions and heat exchanger outflow temperatures are

presented in figure 2.25. Correspondence of simulations and measurements is qualitatively good in all cases both for the temperature distributions and simulated outflow temperatures. The expected behavior of a nearly uniform temperature above the heat exchanger caused by buoyant plumes is seen in all simulations. In figure 2.25c the behavior when an initial thermocline is present above the heat exchanger is seen. The zone with temperatures higher than the boundary layer outflow temperature is left largely undisturbed in both simulations and experiments. The already existing thermocline is amended with a new thermocline around the bottom of the heat exchanger. The presented model seems to capture this effect relatively well although some differences in temperature at the top of the heat exchanger are observable.

In experiment hex_6 presented in figures 2.25c and 2.25d, the heat exchanger inflow temperature was suddenly decreased to a value below the overall storage tank temperature at that time (around 7500 s from the start of the experiment). This causes the heat exchanger to switch from charging to discharging. The flow in the boundary layer is reversed, and buoyant flows reach the bottom of the storage tank. The resulting decrease in storage tank temperature at the location of the heat exchanger is captured well by the model. Furthermore, the change in heat exchanger outflow temperature is also represented with good accuracy.

In figure 2.26, normalized RMSE values for the temperature distribution and heat exchanger outflow temperature are presented. The values are normalized by dividing the root mean squared difference between simulation and experimental temperature by the difference between largest and smallest temperature measured during the experiment. Most often this is the difference between maximum inflow temperature and minimum storage temperature. Temperature distribution RMSE values are seen to be less than 3% for all experiments except hex_10 where an initial thermocline was present in the storage tank. Outflow temperature RMSE are always less than 6%.

An attempt was made to enhance the correlation for $\mathrm{Nu_{hx,ext}}$ by introducing a local dependence on the Rayleigh number in accordance with [107]. The external Nusselt number in layer j can then be written as:

$$\mathrm{Nu}_{\mathrm{hx,ext}}^{j} = \mathrm{Nu_{hx,ext,0}} + \mathcal{C}_{\mathrm{hx,bdl,ext}} \left(\mathrm{Ra}_{\mathrm{hx}}^{j} \right)^{0.25} \tag{2.53}$$

With $\mathrm{Nu_{hx,ext,0}}$ and $\mathcal{C}_{\mathrm{hx,bdl,ext}}$ constants to be fitted and $\mathrm{Ra_{hx}}$ the Rayleigh number with respect to the external heat exchanger diameter and the difference between heat exchanger and storage tank layer temperature, computed as:

$$\mathrm{Ra}_{\mathrm{hx}}^{j} = \frac{g \beta d_{\mathrm{hx,ext}}^{3} |T_{\mathrm{hx}}^{j} - T_{\mathrm{bdl}}^{j}|}{\nu \lambda} \tag{2.54}$$
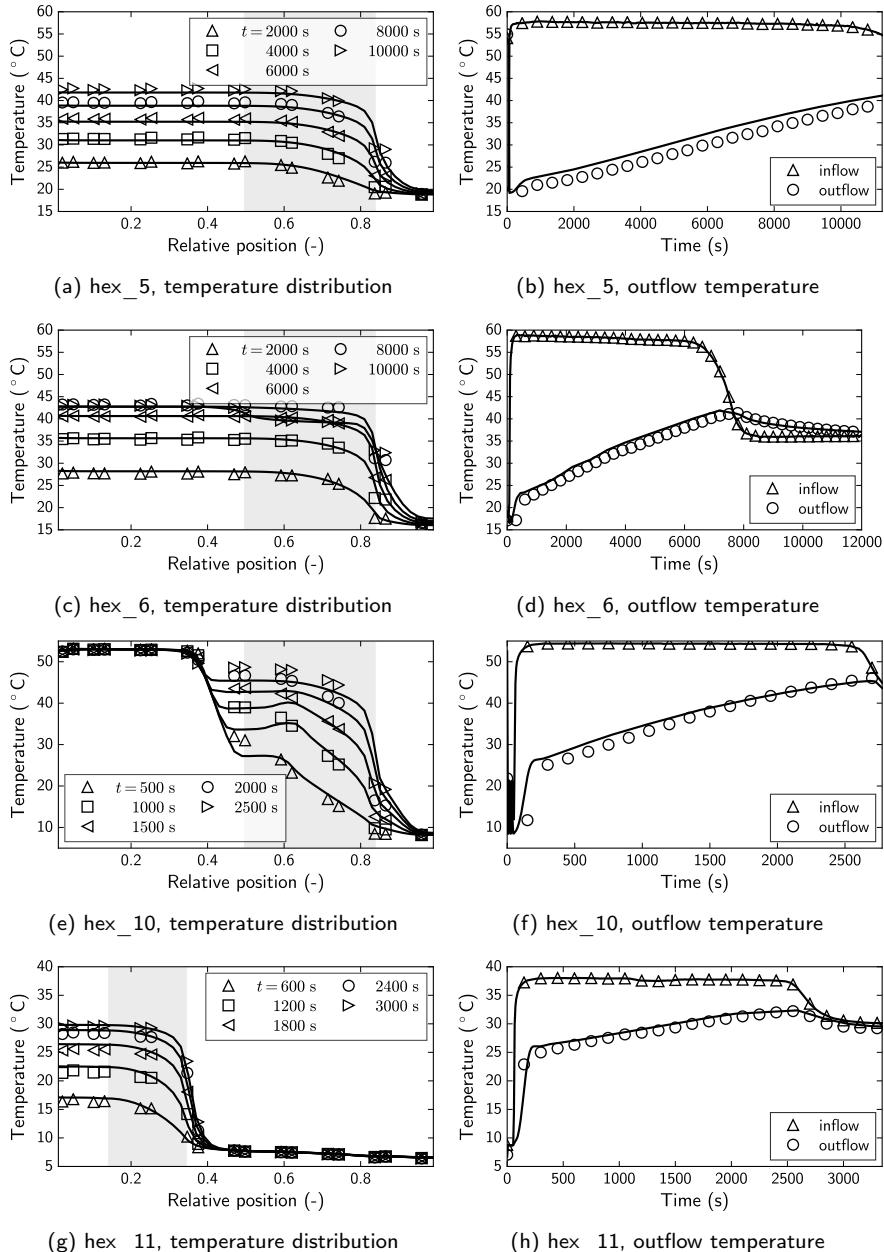
Figure 2.25: Comparison of experimental and simulated storage temperature profiles (left) and outflow temperature (right) for the heat exchanger charging experiments. For clarity, not all measurement times are presented. The location of the heat exchanger is indicated by the shaded area in each figure. The uncertainty on temperature measurements is $\pm 0.2°C$, the uncertainty on the relative measurement positions is ± 0.008.

(a) storage temperature RMSE

(b) outflow temperature RMSE
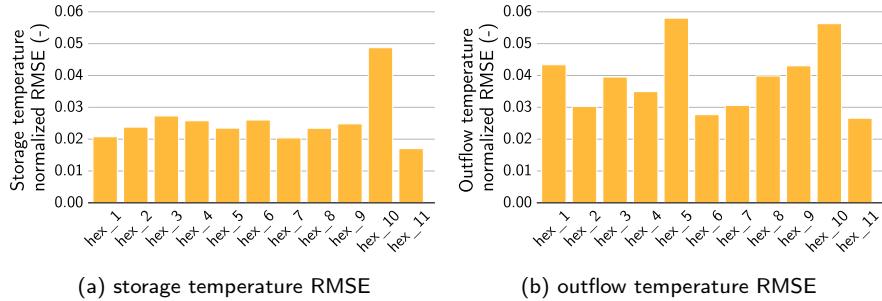
Figure 2.26: Normalized RMSE values of the measured and simulated temperatures for the heat exchanger charging experiments. Values are normalized with respect to the largest temperature difference measured in the experiment.

However, this refinement did not improve the quality of the results and thus was abandoned.

As the presented correspondence with experiments is based on results for the same experiments which were used to fit the parameters, this is not a model cross-validation. To cross-validate the presented heat exchanger charging model an independent set of experiments, preferably on another storage tank, is required. However, as the parameter values were fit for each experiment separately and afterwards a single parameter was chosen, the presented correspondence does give insight into the validity of the presented model and parameters for the storage tank used in the experiments. Furthermore, for the final experiment (hex_11), the same parameter values were used and provided good results even though a different heat exchanger is used to charge the storage tank.

2.5.4 Heat loss

Both methods for modeling the heat loss from a hot water storage tank (see section 2.4.3) are compared with experiments. The boundary layer heat loss model requires two parameters to be estimated from experiments, the average heat loss model requires only one parameter. Due to the long duration of heat loss experiments, too few experiments were carried out to perform a full parameters estimation and model validation. General data on the three standby phase experiments (sto_1 to sto_3) are presented in table 2.7. As the experiments were carried out in an unheated space the heat loss temperature was not constant. Daily variations of around 5°C were observed in all experiments. In the simulations, the storage tank model is subjected to the measured heat loss temperature.

run	$T_{0,\mathrm{avg}}$ (°C)	$T_{\mathrm{hl,avg}}$ (°C)	duration (h)
sto_1	29.6	13.0	165
sto_2	40.8	17.3	163
sto_3	46.0	15.9	20

Table 2.7: General data on the standby phase experiments.

For each of the experiments, the parameters of both models are fitted independently, minimizing the temperature distribution RMSE over the entire experiment duration. The resulting parameters of the boundary layer and the average heat loss model are presented in figure 2.27. Overall coefficients of heat transfer resulting from both optimizations are similar, around 1.20 W/m²K and the ranges of good fit quality are relatively small. For the average heat loss model, a value of 1.20 W/m²K lies within all ranges of good fit quality, where the parameter fit objective function is less than 5% larger than the optimal value. This overall heat loss coefficient is substantially larger than the one obtained through a one-dimensional analysis of the storage tank heat loss. This difference can be attributed to the large number of fittings penetrating the insulation mantle and the adaptations made to the storage tank to insert the temperature distribution sensors. The parameters computed for the boundary layer model, present no overlap in their ranges of good fit quality. Even the boundary layer parameter $\mathcal{C}_{\mathrm{hl,bdl}}$, to which the model is rather insensitive, shows no overlap.

For further analysis the values $U = 1.24$ W/m²K and $\mathcal{C}_{\mathrm{hl,bdl}} = 60$ are selected for the boundary layer model and $U = 1.20$ W/m²K is selected for the average heat loss model. With these values, the experiments were replicated in the simulation environment. In figure 2.28, simulations with the boundary layer model and the average heat loss model, calculated with the overall model parameters presented above, are compared with measured temperature profiles. Both models give a qualitatively good representation of the temperature profile for all runs. From these runs it seems that the boundary layer model is better suited for representing the dynamics near the bottom part of the storage tank. Nevertheless, the differences between both models are very small.

The normalized temperature distribution RMSE is compared for both models and all experiments in figure 2.29. Normalization is done with respect to the maximum difference of storage tank and heat loss temperature measured in the experiment. The boundary layer model has lower errors in all experiments, which is expected as this model has two parameters instead of one in the average heat loss model giving more freedom to the parameter estimation. As these results are obtained for the same experiments as used for the parameter estimation, no definitive conclusion considering the models merit can be made.

(a) U, boundary layer model

(b) U, average model

(c) $\mathcal{C}_{\mathrm{hl,bdl}}$, boundary layer model
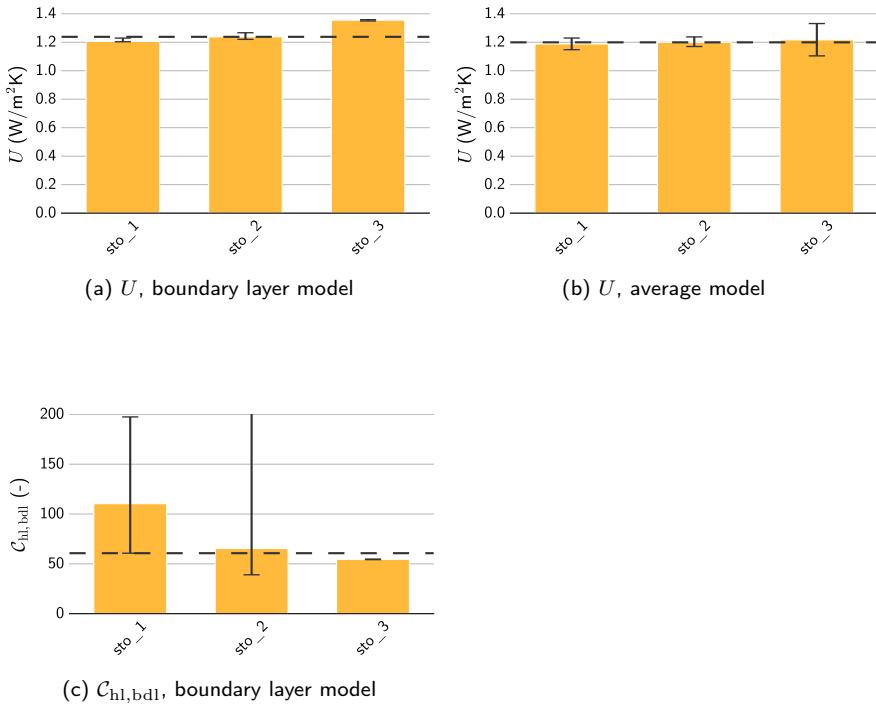
Figure 2.27: Parameter values of the heat loss models resulting from the fitting of individual experiments with their ranges of good fit quality. Parameters of the boundary layer model are presented on the left, parameters of the average heat loss model on the right. The uncertainty on temperature measurements is $\pm 0.2°$C, the uncertainty on the relative measurement positions is ± 0.008.

In the boundary layer model the location for re-injecting the flow must be computed for all nodes. This can be implemented in the Modelica modeling language by introducing a number of layers squared distribution variables. When the number of layers rises, the number of variables thus rises very quickly. This makes the boundary layer model rather computationally expensive, especially during model compilation. The above results were obtained for 50 storage tank layers, which cause the simulations using the boundary layer model to be around a factor 4 slower than the simulations using the average heat loss model. As the latter model involves only a single parameter and the results when comparing the models with experiments are qualitatively similar, the average heat loss model is used in the remainder of this work.
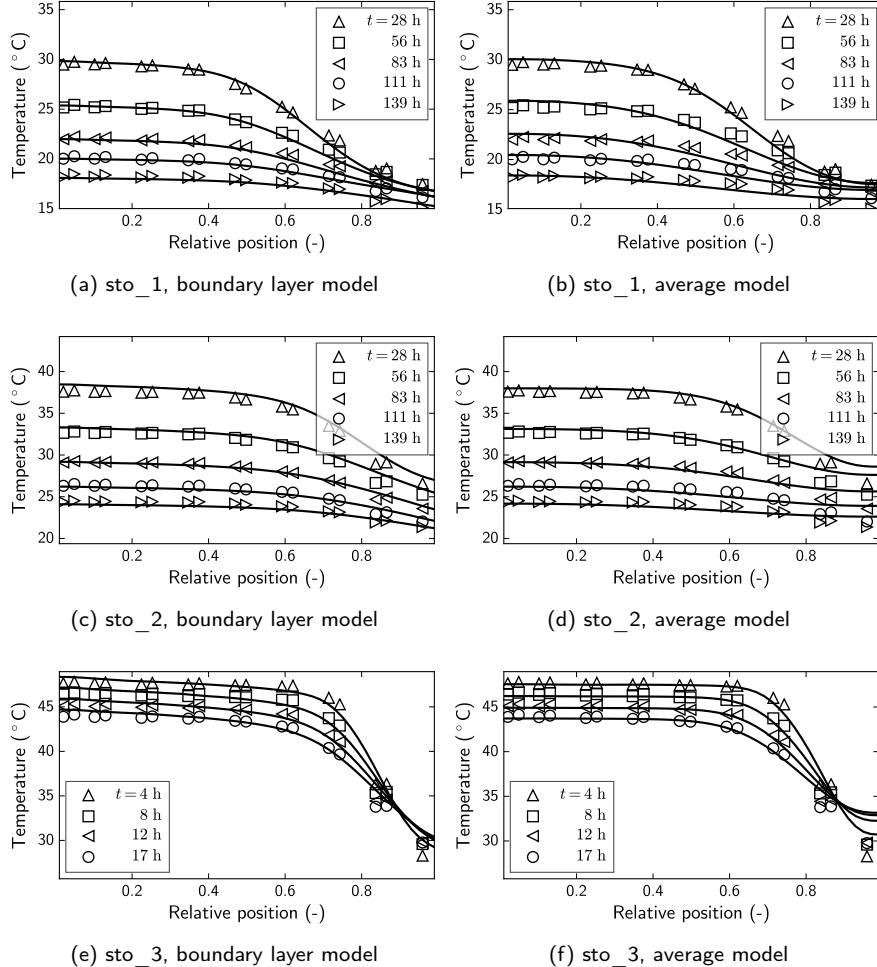
Figure 2.28: Comparison of simulated and measured storage tank temperature profiles for the storage phase experiments. Simulations with the boundary layer model are presented on the left, simulations with the average heat loss model on the right.
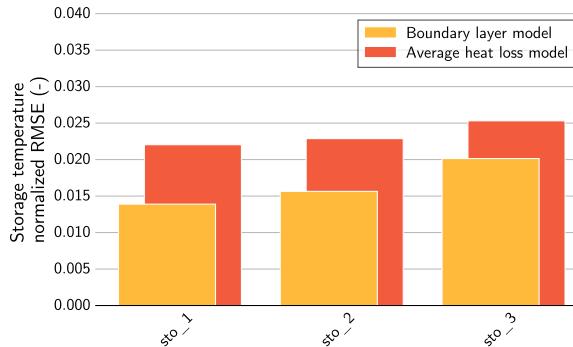
Figure 2.29: Comparison of normalized storage temperature distribution RMSE for both heat loss models obtained with the overall parameter values.

Nevertheless, the boundary layer heat loss model is valuable as it is based more on physical insights in the heat loss process and it provides slightly more accurate results. To validate the model however, a more extensive measurement campaign is required.

2.6   Conclusion

Integrated system simulations are essential for evaluating the benefits of residential heating systems with heat pumps and hot water storage tanks. For these simulations, an accurate but low order storage tank model is required. The model must represent important flow phenomena sufficiently accurate in order to make valid conclusions from such building simulations.

In this chapter a one-dimensional discretization of a hot water storage tank is presented. This model is amended with formulations for energy transfers resulting from three-dimensional phenomena such as direct inflow charging, heat exchanger charging and heat loss. Required parameters have been estimated based on experiments or detailed simulations. For the direct inflow charging model, the resulting correlations have been experimentally validated.

The resulting model is able to predict the variation of temperature profiles inside a hot water storage tank well. Furthermore, the model is sufficiently low order so that full year dynamic building simulations can be performed within a feasible simulation time.

On the contrary, under some circumstances, such as when the inflow temperature is much larger than the average storage tank temperature in a direct inflow

charging situation, the differences between experiments and simulations are larger than the experimental and simulation uncertainty. The three-dimensional nature of the phenomena makes it very difficult to capture the storage tank behavior in a one-dimensional model. Nevertheless, the presented model provides a significant improvement relative to models found in the literature, which most often do not take inflow buoyancy, inflow mixing, natural convection flows from an immersed heat exchanger or the energy redistribution accompanying heat losses into account.

Chapter 3

Operation of heating systems including a hot water storage tank

3.1 Introduction

In European residential heating systems, water is most often used to transfer energy from the heat generation system e.g. gas boiler, heat pump, to the heat emission system e.g. radiator, floor heating. To control the power of such energy transfer, two variables are available: supply temperature and flow rate. If the supply temperature is kept constant, and the flow rate increases, energy transfer will increase. Likewise, if the flow rate is constant, a rise in the supply temperature will cause a rise in energy flow rate. In the above statements, care must be taken that the supply temperature is generally defined differently for emission and generation systems. For emission systems it is generally defined as the temperature of the fluid entering the system, while for heat generation systems it is the temperature of the fluid leaving the system.

In standard heating systems, heat generation and heat emission are coupled directly or with an intermediate mixing valve. Therefore, all generated heat is transferred to the emission system and must be emitted to the building or accumulated in the system. Integrating a hot water storage tank in a heating system allows decoupling the heat generation from heat emission. A hot water storage tank thus adds flexibility to the heating system as the heat generation

can be shifted in time.

In a heating system with a hot water storage tank, the entering mass flow rate is related to the charging or discharging power and thus affects the temperature distribution inside the storage tank [9]. However, the temperature of the water entering the storage tank, both during charging and discharging, can also be controlled to some extent, which affects the required mass flow rate. This gives rise to different charging and discharging strategies. As presented in chapter 2, different storage charging methods result in significantly different temperature distributions inside the storage tank. Likewise, the charging or discharging strategy influences the distribution of energy in a storage tank. In the literature, storage tank stratification is suggested to strongly influence the performance of a storage tank [31, 127, 153, 197, 198].

In this chapter, the effect of different charging and discharging strategies on the operation of a storage tank in a heating system is investigated. The investment in a storage tank is substantial, both from a financial and an environmental viewpoint. Using suboptimal strategies implies the investment is not used to it's full extent, leading to an increased environmental impact and/or cost.

The chapter goal is to determine which storage tank charging and discharging strategies are most suitable for use in a building participating in a DR program.

The chapter is structured as follows: In section 3.2 the different charging and discharging strategies and their implications are presented. Next, in section 3.3, a methodology is developed for evaluating the performance of a storage tank in a DR context. Section 3.4 evaluates the strategies presented in section 3.2 based on the methodology developed in section 3.3. Finally, in section 3.5, concluding remarks are formulated.

3.2 Storage charging and discharging strategies

Several methods for integrating thermal energy storage in solar, combined heat and power and heat pump heating systems were presented by Gang and Xuefei [74]. However, no attention is given to the operation of a storage tank in the presented system. When a hot water storage tank is used in a heating system, several charging and discharging strategies are possible.

3.2.1 Storage charging

When charging a storage tank, two extreme strategies can be identified. First, it is possible to ensure the fluid entering the storage tank has a constant temperature. This strategy implies fluid at the final, desired storage tank temperature is delivered to the storage tank. Second, it is possible to control the temperature of the fluid entering the storage tank such that a constant temperature difference between inflow and outflow is maintained. Here, fluid at a temperature lower than the desired storage tank temperature is sent to the storage tank. As the storage tank outflow temperature increases, the inflow temperature is increased to maintain a fixed temperature difference until the desired storage tank temperature is reached. The energy flow to the storage tank is in both cases controlled by controlling the mass flow rate through the use of control valves, or more efficiently, frequency controlled pumps. Both strategies can be used with a direct charging system or a system with an immersed heat exchanger.

The two charging strategies cause different intermediary storage tank temperature profiles. When applying a fixed temperature strategy while charging the storage tank through properly located direct inflow ports, the fluid inside the storage tank is gradually replaced with fluid at the fixed inflow temperature. During the charging some mixing will occur, but overall the storage tank behaves rather stratified. If however the fixed temperature charging strategy is used to charge a storage tank through an immersed heat exchanger, a more mixed intermediary temperature profile results due to the natural convection heat transfer from the heat exchanger.

The fixed temperature difference strategy, when used with direct inflow charging, causes the fluid in the storage tank to be replaced with fluid at a slightly higher temperature. To charge the storage tank to a certain temperature level, multiple passes are required. Although the storage tank is charged stratified within a single pass, when observing the storage temperature profile with respect to the final temperature difference, it behaves more mixed than stratified. Charging a storage tank through an immersed heat exchanger with a fixed temperature difference strategy does not necessarily cause additional destratification.

When a storage tank is fully charged, up to the desired temperature level, the charging method has no influence on the discharge performance of the storage tank as the final temperature distribution is the same. However, if the discharge process requires heat to be delivered at a certain minimum temperature, the two charging methods presented above are not equivalent with respect to discharging performance as long as the required stored energy is less than the amount that can be stored in a fully charged storage tank.

3.2.2 Storage discharging

In many floor heating emission systems, the energy flow rate to the system is controlled by means of a mixing valve. In such a system, the flow rate through the emission system is constant and the supply temperature is controlled by mixing colder fluid from the emission return flow with the generation supply flow. On the other hand, the power flow can also be controlled by controlling the flow rate through the emission system and keeping the emission supply temperature equal to the generation supply temperature. In this text, the former is referred to as temperature modulation, the latter as flow modulation.

In a heating system without storage tank, the two emission control strategies result in a different emission return temperature. In a heating system, the emission system can be viewed as a heat exchanger, exchanging heat between the flow through the emission system and the air inside the building. If the air inside the building is at a rather uniform temperature, the heat exchanger effectiveness will be predominantly dependent on the water flow rate through the emission system. Under temperature modulation, the constant flow rate through the emission system implies the system operates at a fixed effectiveness. In a flow modulation system with equal maximum power, the flow rate through the heat exchanger is always smaller, leading to to a higher effectiveness. An emission system with temperature modulation will thus have a higher return temperature than a system with flow modulation supplying the same power. When the heat is supplied by a condensing gas boiler, a lower return temperature enables more condensation and thus a higher efficiency. When the heat is supplied by a heat pump, the lower return temperature allows for a decreased refrigerant mass flow rate which also slightly increases efficiency.

However, these differences only manifest at powers lower than the nominal power. Under nominal conditions, the mixing valve is set such that no mixing occurs making the two systems equivalent. Furthermore, the presented gains in efficiency are small compared to the required additional investments in a frequency controlled pump in the emission system and additional sensors and control actuators in the generation systems.

In a heating system including a storage tank, the reduction in emission return temperature has an additional benefit. When the storage tank is discharged, a lower emission return temperature could allow a lower average storage tank temperature at the end of the discharge phase. This effectively increases the storage tank capacity as the average temperature difference between a fully charged and fully discharged storage tank increases. This increased storage capacity leads to an increased system flexibility implying the investment in the storage tank pays off sooner.

In the literature, no studies analyzing the benefits or disadvantages of the above presented charging and discharging strategies were found. As there is a difference in operation depending on the selected strategy, such an analysis is useful and is the subject of this chapter.

3.3 Characterizing storage cycle performance

In this section, a methodology is developed to quantitatively compare the storage charging and discharging strategies presented in section 3.2 in the context of DR with heat pumps. When a building owner participates in a DR program, an incentive is given to lower the electricity demand during a certain period. To compensate for this reduction in demand, a period where higher demand is allowed must precede the reduction period. If this is not the case, the end user is not offered the same services as a user not participating in a DR program.

When DR is provided by space heating with heat pumps, a reduction in demand corresponds to a decrease in heat pump heat output. To ensure thermal comfort in the building is maintained, the reduction in heat supply from the heat pump can be compensated by discharging a hot water storage tank. Some time before the reduction or the discharge period, the storage tank must have been charged by the heat pump, leading to an increased electricity demand in that period.

In section 3.3.1 the methodology and used models are presented. Next in section 3.3.2, performance indicators for comparing storage systems are discussed.

3.3.1 Characterization methodology

The effects of the charging and discharging strategies are investigated based on periodic simulations of a heating system. The building heating system is simplified to an ideal emission system, a hot water storage tank, and a heat generation system. The three subsystems involved are connected in a parallel configuration as presented in figure 3.1.

The cycle of storage charging and discharging in response to DR incentives is simplified by assuming storage charging is allowed during the first half of a fixed period (charge phase), and heat pump operation must be minimized during the second half of the period (discharge phase). The entire time period, a fixed heat flow rate must be supplied to the building by the emission system. This assumes no storage capacity is present in the building or that the flexibility available through the building thermal mass is already used to its full extent
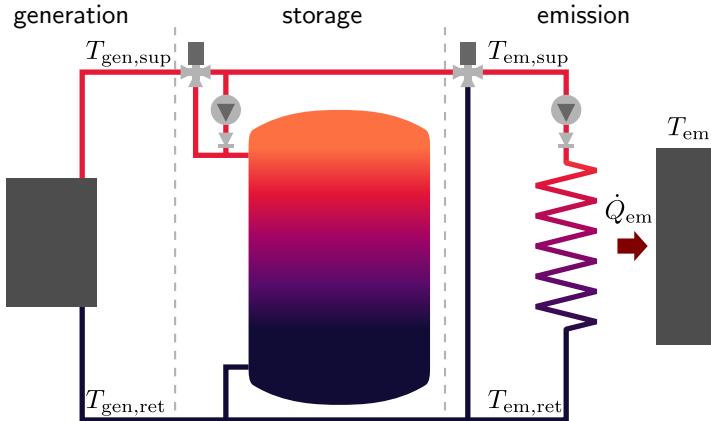
Figure 3.1: Schematic representation of the simplified heating system.

and that heat losses and gains in the building are constant. This allows to focus on the heating system.

During the charge phase, the storage tank is charged with constant power, until this power can no longer be supplied by the heat generation system because the temperature difference between storage inflow and outflow temperature is too small or the maximum supply temperature is reached. During the charge phase, the heat generation system must also supply the required emission power. When the requested charging power can no longer be supplied, the storage charging stops. During the discharge phase, the heat generation system is switched off and the full emission power demand must be met by discharging the storage tank. When the storage tank can no longer supply the demanded minimum emission temperature, storage discharging is stopped and the heat generation system again takes over to supply the demanded emission power. This charging-discharging cycle is schematically presented in figure 3.2.

The emission system is controlled to supply heat at constant power ($\dot{Q}_{\mathrm{em}}$) to the building which is at a constant temperature (T_{em}). Heat losses from piping to unheated spaces are neglected. Under these assumptions, the emission power and effectiveness ($\varepsilon_{\mathrm{em}}$) are written as:

$$\dot{Q}_{\mathrm{em}} = \varepsilon_{\mathrm{em}} \dot{m}_{\mathrm{em}} c \left(T_{\mathrm{em,sup}} - T_{\mathrm{em}} \right) \tag{3.1}$$

$$\varepsilon_{\mathrm{em}} = 1 - \exp\left(-\frac{U A_{\mathrm{em}}}{\dot{m}_{\mathrm{em}} c} \right) \tag{3.2}$$
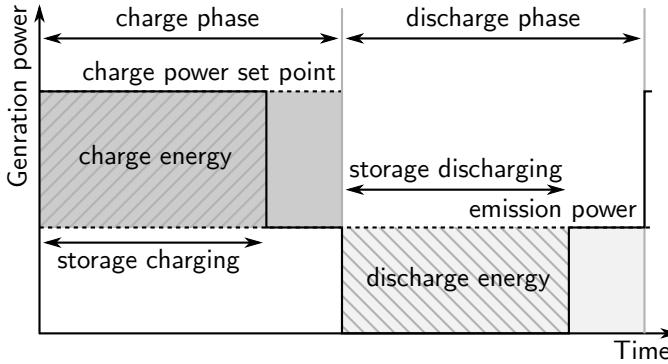
Figure 3.2: Schematic representation of a periodic storage cycle simulation. The dark gray area represents the requested storage charging energy while the dark gray hatched area represents the actual charge energy. The light gray area represents the requested storage discharging energy while the dark gray hatched area represents the actual discharged energy.

With UA_{em}, the average overall heat transfer coefficient, which is assumed to be constant, multiplied with the emission area, $\dot{m}_{\mathrm{em}}$ the mass flow rate through the emission system and $T_{\mathrm{em,sup}}$ the temperature of the water supplied to the emission system. The emission system nominal mass flow rate and UA value can be derived from the systems nominal heat flow rate ($\dot{Q}_{\mathrm{em}}^{\mathrm{nom}}$, supply temperature ($T_{\mathrm{em,sup}}^{\mathrm{nom}}$) and effectiveness ($\varepsilon_{\mathrm{em}}^{\mathrm{nom}}$):

$$\dot{m}_{\mathrm{em}}^{\mathrm{nom}} = \frac{\dot{Q}_{\mathrm{em}}^{\mathrm{nom}}}{\varepsilon_{\mathrm{em}}^{\mathrm{nom}} c \left(T_{\mathrm{em,sup}}^{\mathrm{nom}} - T_{\mathrm{em}}\right)} \tag{3.3}$$

$$UA_{\mathrm{em}} = -\dot{m}_{\mathrm{em}}^{\mathrm{nom}} c \ln\left(1 - \varepsilon_{\mathrm{em}}^{\mathrm{nom}}\right) \tag{3.4}$$

In this chapter, these nominal values are chosen to be 10 kW, 35°C and 0.4 for the heat flow rate, supply temperature and effectiveness respectively. These values are derived from a typical residential floor heating system [97].

The heat flow to the emission system can be controlled by modulating the flow rate to the emission system or by using the emission mixing valve and controlling the emission supply temperature. It must be remarked that at the nominal emission power, the mixing valve will be completely closed and the two systems are identical. When using the mixing valve control system, the mass flow rate through the emission system is always the nominal mass flow rate. The emissions system effectiveness will thus be the nominal effectiveness.

The requested power can only be supplied by the emission system if the emission supply temperature is above a certain minimum emission supply temperature.

This minimum temperature is dependent on the requested power and can be evaluated as:

$$T_{\text{em,sup}}^{\min} = T_{\text{em}} + \frac{\dot{Q}_{\text{em}}}{\varepsilon_{\text{em}}^{\text{nom}} c \dot{m}_{\text{em}}^{\text{nom}}} \tag{3.5}$$

When during the discharge phase, the emission supply temperature threatens to fall below this temperature, the heat generation system is switched back on and storage discharging stops.

The system for heat generation is simplified as having no thermal inertia and no heat losses to the surroundings. Furthermore, it is assumed to be able to supply nominal power to the hydronic system at any temperature below the nominal supply temperature. The temperature of the fluid entering and leaving the heat generation system are termed $T_{\text{gen,ret}}$ and $T_{\text{gen,sup}}$ respectively. With $\dot{m}_{\text{gen}}$ the heat generation mass flow rate, the generation power is written as:

$$\dot{Q}_{\text{gen}} = \dot{m}_{\text{gen}} c \left(T_{\text{gen,sup}} - T_{\text{gen,ret}} \right) \tag{3.6}$$

The generation power can be controlled by altering the generation mass flow rate ($\dot{m}_{\text{gen}}$) or the generation supply temperature ($T_{\text{gen,sup}}$). With the fixed temperature charging strategy, $T_{\text{gen,sup}}$ is fixed to it's nominal value of 35°C during storage charging. When the storage tank is not charged, the the generation supply temperature is set to the minimum emission supply temperature. With the fixed temperature difference charging strategy, $T_{\text{gen,sup}}$ is kept minimum 2°C above the return temperature ($T_{\text{gen,ret}}$) and above the minimum emission supply temperature. In both cases, the generation mass flow rate is varied to ensure the requested heat output is met. When during the charge phase, the mass flow rate required to supply the requested charging power tends to rise above the nominal mass flow rate, storage charging is stopped. The nominal generation mass flow rate is chosen equal to the nominal emission mass flow rate.

In section 3.4, the effect of the different charging and discharging strategies on a storage tank charged through direct inflow ports is investigated. The approach however holds for different types of storage charging and discharging methods.

Periodic simulations are performed for different values of the simulation period, emission power, charge power set point and the different storage charging and discharging strategies. The periodicity of the simulations is important since otherwise, unfair comparisons are made as different amounts of energy could be stored in the system at the end of the simulation while the starting energy would be the same. This is achieved by running the simulation over multiple periods, ensuring that the difference in start and final storage energy is below 0.01% of the final storage energy.
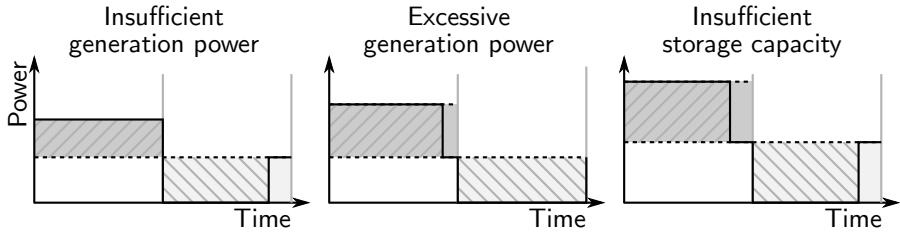
Figure 3.3: Schematic representation of the three possible scenarios in the storage cycle simulation.

In these simulations three scenarios can be distinguished which are schematically represented in figure 3.3. First, if the charging power set point is low, the storage tank will not contain sufficient energy at the end of the charge phase to supply the requested emission power during the discharge phase. Discharging will thus end before the end of the discharge phase. Second, at larger charge power set points, the storage tank will contain sufficient energy to supply the emission power during the full discharge phase. As there is only a single charge power set point value where charging and discharging are perfectly balanced, the average temperature of the storage tank will increase. This increase causes the storage charging to end before the end of the charge phase while storage discharging will last the complete discharge phase. The increased average temperature also causes an increase in storage heat losses which should be avoided. Finally, as the demanded emission power rises, the storage tank capacity may be too small to supply the demanded emission power during the complete emission phase. As the storage tank capacity is reached, charging will end before the end of the charge phase and discharging will also end before the end of the discharge phase. In this scenario, the storage tank is under-sized.

From the simulation results, a comparison between different charging and discharging strategies can be made.

3.3.2 Storage cycle performance indicators

To compare different situations, indicators describing the system performance are required. Njoku et al. [131] summarized several indicators to represent the performance of a storage tank by energy or exergy based measures. In a space heating context, the maximum generation temperature and minimum emission supply temperature are important. Energy based indicators fail to represent this temperature dependency. On the other hand, exergy based measures assign a higher value to fluid at higher temperatures. However, in a space heating

context, when the storage fluid temperature is above the emission system minimum supply temperature, the amount of energy that can be supplied to the emission system increases with the energy content of the storage fluid, not the exergy. Exergy based measures thus include temperature dependency but in a way which is not appropriate for space heating systems.

Dincer and Rosen [47] also presented several energy based and exergy based efficiencies for a storage charging-standby-discharging cycle and each phase separately. They argue exergy based efficiencies provide a more complete view and are more intuitive measures. However, they considered a thermal energy storage outside the context of a complete system. If the entire system, in this case the heating system, is considered, temperature related effects are contained within the system and storage tank inflow and outflow temperatures are constrained by the system reducing the added value of an exergy analysis. As the quantities of interest, such as energy delivered to the building and energy required by the heat pump, are energy related, an energy based evaluation of the complete system is more useful.

S. Zhang and Niu [200] defined a volumetric thermal storage capacity based on a charging or discharging process of a cold storage using a phase change material slurry. They computed the discharge and charge energy based on an experiment of a storage tank connected to a radiant cooling panel and took theoretical heat losses into account. González-Altozano et al. [79] used thermocline widths as performance indicators, computed using a temperature distribution function fitted to measurements. Castell et al. [30] applied several stratification indices found in the literature on a charging process. Arslan and Igci [8] investigated the effects of simultaneous charging and discharging flow rates on stratification indices for a solar domestic hot water storage tank charged through a mantle heat exchanger. However, no indicator for system performance was presented. Haller et al. [84] presented an extensive literature review on measures representing the stratification efficiency for a charging, discharging or storage process. A stratification efficiency measure based on the internal loss of exergy, including the effects of heat losses, was developed by Haller et al. [85]. They applied the methodology to a charging - standby - discharging cycle but limit the system boundaries to the storage tank.

Dincer [46] compared two theoretical storage systems in a complete storage cycle. Temperatures and flow rates of theoretical charging and discharging flows were taken into account in an exergy based efficiency measure. However, only the charging and discharging flows were taken into account and not an actual heat pump or heat emission system.

The indices used to characterize stratification found in the literature are useful for comparing the effects of changing geometry on a single storage

tank process (charging, discharging or standby). However, they do not allow a quantitative comparison between different storage tanks, or charging and discharging strategies of a storage tank operating in a heating system as they only represent the amount of stratification and not the benefits of stratification for the complete system. When developing performance indicators for a hot water storage tank, this is best done in the context of the operation of the storage tank in the system of interest. Such indicators for hot water storage tank operation in a heating system, with a heat pump and heat emission system, were not found in the literature.

In the following paragraphs, energy based indicators for the operation of a storage tank in a heating system are presented. The indicators are defined in accordance with, and in the context of the above presented periodic simulations of a heating system. The *discharge ratio*, *storage efficiency*, *ideal charge ratio*, *ideal discharge ratio* and *effective storage capacity ratio* are indicators considering thermal energy. As this work considers a heat pump, two indicators considering electrical energy (the *electrical discharge ratio* and the *electrical storage efficiency*) are defined.

The amount of energy that the storage can supply to the emission system at the requested power is the first important quantity for evaluating storage performance. The ratio of actual discharged energy to the requested amount of discharge energy is defined as the *discharge ratio*.

$$\text{discharge ratio} = \frac{\text{discharge energy}}{\text{requested discharge energy}} \tag{3.7}$$

In figure 3.2 it is represented as the ratio of the light gray hatched area and the total light gray area. When the storage tank can supply the requested emission power during the full discharge phase, the discharge ratio is 1, otherwise it is less. The discharge ratio can thus be used to asses the storage capacity which is effectively usable during a storage cycle.

Another important indicator is the amount of discharged energy with respect to the amount of charged energy. The ratio of these quantities is a measure of the efficiency of the storage process and is thus called the *storage efficiency*.

$$\text{storage efficiency} = \frac{\text{discharge energy}}{\text{charge energy}} \tag{3.8}$$

As the simulations are periodic, the energy content of the storage is equal at the beginning and end of the simulations, and the storage efficiency is only influenced by the heat losses. In figure 3.2 the storage efficiency is represented as the ratio of the light gray hatched area and the dark gray hatched area. This definition is in line with the definition for thermal energy storage in the

structural thermal mass of a building presented by Reynders [148] and the overall energetic storage efficiency presented by Dincer and Rosen [47].

The storage efficiency is an important parameter as it determines the viability of shifting a heat load in time. Assume there is an incentive for shifting a heat load represented by low price of heat p_l at some time and a high price of heat p_h some time Δt later. If energy is stored at the time of the low price, only a part of this energy can be recuperated at the time of the high price due to heat losses. Let η denote the storage efficiency, which is naturally dependent of the time difference Δt, then shifting energy to the low price period is only viable if the cost of the recoverable energy is larger than the cost of the stored energy:

$$p_h \ \eta \ E \geq p_l \ E \qquad (3.9)$$

For load sifting to occur, the storage efficiency thus should be larger than the price ratio:

$$\eta \geq \frac{p_l}{p_h} \qquad (3.10)$$

It should be noted that in this analysis, the price of heat does not need to signify a monetary value. Different cost indicators, e.g. environmental impact, can be used as well.

The above presented indicators are dependent on the storage charge power set point and the requested emission power. To represent the results in a generic way, an *ideal charge ratio* is defined as the ratio of energy an ideally stratified storage tank would be able to store during the charge phase, divided by the maximum capacity of such an ideally stratified storage.

$$\text{ideal charge ratio} = \frac{\text{requested charge energy}}{\text{ideal storage capacity}} \qquad (3.11)$$

The capacity of an ideally stratified storage tank operating between the nominal generation supply temperature and the minimum emission return temperature can be computed as:

$$E_{\text{ideal}}^{\text{max}} = mc \left(T_{\text{gen,sup}}^{\text{nom}} - T_{\text{em,ret}}^{\text{min}} \right) \qquad (3.12)$$

With m the storage fluid mass.

If the maximum charge energy during the charge phase is less than the ideal storage capacity, the ideal storage ratio can be computed as the total dark gray area in figure 3.2 divided by the ideal storage capacity. For a real storage tank, the maximum charge energy will always be less than the ideal storage capacity.

It thus makes no sense to increase the charging power set point to values where the ideal charge ratio would be larger than 1 as no more energy will be stored.

If the emission power rises or the discharge phase lengthens, the amount of energy which needs to be stored to supply the requested power increases likewise. This can be represented as an *ideal discharge ratio* computed by dividing the requested energy during the discharge phase (the total light gray area in figure 3.2) by the capacity of an ideally stratified storage tank.

$$\text{ideal discharge ratio} = \frac{\text{requested discharge energy}}{\text{ideal storage capacity}} \tag{3.13}$$

If the ideal discharge ratio is larger than 1, the storage tank will not be able to supply the total amount of energy. However, it is interesting to investigate these situations as there will be differences in the actual amount of delivered energy between the possible charging and discharging strategies.

It should be noted that the ideal storage capacity, used in the definition of the ideal charge ratio and ideal discharge ratio, is not a storage tank property. As seen in equation (3.12), it depends on the generation system nominal supply temperature ($T_{\text{gen,sup}}^{\text{nom}}$) and the minimum emission return temperature ($T_{\text{em,ret}}^{\text{min}}$). The dependency on the minimum emission return temperature even causes it to be emission power dependent. If the emission temperature (T_{em}) remains constant, as is throughout this chapter, the minimum possible emission return temperature is dependent on the emission effectiveness which is mass flow rate and thus power dependent. Therefore, the ideal storage capacity can also be written as:

$$E_{\text{ideal}}^{\text{max}} = \varepsilon_{\text{em}} mc \left(T_{\text{gen,sup}}^{\text{nom}} - T_{\text{em}} \right) \tag{3.14}$$

This allows defining the emission system power independent ideal storage capacity, denoted as $E_{\text{ideal,em}}^{\text{max}}$, which is the maximum energy a storage tank can hold when operating between a nominal generation temperature ($T_{\text{gen,sup}}^{\text{nom}}$) and a building requiring energy at the emission temperature (T_{em}).

$$E_{\text{ideal,em}}^{\text{max}} = mc \left(T_{\text{gen,sup}}^{\text{nom}} - T_{\text{em}} \right) \tag{3.15}$$

For an ideal storage tank to be able to deliver this amount of energy at a power above zero, the emission system would have to be infinitely large. The merit of this measure is that it is emission power independent and thus provides an upper limit to the effective storage capacity.

A final interesting indicator is the maximum amount of energy a storage tank can discharge. For an ideally stratified storage tank, the discharge ratio is proportional to the ideal charge ratio until the ideal charge ratio is equal to the

ideal discharge ratio or the ideal charge ratio equals 1. For an actual storage tank, the discharge ratio will be less, suggesting a maximum discharge ratio occurring at an ideal charge ratio less or equal to 1. This maximum discharge ratio represents the maximum amount of energy that can be discharged at a specific ideal discharge ratio or emission power. This amount of energy can be seen as the effective storage capacity. Dividing the effective storage capacity by the power independent ideal storage capacity, the effective storage capacity ratio is formed:

$$\text{effective storage capacity ratio} = \frac{\text{maximum discharge energy}}{\text{power indep. ideal storage capacity}} \quad (3.16)$$

For an ideally stratified storage tank, the effective storage capacity ratio is equal to the emission system effectiveness. The reason to use the power independent ideal storage ratio in the definition is to be able to easily compute the effective capacity, in absolute units, from an effective capacity ratio. If the ideal storage capacity was used, the emission system effectiveness, which varies with emission power, would be required to compute the effective storage capacity in dimensional terms.

In the indicators described above, no assumptions were made concerning the heat generation system. All indicators are computed using the thermal energy transferred to the hydronic system. In a DR context, it is evident that this heat is generated using electricity as energy vector. If the heat is generated electrically with resistance heating elements, the efficiency of the heat generation will not depend significantly on the temperatures in the hydronic system and the above indicators can be directly used. However, if the heat is generated by a heat pump, the efficiency will depend on the generation supply temperature. Higher supply temperatures considerably decrease the heat pump coefficient of performance (COP). As the storage tank charging strategy affects the generation supply temperature, and thus the electrical power used by the heat pump, it is interesting to define indicators with respect to the electricity use of the system.

During storage tank discharging, the storage tank delivers the requested heat to the emissions system. The electrical energy that would be used by the heat pump if this amount of heat was supplied directly by the heat pump is called the discharge electrical energy. If the heat pump were to supply the requested heat during the entire discharge phase, its electricity use is denoted as the requested discharge electrical energy. In accordance with the above definitions, an *electrical discharge ratio* is defined as the ratio of the discharge electrical energy and the requested discharge electrical energy. This definition is equivalent to the definition of the *discharge ratio* on the electrical side.

$$\text{electrical discharge ratio} = \frac{\text{discharge electrical energy}}{\text{requested discharge electrical energy}} \quad (3.17)$$

During storage tank charging, the heat pump uses more electrical energy then it would to only supply the requested emission power. The difference between the electrical energy used by the heat pump while charging the storage tank and the electrical energy that would be required to only supply the requested emission power is called the charge electrical energy. In accordance with the *storage efficiency*, the *electrical storage efficiency* is defined as the ratio of the discharge electrical energy and the charge electrical energy.

$$\text{electrical storage efficiency} = \frac{\text{discharge electrical energy}}{\text{charge electrical energy}} \qquad (3.18)$$

This indicator thus represents the electrical energy used to compensate for the storage tank heat losses.

An effective capacity measure can also be defined from an electrical point of view. Here the effective electrical storage capacity ratio is defined as the maximum discharge electrical energy divided by the power independent ideal storage capacity.

$$\begin{array}{l}\text{effective electrical}\\\text{storage capacity ratio}\end{array} = \frac{\text{maximum discharge electrical energy}}{\text{power indep. ideal storage capacity}} \qquad (3.19)$$

These indicators can be used to compare storage cycles from an electrical viewpoint. However, to compute them, the temperature and load dependency of the heat pump performance is required, thus losing generality of conclusions.

3.4 Effects of operating strategy on storage cycle performance

A parametric study of the different charging and discharging strategies is performed. Periodic simulations are performed for 3 charging/discharging strategies: a storage tank which is charged at constant temperature and discharged with flow modulation, a storage tank which is charged with a minimum temperature difference and discharged with flow modulation and a storage tank which is charged at constant temperature and discharged with temperature modulation. The presented results are obtained for a 2 m^3 storage tank with an uninsulated height of 2 m. The in- and outflow ports are located 0.20 m from the top and bottom of the tank. The storage tank is insulated with 0.20 m flexible polyurethane foam with a conduction coefficient of 0.04 W/m K and is assumed to reside in a space with a constant temperature of 15°C. The storage tank is modeled in accordance with the model described in chapter 2.

Each simulation considered the variation of ideal discharge ratio of 0.5, 1.0, 1.5 and 2.0, ideal charge ratios between 0.2 and 1.0 and a period of 12h and 24h.

Examples of the resulting storage temperatures with an ideal discharge ratio of 1.0 and an ideal charge ratio of 0.8 are presented in figure 3.4. From these examples, the effects of the different charging and discharging strategies are clear. If the storage tank is charged at constant temperature and discharged with flow modulation (figure 3.4a), very stratified temperature distributions are seen throughout the entire storage cycle. Furthermore, the average temperature inside the discharged storage is close to the emission temperature. The slight increase in storage tank temperatures observed at the end of the discharge phase is caused by the increase of the emission return temperature. When the storage is nearly discharged, the emission supply temperature drops. To supply the same power, the emission mass flow rate rises, leading to a decrease in emission effectiveness and an increase in emission return temperature. As this higher temperature fluid enters the storage tank at the bottom, a rising buoyant jet is formed, leading to an overall increase in storage temperature.

On the other hand, if the storage tank is charged with a minimum temperature difference (figure 3.4b), initially a small stratification front is observed, however as soon as the storage fluid is replaced entirely, a nearly uniform temperature profile is observed throughout the storage tank. Mixing at the storage tank inflow port due to formation of a jet causes the small temperature difference between the inflow fluid and the storage fluid to dissipate even further. As the small temperature difference requires much higher mass flow rates, this effect is amplified.

Finally, if the emission system uses a mixing valve, and the emission power is controlled by altering the emission supply temperature (figure 3.4c), the average temperature in the discharged storage tank is higher than when flow modulation is used. If a mixing valve is used, the emission supply temperature is always less or equal to the temperature of the fluid exiting the storage tank and the mass flow rate through the emission system is the nominal mass flow rate. This leads to an increase in emission return temperature, which causes the discharged storage tank to be at a higher temperature. Thus, the effectively usable storage capacity is less.

In figure 3.5, the discharge ratio for all strategies is presented with varying ideal charge ratio and ideal discharge ratio. For comparison, the discharge ratio of an ideally stratified storage, without heat losses is also presented. From the definitions presented above, the discharge ratio of an ideally stratified storage is the ideal charge ratio divided by the ideal discharge ratio, limited to 1. If the ideal charge ratio is less than the ideal discharge ratio, the storage tank can never supply the complete requested emission energy during the discharge

(a) Fixed temperature charging, flow modulation discharging

(b) Minimum temperature difference charging, flow modulation discharging

(c) Fixed temperature charging, temperature modulation discharging
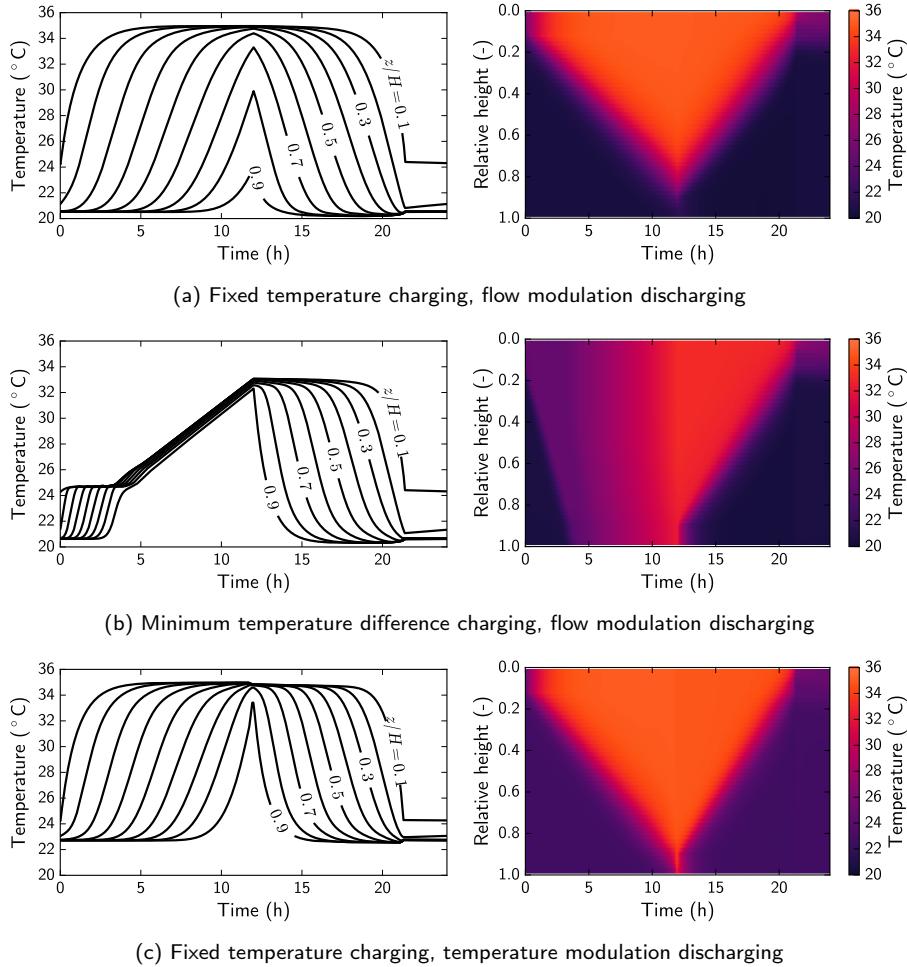
Figure 3.4: Examples of the storage temperature resulting from periodic simulations with different charging and discharging strategies, an ideal discharge ratio of 1.0 and an ideal charge ratio of 0.8 and a simulation period of 24 h. Temperature progress with time at different relative heights in the storage tank is presented on the left, the temperature profiles at different times are presented on the right.

phase. The used generation power is too small and the discharge ratio is less than 1 but close to the discharge ratio of an ideally stratified storage. There is a slight observable difference caused by heat losses. This situation corresponds to the situation with insufficient generation power in figure 3.3.

If the discharge ratio is 1, the storage tank can supply the full requested emission energy. As the ideal charge ratio rises, the actual period the storage tank is charged decreases and the average storage tank temperature rises. This corresponds to the situation with excessive generation power in figure 3.3.

At high ideal charge ratios and relatively large ideal discharge ratios, the storage tank charging ends before the end of the charge phase because no more energy can be transferred to the storage tank. Discharge ratios drop as the storage tank cannot supply the requested emission energy. This corresponds to the situation with insufficient storage capacity in figure 3.3. The maximum value of the discharge ratio can be seen as a measure for the effective storage tank capacity as it is the ratio of the maximum energy the storage tank can supply to the emission system and the requested amount of discharge energy.

Here differences between the different charging or discharging strategies are visible. The fixed temperature charging and flow modulation discharging strategy always has the highest maximum discharge ratio. The minimum temperature difference charging strategy follows, except at an ideal discharge ratio of 2 in the 12 h period simulations. The difference between maximum discharge ratio for the fixed temperature and minimum temperature difference charging strategies amounts up to 0.11 in the 12 h period simulations. In the 24 h period simulations the maximum difference is less. Overall differences between the 12 h period and 24 h period are small. Only when the storage capacity is insufficient, a slight increase in discharge ratio is observed in the 24 h period simulations. This can be explained as with equal ideal discharge ratio, the actual emission heat flow drops as the emission phase lengthens. This causes a lower flow rate through the emission system and thus a higher effectiveness and a lower return temperature. Furthermore, lower flow rates will induce less mixing in the storage tank, increasing stratification and its effective capacity.

In figure 3.6, the effective storage capacity ratio is presented as a function of the ideal discharge ratio. The effective storage capacity of an ideally stratified storage tank is also presented. For the discharge ratio of 0.5, no maximum discharge ratio could be computed as the storage tank never reached full capacity, the complete requested discharge energy was always supplied. For the 12 h period, the maximum discharged energy is 25.8 kWh, this amount can be discharged with the fixed temperature charging, flow modulation discharging strategy with an ideal discharge ratio of 1 and an ideal charge ratio of 0.9. For the 24 h period, the maximum discharged energy increases to 30.7 kWh which
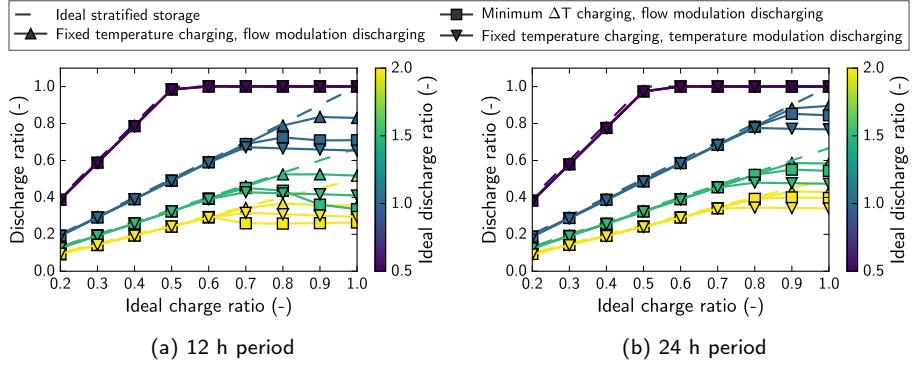
Figure 3.5: Discharge ratio with varying of ideal charge ratio, ideal discharge ratio and charging/discharging strategy for the 12 h period (left) and 24 h period (right) simulation.
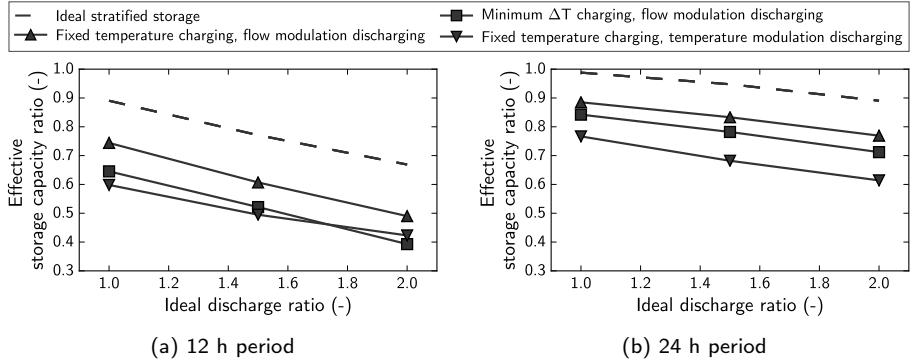
Figure 3.6: Effective storage capacity ratio with varying ideal discharge ratio and charging/discharging strategy for the 12 h period (left) and 24 h period (right) simulation.

occurs with the same strategy and an ideal discharge ratio of 1 and an ideal charge ratio of 1. In the former case, the capacity of an ideally stratified storage tank is 30.9 kWh while in the latter case it is 34.2 kWh. The power independent ideal storage capacity in both cases is 34.8 kWh. The increased energy storage capacity for the longer period is a result of lower flow rates and thus lower emission return temperatures.

In figure 3.7 the storage efficiency is presented with varying ideal charge ratio and ideal discharge ratio. Values are between 0.90 and 0.99. Differences between the different strategies are rather small and unclear. However, in the 24 h simulations the fixed temperature charging, flow modulation discharging strategy performs slightly better, especially at low ideal charge ratios.
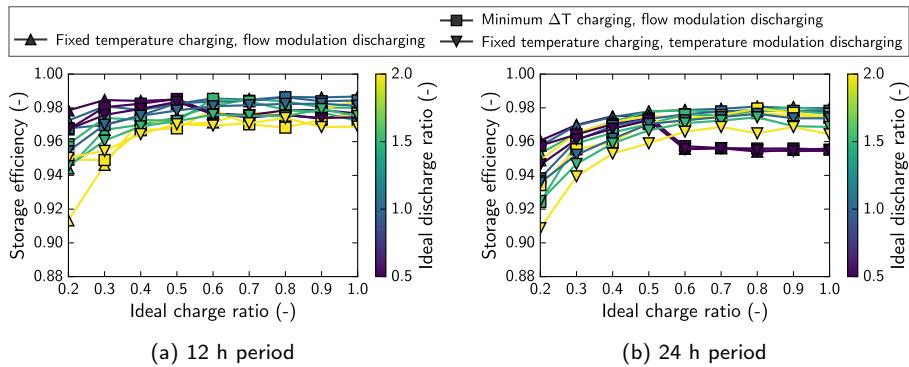
Figure 3.7: Storage efficiency with varying ideal charge ratio, ideal discharge ratio and charging/discharging strategy for the 12 h period (left) and 24 h period (right) simulation.

For ideal discharge ratios below 1, a decrease in efficiency is observed if the ideal charge ratio is above the ideal discharge ratio. In these cases, there is excessive generation power and the resulting average temperature increase implies a decrease in storage efficiency. For all other cases, the storage efficiency is seen to rise with rising ideal charge ratio and drop with increasing ideal discharge ratio. As the ideal charge ratio rises, the mixed zones near the inflow ports become less determining for the complete storage temperature distribution. This results in an increase in average emission supply temperature, and a reduction in emission return temperature. The result is that the unused part of the storage tank is at a lower temperature with higher ideal charge ratios. This leads to lower heat losses and a higher storage efficiency. An increase in ideal discharge ratio causes a decrease in emission effectiveness which in turn increases the emission return temperature, resulting in higher heat losses. In the 12 h period simulation, these observations are less clear.

The above presented results are independent of the type of heat generation system, as long as it can provide the requested temperatures and flows. If the heat is supplied by a heat pump, the heat pump COP can be taken into account in assessing the storage efficiency on the electrical side. As the COP varies with the generation supply temperature and the generation power, different values for storage efficiency are obtained. The results presented below are computed with the performance map of a commercial air to water heat pump with a fixed ambient temperature of $2°C$ [40].

Values of the electrical discharge ratio are similar to the thermal discharge ratio. Nevertheless, the effective electrical storage capacity ratio is a very useful indicator for comparing strategies and is presented in figure 3.8. The fixed
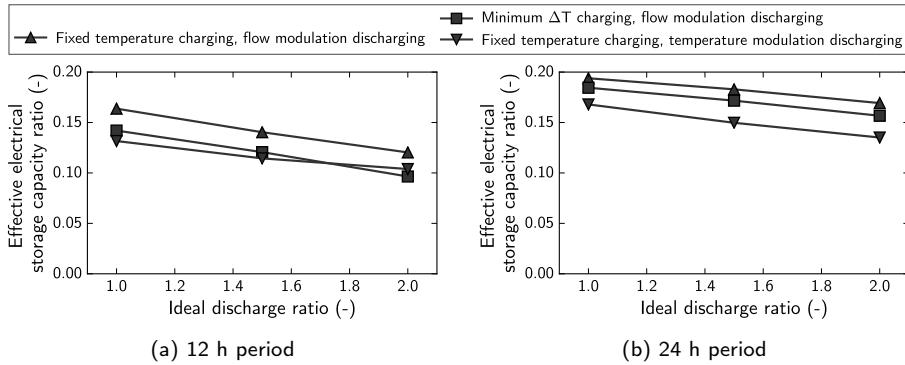
Figure 3.8: Effective electrical storage capacity ratio for different values of ideal discharge ratio and charging/discharging strategy for the 12 h period (left) and 24 h period (right) simulation.

temperature charging and flow modulation discharging strategy has the largest effective capacity ratio for all ideal discharge ratios. With increasing ideal discharge ratio, the effective capacity decreases due to a decrease in emission effectiveness and an increase of mixing inside the storage tank.

From figure 3.8, absolute values of maximum discharge electrical energy which represent the electrical storage capacity of the storage tank can be computed. For the 12 h simulation period, the 2 m³ storage tank can replace the use of 5.7 kWh, 4.9 kWh and 4.6 kWh for the strategy with fixed temperature charging and flow modulation discharging, the strategy with minimum temperature difference charging and flow modulation discharging and the strategy with fixed temperature charging and temperature modulation discharging respectively. For the 24 h simulation period, the electrical discharge energy is 6.7 kWh, 6.4 kWh and 5.8 kWh for the strategy with fixed temperature charging and flow modulation discharging, the strategy with minimum temperature difference charging and flow modulation discharging and the strategy with fixed temperature charging and temperature modulation discharging respectively. The observed difference in effective electrical storage capacity between the fixed temperature charging and minimum temperature difference charging strategies is rather large, 4 to 14%.

The above described variation of the maximum discharge energy, both thermal and electrical, illustrates the difficulty in defining a state of charge measure for hot water storage tanks similar to the state of charge as defined for electrical batteries. The maximum amount of discharge energy or the effective storage capacity is strongly affected by the requested emission power. Thus defining an independent state of charge measure representing how much energy can be

discharged is not possible.

However, when the average required emission power can be predicted or estimated, for example through prediction of the average ambient temperature and solar gains, a useful and approximative measure can be computed. Starting from a storage tank temperature profile and average emission power, a discharging simulation much like the 2nd half of the simulation presented above can be performed. This simulation leads to the amount of energy that can be discharged starting from the temperature profile. This amount of energy can then be compared to the effective storage capacity at the specific emission power to obtain a state of charge measure. The state of charge could thus be computed as:

$$\text{state of charge} = \frac{\text{discharge energy}}{\dfrac{\text{effective storage}}{\text{capacity ratio}} \times \dfrac{\text{emission indep.}}{\text{storage capacity}}} \quad (3.20)$$

The emission independent storage capacity is easy to compute and the effective storage capacity ratio can be computed in advance for the specific storage tank - generation system - emission system combination as described above. The computation of the discharge energy is not straightforward as it requires a dynamic simulation and the knowledge of the storage temperature distribution. In practice this distribution is hard to obtain as measuring it would require many temperature sensors distributed vertically inside the storage tank to properly estimate the location and height of the thermocline. However, state estimation techniques exist utilizing the measurement history of only two to three temperature sensors and a flow rate measurement which can provide an adequate estimation of the storage tank temperature profile [113].

In figure 3.9 the electrical storage efficiency is presented. This figure differs significantly from figure 3.7, presenting the thermal storage efficiency. The most notable change is the difference in efficiency when the storage is charged with the minimum temperature difference strategy. For the 24 h period simulations, the difference goes up to 40 percentage points. As the heat pump efficiency is strongly dependent on the generation supply temperature, less electrical energy is required to charge the storage tank with the minimum temperature difference strategy as the average generation supply temperature is lower. With the minimum temperature difference strategy, if the charge ratio increases the average generation supply temperature increases, leading to a large decrease in electrical storage efficiency. If the generation supply temperature is fixed, the electrical storage efficiency increases, reflecting the increase in thermal storage efficiency. Differences between discharging strategies are negligible.
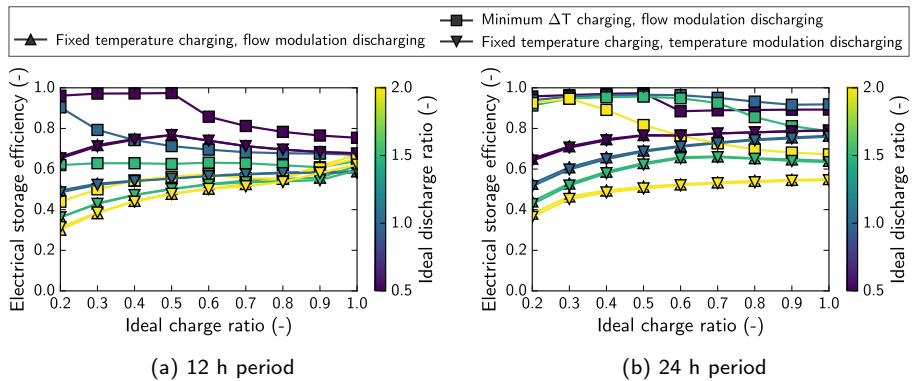
Figure 3.9: Electrical storage efficiency with varying ideal charge ratio, ideal discharge ratio and charging/discharging strategy for the 12 h period (left) and 24 h period (right) simulation.

Overall, the electrical storage efficiency is much less than the thermal storage efficiency. The electrical storage efficiency ranges from 0.30 to 0.97. Without storage, the generation supply temperature does not need to be higher than the minimum emission supply temperature, which results in high COP's. When the storage tank is charged, the generation supply temperature necessarily increases, decreasing the COP. Therefore, significantly more electrical energy is used to charge the storage tank, than would be required to directly supply heat to the emission system during the discharge phase, reducing the electrical storage efficiency.

3.4.1   Discussion

The presented results provide several insights into the selection of charging and discharging strategy of a hot water storage tank included in a heating system. First of all, discharging the storage tank with a temperature modulation emission system is inferior to flow modulation in all cases. Temperature modulation causes the effectively useful storage capacity to decrease, results in a slightly lower thermal storage efficiency and causes a very small decrease in electrical storage capacity. A variable flow emission system is thus preferred over an emission system using a mixing valve. This however requires a frequency controlled pump in the emission system which will increase the investment costs. On the other hand, a frequency controlled pump will consume less electricity which might result in an overall reduction in costs related to the emission system.

The selection of charging strategy is less obvious. Charging at a fixed temperature results in the highest effective storage capacity ratios, meaning more energy can be stored. On the other hand, if the storage tank is charged with a heat pump, minimum temperature difference charging results in higher electrical storage efficiencies leading to less overall energy use.

A combination of both strategies could be useful. When predictions indicate only small gains can be achieved when the storage tank is used to the full extent, the storage can be charged with a minimum temperature difference. When in another period the full storage tank capacity is required, it can be charged with a fixed generation supply temperature. This hybrid charging strategy would result in optimal electrical storage efficiency when only part of the storage tank capacity is required while retaining the maximum effective capacity when it is necessary. To determine whether or not to the full storage capacity is required, several optimal control problems, or a mixed integer optimal control problem must be solved applying the different charging strategies at different times. The optimization must take into account that a change in strategy is only allowed when the storage tank is nearly full or nearly empty.

Minimum temperature difference charging however poses another downside. If the storage tank is charged up to a certain level, the available emission power from the storage tank is fixed. A lower ideal charge ratio leads to a decrease in available emission power. If predictions considering the required future emission power are correct, this poses no threat. However, predictions are seldom correct and if the required emission power is underestimated, the storage tank will not be able to supply the requested power and the heat generation system must be addressed at undesirable times. If the storage tank is charged with a fixed generation supply temperature, the available emission power is rather independent of the ideal charge ratio as fixed temperature charging leads to a more stratified temperature profile. Thus, from a robustness point of view, fixed temperature charging has the advantage.

The analysis conducted above could easily be repeated for a storage tank charged through an immersed heat exchanger. However, from the results presented in chapter 2 it is clear that charging through an immersed heat exchanger induces more mixing than direct inflow charging. The difference in temperature profiles, and thus effective storage capacity, between the fixed temperature charging and minimum temperature difference charging will be smaller. Furthermore, the additional limited heat exchanger effectiveness poses an additional constraint on the charging power. This makes charging a storage tank through an immersed heat exchanger less suitable for use in a heat pump space heating context, where strict separation of storage fluid and charging fluid is not required.

3.5 Conclusion

When a storage tank is integrated in a heating system, several strategies are available for charging and discharging the storage tank. In order to maximize the benefit of the storage tank, strategies which deliver most merits must be selected.

In this chapter a methodology for evaluating the operation of a storage tank integrated in a simplified heating system is developed. In relation to this, several performance indicators are derived, the most interesting of which are the effective storage capacity ratio and the electrical storage efficiency. Several charging and discharging strategies are presented and compared qualitatively and quantitatively based on the developed methodology and indicators. Furthermore, a state of charge measure is defined which can be computed similarly to the presented methodology and is a representation of the amount of energy that can be discharged by a storage tank constrained by an emission system.

Finally, fixed temperature charging and flow modulation discharging are selected as the strategies most suitable in a residential DR heat pump space heating context. Furthermore, direct inflow charging is chosen above immersed heat exchanger charging in applications where mixing of storage and charging fluid is allowed. In the following chapters these charging and discharging strategies will be used.

Chapter 4

Optimal control of hot water storage tank based space heating systems

4.1   Introduction

The control of a system including any form of energy storage is a non-trivial task. Such a storage based system requires the control to take into account predictions of the energy requirement and to estimate the future state of the system in response to current control actions. Model predictive control is able to perform these tasks provided that a model representing the system behavior sufficiently well is available.

The goal of this chapter is to compare different optimal control formulations for a residential heating system with a heat pump and hot water storage tank. The accuracy of results obtained by open-loop optimizations is assessed and

an optimal control formulation suitable for use in a full year model predictive control simulation is selected.

This chapter is structured as follows. In section 4.2, the concepts of optimal control and model predictive control are introduced with emphasis on the methods used in this work. Subsequently, in section 4.3, optimal control approaches for heating systems using thermal energy storage found in the literature are discussed. Next, in section 4.4, several optimal control formulations for a system including a hot water storage tank are developed and compared based on their open-loop performance. In section 4.5, a subset of the formulations developed in the previous section is used in a model predictive control simulation to assess their merits. Finally, in section 4.6, conclusions are formulated.

4.2   Optimal control and model predictive control

Given a controlled system represented in state-space form with the vector $\boldsymbol{x}(t)$ representing the state of the system, the vector $\boldsymbol{u}(t)$ representing the control inputs and the vector $\boldsymbol{p}$ representing known parameters, the variation of the state vector in time can be computed from a system of 1st order ordinary differential equations (ODE):

$$\frac{\mathrm{d}\boldsymbol{x}(t)}{\mathrm{d}t} = \boldsymbol{f}\left(\boldsymbol{x}(t), \boldsymbol{u}(t), \boldsymbol{p}, t\right) \tag{4.1}$$

Optimal control attempts to find the value of control inputs, $\boldsymbol{u}(t)$, over time, so that the performance of the system is optimal in some way. Optimality can mathematically be expressed as a certain objective functional which is minimized [77, 135]. In general, the objective functional can be written in the Lagrange form [120]:

$$J = \int_{t_0}^{t_\mathrm{f}} \mathcal{L}\left(\boldsymbol{x}(t), \boldsymbol{u}(t), \boldsymbol{p}, t\right) \mathrm{d}t \tag{4.2}$$

Where $t_f - t_0$ is the control horizon. In the literature, a distinction is made between the control horizon, the time span for which the inputs are computed, and the prediction horizon, the time span for which the system output is computed [2]. Throughout this work however, the prediction horizon and control horizon are taken equal.

Usually, the operation of the system is constrained, which implies certain combinations of states and inputs can or should not occur. This can be written as:

$$c\left(\boldsymbol{x}(t), \boldsymbol{u}(t), \boldsymbol{p}, t\right) \leq 0 \tag{4.3}$$

As all possible control inputs $\boldsymbol{u}$ are continuous, this forms an infinite dimensional problem which can be solved by solving the Hamilton-Jacobi-Bellman equation [77]. An alternative approach is to discretize the states and inputs over time, transforming the problem to a finite dimensional problem. The differential equation governing the state of the system (equation (4.1)) is then transformed to a set of equality constraints for the optimization problem. Such a method is called a *direct collocation method* [135].

The direct collocation method used in this work goes as follows: divide the control horizon in M intervals. Approximate the states ($\boldsymbol{x}$) as a quadratic function in each interval and the control inputs ($\boldsymbol{u}$) as constant over each interval. Let $\boldsymbol{x}_i$ denote the value of $\boldsymbol{x}$ at time t_i. In the interval t_i to t_{i+1} the continuous state equation (4.1) is transformed to:

$$\frac{\boldsymbol{x}_{i+1} - \boldsymbol{x}_i}{t_{i+1} - t_i} = \frac{1}{2}\Big(\boldsymbol{f}\left(\boldsymbol{x}_i, \boldsymbol{u}_i, \boldsymbol{p}, t_i\right) + \boldsymbol{f}\left(\boldsymbol{x}_{i+1}, \boldsymbol{u}_i, \boldsymbol{p}, t_{i+1}\right)\Big) \tag{4.4}$$

The ODE system governing the states of the system is thus represented by $M - 1$ equality constraints. The integral in the objective functional is now written as a function of the discrete states and inputs by using the trapezoidal rule:

$$J = \sum_{i=1}^{M-1} \frac{1}{2}\Big(\mathcal{L}\left(\boldsymbol{x}_i, \boldsymbol{u}_i, \boldsymbol{p}, t_i\right) + \mathcal{L}\left(\boldsymbol{x}_{i+1}, \boldsymbol{u}_i, \boldsymbol{p}, t_{i+1}\right)\Big)\left(t_{i+1} - t_i\right) \tag{4.5}$$

Other system constraints are only enforced in the discretization points resulting in:

$$c\left(\boldsymbol{x}_i, \boldsymbol{u}_i, \boldsymbol{p}, t_i\right) \leq 0 \qquad \forall\ i \tag{4.6}$$

The infinite dimensional continuous optimal control problem is thus transformed into a finite dimensional mathematical optimization problem with variables $\boldsymbol{x}_i$ and $\boldsymbol{u}_i$:

$$\underset{\boldsymbol{x}_i, \boldsymbol{u}_i}{\text{minimize}} \ J = \sum_{i=1}^{M-1} \frac{1}{2} \Big(\mathcal{L}\left(\boldsymbol{x}_i, \boldsymbol{u}_i, \boldsymbol{p}, t_i\right) + \mathcal{L}\left(\boldsymbol{x}_{i+1}, \boldsymbol{u}_i, \boldsymbol{p}, t_{i+1}\right) \Big) \big(t_{i+1} - t_i \big)$$

subject to (4.7)

$$\frac{\boldsymbol{x}_{i+1} - \boldsymbol{x}_i}{t_{i+1} - t_i} = \frac{1}{2} \Big(\boldsymbol{f}\big(\boldsymbol{x}_i, \boldsymbol{u}_i, \boldsymbol{p}, t_i\big) + \boldsymbol{f}\big(\boldsymbol{x}_{i+1}, \boldsymbol{u}_i, \boldsymbol{p}, t_{i+1}\big) \Big) \qquad \forall\, i$$

$$\boldsymbol{c}\left(\boldsymbol{x}_i, \boldsymbol{u}_i, \boldsymbol{p}, t_i\right) \leq 0 \qquad\qquad\qquad \forall\, i$$

The input vector $\boldsymbol{u}^*$ which minimizes the cost function is called the optimal program. Depending on the characteristics of the functions $\mathcal{L}$, $\boldsymbol{f}$ and $\boldsymbol{c}$, the optimization problem can be categorized. If the objective is an affine function and all constraints are linear functions of the optimization variables, the problem is called a *linear programming problem* (LP). LPs are easy to solve with state-of-the-art algorithms and problems with thousands of variables and constraints are solved with a computation time in the order of seconds.

Algorithms exist to solve problems with variables that are constrained to only have integer values. If the the relaxed problem, obtained by omitting the integer requirements, is an LP, the problem is called a *mixed integer linear programming problem* (MILP). Although the solution of such problems is possible if the amount of integer variables is limited, the required solution time is often considerably longer than for an LP of the same size.

If the cost function and inequality constraints are convex functions and the equality constraints are linear functions, the problem is called a *convex programming problem*. Very efficient algorithms exist for solving convex programming problems [23]. A special case, where the function $\mathcal{L}$ is a quadratic function and all constraints are linear functions, is called a *quadratic programming problem* (QP). If the problem also contains quadratic terms in the inequality constraints, it remains convex as long as the matrix describing the quadratic terms in the constraints is positive semidefinite. Such a problem is called a *quadratically constrained quadratic programming problem* (QCQP).

If at least one constraint or the objective function is non-convex, the optimization problem is non-convex and it is generally called a *non-linear programming problem* (NLP). In general it is very difficult to find the global optimum of an NLP. Starting from an initial guess, it is possible to find a local optimum, and efficient algorithms, capable of handling large scale problems, are available. However, solver settings required for a good solution are often very problem specific [23].

If a physical system is to be controlled, solving an open-loop optimal control

problem (OCP) and applying the complete solution as system inputs, called open-loop optimal control, may lead to undesired system behavior as there is no stabilizing feedback and disturbances present in reality are not anticipated in the OCP. One way to introduce feedback is to only apply a single time step of the OCP solution to the actual system. After the system has evolved during that time step, the states of the OCP are estimated from measurements and the process is repeated. Such a control strategy is generally referred to as model predictive control (MPC) [4, 27].

This chapter investigates the performance of different OCP formulations in an MPC by simulation. Here, the actual system is replaced by a system emulator which uses a relatively detailed model, able to predict the system response. The time interval of interest is divided in several control time steps. Each control time step, an OCP is solved, minimizing an objective function over a certain control horizon. The first element of the control input vector is then applied to the system emulator, which simulates the system behavior during the time step. At the end of the time step, the system states required for the OCP are determined from the system emulator results and the process is repeated. Such an approach is sometimes referred to as moving horizon optimal control or receding horizon optimal control.

4.3 Optimal control of hot water storage tanks: literature review

Several authors have applied open-loop optimal control to various systems with hot water storage tanks. In most publications the storage tank is modeled as an energy storage for which the energy transfers to and from the storage tank are independent of the storage tank temperature distribution. In this work such a model is referred to as a temperature independent state-of-charge model. Ren et al. [147] used such a model to optimize the operation and sizing of several components in a combined heat and power plant (CHP). Fragaki et al. [70] optimized the size of a storage tank connected to a CHP unit and a backup boiler to maximize the net present value of the investment in the context of the UK electricity market. Streckiené et al. [167] performed a similar analysis for the German spot market. The thermal energy storage tank is modeled as a temperature independent state-of-charge model in both studies. Kopanos et al. [111] investigated the benefits of a micro-grid including a heat network where electricity and heat are supplied by a CHP. They considered local hot water storage tanks and a centralized energy buffer which were all modeled as temperature independent state-of-charge storages. Mehleri et al. [121] used a similar model in a distributed electricity generation context with

CHP and photovoltaic (PV) electricity production combined with a heat network and thermal energy storage. Using this model they computed optimal control programs and optimal distributed generation and storage tank capacities for a small network of 5 buildings in Greece while minimizing the total annual energy cost. Henze et al. [89] used a loss-free temperature independent state-of-charge model to generate optimal programs for a base chiller and a dedicated thermal energy storage chiller to shift cooling loads for an office building. They considered a chiller with constant COP, independent of ambient or outflow temperatures which further affects the accuracy of the results. Menon et al. [122] computed optimal control programs for thermal and electrical energy converters, including heat pumps distributed over a set of 5 buildings. They included a thermal storage tank which was modeled as a temperature independent state-of-charge storage.

In the literature, the temperature independent state-of-charge model is often used for optimal scheduling of CHP plants or chillers connected to a thermal energy storage tank. As this model simplifies the storage tank behavior considerably, there is no guarantee that an actual storage tank is able to supply the predicted amount of energy. In the context of space heating by CHP, this simplification might be justifiable as the generation temperature is probably considerably higher than the heat demand temperature. If however the temperature difference is smaller, as in the context of residential heating with heat pumps, the assumption of temperature independence is flawed. As shown in chapter 3, the effective storage capacity of a storage tank in such a system is considerably lower than the capacity of an ideal stratified storage tank and decreases with discharge power. The system energy use obtained from an open-loop optimization with a temperature independent state-of-charge storage tank model is thus questionable as the effective storage capacity of a real storage tank differs and the power a storage tank can deliver to an emission system is temperature dependent.

Some authors use moving horizon optimal control simulations with the same model for the emulator and the optimization problem to compute the optimal operation of systems for a full year period. When long time span results are required, the solution of an OCP spanning the entire time span may require too much memory or computation time. With a moving horizon optimal control approach this can be resolved by optimizing a limited control horizon, for instance a week, and assuming the solution of the OCP represents the actual system state. The control horizon can then be shifted to some extent, for instance a day, for the next optimization problem. The control horizon length and overlap between subsequent control horizons are crucial in such a simulation. The length of the horizon must be sufficiently larger than the largest time constant in the system to ensure current actions are optimal for

future needs. The required overlap between horizons is more difficult to quantify, however, larger overlaps lead to more optimal operation as information about future conditions is taken into account in more intervals.

Kriett and Salani [114] used a temperature independent state-of-charge storage tank model in such a moving horizon optimal control simulation of a residential micro grid. They computed optimal operation for a boiler and CHP unit in a system with solar thermal collectors, PV electricity production and thermal and electrical energy storage. Arteconi et al. [11] used a similar approach with a state-of-charge domestic hot water storage tank model to determine optimal heat pump operation in a DR context. They constrained the operation of the storage tank tightly by stating that the minimum average storage temperature must always be higher than the domestic hot water demand temperature. This ensures that even if the storage tank behaves like a completely mixed tank, domestic water comfort is always guaranteed.

Fux et al. [73] combined a temperature independent state-of-charge model with a multi layer storage tank model embedded in a detailed building emulator to schedule the operation of several heat generation systems. They computed the net present value of investments and operational greenhouse gas emissions for various component sizes and presented a trade-off curve between both. However, as in the emulator the storage tank is able to operate at multiple temperature levels and in the OCP formulation this is almost completely neglected, the resulting control programs are expected to be suboptimal. As a consequence, different combinations of component sizes could be on the Pareto-front. A comparison between the emulator and controller model should be made to check the model mismatch.

Patteeuw and Helsen [137] proposed a multi temperature-level linear approach for a domestic hot water storage tank, and compared the average temperature profiles resulting from an open-loop optimization with the results from a detailed emulator. The multi-level approach combines 3 temperature independent state-of-charge models operating between different temperature levels and enables storage charging at different temperature levels. During discharging, the average storage tank temperature must be larger than the demand temperature leading to a tight discharging constraint. They found a reasonable accordance between the optimization and the emulator, however the average temperature computed by the emulator is up to 6 K less than the temperature predicted by the optimization. This could lead to significant discomfort for the domestic hot water users if the errors are not corrected.

From the analysis in chapter 3 it is concluded that when an actual hot water storage tank is installed in a heating system with finite size heat exchangers, the temperature distribution inside the storage tank is important. Due to the

non-linear nature of such a system, the use of linear optimal control formulations might be insufficient to obtain good control performance [4]. However, in the literature, only temperature independent state-of-charge models are used to generate optimal programs for systems including a hot water storage tank. In an open-loop OCP this gives rise to uncertainty on the results, while in an MPC simulation optimal control formulations which lead to better system performance may exist.

This work presents several OCP formulations for a residential heating system with a heat pump and storage tank. The open-loop solutions of the formulations are compared with an emulator containing a detailed model for the storage tank to asses the accuracy of an open-loop OCP. Next, some formulations are implemented in an MPC simulation of the heating system to select the OCP formulation most suitable for this application.

4.4 Comparing hot water storage tank models for optimal control

To compare the open-loop performance of OCP formulations containing different hot water storage tank models, a system similar to that in chapter 3 is considered. The system consists of a heat generation unit, hot water storage tank and idealized emission system supplying heat to a building (figure 4.1). As in chapter 3 was concluded that a flow modulation emission system is superior to a temperature modulation emission system, the mixing valve is omitted. The heat generation unit supplies water at the generation supply temperature ($T_{\mathrm{gen,sup}}$) to the hot water storage tank or to the emission system. The emission system receives water at the emission supply temperature ($T_{\mathrm{em,sup}}$) which originates from the heat generation unit or the hot water storage tank or a combination of both. The emission return temperature ($T_{\mathrm{em,ret}}$) is returned to the storage tank or heat generation unit. During storage charging, the heat generation unit receives water from the storage tank and emission system, resulting in the generation return temperature ($T_{\mathrm{gen,ret}}$). An auxiliary heater is added which can supply heat ($\dot{Q}_{\mathrm{aux}}$) to the emission system directly. The building dynamics are not included in the presented optimizations, to focus on the effects of the storage tank model. However, the emission system temperature (T_{em}) and power demand ($\dot{Q}_{\mathrm{em}}^{\mathrm{dem}}$) are computed from a prior optimization including a simplified building model, and used as input here.
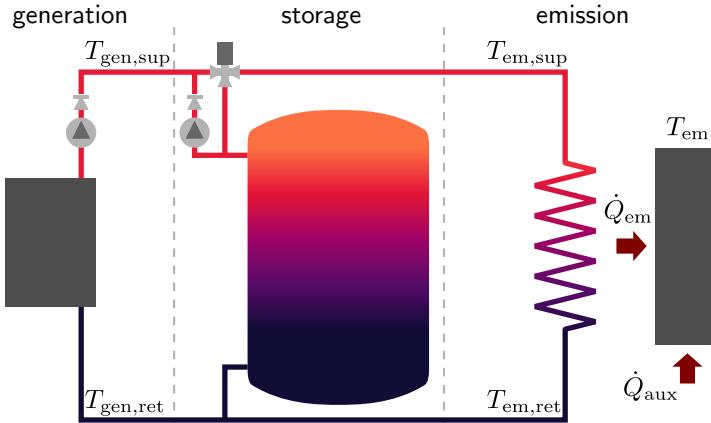
Figure 4.1: Schematic representation of the simplified heating system.

4.4.1 Methodology

The methodology followed for comparing different OCP formulations is presented schematically in figure 4.2. The methodology starts from a fixed set of boundary conditions, representing known disturbances over the comparison time horizon, e.g. heat flow demand, electricity price,... . In this section, and throughout this thesis, perfect predictions of all disturbances are assumed. With these boundary conditions, an OCP is solved using an objective of minimum energy cost. This results in a set of control signals for the generation heat flow rate and the generation supply temperature over the control horizon. Subsequently, these signals serve as input to a dynamic system simulation, the system emulator, where the storage tank is modeled in detail as presented in chapter 2. Other system components are modeled more simplified, similar to how they are implemented in chapter 3 and the OCP.

The three dimensional phenomena occurring in a storage tank during charging, cannot be easily implemented in an OCP. The resulting formulation would be non-convex to such an extent that solving them in a reasonable time is no longer possible without using a super computer. When constructing models for these three dimensional phenomena, often mass flow rates and temperatures are multiplied in for instance an energy balance. As this results in the multiplication of optimization variables in an equality constraint, the formulations are non-convex [23]. In an OCP therefore, simplifications of the storage tank model are required. These simplifications lead to a model mismatch between the storage tank model in the OCP and the emulator. The result is that if the heat generation schedule is followed strictly, the requested heat demand is probably
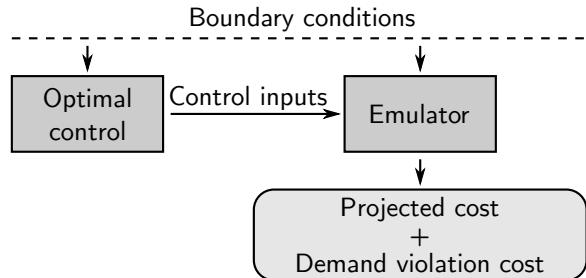
Figure 4.2: Schematic representation of the followed methodology for comparing different OCP formulations.

not delivered at all times. If this is not handled properly, it results in a different thermal comfort for the building inhabitants depending on the OCP formulation, making it difficult to compare formulations. In this section this issue is handled by including an auxiliary heat generation unit, which can supply heat directly to the emission system and makes up the difference between the heat supplied by the primary heating unit and the heat demand. If a cost is assigned to heat generated by the auxiliary heater, it can be added to the costs incurred by the primary heating unit and a quantitative comparison based on a single cost is possible. As the heat generation unit model is the same in the OCP and emulator, the costs incurred by the primary heating unit are equal to the costs predicted by the OCP and are thus called projected costs. Auxiliary heater costs are called demand violation costs.

It must be noted that in the above presented approach, the cost assigned to auxiliary heat generation is arbitrary, thus making the comparison arbitrary. It is however reasonable to assume a specific, low investment, heat generation unit to serve as auxiliary heater, eliminating the arbitrary nature. In the current section an electric resistance heater is assumed to supply auxiliary heat.

Another option to compare different formulations is not to add the projected and demand violation costs but to present them as independent quantities and generate a trade-off curve. The demand violation cost can then also be seen as discomfort for the inhabitants as it is the cost of alleviating the discomfort. If this is done, the selection of the most suited formulation is less clear, however, formulations away from the Pareto-front can be easily discarded as they are sub-optimal.

(a) Ambient temperature
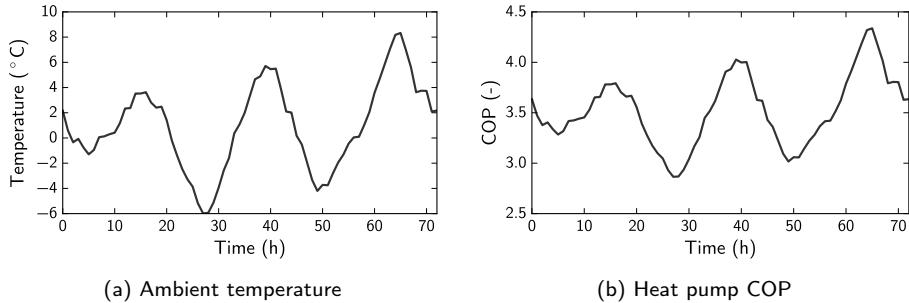
(b) Heat pump COP

Figure 4.3: Assumed ambient temperature (left) and corresponding heat pump COP for a generation supply temperature of 35°C (right).

4.4.2   System emulator and boundary conditions

In the system emulator a 2 m^3 hot water storage tank is modeled in accordance with the method presented in chapter 2. The storage tank has an uninsulated height of 2 m and is charged and discharged through direct inflow ports located at 0.20 m from the top and bottom. The storage tank is insulated with 0.20 m thick flexible polyurethane foam with a heat conduction coefficient of 0.04 W/m K and is assumed to be located in an unheated technical room at a constant temperature of 15°C (T_{hl}).

The heat generation unit is assumed to be an air coupled heat pump and is modeled as a heat supply with a controllable generation supply temperature ($T_{\mathrm{gen,sup}}$). In most OCP formulations, this supply temperature is chosen constant at 35°C as this maximizes the effective storage capacity. However, a formulation which allows variations in the supply temperature is also presented. The heat pump COP is assumed to be dependent on the temperature difference between generation supply temperature and ambient temperature according to:

$$\mathrm{COP} = \frac{1}{a_0 + a_1(T_{\mathrm{gen,sup}} - T_{\mathrm{amb}}) + a_2(T_{\mathrm{gen,sup}} - T_{\mathrm{amb}})^2} \qquad (4.8)$$

With T_{amb} the ambient temperature and coefficients $a_0 = 0.1499$, $a_1 = -0.4002 \times 10^{-3}$ 1/K and $a_2 = 0.1283 \times 10^{-3}$ 1/K^2 fitted from manufacturer data [40]. If the generation supply temperature is fixed, this results in a COP which is only time dependent and thus can be implemented as a parameter in the optimization problem. Values for the assumed ambient temperature and the COP variation in time with a fixed generation supply temperature of 35°C are presented in figure 4.3.

The auxiliary heater is assumed to be an electric resistance heater supplying heat directly to the building. The efficiency at which this occurs is assumed to be 100%.

The emission system is modeled as a heat exchanger transferring heat between the emission fluid flow and a uniform emission temperature (T_{em}). Dynamic effects in the emission system are not taken into account. The system nominal mass flow rate ($\dot{m}^{nom}$) is chosen to be 0.5 kg/s with a nominal effectiveness (ε_{em}^{nom}) of 0.4 which are typical values for a residential floor heating system [97]. The emission system effectiveness can then be calculated from:

$$UA_{em} = -\dot{m}^{nom} c \ln\left(1 - \varepsilon_{em}^{nom}\right) \tag{4.9}$$

$$\varepsilon_{em} = 1 - \exp\left(-\frac{UA_{em}}{\dot{m}_{em} c}\right) \tag{4.10}$$

The emission temperature (T_{em}) and emission power demand ($\dot{Q}_{em}^{dem}$) are assumed to be known in advance. Hereby it is assumed that no flexibility is available in the building, f.i. with strict temperature set-point tracking, or that the building's storage capacity is already used to its full extent. The current approach thus focuses on the storage tank as the sole source of flexibility. The emission system temperature (T_{em}) varies slightly in time with values between 24°C and 25°C. The emission power demand is presented in figure 4.4a.

In the above described system, interactions of the heating system with the electricity grid are assumed static. This results in fixed signals for the electricity price (p_{el}) and a maximum generation heat flow rate ($\dot{Q}_{gen}^{max}$) profile which are treated as boundary conditions.

Two reference scenarios have been chosen as two distinct control situations can arise in a DR context. On the one hand we can assume the control has a strong power limitation. This results in the *power limit* scenario (figure 4.4a and 4.4b). On the other hand we can assume that strong variations in electricity price may exist as would be the result of a very open electricity market. This results in the *price variation* scenario (figure 4.5a and 4.5b). A relative electricity price is presented here by dividing the price by its average. In both scenarios possible feedback of the heating system to the electricity generation side is neglected. For both cases the demanded emission heat load is equal and varies in time as depicted in figure 4.4a and 4.5a.

As inputs, the emulator receives the values of the desired heat pump power ($\dot{Q}_{gen}$), the desired heat pump supply temperature ($T_{gen,sup}$) and the emission power demand ($\dot{Q}_{em}^{dem}$). These are converted to mass flow rate values through

(a) *Power limit* scenario, heat flow rates

(b) *Power limit* scenario, relative electricity price
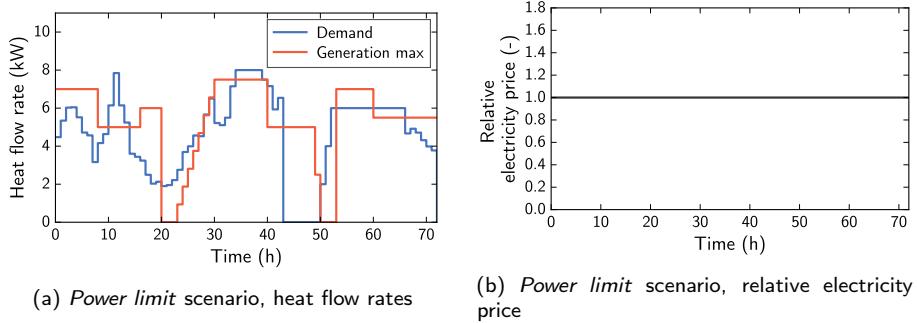
Figure 4.4: System boundary conditions related to the *Power limit* scenario.

(a) *Price variation* scenario, heat flow rates

(b) *Price variation* scenario, relative electricity price
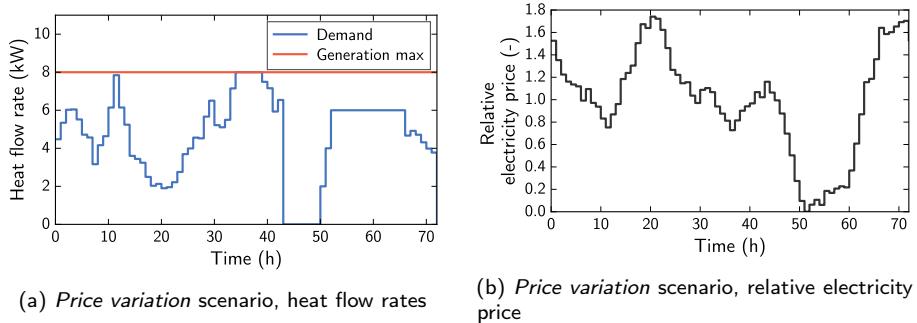
Figure 4.5: System boundary conditions related to the *Price variation* scenario.

the generation and emission system based on in- and outflow temperatures or set-points.

4.4.3 OCP formulations

In this subsection, different storage tank models are implemented in an optimal control formulation for the above described system. The generation heat flow rate ($\dot{Q}_{\mathrm{gen}}$) and generation supply temperature ($T_{\mathrm{gen,sup}}$) can be selected as the main optimization variables. The auxiliary heater power ($\dot{Q}_{\mathrm{aux}}$) is added to ensure feasibility at all times.

Throughout this section, the optimization problem objective is defined to minimize the cost of heating. For heat generated by the heat pump with a certain COP and by the auxiliary heater with a time dependent electricity price $p_{\mathrm{el},i}$, this is formulated as:

$$\underset{\dot{Q}_{\mathrm{gen},i},\dot{Q}_{\mathrm{aux},i},T_{\mathrm{gen,sup},i}}{\text{minimize}} \quad J = \sum_{i} \left(\dot{Q}_{\mathrm{gen},i} \frac{p_{\mathrm{el},i}}{\mathrm{COP}} + \dot{Q}_{\mathrm{aux},i} p_{\mathrm{el},i} \right) \Delta t \qquad (4.11)$$

Where an expression for the heat pump COP must be substituted, depending on the generation supply temperature (equation (4.8)).

The optimization variables are subject to certain constraints. For the heat generation unit these constraints are that the generation power remains below its maximum and that the generation mass flow rate remains below its maximum. The latter requires knowledge of the generation supply and return temperatures which will be further specified depending on the storage tank optimal control formulation.

$$\dot{Q}_{\mathrm{gen},i} \leq \dot{Q}_{\mathrm{gen},i}^{\max} \qquad\qquad\qquad \forall\, i \qquad (4.12)$$

$$\dot{Q}_{\mathrm{gen},i} \leq \dot{m}^{\mathrm{nom}} c \left(T_{\mathrm{gen,sup},i} - T_{\mathrm{gen,ret},i} \right) \qquad\qquad \forall\, i \qquad (4.13)$$

To avoid infeasibility whenever the storage tank capacity is taken too small to supply the heat demand, the auxiliary heater is explicitly modeled in all optimal control formulations. The heat demand must thus always be supplied by either the emission system, or the auxiliary heater, leading to:

$$\dot{Q}_{\mathrm{em},i}^{\mathrm{dem}} = \dot{Q}_{\mathrm{em},i} + \dot{Q}_{\mathrm{aux},i} \qquad \forall\, i \qquad (4.14)$$

The emission system is subject to a similar constraint as the generation unit, although here, the emission system effectiveness must be taken into account. The maximum emission heat flow rate with a given emission supply temperature, will always coincide with nominal emission mass flow rate and thus nominal emission effectiveness. The emission heat flow rate is thus subject to:

$$\dot{Q}_{\mathrm{em},i} \leq \varepsilon_{\mathrm{em}}^{\mathrm{nom}} \dot{m}^{\mathrm{nom}} c \left(T_{\mathrm{em,sup},i} - T_{\mathrm{em},i} \right) \qquad \forall\, i \qquad (4.15)$$

Values for $T_{\mathrm{gen,ret},i}$ and $T_{\mathrm{em,sup},i}$ depend on the assumptions required to include a storage tank model in the OCP formulation. In the subsequent paragraphs, several storage tank models, suitable for implementation in the OCP are developed and presented.

Non-linear program (nlp)

The most common way of modeling a stratified hot water storage tank is to divide the storage volume in N equal volumes and computing the average temperature in each volume. In an optimization context, both the average

layer temperatures (T^j) and mass flow rates to and from the storage tank are regarded as variables. The differential equations that govern the changes in layer temperature are implemented as state constraints. With the assumption of an incompressible storage fluid, constant specific heat and no heat flow rate due to diffusion, the energy balance for layer j becomes:

$$m^j c \frac{\mathrm{d}T^j}{\mathrm{d}t} = \dot{H}_{\mathrm{b}}^{j-1/2} - \dot{H}_{\mathrm{b}}^{j+1/2} + UA^j \left(T_{\mathrm{hl}} - T^j\right) \tag{4.16}$$

Where the enthalpy flows across the upper and lower boundary ($\dot{H}_{\mathrm{b}}^{j-1/2}$ and $\dot{H}_{\mathrm{b}}^{j+1/2}$) require an estimate of the temperature at the boundary which can be computed from the average temperatures through an upwind discretization. Heat losses are added for each layer using a fixed UA value and the temperature to which the heat is lost (T_{hl}). As the upwind convection equations change with the flow direction, the mass flow rate inside the storage tank is split into a downward, $\dot{m}_{\mathrm{down}}$, and an upward component, $\dot{m}_{\mathrm{up}}$. Evidently only one of both can be non-zero at any time. The differential equation governing the temperature of layer j (with layer 1 at the top of the storage tank and layer N at the bottom) becomes:

$$m^j c \frac{\mathrm{d}T^j}{\mathrm{d}t} = \dot{m}_{\mathrm{down}} c \left(T^{j-1} - T^j\right) \tag{4.17}$$

$$+ \dot{m}_{\mathrm{up}} c \left(T^{j+1} - T^j\right)$$

$$+ UA^j \left(T_{\mathrm{hl}} - T^j\right)$$

The control horizon is split up in intervals with length Δt. Using a second order collocation scheme, the state constraint for layer j at time step i is written as:

$$m^j c \frac{T_{i+1}^j - T_i^j}{\Delta t} = \frac{1}{2} \dot{m}_{\text{down},i} c \left(T_i^{j-1} - T_i^j \right) \tag{4.18}$$

$$+ \frac{1}{2} \dot{m}_{\text{up},i} c \left(T_i^{j+1} - T_i^j \right)$$

$$+ \frac{1}{2} U A^j \left(T_{\text{hl},i} - T_i^j \right)$$

$$+ \frac{1}{2} \dot{m}_{\text{down},i} c \left(T_{i+1}^{j-1} - T_{i+1}^j \right)$$

$$+ \frac{1}{2} \dot{m}_{\text{up},i} c \left(T_{i+1}^{j+1} - T_{i+1}^j \right)$$

$$+ \frac{1}{2} U A^j \left(T_{\text{hl},i+1} - T_{i+1}^j \right) \qquad \forall \, i, j$$

At layer 1 and N the temperatures with index 0 and $N+1$ must be replaced with the generation supply and emission return temperatures respectively.

Here, the emission supply temperature is assumed fixed at 35°C. Under this assumption, the heat pump COP is ambient temperature, and thus time dependent only and can be pre-computed according to equation (4.8), as presented in figure 4.3b. The COP value to be substituted in equation (4.11) thus becomes:

$$\text{COP} = \frac{1}{2} \left(\text{COP}_i + \text{COP}_{i+1} \right) \tag{4.19}$$

As in the state constraints the layer temperature, a state variable, is multiplied by the mass flow rate, a decision variable, this results in a bilinear, non-convex optimization problem. Hence it is designated as nlp. It is important to notice that no mixing or buoyancy is implemented in this formulation which will result in a model mismatch between the OCP and emulator.

Temperature discretization (lp_td)

Instead of a spatial discretization of the storage tank in equal volumes, one could also consider to split the storage tank in parts with different, constant temperature and varying mass. Each part j has a variable mass m^j and a fixed temperature T^j which drops with rising index j. The sum of all masses must always be equal to the total mass of the storage tank, m. A mass balance for node j can be written as:

$$\frac{\mathrm{d}m^j}{\mathrm{d}t} = \sum_{k>j} \dot{m}_{\mathrm{gen}}^{k,j} - \sum_{j>k} \dot{m}_{\mathrm{gen}}^{j,k} + \sum_{k<j} \dot{m}_{\mathrm{em}}^{k,j} - \sum_{j<k} \dot{m}_{\mathrm{em}}^{j,k} \qquad (4.20)$$

$$+ \dot{m}_{\mathrm{hl}}^{j-1} - \dot{m}_{\mathrm{hl}}^{j}$$

Here $\dot{m}_i^{k,j}$ represents the generation or emission mass flow rate from node k to node j and $\dot{m}_{\mathrm{hl}}^{j}$ represents a mass flow rate to the node at lower temperature caused by heat transfer to the surroundings.

This formulation assumes that, through buoyancy effects, injected fluid is transported to the height where its temperature matches the storage tank temperature without mixing.

With the emission and generation mass flow rates are assumed constant during each time step, the state constraint for node j at time i is written as:

$$\frac{m_{i+1}^j - m_i^j}{\Delta t} = \sum_{k>j} \dot{m}_{\mathrm{gen},i}^{k,j} - \sum_{j>k} \dot{m}_{\mathrm{gen},i}^{j,k} + \sum_{k<j} \dot{m}_{\mathrm{em},i}^{k,j} - \sum_{j<k} \dot{m}_{\mathrm{em},i}^{j,k} \qquad (4.21)$$

$$+ \frac{1}{2}\, \dot{m}_{\mathrm{hl},i}^{j-1} - \frac{1}{2}\, \dot{m}_{\mathrm{hl},i}^{j} + \frac{1}{2}\, \dot{m}_{\mathrm{hl},i+1}^{j-1} - \frac{1}{2}\, \dot{m}_{\mathrm{hl},i+1}^{j} \qquad \forall\, i, j$$

with additional constraints:

$$\sum_j m_i^j = m \qquad\qquad \forall i \qquad (4.22)$$

$$\dot{m}_{\mathrm{gen},i}^{k,j} = 0 \qquad\qquad \forall\, i, j, k \leq j \qquad (4.23)$$

$$\dot{m}_{\mathrm{em},i}^{k,j} = 0 \qquad\qquad \forall\, i, j, k \geq j \qquad (4.24)$$

$$\sum_{j,k} \dot{m}_{\mathrm{gen},i}^{k,j} \leq \dot{m}^{\mathrm{nom}} \qquad\qquad \forall i \qquad (4.25)$$

$$\sum_{j,k} \dot{m}_{\mathrm{em},i}^{k,j} \leq \dot{m}^{\mathrm{nom}} \qquad\qquad \forall i \qquad (4.26)$$

Heat lost to the surroundings by node j is translated into a mass flow rate $\dot{m}_{hl}^{j}$ to node $j+1$ which is at a lower temperature according to:

$$\dot{m}_{\mathrm{hl},i}^{j} = \frac{m^j}{m}\, \frac{UA}{c}\, \frac{T^j - T_{\mathrm{hl},i}}{T^j - T^{j+1}} \qquad \forall\, i, j \qquad (4.27)$$

Here the heat loss area of a node is assumed to be proportional to the node mass. For the top and bottom nodes this is definitely not the case. However, the assumption is in agreement with the average heat loss model presented in section 2.4.3 which showed good accordance with experiments.

The emission heat flow rate is written as:

$$\dot{Q}_{\text{em},i} = \sum_{j,k} \dot{m}_{\text{em},i}^{j,k} \, c \, (T^j - T^k) \qquad \forall \, i \tag{4.28}$$

Furthermore, equation (4.15) is rewritten to include the mass flow rates from different layers:

$$\dot{m}_{\text{em},i}^{j,k} \, c \, (T^j - T^k) \leq \varepsilon_{\text{em}}^{\text{nom}} \dot{m}_{\text{em},i}^{j,k} \, c \, (T^j - T_{\text{em},i}) \qquad \forall \, i,j,k \tag{4.29}$$

Note that the emission mass flow rate appearing on both sides of the inequality cannot be omitted. If the mass flow rate is zero, the constraint should always hold, which is ensured in the above formulation. The use of the nominal effectiveness in the above constraint is also more restrictive than required. The above model assumes multiple flow rates, with multiple supply temperatures, and more impractical, multiple return temperatures are possible through the emission system. This is as if multiple emission systems are present, each with its own supply and return temperature, mass flow rate and effectiveness. In this situation, the actual effectiveness should be used in the above inequality. This would however, make the model non-linear and difficult to solve. The nominal effectiveness is used to constrain the model a bit more as the implicit assumption of multiple emission systems allows for too much freedom.

The objective function is now altered to:

$$J = \sum_{i} \left(\sum_{j,k} \dot{m}_{\text{gen},i}^{k,j} \, c \, (T^j - T^k) \frac{p_{\text{el},i}}{\frac{1}{2}(\text{COP}_i^j + \text{COP}_{i+1}^j)} + \dot{Q}_{\text{aux},i} \, p_{\text{el},i} \right) \Delta t \tag{4.30}$$

Where COP_i^j is the heat pump COP at time step i with a heat pump generation supply temperature assumed to be T^j, the temperature of node j. This quantity can again be pre-computed from equation (4.8) and the discrete storage tank temperatures.

The main advantage of this formulation is that it is an LP where the generation temperature is allowed to vary. Therefore it is designated as lp_td, where "td" stands for temperature discretization. The main disadvantage of this formulation is that multiple simultaneous charging or discharging flow rates, with different supply and return temperatures, are possible which is unrealistic.

As in the real world this is not possible, it will lead to an underestimation of costs and an increase in demand violation.

This issue can be resolved by including binary variables for both generation and emission flow rate, and an additional constraint stating that the sum of binaries must be less or equal to one at each time step. The resulting formulation is however a MILP which is much more difficult to solve and due to the many boolean variables does not converge to an acceptable solution within the control time step of 1 hour. It is thus abandoned as it is not applicable for real-time MPC.

Another issue is the assumption that any entering water is injected in the tank layer with the same temperature. In an actual storage tank this can partially be obtained through the use of inlet stratifiers [24, 72, 159] or multiple controlled inflow valves but as these devices would increase the investment costs, they are not considered.

Ideal stratification (lp_strat)

Two extreme storage tank configurations can be considered: ideal stratified tanks and ideal mixed tanks. Reducing the above lp_td formulation to a situation with only 2 nodes results in ideal stratification (lp_strat), where one part of the storage fluid is always at a high temperature T_h and the rest is at a low temperature T_l. As lp_td was a linear formulation, so is lp_strat.

From an energy balance with the assumption of constant specific heat capacity and density, the differential equation governing the average temperature (T_avg) is written as:

$$mc\frac{\mathrm{d}T_\mathrm{avg}}{\mathrm{d}t} = \dot{Q}_\mathrm{gen} - \dot{Q}_\mathrm{em} + UA\left(T_\mathrm{hl} - T_\mathrm{avg}\right) \tag{4.31}$$

With emission and generation power constant during a time step, the state constraints become:

$$mc\frac{T_\mathrm{avg,i+1} - T_\mathrm{avg,i}}{\Delta t} = \dot{Q}_\mathrm{gen,i} - \dot{Q}_\mathrm{em,i} \tag{4.32}$$

$$+ \frac{1}{2}UA(T_\mathrm{hl,i} - T_\mathrm{avg,i})$$

$$+ \frac{1}{2}UA(T_\mathrm{hl,i+1} - T_\mathrm{avg,i+1}) \qquad \forall\, i$$

with:

$$T_\mathrm{l} \leq T_{\mathrm{avg},i} \leq T_\mathrm{h} \qquad \forall\, i \tag{4.33}$$

Under the assumption of ideal stratification, the generation return temperature and the emission supply temperature used in equations (4.13) and (4.15) become the low and high temperature respectively:

$$T_{\mathrm{gen,ret},i} = T_\mathrm{l} \qquad\qquad\qquad \forall\, i \tag{4.34}$$

$$T_{\mathrm{em,sup},i} = T_\mathrm{h} \qquad\qquad\qquad \forall\, i \tag{4.35}$$

These temperatures are model parameters and must be fixed in advance. If the heat generation unit is assumed to supply energy at a fixed temperature, the choice of T_h is obvious. During storage charging, the storage tank is gradually filled with fluid at the generation supply temperature. Even though, because of mixing and heat losses, the temperature supplied to the emission system during storage discharging will be less, the generation supply temperature is a good estimate.

The choice of the low temperature, T_l, is less obvious. During discharging of the storage tank, its fluid is replaced with fluid at the emission return temperature. However, as the emission heat flow rate changes, so does the emission return temperature. The emission return temperature is thus not known in advance. Furthermore, in a real storage tank discharged through direct inflow ports, if the emission return temperature rises, the part of the storage tank at a lower temperature is mixed by the buoyant jet generated. If however, the emission return temperature falls, a new thermocline can form. To make a choice for T_l, a prediction of the emission heat flow rate is required. In the present investigation, the prediction of $\dot{Q}_\mathrm{em}$ is available and T_l is chosen as the minimum value of the emission return temperature given that the emission supply temperature is T_h.

This formulation is similar to the state-of-charge formulation most commonly found in the literature [11, 70, 73, 89, 111, 114, 121, 122, 147, 167]. The generation and emission constraints (equation (4.13) and (4.15)) however include some temperature dependence in the formulation which is generally not the case in the literature.

As the generation supply temperature is assumed to be known, the COP required in the objective function becomes time dependent only and is pre-computed:

$$\mathrm{COP} = \frac{1}{2}\left(\mathrm{COP}_i + \mathrm{COP}_{i+1}\right) \tag{4.36}$$

Ideal mixing (lp_mix)

An ideal mixed storage tank can also be approximated as a linear program (lp_mix). If a storage tank behaves completely mixed, the temperature of the fluid exiting the storage tank is the average storage tank temperature. Therefore, the constraints on the generation and emission heat flow rate must be adapted.

If the generation power is smaller than the emission power, the storage tank is discharged, and the generation return temperature is equal to the emission return temperature which can be approximated by a fixed low temperature (T_l). However, if the generation power is larger than the emission power, the generation return temperature is formed by mixing the emission return temperature with the storage tank outflow temperature, which, under the ideal mixing assumption, is the average storage tank temperature. As the computation of the actual generation return temperature in this situation requires multiplication of the mass flow rate with the average storage temperature, this would generate a non-convex formulation. The generation return temperature is therefore approximated as the average storage tank temperature. The generation supply temperature is assumed to be constant at T_h. The generation power limiting constraint is then implemented as:

$$\dot{Q}_{\text{gen},i} \leq \dot{m}^{\text{nom}} c \, (T_h - T_{\text{avg},i}) \qquad \forall \, i \qquad (4.37)$$

$$\dot{Q}_{\text{gen},i} \leq \dot{m}^{\text{nom}} c \, (T_h - T_{\text{avg},i+1}) \qquad \forall \, i \qquad (4.38)$$

The generation power is limited by both the storage tank temperature at the current time step and the storage tank temperature at the next time step. As the storage tank temperature evolves during the time step while the generation heat flow rate is constant, both constraints are required.

For the emission power a similar set of constraints is added:

$$\dot{Q}_{\text{em},i} \leq \varepsilon_{\text{em}}^{\text{nom}} \dot{m}^{\text{nom}} c \, (T_{\text{avg},i} - T_{\text{em}}) \qquad \forall \, i \qquad (4.39)$$

$$\dot{Q}_{\text{em},i} \leq \varepsilon_{\text{em}}^{\text{nom}} \dot{m}^{\text{nom}} c \, (T_{\text{avg},i+1} - T_{\text{em}}) \qquad \forall \, i \qquad (4.40)$$

As stated above, these constraints imply an approximation of the actual generation return and emission supply temperature in a system with an ideally mixed storage tank. Furthermore, the approximation is overly conservative. In the idealized system, when discharging, the emission supply temperature is larger or equal to the average storage tank temperature, depending on the generation power. The maximum emission power is thus larger or equal to the maximum power allowed by the above constraints.

The COP required for the objective function is pre-computed as in lp_strat.

The main disadvantage of the ideal linear programs is that the assumptions of the water temperatures exiting the storage tank do not always hold. In an attempt to resolve this issue, an iterative linear program is developed.

Iterative linear program (lp_iter)

The description of the storage tank as an energy buffer with heat entering from the generation side and heat exiting to the emission system results in the linear program describing ideal stratification. However, this approach holds an implicit assumption concerning the storage tank outflow temperature. As the heat supplied to the emission system is delivered by a heat exchanger with a slow varying temperature at the emission side, the flow rate must rise when the storage tank outflow temperature drops. The possible heat flow rate is thus limited by the maximum flow rate and dependent on the storage tank outflow temperature. In the ideal stratified model this storage tank outflow temperature is fixed at T_h, while in a real storage tank the outflow temperature varies in time. On the generation side a similar reasoning holds.

To accurately represent a real storage tank the generation return temperature and emission supply temperature in equations (4.13) and (4.15) must be computed more accurately. However, if these temperatures are computed as a function of the average storage tank temperature and implemented directly in the stated constraints it would make the optimization problem non-convex. Furthermore, the direct computation of the storage tank outflow temperature as a function of the average temperature is difficult. The storage tank outflow temperature can however be computed from a dynamic simulation of the considered system.

When an actual energy storage tank is nearly empty, the outflow temperature approaches the average temperature. As the outflow temperature decreases, the available emission power is decreased. As the emission power is an input to the optimal control formulation, the constraint limiting the emission power (equation (4.15)) results in an increased minimum average storage tank temperature. This results in an iterative solution of the linear program lp_iter:

1. Estimate the storage tank outflow temperature and the minimum average storage tank temperature over the control horizon.

2. Solve the linear program lp_strat with the estimated outflow temperature.

3. Perform a simple simulation of the system with the found control inputs and a storage tank model capable of estimating the outflow temperatures.

4. Calculate the generation return temperature and update the minimum storage tank temperature by increasing it by a small amount at times the emission heat flow demand cannot be supplied.

5. If the simulation satisfies the constraints finish, else return to step 2.

This iterative approach resolves the issues present in the other linear programs as the unknown temperatures are computed from a simulation. It is however not guaranteed that the final solution is optimal. As the constraints applied to the stratified linear program are successively tightened according to the simulation output, overall optimality cannot be assured. Furthermore, model mismatch between the OCP and emulator is still possible as the simplified simulation used in the iterative approach uses a less detailed storage tank model than the emulator to limit the overall computation time.

In this chapter, the simplified storage tank model used in the iterative linear program consists of a one-dimensional upwind discretization of the convection equation for a storage tank with 20 layers. In- and outflows are assumed to be at the top and bottom respectively and the bottom and top two layers are completely mixed at the end of each simulation time step to account for inflow and outflow mixing. Furthermore, at the end of each time step the storage layers are sorted to obtain a realistic temperature profile if required.

Implementation and optimization algorithms

All above formulations are implemented with a control time step of 1 hour. The non-linear program was solved with a primal-dual interior point optimization algorithm implemented in IPOPT [187]. The linear formulations were solved with a simplex algorithm implemented in IBM ILOG CPLEX. The non-linear program was solved for 20 and 10 layers. An initial guess was obtained by first running the non-linear program without restrictions on computation time, adding small random disturbances to the control signals and removing the final sample. This represents a long running MPC with a moving optimization horizon. The linear temperature discretization program was solved for 20 and 10 layers. In table 4.1 a summary of the formulations and their main properties is presented.

Formulation	Linearity	Discretization	Layers	Remarks
nlp_20	Non-convex	Spatial	20	
nlp_10	Non-convex	Spatial	10	
lp_td_20	Linear	Temperature	20	multiple flows
lp_td_10	Linear	Temperature	10	multiple flows
lp_strat	Linear	-	-	
lp_mix	Linear	-	-	
lp_iter	Linear	-	-	iterative solution

Table 4.1: Summary of the tested optimal control formulations and some of their key properties

4.4.4   Results

In figure 4.6 relative projected costs, relative demand violation costs and computation times are presented for all formulations. Actual costs are divided by the cost a direct supply of the heat demand would have if the electricity price was constant and equal to the average price. As in the *power limit* scenario, limited power is available and the variation in heat price is related to the COP variation only, the relative projected costs are close to one. In the *price variation* scenario, relative projected costs below one are expected as the heat generation can be shifted to periods of lower electricity prices.

When comparing total cost, the iterative linear program (lp_iter) performs best in both scenarios. Furthermore, its demand violation cost is lowest in the *power limit* scenario and only preceded by the mixed linear program in the *price variation* scenario. The simplified simulation in the iterative approach thus enables an adequate estimation of the storage tank outflow temperatures.

The non-linear formulations show a relatively high constraint violation cost, especially in the *price variation* scenario. Although the model takes a temperature distribution inside the storage tank into account, the absence of a model for mixing or buoyancy can lead to temperature inversions in the optimization, caused by a changing emissions return temperature, which are not realistic.

Although the increased degree of freedom of the heat pump supply temperature in the temperature discretization formulations (lp_td_20 and lp_td_10) results in lower projected costs, this reduction is offset by the increase in demand violation costs. Due to the possibility of simultaneous inflows, there is a large mismatch between control and simulation models. This also causes the model with less layers to perform better with respect to demand violation cost as there are less possible inflows.

The rough approximation of the storage tank outflow temperature in the

(a) *Power limit* scenario

(b) *Price variation* scenario
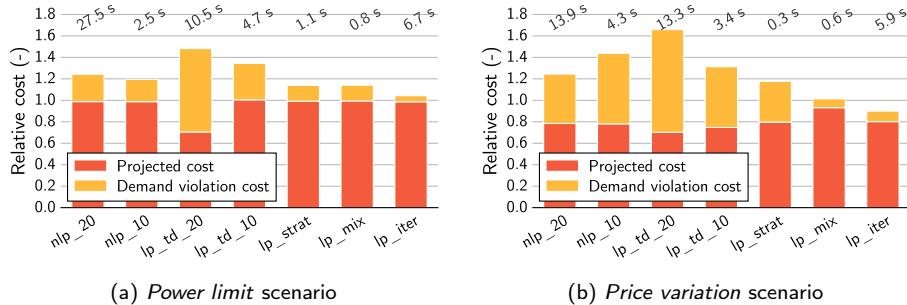
Figure 4.6: Projected costs, demand violation costs and computation time for the presented formulations in the two reference scenarios. Computation times were obtained by taking the 5 run average solution time on a 64-bit 2.56 Ghz Quad-Core machine.

stratified linear program causes a high demand violation specifically in the *price variation* scenario. The mixed linear program on the other hand has much less demand violation but the storage tank is not used to its full extent leading to a higher projected cost. The iterative approach combines the full storage tank use of the stratified linear program with a better estimate of the outflow temperatures.

In the *price variation* scenario, the projected costs computed by the stratified linear program are also around 10 percentage points lower than the overall minimum costs as obtained by the iterative linear program. In the *power limit* scenario the difference is less. If the stratified formulation is used in an open-loop optimization to estimate energy costs or other related quantities, an underestimation is made. On the other hand, with the mixed linear program, projected costs are overestimated in the *price variation* scenario as the storage tank is not used to its full extent.

In figure 4.7, the same data are presented as a trade-off between projected costs and demand violation costs. This allows for a less arbitrary comparison between formulations as the price of demand violation in the current methodology is chosen freely. Here can be seen that the iterative linear program performs well in both scenarios, with a low demand violation cost compared to the other formulations and a relatively low computation time.

In the *power limit* scenario, no trade-off curve is formed, only the iterative linear program is Pareto-optimal as it has both the lowest projected cost and demand violation cost. In the *price variation* scenario, all formulations except the non-linear program with 10 nodes are on the Pareto-front.

Compared to the other formulations, the stratified and mixed linear programs

(a) *Power limit* scenario

(b) *Price variation* scenario
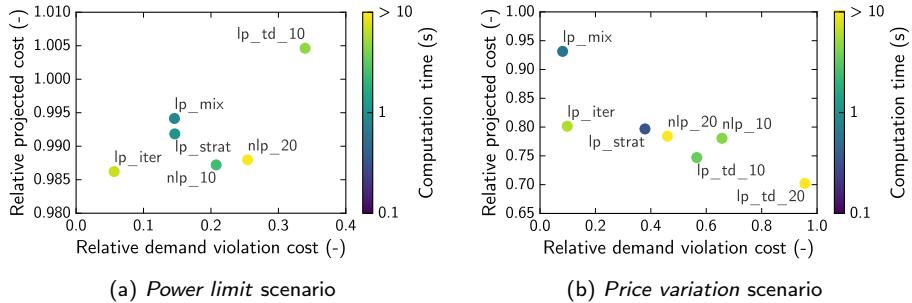
Figure 4.7: Trade-off between projected costs, demand violation costs and computation time for the presented formulations in the two reference scenarios. Computation times were obtained by taking the 5 run average solution time on a 64-bit 2.56 Ghz Quad-Core machine and are presented on a logarithmic color scale.

perform relatively well in both scenarios. In the *price variation* scenario, the demand violation cost of the mixed linear program is similar to that of the iterative solution, however due to the underestimation of the storage capacity, its projected costs are substantially higher.

The presented computation times are calculated as the 5 run average required cpu-time to solve the optimal control problems on a 64-bit 2.56 Ghz Quad-Core machine. Although the computation times of the non-linear programs are acceptable, the presented times are strongly influenced by the initial guess supplied to the optimization solver. When due to an update in predictions this initial guess significantly differs from the optimum, the solution requires significantly more time. Furthermore, the solution times are very sensitive to changes in solver settings. Considerable tweaking of setting was required to obtain the presented solutions. Thus from a robustness point of view, these formulations are depreciated.

In the literature, many authors use an optimal control approach with a formulation similar to the stratified linear program for assessing the benefits of a storage tank in a heating system [11, 70, 73, 89, 111, 114, 121, 122, 147, 167]. This analysis however shows that using a stratified OCP formulation without updating the actual state of the storage tank through a more detailed simulation, as is done in an MPC simulation, leads to a significant underestimation of the actual costs depending on the boundary conditions. The use of a mixed formulation can lead to considerably less underestimation, however, this is caused by the too restrictive constraints in the model which imply the storage tank is not used to its full extent. In a situation where the heat generation power is limited, it is possible that the mixed formulation leads to insufficient storage capacity to supply the requested heat demand while in reality the

storage capacity is sufficient. Results obtained from the solutions of open-loop optimal control problems thus must be interpreted with caution.

The iterative linear program shows a relatively good prediction of costs in both scenarios. However, if applied in an MPC approach, the difference between the stratified and iterative approach may decrease. As the storage tank state is updated each time step, errors made by the stratified approach are no longer propagated over the entire control horizon which is expected to lead to a similar performance. Furthermore, in an MPC framework, the sequential solution of the OCP allows for a comparison of the OCP solution with the actual behavior over time. This comparison can be used to adapt the OCP similarly to the iterative approach, which is expected to result in a similar performance and is investigated in the following section.

4.5 Model predictive control of heat pump space heating with hot water storage tank

In this section the most promising optimal control formulations presented above are compared while applied in an MPC simulation. In MPC, an OCP is solved resulting in optimal control inputs. However, only the first time step of these inputs is used and supplied to the system emulator. The emulator then computes the system response for that time step. At the end of the time step, the values of state variables required in the OCP are estimated from the emulator results and the process is repeated.

To compare different OCP formulations, the system and boundary conditions from the previous section are reused. However, instead of supplying the full control program to the emulator, only the first control input is used by the system emulator and the optimal control problem is solved each time step using the states computed by the system emulator as initial state. After the complete time horizon is emulated, the projected costs and demand violation costs are computed as described above. This approach is schematically presented in figure 4.8. In the current section, only the stratified (lp_strat) and mixed linear program (lp_mix) and the iterative linear program (lp_iter) are compared as the other formulations were shown to be sub-optimal or not suitable for use in a full year MPC simulation.

As in the previous section, there was no feedback from the emulator to the OCP, a state estimator was not required. In the current approach a value for the storage tank temperature profile or average temperature must be computed from the emulator results. For the stratified and mixed linear programs, the
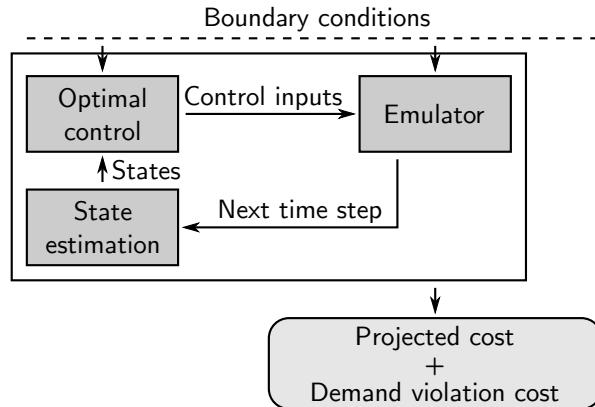
Figure 4.8: Schematic representation of the followed methodology for comparing different OCP formulations in the context of an MPC simulation.

average storage tank temperature is required and is computed as the actual average storage tank temperature in the emulator. For the iterative linear program, the temperature profile is interpolated to the layer center positions in the simplified model.

As suggested in section 4.4, the stratified linear program can utilize the emulator results in a way similar to the iterative linear program. As the selection of the low storage tank temperature (T_l) strongly influences the accuracy of the formulation, a modified approach is presented here. After every emulation, the state of the storage tank estimated from the emulator is compared with the state as estimated from the previous control optimization. If the average temperature determined by the emulator is higher than the temperature determined from the OCP, the storage tank lower temperature bound is increased by the difference. With this approach, if the emission heat demand is violated due to a storage outflow temperature below the required minimum emission supply temperature, the average storage tank temperature in the emulator will be higher than the average temperature in the optimal control problem. From then on, the minimum average storage tank temperature is increased so such an event can no longer occur. If the average heat demand decreases, the required minimum emission supply temperature decreases and the storage tank minimum temperature bound can be decreased to its original value or even lower. This way, many of the heat demand violation situations are avoided while maintaining a large effective storage capacity.

As in an MPC simulation, the optimization horizon moves, additional values are required for the boundary conditions. To allow for a comparison between the

(a) *power limit*   (b) *price variation*
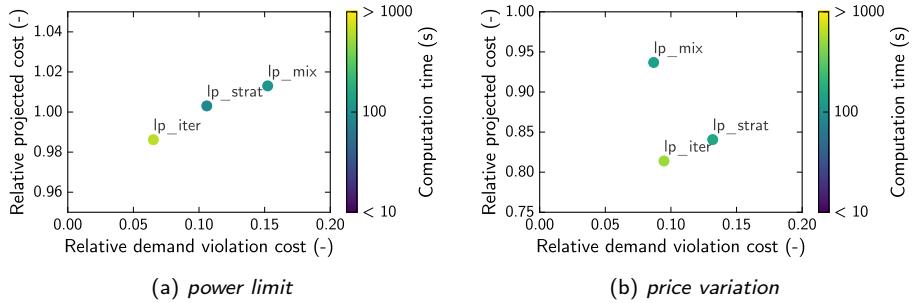
Figure 4.9: Trade-off between projected costs, demand violation costs and computation time for the presented formulations in the two reference scenarios using an MPC simulation. Computation times are single run times on a 64-bit 2.56 Ghz Quad-Core machine and are presented on a logarithmic color scale.

formulations in the OCP approach and the MPC approach, the heat demand as well as the electricity price after the 3 day time horizon are assumed zero, while the maximum heat generation power is assumed large.

4.5.1 Results

The trade-offs between projected costs and demand violation costs are presented in figure 4.9. From these figures it is seen that the iterative linear formulation offers the lowest projected cost and a very low demand violation cost. Due to the storage tank state updates and the variable lower temperature limit added to the stratified linear program (lp_strat), its demand violation cost is significantly decreased. The mixed linear program (lp_mix) still suffers from an underestimation of the effective storage capacity leading to higher projected costs.

The computation time results are similar to those obtained for the open-loop optimization. The time scale presented in figure 4.9 represents the time for the complete MPC simulation, including 72 control optimizations and the emulation time. The stratified linear program thus results in a 3 to 7 times faster MPC simulation which is an important speed increase if full year simulations are to be performed.

From this analysis it is concluded that for an MPC simulation of a heating system with a hot water storage tank and heat pump, the use of a stratified optimal control formulation provides a good compromise of optimality and computation time stated that the minimum storage tank temperature is updated regularly by

comparing the optimization predictions and the emulator results, and modifying accordingly.

4.6 Conclusion

The control of a heating system including thermal energy storage must take into account the future effects of current actions. In a residential space heating system with a heat pump and hot water storage tank MPC can be used to this end. However, several underlying OCP formulations are possible and the formulation most suitable for the system at hand must be selected.

In an open-loop optimization, the stratified linear OCP formulation, most common in the literature, is shown to significantly overestimate the effective storage capacity and to cause an underestimation of actual energy costs of up to 10 percentage points. The use of the iterative approach developed in this section provides more certainty on the results as temperature dependency, and effects of mixing and buoyancy are taken into account. This however comes at the expense of an increased computation time.

The non-linear formulations presented are depreciated for use in MPC simulations as their computation time is very sensitive to initial conditions and solver settings, and their results are disappointing. Furthermore, a temperature discretization linear formulation also shows suboptimal performance due to too much freedom in the optimization problem.

In a real time MPC of a space heating system with heat pump and storage tank, the use of the iterative linear program is recommended as the optimization solution time is less critical. In an MPC simulation, results from the emulator can be used to update the constraints of a stratified linear program to achieve similar results 3 to 7 times faster. In the remainder of this work, the stratified linear programing approach presented in section 4.4.3 is used, where the lower temperature limit is updated based on emulator results.

Chapter 5

Demand response with residential heat pumps and hot water storage tanks

5.1   Introduction

Residential space heating is a thermal load with a high level of simultaneity as it is governed mainly by ambient temperature. If heat pumps are used for heating on a large scale, the resulting additional electrical load is significant. The heat pump operation thus affects the scheduling of power plants and can induce large peak loads in winter times [184]. Demand response (DR) is referred to in the literature as technologies or programs that concentrate on shifting energy use to help balance supply and demand [190]. At times of abundant electricity generated from renewable sources, heat generated by a heat pump can be stored in the structure of the heated building or in a thermal energy storage tank. During a subsequent period of large electricity demand, the heat production of the heat pump can be decreased while releasing the stored thermal

energy. This way the peak loads in the electricity grid are decreased while the thermal comfort of the building inhabitants is maintained provided the system is well-controlled. Furthermore, it is possible to shift energy use in time to enhance the use of more efficient power plants. By using a hot water storage tank as thermal energy buffer, the amount of energy which can be stored is increased, thus increasing system flexibility.

The goal of this chapter is to quantify the effect on electricity generation mix and peak loads of introducing a large number of heat pumps for residential heating in an electricity system. The heat pump control system can attempt to minimize the local costs of heating, or take the effects on the electricity system into account to some degree. A method to include the impact of peak load in a moving horizon optimal control approach is developed. This results in a multi-objective model predictive control strategy. Furthermore, the effects on electricity generation mix and peak loads of adding a hot water storage tank of different sizes to a heat pump heating system are investigated.

The remainder of this chapter is structured as follows: First, section 5.2 presents an overview of studies investigating DR with heat pumps, highlighting the novelties of this work. Next, in section 5.3, the system under consideration is described and a mathematical model for the system is developed. In section 5.4 the multi-objective optimal control problem used in the MPC strategy is described. Section 5.5 presents the results of a case study inspired by the Belgian electricity grid with a large amount of intermittent renewable energy sources and heat pumps. Finally, in section 5.6, concluding remarks are formulated.

5.2 Demand response with heat pumps and thermal energy storage: literature review

Several studies investigated the potential of residential DR with heat pumps. Kreuder and Spataru [112] used a simplified model of heat pump space heating for residential buildings to investigate the effect of demand response on the peak load at household level and electricity generation level. They assumed a DR algorithm which alters the heat pump load to have a constant daily electricity demand profile in each household. Without demand response, the heat pumps cause an increase in peak load of about 2500 W at household level. By introducing a DR method, this peak load is decreased by about 700 W per household. In the model, they calculated the heating loads and heat pump efficiency based on the daily average temperature. Furthermore, effects of part load on heat pump efficiency were neglected. These model simplifications could have a large effect on the results as daily temperature variations significantly

affect the heat pump load. Vanhoudt et al. [184] experimentally investigated
the effect of an actively controlled heat pump on the buildings energy demand
profile. They found that their multi-agent market-based control algorithm
decreases the peak load but does not decrease the consumption of fossil-based
electricity. The combination of heat pumps and a hot water storage tank for
space heating was investigated by Arteconi et al. [10]. They showed that even
without a storage tank, when sufficient thermal mass is present in the emission
system, the heat pump can be turned off during a 3 h peak period without
affecting thermal comfort. Arteconi et al. [11] also investigated the effect of
the number of DR participants on the total operational costs of electricity
generation. In that study, DR is supplied by space heating and domestic hot
water production (DHW) using a domestic hot water tank, no space heating
storage tank is considered. In several scenarios of the future Belgian electricity
grid they showed that with more DR penetration the operational costs decrease
but the savings per customer also decrease. As the DR penetration increases
the peak residual demand also decreases. However, it remains well above the
fixed peak residual demand. The peak demand decrease is driven by the higher
energy costs assigned to high demand by a merit order model. Patteeuw et al.
[139] computed the cost of a reduction in CO_2 emissions through DR and the
use of heat pumps in residential buildings on a large scale. They found that
DR reduces the cost although there is a large spread in costs depending on the
building insulation level and the heating system. Hedegaard et al. [87] discussed
the investment in storage tanks used for space heating with heat pumps in
a DR context and compared this investment with using the building thermal
mass to offer flexibility to the electricity generation park. Using simplified
models for building and storage tank, they concluded that the fuel savings
cost is higher for the cases with storage tank than with passive thermal energy
storage. However, in the case of passive thermal energy storage the building
temperature was allowed to fluctuate in a temperature band around the reference
temperature. This implies that there are times the temperature is below the
reference temperature meaning that the building inhabitants thermal comfort
is decreased. This difference in thermal comfort results in an unfair comparison
between cases.

The afore mentioned studies employ open-loop optimal control with either
perfectly stratified or perfectly mixed models to represent the dynamics of hot
water storage tanks. However, as shown in chapter 3, when using a hot water
storage tank for space heating in a DR context, the effective storage capacity
is highly dependent on the degree of stratification inside the tank. The use of
simplified models to represent the storage tank behavior in an open-loop optimal
control approach thus may over- or underestimate the energy retrievable from
the storage tank as was shown in chapter 4. On the other hand, the solution of
an optimization problem with an accurately modeled hot water storage tank is

difficult and requires too much computing power when results on a yearly time scale are required. To resolve this problem a moving horizon optimal control or model predictive control (MPC) simulation can be used. In an MPC simulation a simplified OCP is used to generate control signals for a simulation with a detailed model, known as the system emulator.

In the literature, several authors used MPC or other advanced control strategies to investigate the operation of thermal energy storage in an energy system [18, 39, 41, 118, 156, 185, 202]. Bianchini et al. [18] presented an MPC algorithm for a large multi-zone building heated by a heat pump. They considered a scenario where an aggregator proposes DR requests, in the form of a price-volume signal, to the building management system. The building owner is rewarded if the requests are fulfilled. Results indicate good thermal comfort while addressing the DR requests. However, the effects on the electricity generation were not investigated. Another MPC algorithm which minimizes the cooling costs of a large building based on the day-ahead electricity price was proposed by Zhao et al. [202]. They concluded that using combined cooling and power generation could reduce the buildings primary energy use and CO_2 emissions. Adding a 125 m^3 chilled water energy storage further enabled savings in the building energy cost. However, these results are only valid when the penetration of such buildings in the electricity market is low, as no feedback effects were taken into account. Dahl Knudsen and Petersen [39] presented an MPC controller which minimizes electricity costs or CO_2 emissions for electric space heating. Depending on the controller settings lower emissions or lower costs compared to a PID control could be obtained. However, the presented control strategies neglect the feedback effects of the demand side changes on the electricity generation side which can be significant [136].

An MPC simulation for electric DHW production was described in [105] and a corresponding field test in [106]. They used a mixed storage tank approach in the OCP and a day-ahead electricity price based or energy based objective function. With typical user behavior they computed cost or energy savings of approximately 12% with respect to a system only allowed to charge the DHW tank at night. In the field testing campaign a reduction in cost per unit heat of around 12% was observed using a day-ahead electricity price based MPC strategy. However, as a price signal was used, the results do not account for the effects of a large scale integration of such systems in the electricity system.

Simulations with a control strategy designed to maximize self consumption of a buildings containing PV electricity generation and heat pumps with thermal storage in the building thermal mass or hot water storage tanks are described in [143, 171, 172]. They found self consumption of PV energy increases with increasing storage tank size. However, when the complete energy system is considered, self consumption might not be the most suitable objective.

Schibuola et al. [156] investigated several price signal based control strategies for maximizing self consumption in an apartment building. Here, a decrease of imported and exported energy of up to 11% and 21% respectively was seen. Dar et al. [41] found that with different rule based control strategies, self consumption or the energy bill of a net-zero energy building could respectively increase by 40% and decrease by 19%. However, both values were obtained with mutually exclusive control strategies and effects on the electricity generation side were not taken into account.

When DR is applied on a large scale, individual controllers impact loading and even commitment of electricity generation units, hereby altering the generation mix. Existing studies on building-level MPC with DR objectives do not take these effects into account. Often price signals are used to represent the electricity generation side. This approach neglects the feedback of DR on the supply side which actually is its prime objective [136].

This work aims at investigating the effects of a large-scale introduction of actively controlled heat pumps and hot water storage tanks used as space heating energy buffer, incorporating feedback of these systems on the electricity generation side. To correctly assess the value of a hot water storage tank in such a system, an MPC approach is developed using the detailed, validated model for a hot water storage tank, presented in chapter 2, in the system emulator. To the author's knowledge, such an analysis is not present in the literature.

5.3   System description and model

This section describes the system under consideration and its mathematical model. The system consists of a set of similar residential buildings with an underfloor heating system to which heat is supplied by an air to water heat pump. The heat pump uses electricity generated by different renewable and classic power plants. At the building level thermal energy storage capacity is available through the building thermal mass, the underfloor heating, a domestic hot water storage tank and a space heating buffer tank (figure 5.1).

An emulator for the building and heating system is created using the Modelica physical modeling language [123]. In the emulator the governing equations are solved numerically using a variable time step differential-algebraic equation solver implemented in Dymola 2016.

The current study applies an MPC control strategy to the system emulator. Every hour, values for the required control signals are computed through the solution of an OCP over a 4 day control horizon. The optimal control problem
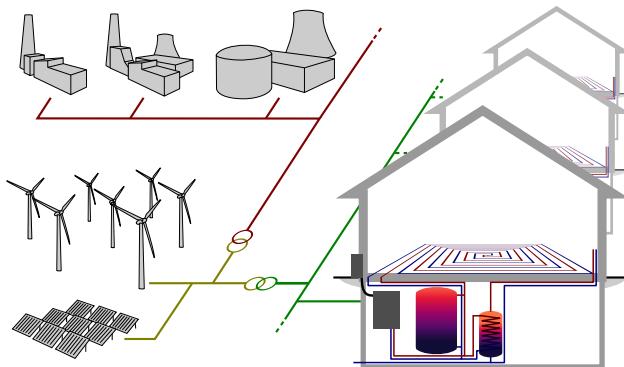
Figure 5.1: Schematic representation of the system under consideration, including a set of buildings heated by a heat pump with a hot water storage tank used for space heating and a domestic hot water tank. The electricity production park consists of renewable based and classic electricity generation units.

consists of a simplified model of the system, constraints limiting the allowable operating range and an objective function which is minimized by altering the control signals. The optimal control signals are applied to the system emulator which calculates the system behavior for the next hour. Then, the states of the optimal control problem variables are estimated from the emulator results. Hereafter, the optimal control problem is updated with new initial states and boundaries and the process is repeated.

In the following subsections the emulator and controller models for each subsystem are described. As a case study, parameter values derived from the Belgian housing stock and electricity generation park are used. The results presented are thus to be seen within the context of the Belgian electricity system. Nevertheless, the presented multi-objective control strategy can be used independently of the presented case.

5.3.1 Building

In this study the set of buildings under consideration is modeled by scaling the results of a single building simulation [138]. This simplification assumes the averaged behavior of the building set is equal to the behavior of the average building, including average user behavior. This assumption is based on the simultaneity of the space heating requirement for all buildings. As heat pumps currently available on the market operate more efficiently in part load operation, this assumption is further justified.

Volume (m^3)	741
Ground floor area (m^2)	132
External surface area (m^2)	530
Total window area (m^2)	44
Average insulation value (W/m^{2}K)	0.44

Table 5.1: Key parameters for the building under consideration.

The building under consideration is a new built, detached single family home, insulated according to the Flemish building performance legislation of 2010, built with massive construction elements, as is common in Belgium [38]. The building is assumed to have an underfloor heat emission system which covers the entire ground floor area. Key parameters for the building are presented in table 5.1.

In figure 5.2, a simplified model of the building under consideration is presented as an RC-network. This building model is used in the emulator as well as in the OCP. The model was extended from Reynders model [148] to include a basement which functions as technical room where the heating system, including space heating storage tank and domestic hot water tank, are set up. The building interior air (in), internal walls and furniture (wi), external walls (we), floor (fl) and technical room (tr) temperatures are chosen as state variables. Heat losses from the building are transferred to the ambient air (amb) by transmission and ventilation, and to the ground (gnd), which is assumed to be at a constant temperature. As the floor and all walls are assumed to be built using heavy-weight materials, the floor and external walls thermal resistance is split into parts (R_{w1} - R_{w2} and R_{f1} - R_{f2}) on either side of a lumped thermal capacity. The ventilation heat loss is modeled as a thermal resistance (R_{ve}).

Solar and internal gains are modeled as heat flows to all thermal capacities (contained in $\dot{Q}_{in}$, $\dot{Q}_{wi}$, $\dot{Q}_{we}$, $\dot{Q}_{fl}$). The solar gains are calculated as a fraction of maximum solar gains, determined by the shading position, and distributed over the internal air, internal walls, external walls and floor according to fixed distribution factors [149]. Internal gains are supplied to the interior air temperature.

The heating system is assumed to be located in the technical room (tr) of the building. All parts of the heating system are assumed to have linear heat losses to the technical room. These heat losses can be represented as thermal resistances for the heat pump (hp), space heating storage tank (sh) and domestic hot water storage tank (dw).

From this schematic presentation, differential equations governing the behavior of the system are derived which are used in the system emulator. In the OCP
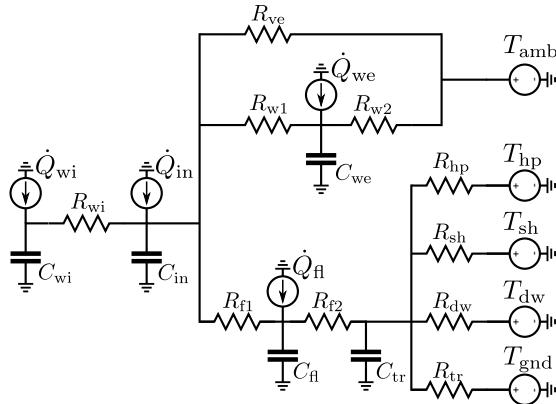
Figure 5.2: A detached house with underfloor heating including a basement acting as technical room, modeled as an RC-network.

these equations are discretized with respect to time using a 2nd order collocation scheme and considered as equality constraints (see appendix A).

5.3.2   Heating system

In figure 5.3 the heating system consisting of heat pump, space heating storage tank, domestic hot water storage tank and electric domestic water heater is presented schematically. In the system under consideration, an air source heat pump is used to supply heat to a space heating storage tank, to the building heat emission system or to the domestic hot water tank. The heat pump and space heating storage tank are connected in parallel to the heat emission system and can be used independently to supply heat to the building. In the present study, cooling of the building is not considered since residential cooling can be avoided in a Belgian climate when the building is well-designed. However, the methodology can be easily extended to include cooling.

In the system emulator, the condenser of a modulating air to water heat pump, with 7.0 kW rated heating capacity, is modeled as a heating element in the hydronic circuit. The heating capacity ($\dot{Q}$) and required power input (P) are modeled using performance maps obtained from manufacturer data [40]. The performance maps relate the heating capacity and the required power to the ambient air temperature, the heat pump supply temperature and the compressor modulation. The heat pump supply temperature can be set at three different temperature levels, 35°C, 45°C and 55°C designated low (lt), medium (mt) and high (ht) temperature respectively. The compressor is assumed to
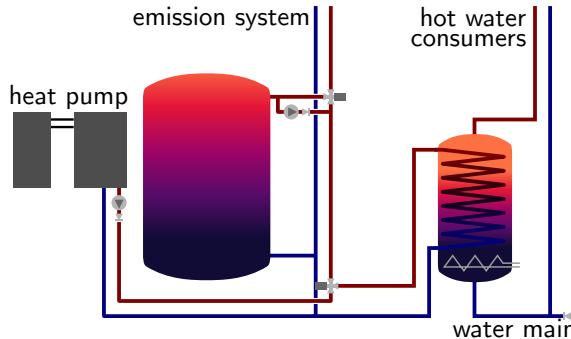
Figure 5.3: Diagram of the heating system including a space heating energy storage tank besides the heat pump, domestic hot water storage tank and electric domestic water heater.

modulate continuously from 0% to 100%. Most commercial heat pumps only allow modulation down to 30%. However, including this lower limit in an OCP requires an integer constraint which makes the OCP much more difficult to solve.

In the OCP, the power required by the heat pump operating at a temperature level is modeled to be quadratically dependent on the heat transferred at the condenser. For each supply temperature level, the polynomial coefficients were fit for different ambient temperatures creating a model which is dependent on the heat pump supply temperature, ambient temperature and modulation. Examples of the fitted data are presented in figure 5.4. This procedure leads to a small heat pump model mismatch between the emulator and the controller. For each temperature level, an inequality constraint is required to maintain convexity of the resulting optimization problem. As additional power use will always result in higher costs this constraint will however always be active.

$$P_{\mathrm{hp,lt}} \geq \zeta_{\mathrm{lin,lt}}(T_{\mathrm{amb}})\dot{Q}_{\mathrm{hp,lt}} + \zeta_{\mathrm{qua,lt}}(T_{\mathrm{amb}})\dot{Q}_{\mathrm{hp,lt}}^2 \tag{5.1}$$

$$P_{\mathrm{hp,mt}} \geq \zeta_{\mathrm{lin,mt}}(T_{\mathrm{amb}})\dot{Q}_{\mathrm{hp,mt}} + \zeta_{\mathrm{qua,mt}}(T_{\mathrm{amb}})\dot{Q}_{\mathrm{hp,mt}}^2$$

$$P_{\mathrm{hp,ht}} \geq \zeta_{\mathrm{lin,ht}}(T_{\mathrm{amb}})\dot{Q}_{\mathrm{hp,ht}} + \zeta_{\mathrm{qua,ht}}(T_{\mathrm{amb}})\dot{Q}_{\mathrm{hp,ht}}^2$$

As the maximum heat pump capacity occurs at 100% modulation, it is only ambient temperature dependent. Thus for the maximum condenser heat flow rate, the manufacturer data are linearly interpolated in the optimal control formulation.

To avoid integers in the optimization problem, the heat pump is allowed to
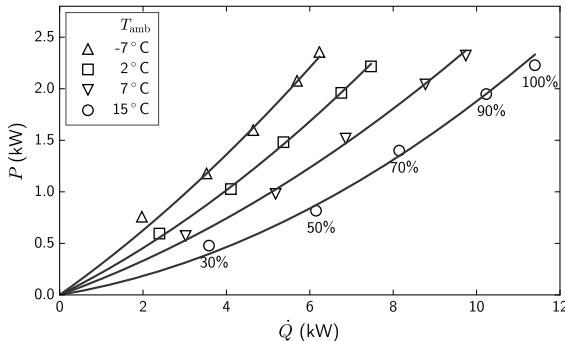
Figure 5.4: Example of the heat pump performance data and quadratic curve fit as used in the optimal control problem for the low heat pump supply temperature level. Markers represent the manufacturer data used in the emulator while the solid lines represent the quadratic fit used in the OCP. The amount of modulation at different markers is indicated for the highest ambient temperature.

operate at the different heat pump supply temperatures simultaneously. As this is not possible in reality or in the system emulator, after the optimization, a post processing step reorders the condenser heat flow rates so they occur sequentially within a single control time step while ensuring equal energy transfers at each heat pump supply temperature level.

The space heating storage tank is assumed to be a vertical cylindrical tank with rounded heads as is available on the market. Several storage tank volumes are simulated by changing the storage diameter while keeping the height fixed at 2 m. The tank is insulated using 0.20 m flexible poly-urethane foam with a thermal conductivity of 0.04 W/m K. Fittings attached to the storage tank and penetrating through the insulation are assumed to increase heat losses and are modeled with a heat transfer rate of 0.16 W/K. The space heating storage tank is charged and discharged through direct inflow ports positioned horizontally and located at a distance of 0.04 m from the top and bottom. When the monthly average ambient temperature rises above 13°C, the space heating requirement is very small. The space heating storage tank is then disconnected from the heating system to reduce heat losses. If during this period space heating is required, it is directly supplied by the heat pump.

Domestic hot water is supplied to the building occupants from a 0.2 m^3 domestic hot water storage tank. The domestic hot water tank is charged by the heat pump through an immersed coil heat exchanger spanning the entire storage tank height. An auxiliary immersed resistance heater, located at the bottom of the tank, can be used to further heat the tank up to 80°C, designated the very high temperature level (vht). As a result of the charging methods, the

domestic hot water tank is mixed during charging, so afterwards the storage tank temperature is nearly uniform. To ensure the building users domestic hot water comfort, the storage tank is controlled to be at a temperature of $50°C$ every morning at 7:00 and to be at $60°C$ every evening at 20:00. A high temperature is set every day to avoid legionella contamination as suggested by De Vlieger et al. [43]. During a 4 h period after both high temperature set points no storage charging is allowed as domestic hot water draws are assumed to occur in this period. During the morning period 0.09 m^3 and during the evening period 0.15 m^3 water at $45°C$ are used every day. When the water in the storage tank is at a higher temperature, a thermostatic mixing valve mixes the water from the storage tank with cold water from the water mains.

In the emulator, both storage tanks are modeled in accordance with the models presented in chapter 2. In the OCP the space heating storage tank is modeled as a perfectly stratified storage tank as was shown to be appropriate in chapter 4. The domestic hot water storage tank is modeled in the OCP as being charged perfectly mixed, and discharged perfectly stratified. As the domestic hot water storage tank is charged through an immersed heat exchanger, natural convection will impede strong stratification during charging, justifying the mixed charging approach. Mixed charging implies a reduction in power supplied by the heat pump as the average storage tank temperature rises. Furthermore, the heat pump cannot deliver any heat to the domestic hot water storage tank when it is heated by the auxiliary heater above the maximum heat pump supply temperature. To model this in the OCP, the domestic hot water tank is split in a low, medium, high and very high temperature part which can only be used in sequence as described by Patteeuw and Helsen [137]. Discharging occurs using direct inflow ports of water from the mains and will thus result in stratification of the storage tank.

5.3.3 Electricity generation

The electricity use of the heat pumps and auxiliary water heaters in the building set is added to the fixed demand in the electricity grid. This total electricity demand needs to be supplied by the available electricity generation units. The electricity generation park is simplified by dividing it into four categories: Wind generation, photovoltaic (PV) generation, base load generation and peak load generation units. At all times the sum of outputs of each part of the electricity generation park must equal the total electricity demand. In this approach, losses in the electricity grid are neglected. Wind, PV and base load generation are assumed to have a limited, fixed capacity. The capacity of all peak load generation units is assumed large enough to be able to fulfill the balance of supply and demand at all times. The required peak load capacity is an output

of the simulations. To schedule the electricity generation, a merit order model
is used, as suggested by Patteeuw et al. [136].

The maximum power of wind and PV generation is obtained by upscaling
measured power generation data for the Belgian electricity grid in the year
2013 [51]. The capacities are scaled up to 4080 MW wind power and 5750 MW
PV power, chosen based on the Europe 2030 goals for increasing the share of
renewable energy in Belgium [58]. The ratio between wind capacity and PV
capacity is equal to the 2015 capacity ratio in Belgium. No distinction is made
between on- and offshore wind power. As producing electricity using these
renewable technologies releases very little greenhouse gases into the atmosphere,
e.g. emissions related to maintenance, they are scheduled first. In this work the
total load minus the available renewable based production is called the residual
load. When the renewable sources can generate more than the total electricity
demand, residual load is zero and renewable production will be curtailed. When
the residual load is larger than zero, it must be supplied by base and peak load
power plants. Part of this residual load originates from the fixed load in the
electricity grid and thus is also fixed. This part is designated the fixed residual
load.

A fixed capacity of low greenhouse gas emission power plants (e.g. nuclear power
plants and combined cycle gas turbines (CCGT)) is assumed to be available
in the electricity production park. These plants are designated as base load
plants and are scheduled second. Throughout this work a base load generation
capacity of 10 000 MW is assumed. This amount is derived from the present
relative nuclear and combined cycle gas turbine capacity in Belgium.

Due to technical constraints in the assumed base load power plants, the base load
generation has a limited ramping rate. When the available renewable capacity
increases, the variations in the residual load increase accordingly. When the
residual load suddenly drops below the base load capacity, for instance due to
rapidly changing weather conditions, base load power plants may not be able to
follow the residual load. They need to anticipate these changes and gradually
lower their output in advance. In this study a maximum ramping rate for the
entire base load fleet of 10 MW/min is assumed. Table 5.2 presents a summary
of the available capacity and maximum ramping rates for the generation units
used in this work.

The difference between the residual load and the base load plant generation
is supplied by peak load power plants (assumed to be open cycle gas turbines
(OCGT)). The capacity of the peak load generation units is not fixed in
advance. The required peak load generating capacity is determined by simulation.
However, to limit peaks in the total demand, an additional cost is added when
the total demand is higher than a preset threshold. The determination of

Generation unit	Capacity (MW)	Maximum ramping rate (MW/min)
Wind	4 080	-
PV	5 750	-
Base	10 000	10
Peak	-	-

Table 5.2: Summary of the electricity generation units capacity and maximum ramping rate as used in this work.

this parameter is described in section 5.4. The above assumptions lead to an enhanced merit order model for the electricity generation park, taking maximum base load ramping into account, but neglecting start-up, shut-down, and part load running costs. Including start-up, shut-down, and part load running costs requires integer constraints making the OCP much more difficult to solve.

In this chapter the required energy, generation capacity and consumer heating cost are compared for different systems and control parameters. To compute the consumer cost a day-night time-of-use electricity tariff, as is common in Belgium, is used with an electricity price of 0.25 EUR/kWh during weekdays from 7:00 to 22:00 and 0.22 EUR/kWh otherwise.

5.4 Control approach

A direct collocation OCP with a time step of 1 h is formulated as described in chapter 4. The model equations of the system presented above are discretized and implemented as equality constraints. For the hot water storage tanks additional constraints are implemented to specify whether the storage tank behaves stratified or mixed. The complete OCP formulation is presented in appendix A.

Different control objectives can be defined. First, from the individual consumer viewpoint, a consumer wants to minimize his own cost for providing thermal comfort and domestic hot water. This can be attained by minimizing the individual cost of energy over the control horizon, stated that thermal comfort is maintained. In the present OCP formulation, a large cost for discomfort is added to the objective function thus treating thermal comfort as a soft constraint:

$$\text{minimize} \quad \sum_i p_{\text{el},i}(P_{\text{hp},i} + P_{\text{aux},i})\frac{\Delta t}{3600 \times 10^3} \tag{5.2}$$

$$+ \sum_i \text{discomfort costs}_i$$

With p_{el}^i the electricity price at time step i and P_{hp}^i and P_{aux}^i the heat pump power and auxiliary heater power respectively. In this study, the discomfort costs are quantified by multiplying the deviation of the operative building temperature (T_{op}) outside set comfort temperature boundaries ($T_{\text{op}}^{\text{min}}$ and $T_{\text{op}}^{\text{max}}$) with a discomfort price p_d:

$$\text{discomfort costs}_i = p_{\text{d}} \left(\Delta T_{\text{d,cold},i} + \Delta T_{\text{d,warm},i}\right) \frac{\Delta t}{3600} \qquad \forall\, i \tag{5.3}$$

$$\Delta T_{\text{d,cold},i} \geq T_{\text{op},i}^{\text{min}} - T_{\text{op},i} \qquad \forall\, i$$

$$\Delta T_{\text{d,cold},i} \geq 0 \qquad \forall\, i$$

$$\Delta T_{\text{d,warm},i} \geq T_{\text{op},i} - T_{\text{op},i}^{\text{max}} \qquad \forall\, i$$

$$\Delta T_{\text{d,warm},i} \geq 0 \qquad \forall\, i$$

The building operative temperature is linearized according to [132]:

$$T_{\text{op},i} = 0.4\, T_{\text{in},i} + 0.6\, (0.3\, T_{\text{we},i} + 0.3\, T_{\text{wi},i} + 0.4\, T_{\text{fl},i}) \qquad \forall\, i \tag{5.4}$$

Second, an environmental impact of energy use viewpoint can be considered, where the environmental impact of the used energy is minimized. As the impact differs for each generation plant, the optimization attempts to run the most environmentally friendly plant as much as possible. The objective function is then written as:

$$\text{minimize} \quad \sum_i \sum_j p_{\text{impact,ene}}^j P_i^j \frac{\Delta t}{3600 \times 10^3} \tag{5.5}$$

$$+ \sum_i \text{discomfort costs}_i$$

With j an index which runs over all power plants, $p_{\text{impact,ene}}^j$ the marginal impact of generating electricity by plant j and P_i^j, the power generated by plant j in time step i.

In this work the impacts of power generation for the different plants are chosen as the single score impact for electricity generated at rooftop pv, on- and offshore wind, nuclear, combined cycle natural gas and open cycle gas turbine power plants derived from the Ecoinvent database [191] with the *ReCiPe Europe H/A* impact assessment method [78].

Finally, one must remark that not only energy use is important when considering the environmental impact of electricity generation. For many power plants, a large amount of emissions is associated with the construction and decommissioning of the plant itself. Furthermore, the construction and maintenance of electricity transmission and distribution infrastructure also entail significant emissions and are peak power dependent. The costs or emissions assigned to peak loads are difficult to implement in a moving horizon optimal control approach as the maximum load will occur only in a few optimization horizons. To handle this problem, an overload threshold ($P_{\text{overload}}^{\text{max}}$) is defined. When the residual power generation rises above the overload threshold, an additional cost is assigned to the square of the overload power:

$$\text{minimize} \quad \sum_i p_{\text{cap}} \left(P_{\text{overload},i} \right)^2 \frac{\Delta t}{3600 \times 10^6} \qquad (5.6)$$

$$+ \sum_i \text{discomfort costs}_i$$

subject to :

$$P_{\text{overload},i} \geq \sum_j P_i^j - P_{\text{overload}}^{\text{max}} \qquad \forall \, i$$

As this is an approximation to include the impact of installed capacity in the objective function, the price of capacity assigned here, $p_{\text{impact,cap}}$, has little physical meaning. In this study, it is chosen such that the impact of an overload situation, if it occurs, is substantially larger than the impact of generating electricity at a power just below the overload threshold.

In the present work, the three viewpoints, consumer cost, energy impact and capacity impact, are merged in a single multi-objective function. To include the energy impact in the consumer cost function, a weighting factor for the environmental impact of energy (w_{EIE}) is introduced which scales the environmental impact of electricity generation to a cost for the consumer. If this factor is small, the controller will disregard the impact of the generated electricity, if it is large, the controller will attempt to minimize the impact. The capacity impact viewpoint can simply be added to the cost function. To alter

controller behavior, to attempt to minimize the required capacity or not, the
overload threshold is changed. A capacity limiting factor (l_{cap}) is introduced,
which relates the overload threshold to the maximum fixed residual load:

$$P_{\mathrm{overload}}^{\max} = l_{\mathrm{cap}} P_{\mathrm{fixed}}^{\max} \tag{5.7}$$

When the capacity control factor is much larger than 1, overload situations are
not recognized by the controller, and load peaks are not avoided. When l_{cap} is
near 1 or even below 1, the controller attempts to keep the residual load below
the threshold unless thermal comfort is jeopardized.

Combining the above objective functions and definitions, the total objective
function is written as:

$$\text{minimize} \quad \sum_i p_{\mathrm{el},i}(P_{\mathrm{hp},i} + P_{\mathrm{aux},i})\frac{\Delta t}{3600 \times 10^3} \tag{5.8}$$

$$+ \sum_i \sum_j w_{\mathrm{EIE}} \, p_{\mathrm{impact,ene}}^j P_i^j \frac{\Delta t}{3600 \times 10^3}$$

$$+ \sum_i p_{\mathrm{cap}} \left(P_{\mathrm{overload},i}\right)^2 \frac{\Delta t}{3600 \times 10^6}$$

$$+ \sum_i \text{discomfort costs}_i$$

subject to :

$$P_{\mathrm{overload},i} \geq \sum_j P_i^j - l_{\mathrm{cap}} P_{\mathrm{fixed}}^{\max} \qquad \forall \, i$$

The resulting optimal control problem is a convex, quadratically constrained
quadratic programming problem (QCQP) and is solved with IBM ILOG CPLEX.

5.5 Effect of space heating storage buffers on electricity generation: results

The results of different settings of the two controller parameters (w_{EIE} and
l_{cap}) are analyzed in a parametric study with different space heating storage
tank sizes. MPC simulations spanning a whole year are executed for w_{EIE}

equal to 10^{-2}, 10^0 and 10^2 and l_{cap} equal to 1.10, 1.00 and 0.95. The case with $w_{\text{EIE}} = 10^{-2}$ and $l_{\text{cap}} = 1.10$ represents no DR, where every consumer minimizes his own energy bill. In all other cases DR is present to some degree. To investigate the effects of adding extra storage capacity at the demand side, results are computed for a heating system without space heating storage tank, with a 1 m^3, 2 m^3, and a 4 m^3 space heating storage tank.

During all simulations perfect weather predictions and predictions of available renewable energy sources are assumed. Furthermore, a perfect estimation of the building states is assumed which is possible since the building model in the optimal control formulation is the same as in the system emulator. The states of the storage tanks are also derived directly from the actual average storage tank temperature as calculated by the system emulator.

When comparing different systems or control strategies, it is important that thermal comfort is comparable in all cases. In the present study, the thermal comfort requirements were met almost always. Building operative temperatures never drop below the specified lower comfort limit of 20°C and the demanded domestic hot water is always delivered. Only during a brief period in summer, the operative temperature rises above the maximum allowed operative temperature of 24°C. As the building does not include an active cooling system, this is unavoidable for the given building design. The overheating discomfort lies around 200 K h for all simulated cases, representing a temperature of 1K above the maximum value for less than 10 days per year. As this discomfort is comparable in all cases, a fair comparison between cases is made.

In the following subsections different aspects of the results are highlighted. First, the general behavior of the control strategy is illustrated. Next, the effect of different control parameter settings on the required peak generating capacity is discussed. Subsequently, the effect on energy use is presented. Finally, the associated costs for the consumer are compared.

5.5.1   General control behavior

The effect of adding a space heating storage tank on the residual peak load period is illustrated in figure 5.5 and figure 5.6. In figure 5.5 time series of the fixed residual load, heat pump power and auxiliary heater power for a system without space heating storage tank and with a 4 m^3 space heating buffer are compared for a 7 day period. In figure 5.6 the corresponding building and storage tank temperatures are presented. In the presented figures the control settings are $w_{\text{EIE}} = 10^2$ and $l_{\text{cap}} = 0.95$.

If no space heating buffer is present, the building thermal mass will serve as

thermal energy storage (figure 5.5a and figure 5.6a). However, due to the limits
on indoor operative temperature, the amount of energy that can be stored,
and subsequently the peak load period that can be bridged, is limited. The
4 m^3 storage tank allows the heat pump output to be reduced dramatically
during the time of high fixed load without a reduction in thermal comfort for
the building occupants (figure 5.5b). Remarkable is that the storage tank was
charged almost 5 days prior to discharge during a period of very low loads. In
the period between charge and discharge only the heat losses of the storage tank
and small partial discharge events are being compensated by the heat pump
leading to only a small additional heat pump load. From figure 5.6b, it can
be seen that the space heating storage tank is charged before and discharged
after the thermal mass in the floor and building are addressed. The control
optimization thus sees the storage tank as the more efficient storage option.
Furthermore, it can be seen in figure 5.5 that when a storage tank is used,
a small increase in production from base load plants is possible through the
increased heat pump operation in periods of low fixed residual load.

In figure 5.7 the residual load duration diagrams with different storage tank
sizes are presented for the same control settings as stated above. In addition,
the fixed residual load and the residual load without DR are shown. The
load without DR is computed with the control settings at $w_{\text{EIE}} = 10^{-2}$ and
$l_{\text{cap}} = 1.10$. With these control settings consumers minimize their local cost,
without concerns about the electricity generation efficiency or renewable sources
share. Furthermore, with the high capacity control limit, peak loads are
disregarded by the control strategy. Differences between different storage tank
sizes are difficult to observe in the full load duration diagram. However, the
difference with the case without DR is observable. Even without additional
storage capacity DR decreases energy use at high loads (which occur during
less than 2000 h per year) and increases energy use at lower loads.

Differences between different storage tank sizes are most clear in the region
below 50 h duration. Here can be seen that increasing the storage capacity,
decreases the peak load up to a level similar to the fixed residual peak load.
The decrease of load at low operating hours is made up by an increased energy
use at lower loads.

5.5.2   Peak demand

The peak demand and peak residual load for all simulated cases are presented
in figure 5.8. The peak demand is used to assess the required transmission
and distribution capacity, while the peak residual load determines the amount
of generation capacity required. The difference between the two lies in the

(a) no space heating storage tank

(b) 4 m^3 space heating storage tank
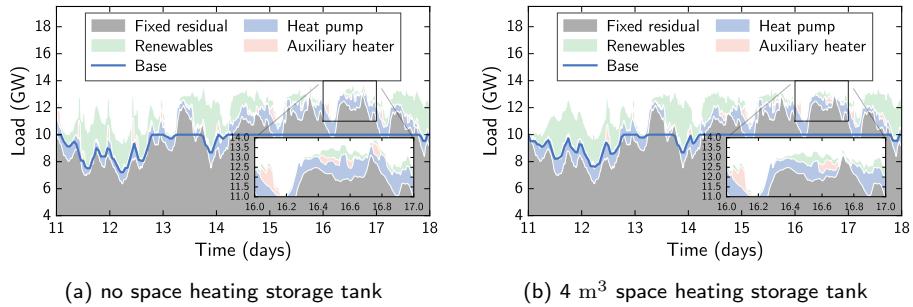
Figure 5.5: Time series of the residual load during the winter peak period. On the left no space heating storage tank is present in the buildings. On the right a 4 m^3 hot water storage tank is used to buffer space heating loads. For both results the environmental impact of energy use weight setting is $w_{EIE} = 10^2$ and the capacity limit setting is $l_{cap} = 0.95$.

(a) no space heating storage tank

(b) 4 m^3 space heating storage tank
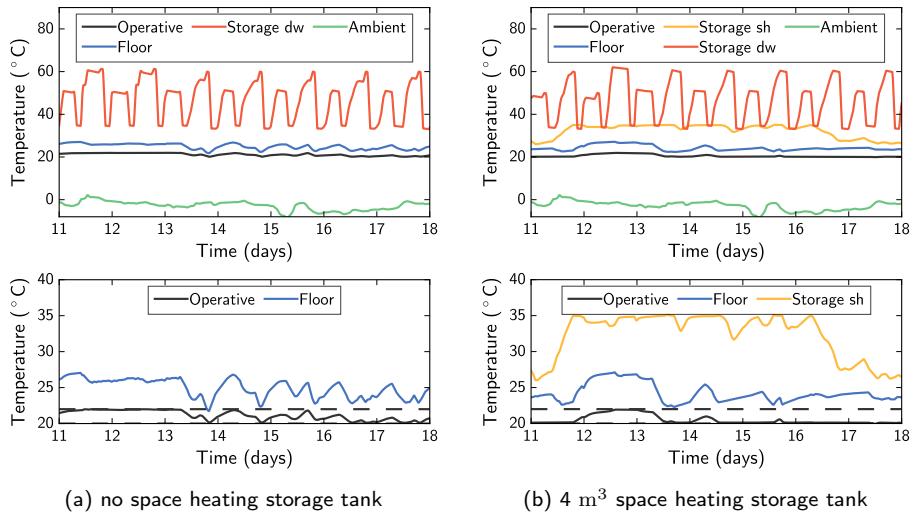
Figure 5.6: Time series of the building temperatures during the winter peak period. On the left no space heating storage tank is present in the buildings. On the right a 4 m^3 hot water storage tank is used to buffer space heating loads. A zoom of the temperatures in the building and storage tank is also presented for both cases where the allowed limits for the operative temperature are indicated by dashed lines. For both results the energy control setting is $w_{EIE} = 10^2$ and the capacity control setting is $l_{cap} = 0.95$.
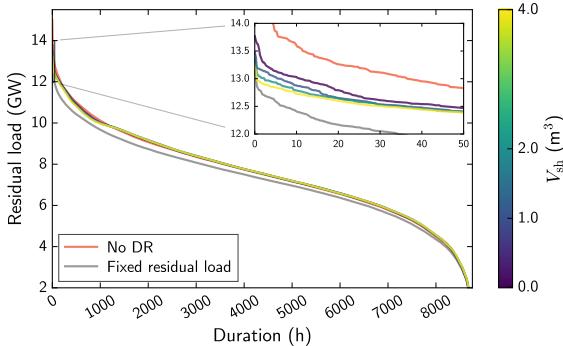
Figure 5.7: Residual load duration diagrams for different storage tank sizes. The fixed residual load and load duration diagram without DR are presented in gray and red respectively.

renewable generation which still requires a certain amount of electricity transport capacity. As almost no differences are observed with changing environmental impact of energy use weight, the peak load is presented with respect to the capacity limit. A lower capacity limit initially is accompanied by a strong decrease in peak demand and residual peak load. However, when the capacity limit is decreased too much, the observed peak residual load increases slightly if a space heating storage tank is not present. The peak demand is however still lowered as it is demanded by the objective function. When the peak load threshold is decreased, the period the heat pump output must be lowered increases. If the available storage capacity is unable to supply heat to the building during this period, the heat pump will supply it to guarantee thermal comfort. Furthermore, due to the complex dynamics of the hot water storage charging and the non-linearity of the heat pump COP, there is a model mismatch between the controller and the actual storage tank and heat pump or the emulator. If the settings become more critical, the OCP will generate solutions which are closer to the boundaries of acceptable operation. A small mismatch between control and emulator could then also lead to the observed increase.

Without a space heating storage tank, the minimum peak demand is around 0.61 GW higher than the fixed peak demand of 13.33 GW while with the same control settings, the residual peak load is 0.65 GW higher than the maximum fixed residual peak load. This minimum is obtained with a control setting $l_{cap} = 0.95$. On the right scales of figure 5.8, the additional peak load, above the fixed load peak, divided by the number of buildings is displayed. This scale thus assigns the additional peak load to the system causing it. Without a space heating storage tank a decrease in peak demand from 3.7 kW without DR to 1.2 kW with DR is observed.

(a) Peak demand   (b) Peak residual load
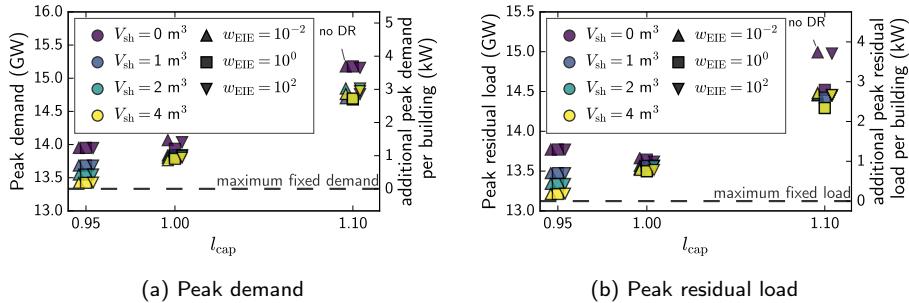
Figure 5.8: Variation of peak demand and peak residual load with variation of the capacity limit (l_{cap}) and environmental impact of energy use weight (w_{EIE}) control parameters and the space heating storage tank size (V_{sh}). The peak load for the total system is presented on the left axis. On the right axis, the increase in peak load above the fixed peak load divided by the number of buildings is presented. For clarity the markers with different environmental impact of energy use weight are slightly shifted left or right.

When a space heating storage tank is used, the peak demand is decreased further. With a 4 m^3 storage tank, the peak demand can be decreased to just above the fixed peak demand with a control setting $l_{\mathrm{cap}} = 0.95$. The heat pumps then only cause an additional peak demand of 0.2 kW per building. Nevertheless, the additional decrease in peak load falls with increasing storage tank size. This suggests that a trade-off can be made between installing larger space heating storage tanks or increasing the peak electricity transport capacity.

The maximum effect of adding a hot water storage tank is obtained with a 1 m^3 tank. In this case, the maximum residual load decreases from 13.95 GW (without space heating storage tank) to 13.68 GW (with a 1 m^3 space heating storage tank in 500 000 buildings) or around 0.54 kW/m^3 storage tank.

5.5.3 Energy use

In figure 5.9a the total residual energy use is shown. In figure 5.9b and figure 5.9c the residual energy is split into the part generated by base load plants and by peak load plants respectively. As the environmental impact of energy use weight control setting is increased, the amount of additional electricity generated by peak load power plants drops from around 2020 kWh to around 940 kWh per building. The amount of electricity generated by base load power plants rises from around 2840 kWh to around 4120 kWh per building. Due to the lower impact assigned to base load electricity generation the control attempts to shift electricity generation from peak to base load plants. Accordingly, the residual energy use rises by around 200 kWh per building on a total yearly electricity

use of around 4860 kWh in the case of no DR. This corresponds to a nationwide increase in electricity use of around 100 GWh. To maintain thermal comfort for the building inhabitants, thermal energy is stored in either the floor heating system or the hot water storage tank. Both imply heat losses counteracting the shift from peak load generation to base load generation and increasing the total energy requirement.

The addition of a storage tank decreases the electricity generated by peak load plants by 40 kWh to 250 kWh per building depending on the energy control setting and storage tank size. A larger storage tank size always results in less electricity generated by peak load plants. When the space heating buffer is added to the system, the residual energy use increases due to the additional heat losses from the storage tank. However, as the storage tank size increases the residual energy use is lowered. With increasing volume the surface area of the storage tank, governing the heat losses, increases with a power of around 2/3 while more load shifting flexibility is offered. The increase in residual energy use with rising space heating storage tank volume is largest with a low environmental impact of energy use weight (w_{EIE}). If this setting is low, the control system attempts to minimize the local electricity cost. As the electricity price is not correlated with the source of electricity or the availability of renewable sources yet, this results in an overall increase in energy use by storing energy when the price is low. With a high energy control setting, the control attempts to reduce the electricity generated by peak load plants and replaces it with electricity produced by base load plants.

When lowering the capacity limit both energy use from base load plants and peak load plants increase slightly in all cases. When the capacity is tightly constrained, the control must decrease the peak load at the expense of energy use.

5.5.4   Consumer cost

Figure 5.10 presents the cost of space heating and domestic hot water production as seen by the consumer as a function of the environmental impact of energy use weight control setting. The general trend in this figure is similar to the residual energy use (figure 5.9a). In the presented case, the difference between day time and night time electricity prices is too small for a significant shift in energy use to the night to occur. Furthermore, the temperature dependence of the heat pump COP further discourages shifting electricity use to the night as the ambient temperature is then lower. As in the presented case no curtailing occurs the figures are alike.

(a) residual

(b) base

(c) peak
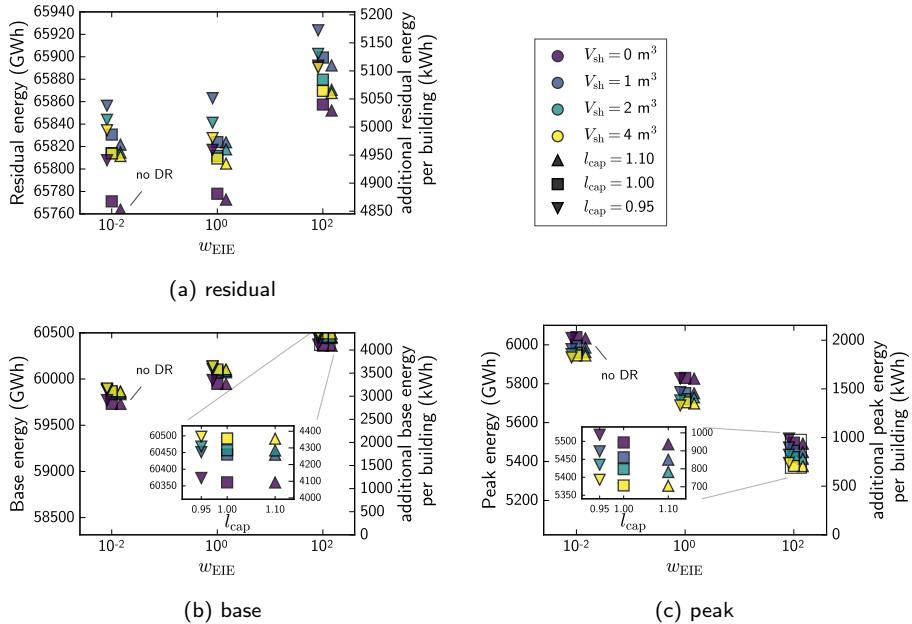
Figure 5.9: Variation of the residual energy use with variation of the capacity limit (l_{cap}) and environmental impact of energy use weight (w_{EIE}) control parameters and the space heating storage tank size (V_{sh}). The total residual energy is shown in (a), electricity generated by base load plants is shown in (b), electricity generated by peak load plants is shown in (c). The energy use for the total system is presented on the left axis. On the right axis, the increase in energy use above the fixed energy use divided by the number of buildings is presented. For clarity the markers with different capacity limit settings are slightly shifted left or right.

When the consumer does not participate in DR, the local costs are minimal. When participating in a DR program the costs carried by the consumer can increase by up to 70 EUR per year. The largest increase is obtained when the energy control setting is maximal and capacity control setting is minimal. In this case the local cost only marginally affects the OCP objective function. Adding a storage tank to the system increases heat losses and thus increases the consumer cost.

From this it can be concluded that if DR is desired by a grid operator, aggregator or other party involved, heat pump owners should be encouraged to participate by compensating them for their additional costs. The services provided by consumers can be remunerated through adapted energy prices [138] or by granting a discount to users who participate in DR programs or a penalty for those that do not.

When figure 5.8 and figure 5.10 are combined a peculiar observation is made.
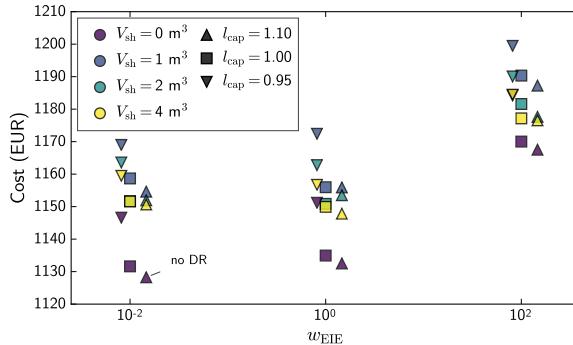
Figure 5.10: Variation of the local operational costs per building with variation of the capacity limit (l_{cap}) and environmental impact of energy use weight (w_{EIE}) control parameters and the space heating storage tank size (V_{sh}). For clarity the markers with different capacity limit control settings are slightly shifted left or right.

When consumers switch from not participating in DR to applying a control strategy which limits the total demand ($l_{cap} = 1.10 \to l_{cap} = 1.00$) the increase in consumer costs never exceeds 2 EUR per year. However, this change in setting causes the peak demand to decrease by 2.2 kW per building from 15.18 GW to 14.07 GW and the maximum residual load to decrease by around 2.5 kW per building from 14.99 GW to 13.77 GW. When a power plant lifetime is assumed to be 25 years, this results in a capacity cost of less than 25 EUR/kW which is very small compared to values for open cycle gas turbine power plants found in the literature which lie between 200 EUR/kW and 400 EUR/kW [57].

Adding a 4 m³ space heating storage tank and lowering the capacity control setting to 0.95 further lowers the maximum residual load from 13.77 GW to 13.21 GW. However, the consumer costs are increased with up to 31 EUR per year compared to the case without DR and storage tank. When comparing this value with the costs for installing additional generation capacity, the investment in the storage tank will probably not be favorable.

5.5.5 Overall merit of different control settings

When discussing the merit of the presented control strategies and their resulting energy use and required generating capacity, several viewpoints are possible. From a financial viewpoint, costs can be assigned to the generation of electricity by different plants and to the construction of generating plants. The resulting cost of electricity generation can then be compared with the total investment cost required for the storage tanks and heat pumps. On the other hand,

emissions from the construction and operation of all subsystems could be calculated through a life-cycle assessment (LCA), resulting in an environmental comparison. In this chapter no specific viewpoint is adopted though, in the presented case study, the controller uses environmental impact costs derived from the Ecoinvent LCA database.

5.5.6 Practical implementation of demand response control strategies

In a real electricity market, the application of the above presented control strategy is more difficult. First, reliable weather forecasts with a sufficient resolution are required. Presently, such forecasts are readily available through several web services although their accuracy and reliability are unproven. If only a small number of heat pumps and other flexible demand are present in the system, a prediction of the total load can be used as an approximation of the fixed load. Together with RES forecasts and an estimate of the number of participants in the system, the presented optimal control problem can be solved in each building separately without an intervention of the grid operator.

If the amount of flexible demand present in the system is large, system operation is much more difficult and support from the grid operator becomes necessary. First of all, the grid operator will require an aggregated model of all systems offering flexibility. Furthermore, information on the state of all systems is required to make a day ahead prediction of the total demand and the optimal demand profile of all flexible systems. These demand profiles can be used in the day-ahead electricity market where balance responsible parties compose their unit commitment schedules. The optimal demand profiles for all flexible systems can be sent to each system as a suggested demand profile and consumers can be rewarded if they follow this profile [138].

5.6 Conclusion

The use of heat pumps for residential heating can reduce greenhouse gas emissions and increase the energy efficiency of buildings. If large numbers of heat pumps are introduced in an electricity system, demand response can be employed to avoid adverse effects of the accompanying decrease in load diversity.

In this chapter, a multi-objective model predictive control strategy for space heating and domestic hot water production using a heat pump and thermal energy storage tank in a residential demand response context is described.

Depending on two control parameters, the controller accounts for consumer costs, impact of energy use in the national electricity system and impact of the total peak demand. Results are presented for a case study inspired by the Belgian electricity system with an increase in renewable based generating capacity and the switch of 500 000 buildings to heating with heat pumps.

In contrast to papers found in the literature, this study employs a detailed emulator model for the hot water storage tank and a heat pump performance map to account for the temperature and modulation dependency of the heat pump output. This results in a more accurate evaluation of the flexibility offered by a hot water storage tank in a residential heat pump heating system. The inclusion of the temperature and modulation dependence of the heat pump is required to correctly assess the effect on energy costs or the electricity generation mix of load shifting. In addition, the heating control system employs an integrated optimization of the electricity generation park and the demand side.

Through demand response with a controller which limits the total residual load, a significant reduction in peak load is possible with only a minor increase in consumer costs. The addition of a storage tank lowers the required generation capacity even further but consumer cost also increases.

By increasing the importance of the environmental impact of the generated electricity, the amount of electricity generated by peak load power plants is reduced significantly independently of the peak load reduction. Adding a hot water storage tank for space heating further reduces load peaks and electricity generated by peak load power plants, however the decrease is less striking.

When further adjusting the control settings and adding a space heating hot water storage tank, the required peak load capacity can be reduced to just above the required capacity without heat pumps. The electricity generated by peak load power plants can be lowered by up to 11% together with only a slightly larger increase in electricity generated by base load plants. However, these control settings cause the costs seen by the consumer, both operational and investment costs, to increase substantially. If this reduction in required capacity or peak energy use is desired by the grid operator or other stakeholders, they can consider encouraging heat pump owners to participate in demand response programs with similar control strategies and remunerating them for their additional expenses.

Chapter 6

Life-cycle assessment of residential heating

6.1 Introduction

The goal of introducing heat pumps for residential heating is to increase the primary energy efficiency of heating and thereby reducing greenhouse gas emissions. As presented in chapter 5, the large scale introduction of heat pumps in an electricity system has an effect on the required electricity generation and transport capacity and the energy mix. The use of demand response and the addition of a hot water storage tank as space heating energy buffer to the system was shown to allow for a shift in electricity generation toward low-emission power plants and a reduction in peak demand. When evaluating the emissions or environmental impact related to heat pump heating, these effects must be taken into account. Furthermore, emissions related to the entire system life-cycle, including resource mining, system construction, the use phase and the waste treatment should be incorporated.

The goal of the current chapter is to asses the life-cycle impact of residential heating with heat pumps and hot water storage tanks. The life-cycle impact of heating with a heat pump is compared to a conventional system using a condensing gas boiler. Furthermore, the effect of the storage tank size on the overall environmental impact and the costs paid by the user are investigated and a trade-off curve is generated.

The remainder of this chapter is structured as follows: First, to provide the

right context for the emission reductions presented at the end of this chapter, in section 6.2, the global warming and sustainability issues are shortly situated. Next, section 6.3 presents an overview of LCA studies related to energy or heating systems found in the literature. The methodology followed in this work is described in section 6.4. Subsequently, in section 6.5, results are presented for a case study of a Belgian inspired electricity system amended with 500 000 heat pumps. Furthermore, the effect of the space heating storage tank size on the total environmental impact and total cost is investigated. Finally, in section 6.6, concluding remarks are formulated.

6.2 Global warming and sustainability

In 2011 global CO_2 emissions from fossil fuel burning and cement production were in the range of 31.9 to 37.8 Gt CO_2 per year [96]. From 1990 up to 2008 the global per capita emissions have increased from 4.2 t/capita to 4.8 t/capita [20]. Over the past decades, these emissions have caused atmospheric CO_2 concentrations to increase from around 280 ppm in 1750 to 320 ppm in 1960 to around 390 ppm in 2010 [32, 103].

Radiative forcing (RF) is defined as the change in difference between energy received by Earth and energy emitted from Earth as a result of a perturbation [125]. It is usually expressed as an energy flow rate per unit area of Earth's surface. In the period from 1750 to 2011 total radiative forcing was between 2.54 and 3.12 W/m^2. The increasing concentration of greenhouse gases in the atmosphere prevent energy from being emitted and cause RF. Anthropogenic emissions of CO_2 are thought to be the largest contributor to RF (64%) followed by CH_4 emissions (18%) [125]. As more energy is received than emitted, the average global temperature rises. Over the period 1880 to 2012 the globally averaged land and ocean surface temperature has risen by 0.85°C [93]. Unless greenhouse gas emissions are substantially reduced, further warming and changes in Earths climate system will occur [96]. If global warming would exceed 4°C above pre-industrial levels by 2100, food insecurity, substantial species extinction and a limited potential for human adaptation are very likely. A multitude of studies have shown the negative effects of climate change on fresh water resources and food security and production [99, 145] and references therein. Furthermore, the risks for human societies are unevenly distributed, being higher for disadvantaged people all over the world [93].

If the temperature increase can be limited to 2°C above pre-industrial levels, the risk of substantial changes is decreased although some unique systems remain threatened and risks associated with extreme weather events remain [93].
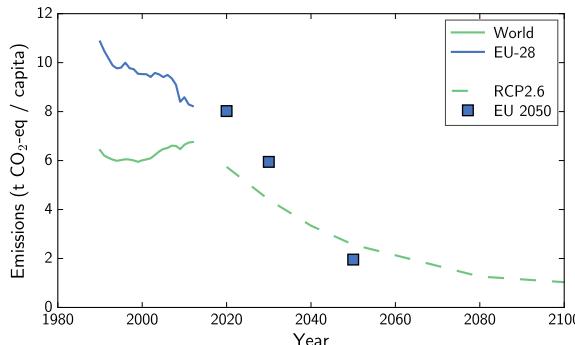
Figure 6.1: Historical emissions and future pathways per capita for the entire world and the EU-28. Historical data compiled from [196]. EU pathway was derived from [55, 56, 59]. RCP2.6 data were derived from [95, 186].

To achieve this limited temperature increase, total cumulative anthropogenic CO_2 emissions since 1870 must remain below 2900 Gt CO_2 while up to 2011 already 1900 Gt CO_2 was emitted [93]. Several scenarios for the future, designated representative concentration pathways (RCP), were investigated by the Intergovernmental Panel on Climate Change [93]. Most notably is RCP2.6 which is expected to limit RF to 2.6 W/m^2 in 2100. In this scenario, greenhouse gas emissions are decreased by 50% by 2050 and by 80% by 2100 relative to 2010 levels and the probability that the temperature increase in the long term remains below 2°C lies between 22% and 73% [186].

In the European Union, the Energy Roadmap 2050 plans a reduction in CO_2 emissions of 20% by 2020, 40% by 2030 and 80% by 2050 [55, 56]. In figure 6.1 historical data of global and European CO_2 equivalent emissions per capita are presented. Moreover, the figure shows the future per capita emissions of the RCP2.6 scenario and the goals set by the European Union. This shows that the long term goals of Europe are in line with a low risk global warming scenario However, short term goals are still significantly above the RCP2.6 scenario. This has a detrimental impact on the feasibility of the long term global warming goals as the cumulative CO_2 emissions are the driver to climate change [186]. Emissions in the first few decades will have a lasting effect on climate change and will impede global warming targets to be met in the future [150].

Although climate change is an important factor which requires urgent action, it is not the only challenge on a global scale. The United Nations General Assembly has defined targets for sustainable development in different sectors to strengthen world peace, eradicate poverty and increase prosperity for all people [180]. Although the presented concept of sustainable economic growth has been
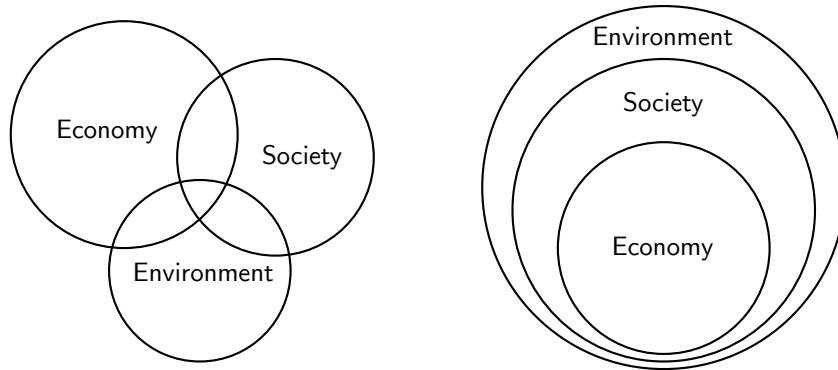
Figure 6.2: The traditional model with overlapping of different aspects of sustainable development (left) and the nested view of sustainable development. Adapted from [1].

criticized for decades [116], the definition of sustainable development provided by Brundtland [25] as "development that meets the needs of the present without compromising the ability of future generations to meet their own needs" is valuable to pursue.

Sustainability can be represented as a balance between economical, social and environmental interests as presented schematically in figure 6.2 [1]. The traditional model of sustainable development, on the left of figure 6.2, depicts the three dimensions of sustainability as separate circles with a possible interaction represented by the overlap. A more recent schematic representation of sustainability recognizes the nested nature of the three dimensions. The economy is a part of the human society which in turn can not grow beyond the natural environment on Earth.

In this work only the environmental impacts are considered.

Finnveden and Moberg [67] presented several tools for environmental system analysis. They concluded that the choice of tool is mainly influenced by the object of study and the impacts of interest. Following their analysis, in this work, life-cycle assessment (LCA) methods are used to study the effect of different systems on the environment.

The principles and framework of an LCA study are described in ISO 14040 [92]. Here, four separate phases are defined which are graphically presented in figure 6.3.

The analysis starts by defining the goal and scope of the study. ISO 14040 mentions the goal should include the reason for carrying out the study as well

as the intended audience. The scope should include the product or service being studied and its functions. A functional unit, quantitatively describing a specific function of the product system, which serves as a unit of comparison between different systems capable of fulfilling the same function, is defined. The boundaries of the study in terms of processes which have and have not been taken into account are also listed. Furthermore, the used allocation procedures must be specified and the methods used for the impact assessment, and any assumptions made must be clearly defined. The purpose of this phase is to enable other researchers to perform similar analyses on different product systems supplying the same function. The scope definition thus should enable a fair comparison between different systems performed by different researchers.

Subsequently, a life-cycle inventory analysis is performed. Here the required inputs for all processes in the product life-cycle are gathered. From the processes, an inventory of required resources and emissions is composed. This is usually the most difficult and time consuming phase of the LCA.

The impact assessment relates the inventory of resources and emissions gathered in the previous step to environmental impacts. Impact assessment methods consist of mathematical models which convert the emission of a substance to a damage indicator at the midpoint level, for instance RF for the emission of CO_2, or to an indicator at the endpoint level, for instance damage to human health. These models always introduce a certain level of uncertainty which must be evaluated carefully. To compute indicators at the endpoint level, more modeling assumptions are always required making them more uncertain than indicators at the midpoint level. Nevertheless, endpoint indicators allow for comparison of different systems that have impacts in different midpoint categories.

6.3 Life cycle assessment of energy systems: literature review

Several studies present LCAs of different electricity generation technologies. Weisser [192] presented emissions of the major generation technologies per unit of generated electricity. Asdrubali et al. [13] focused on renewable generation technologies. Atilgan and Azapagic [14] investigated environmental, social and economic impacts of several electricity generation technologies in the Turkish energy system based on historic data. They presented trade-offs between these impact indicators useful for policy makers. An extensive literature review was performed by Turconi et al. [177]. They presented emissions of the major generation technologies during construction and operation phases based on several studies. They emphasized the importance of data and functional unit
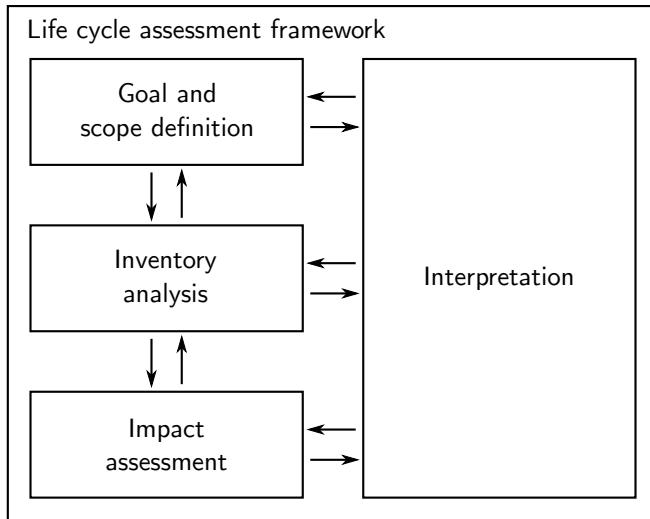
Figure 6.3: Different phases in a life-cycle assessment, adapted from [92].

transparency as large differences were observed between studies. All these studies show a large variation in environmental impact of electricity generation technologies. This variation is partly caused by regional effects. However, differences in assumptions and model boundaries have a large impact as well. Therefore, it is crucial that authors clearly describe the functional unit for which data are presented and are transparent in the assumptions made.

Jones et al. [100] compared consequential LCA with net energy accounting and suggested the combination of both methods for the analysis of distributed electricity generation. They used a functional unit of 1 kWh of electricity delivered to consumers by the complete system, including traditional and distributed electricity producers. Treyer and Bauer [174] investigated the impact of future electricity use in the United Arab Emirates assuming different technological options. They emphasized the importance of energy efficiency measures combined with the introduction of clean generation technologies to cope with expected population growth and rising energy demand. However, they did not take dynamic effects of a changing electricity mix into account. Wolfram et al. [194] presented carbon footprints of electricity generation under different scenarios. Turconi et al. [178] investigated the impact of future electricity use in Denmark. Amor et al. [7] showed that using country average electricity mixes results in significant errors when assessing systems which cause shifts in the electricity mix. They proposed a methodology which uses hourly electricity generation data to identify which technology is displaced when distributed

renewable electricity sources are promoted. García-Gusano et al. [75] combined an optimization of the electricity system with a conventional LCA approach to investigate the future impact of different energy scenarios in Spain. Pehnt et al. [141] used a merit order based optimization model of the electricity generation in Germany combined with an LCA of off-shore wind energy and compressed air energy storage. Turconi et al. [176] used a unit-commitment and economic dispatch model to compute generation schedules of each power plant in the future Irish electricity sector with different scenarios for future generation. They explicitly modeled the impacts of startups and part load operation of the fossil fired plants and concluded that this results in a change in greenhouse gas emissions of less than 5%. Effects of peak loads on the required transmission capacity were not accounted for.

In the above cited studies, no attention is given to the changes in required electricity transmission or distribution grid capacity. Either the impact of electricity transmission is neglected or no information about assumptions is provided even though this is essential to compare different studies. Arvesen et al. [12] presented a detailed attributional LCA of the Norwegian electricity transmission and distribution system. As data of the existing infrastructure was used, the results are not useful for estimating impacts when power flows change.

Only few studies are available in the literature which investigate the life-cycle impact of space heating using heat pumps. Nitkiewicz and Sekret [129] compared an electric heat pump with a gas absorption heat pump and gas boiler to supply heat to several buildings at a specific site in Poland. As this study handled a single specific system only, changes in the electricity system, caused by the introduction of the heat pump, were neglected. Blom et al. [19] analyzed the impact of heating an apartment building using a heat pump or gas boiler. Surprisingly, their results showed a condensing gas boiler has a lower environmental impact than a heat pump. This is however caused by the assumption of a very low performance heat pump, and a very large share of electricity generated by coal fired power plants. Furthermore, the study presented the impact on a single building, so possible changes in the electricity system due to large scale application of heat pumps were neglected.

Some studies estimated the overall CO_2 emissions of a large scale shift from space heating with fossil fuel fired boilers to heat pumps, or other heating technologies using electricity as energy vector, in different countries [29, 80, 104, 119, 155]. Roux et al. [155] computed the life-cycle impact of a building heated electrically or with a gas boiler and included the effects of the changing electricity market and climate over the 50 year life span of the building. They found a small change in impact over the lifetime caused by the changing electricity mix and the need for active cooling in the future due to climate change in

some scenarios. Greening and Azapagic [80] computed a lower global warming indicator for space heating with heat pumps using the 2012 UK electricity mix compared to gas boilers. They showed that ground source heat pumps lower the overall CO_2 emissions much more than air source heat pumps based on fixed average COPs. Furthermore, the effects of changes in the electricity mix were investigated. Carvalho et al. [29] computed the decrease in CO_2 emissions when natural gas boilers in Portugal are gradually replaced by ground source heat pumps. They used projections for the specific emissions of electricity generation to model the electricity use related emissions. Furthermore, emissions related to the production and recycling of the heat pumps were neglected. Similar analyses were performed for Ireland and the USA by Kelly et al. [104] and Lim et al. [119] respectively with more focus on the economic requirements for switching to heat pumps.

In the studies cited above, total CO_2 emissions related to the use of heat pumps were computed using a current or projected average electricity generation mix. However, when heat pumps are integrated into the electricity system on a large scale, this integration will have an effect on the electricity generation dynamics and resulting peak loads. Therefore, the required changes in the electricity system and the resulting changes in generation mix must be taken into account when assessing the impact of switching from fossil fuel fired boilers to heat pumps for residential heating.

Petrović and Karlsson [142] used an optimization model to minimize the operational and investment costs of the future Danish energy system while focusing on residential heat demand. As a by product of the optimization, the operational CO_2 emissions were presented. This approach takes into account the effects on the electricity system of introducing heat pumps. However, emissions related to peak loads and thus electricity generation and transport capacity were neglected.

In the literature, studies focusing on heat pumps and studies focusing on electricity generation are found. The former most often neglect the impacts of a large scale deployment of heat pumps on the electricity sector. The latter most often fail to include a detailed LCA analysis accounting for all environmental impacts.

In the present work a complete LCA of residential heating with heat pumps is presented, including the effects of large scale deployment on the electricity generation and the required electricity transport capacity. Furthermore, the benefits of adding a space heating hot water storage tank to the heating system are analyzed.

6.4 Life cycle assessment of residential heating: methodology

In this section, the LCA methods applied in this work are described in the format specified by ISO 14040 [92].

6.4.1 Goal

The use of heat pumps for space heating and domestic hot water production are recognized as a means to reduce greenhouse gas emissions of buildings. With increasing share of renewable electricity sources (RES) this reduction can be further increased. However, the simultaneity of space heating in all buildings combined with the variability of RES can result in periods with high residual loads and other periods with curtailing. Using thermal energy storage to shift thermal loads can reduce the need for peak generation capacity and can reduce RES curtailing. In residential buildings heated with heat pumps, thermal energy storage in the form of a hot water storage tank can provide additional flexibility to the electricity generation system. This flexibility can be used to lower electricity generation related CO_2 emissions. However, when evaluating all emissions and resources (broader than only CO_2) related to space heating, the investment in an additional energy storage tank, and the associated resources and emissions, must be taken into account.

The goal of the present study is to investigate the environmental impact of residential heating with heat pumps and thermal energy storage. When doing this, the required changes on the electricity generation side must be taken into account. The proposed scenario is compared to a conventional system where buildings are heated with condensing gas boilers. The different scenarios under consideration are denoted (*hp*) and (*gb*) for the scenarios with heat pumps and storage tanks and the scenario with gas boilers respectively.

6.4.2 Functional unit

One of the functions of a residential building is to supply a certain level of comfort to its users at times they request it. The purpose of the heating system in this building is to ensure thermal comfort of the occupants. This is achieved by keeping the indoor temperature within certain limits at all times and by supplying the domestic hot water needed. These limits and amounts depend on several factors and can vary in time [140].

This analysis leads to a description of functional unit definition as follows:

The supply of thermal comfort and domestic hot water to the inhabitants of a reference dwelling with a specified underfloor heating system during a reference year in the Belgian climate and with the Belgian electricity generation boundary conditions.

In this functional unit several terms have to be further quantitatively specified.

Throughout this work thermal discomfort is evaluated as the number of Kelvinhours (K h) calculated as the time integral of the absolute value of the difference of the operative temperature and the comfort boundaries when the temperature is outside a boundary. Thermal comfort is here specified in terms of heating comfort (no cooling is considered), stating that the operative temperature must always be above the minimum operative temperature which is taken 20°C in winter and 21°C in summer and varies as depicted in figure 6.4. In the Belgian climate it is possible to avoid most building overheating in summer, if sufficient attention is given to this aspect during the building design, without installing an active cooling system. Nevertheless, some overheating can occur. Therefore thermal comfort for overheating in this study is translated into the requirement that the overheating Kelvin-hours calculated using a maximum operative temperature limit of 22°C in winter and 24°C in summer (figure 6.4) must remain below 250 K h. From the maximum operative temperature and the ambient temperature in the year 2013 presented in figure 6.4, the amount of overheating thermal discomfort in the ambient environment (if no heating system or building would be in place) is 810 K h. As a cooling system is not within the scope of this study, the upper limit of 250 K h is taken which must be achieved using energy storage in the building thermal mass and active window shading only.

The supply of domestic hot water is further specified as the supply of 0.09 m^3 hot water at 45°C in a period between 7:00 and 11:00 and the supply of 0.15 m^3 hot water at the same temperature in a period between 20:00 and 24:00 every day as described in section 5.3.2.

The reference dwelling with the underfloor heating system used throughout this work is based on [149] and is described in more detail in section 5.3.1.

As the reference year the year 2013 is taken. For this year synchronous data for weather conditions and the Belgian electricity demand and generation from different generating units are available [51].
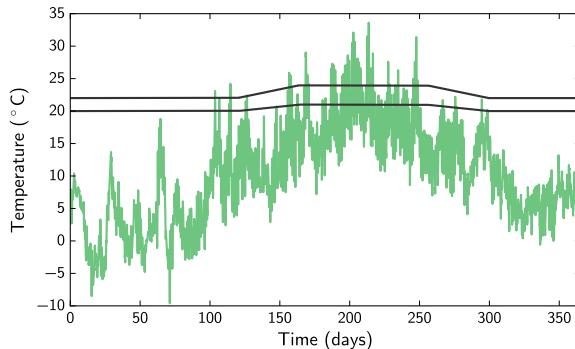
Figure 6.4: Minimum and maximum bound to the indoor operative temperature for evaluating thermal comfort. Additionally the ambient temperature is presented.

6.4.3 System and system boundaries

The system under consideration consists of the set of buildings and the electricity generation park as presented in chapter 5. To correspond to the functional unit defined above, one of the buildings from the set is considered. However, impacts for the electricity generation park will also be presented while including the complete set of buildings.

The system boundaries of the *hp* scenario, with a heat pump and hot water storage tank, and the *gb* scenario, where a condensing gas boiler provides the space heating and domestic hot water, are schematically presented in figure 6.5a and figure 6.5b respectively.

Due to the simultaneity of space heating, the impact of the *hp* scenario on the electricity generation side can not be neglected. Changes in the generation mix, required additional generation units and changes in the electricity transmission and distribution network must be accounted for. To this end, the amount of electricity generated by different types of power plants is included in the system boundaries. As in chapter 5, electricity generated from on- and offshore wind turbines (wind), PV, nuclear power plants (nu), CCGT and OCGT are considered. The required generation capacity for each type of electricity generation is also included. Furthermore, as electric power requirements change, changes in the electricity transmission and distribution network could be required and must therefore also be included within the system boundaries.

The systems responsible for heat generation and heat storage are evidently included. However, as the functional unit fixes the building and the emission system, these are common to both scenarios and can be excluded from the system
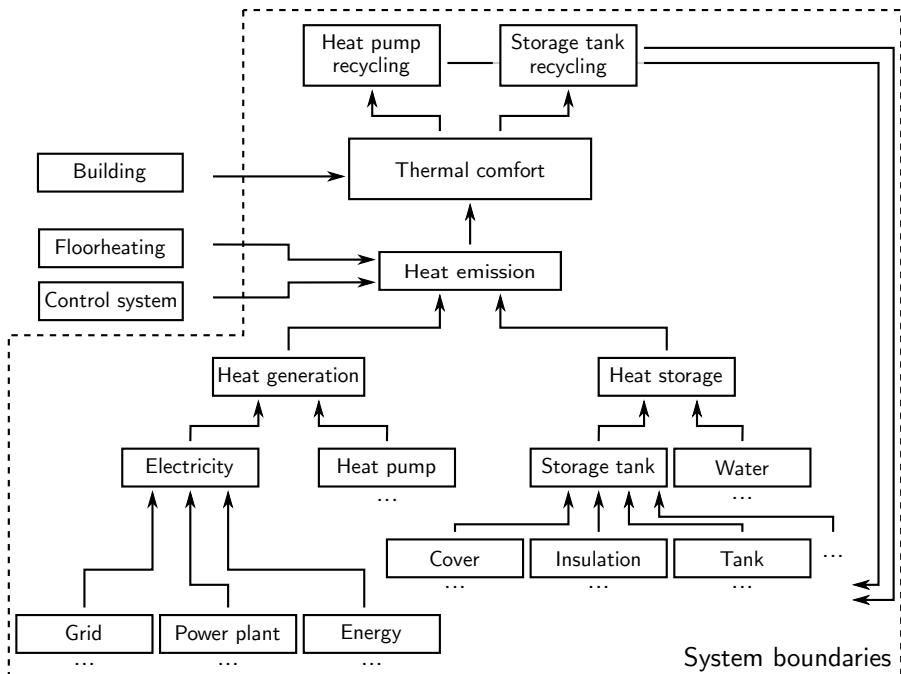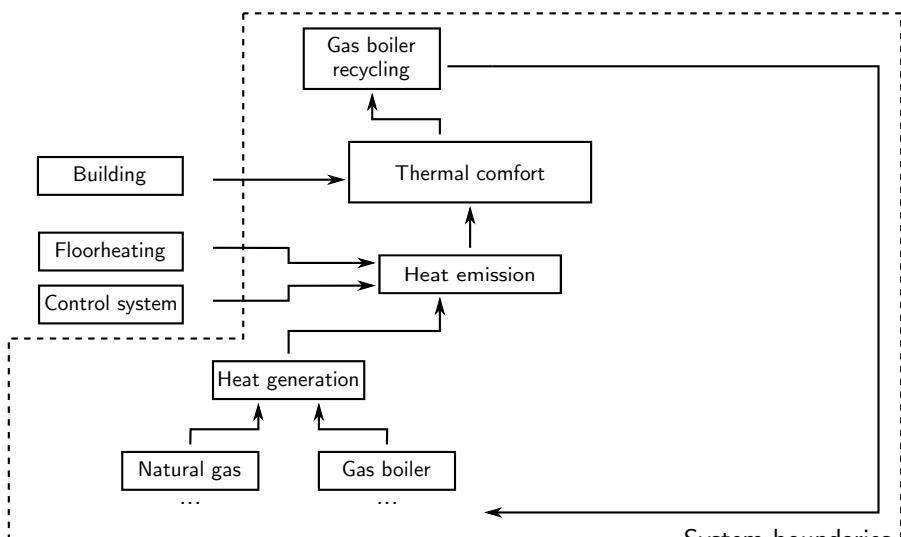
(a) heat pump and hot water storage tank (*hp*)

(b) gas boiler (*gb*)

Figure 6.5: Schematic overview of the boundaries of the systems under consideration. Dots, indicate the inclusion of the complete production chain of a unit-process.

boundaries. This greatly simplifies the analysis as a building is typically a very complex structure with many different materials and construction processes. Furthermore, the building itself has more functions than only providing thermal comfort. It would thus be unfair to assign the total impact of the building to the functional unit under consideration.

However, this simplification does not take into account changes in the building structure required to accommodate for the heating system. For example, the integration of a large storage tank in a building requires a substantial amount of floor area. Therefore, the storage tank is assumed to be located in a technical room in the basement of the building, where it does not significantly detracts from the main building function. This simplification also implies that only absolute differences in the final impact scores can be considered. Relative differences can not be calculated as the total impact required to provide the functional unit is not computed.

The control system itself is also omitted from the system boundaries. In both scenarios an MPC controller is used. The required computing power, and thus circuitry and power use will thus be similar in both cases. Furthermore, the impact and cost of both will be small with recent developments in low power electronics.

Waste treatment and recycling of the heating system (heat pump and storage tanks or gas boiler) are also included in the system boundaries. End-of-life treatment of the required power plants is not included in the system boundaries except for the nuclear power generation where the end-of-life treatment of the generation facility and the treatment of nuclear waste are included within the record.

In the *gb* scenario, all buildings are heated with a modulating, condensing gas boiler. The gas boiler also ensures the production of domestic hot water. A boiler with 11 kW thermal power is selected as this is the combined rated thermal power of the heat pump and electric resistance heater installed in the *hp* system.

6.4.4 LCA methodology and inventory calculation

When computing the inventory of a product system two main modeling assumptions can be made: attributional modeling or consequential modeling.

In an attributional model, the processes required to create a specific product are assigned based on historic values and market averages. In a consequential model, the consequences of a possible change from one product system to an

alternative are estimated [92]. To create a consequential model, assumptions on how the product will alter the current markets must be made and constrained suppliers of alternative products must be excluded from the analysis.

Schmidt et al. [158] described the differences between an attributional and consequential approach for the use of electricity. In an attributional model, the current average country specific electricity mix is used to compute the impact of 1 kWh of electricity use. In the consequential approach, the impact of 1 kWh additional electricity use, on top of the current electricity use, is computed. When applying this approach in a Belgian context, the constrained suppliers of electricity, e.g. nuclear generation and current renewable generation, must be left out of the analysis. As the capacity of renewables is still increasing, part of the additional electricity use will originate from new renewable sources. To include this, data for the growth rate of the renewable capacity is required.

In the scope of the current study, a comparison between alternative systems is made. This dictates a consequential approach. However, the largest consequences in the system under investigation will stem from the additional use of electricity and the electricity source. As the changing electricity mix is modeled explicitly the benefits of a consequential approach would be minimal. Furthermore, as a multitude of assumptions is required, it would lead to a large increase of the uncertainty. For these reasons all analyses in this work are carried out using an attributional approach, while explicitly accounting for the consequences of the additional electricity use.

6.4.5   Data sources and modeling assumptions

All unit-processes used in this work have been derived from the Ecoinvent version 3 database [191]. However, for most processes, default options available in Ecoinvent were not suitable for the analysis and had to be modified. The following subsections provide an overview of the modeling assumptions, a detailed description of the Ecoinvent processes used is given in appendix B.

Electricity generation

In a demand response context, electricity generation is shifted between different types of power plants. The assumed load factors in Ecoinvent will therefore not be valid. To accommodate this change in load factor, for each plant type, the inventory of the generated electricity was split into a part originating from the required generation capacity and a part originating from the generated electricity. This way, the assumed load factors are no longer required as both

the installed capacity and generated electricity are computed from the dynamic simulation or are fixed in advance.

For on- and offshore wind electricity generation all sub-processes are related to the installed capacity, none of the inputs are related to the actual electricity generated by the wind turbine. A reference turbine with 2 MW nominal power and a lifetime of 20 years is assumed [191]. On- and off shore generation are combined into a single wind electricity generation process assuming the installed capacity is divided equally.

For photovoltaic generation, rooftop mounted panels on an inclined roof are considered. Similar to the wind generation process, all impacts are related to the installed capacity of 3 kW and the assumed system lifetime is 20 years [191].

Nuclear generation capacity in Belgium is present in the form of several pressurized water reactors. A 1000 MW power plant with a lifetime of 40 years is assumed. In the existing Ecoinvent process the load factor is assumed 0.886. From this, the unit-process representing the power plant construction and decommissioning is extracted from the main record and used to compute the impact related to the installed capacity. All other processes in the original nuclear generated electricity process are assumed to be related to the generated electricity.

For electricity generated by a CCGT or OCGT a similar approach is followed. A power plant capacity of 400 MW for the CCGT and 10 MW for the OCGT and a lifetime of 25 years are adopted from Ecoinvent [191].

Electricity transport

The transportation of electricity from the generation plants to the end users can be divided in electricity transmission and distribution based on the voltage level. Ecoinvent contains processes for the transport of electricity at voltages above 20 kV, between 1 kV and 20 kV and below 1 kV. The functional unit of these processes is 1 km of electricity network at the specified voltage and all cables and lines are assumed to have a lifetime of 40 years [98].

In this work it is assumed that if the peak power demand in an electricity system changes, the capacity of the electricity transport network changes accordingly. Wind and PV generation are distributed generation technologies. It is assumed that electricity produced at these plants is used within the medium voltage electricity grid. The high voltage electricity transmission network is thus only affected by the residual peak load. The medium and low voltage electricity transportation grids are affected by the total peak load, including RES. In this work, the impact resulting from the required electricity transport infrastructure

Rated power	(kW)	4	6	8	11	16
indoor unit	(kg)	46	48	48	48	48
outdoor unit	(kg)	54	56	56	114	114
refrigerant	(kg)	1.45	1.60	1.60	3.40	3.40

Table 6.1: Mass of air to water heat pump indoor unit, outdoor unit and refrigerant with rated thermal power [154]

at the different voltage levels is computed using the total distance covered by the Belgian electricity grid scaled with the ratio of current total generation capacity and the computed power peak. The Belgian electricity grid consists of 8584 km transmission lines at a voltage higher than 20 kV, 75 742 km line at medium voltage and 159 200 km lines or cables at a voltage lower than 1 kV [170]. As the total generation capacity in 2015 in Belgium was 14 574 MW [52], the required distance of transmission lines at a voltage level higher than 20 kV, $D_{>20 \text{ kV}}$, to accommodate a peak residual power use, $P_{\text{residual}}^{\text{max}}$, is computed as:

$$D_{>20 \text{ kV}} = 8584 \text{ km} \frac{P_{\text{residual}}^{\text{max}}}{14 \text{ } 574 \text{ MW}} \tag{6.1}$$

Values for the other voltage levels are computed similarly but using the total peak power instead of the residual peak power to include the transportation capacity for RES. Other emissions originating from the transport of electricity such as sulfur hexafluoride in switch boxes, and ozone creation around high voltage lines [98] are taken into account by scaling the emissions from the Swiss electricity grid stated in Ecoinvent by the length ratio of the Belgian and Swiss transportation network. Note that to compute the impact of electricity transport, total generation capacity and grid data for the year 2015 were used, while for the electricity demand profile and the the profiles for wind and PV electricity generation, data for the year 2013 were used.

Heat pump and auxiliary heater

To model the air to water heat pump, the mass of the indoor and outdoor unit of a split heat pump and prescribed refrigerant mass were obtained from product specifications [154] and are presented in table 6.1. For the 7 kW rated thermal power heat pump specified in the simulations, a total mass of 104 kg and a refrigerant mass of 1.60 kg are derived from the next larger heat pump.

In Ecoinvent the construction of a brine water heat pump process is available and is used to model all types of heat pumps. From the record details, the total mass of the modeled heat pump is 131 kg. The refrigerant specified in the production data sheets was R410a, which is a common refrigerant in commercial

heat pumps. However, the life-cycle inventory of this refrigerant is not available in the Ecoinvent database. Therefore, the refrigerant is modeled as R134A, for which data is available. The available heat pump construction process is altered by scaling every component except the refrigerant with the ratio of the mass derived from the manufacturer data and the original mass in the model. For the refrigerant the actual refrigerant mass from the manufacturer data is used. The lifetime of the heat pump is assumed to be 20 years.

The auxiliary resistance heater is modeled as a 4 kW electric resistance heating element as specified in the simulations. The lifetime of the auxiliary resistance heater is assumed to be 20 years.

Hot water storage tank

Modeling the impact of a hot water storage tank with varying size forms a critical step in the current analysis. The impact of a storage tank can be split into the impact of its main components and their assembly. The main components are:

- Water: water is used as the thermal energy storage fluid (m^3).

- Pressure vessel: the actual steel tank used to contain the water including several fittings to connect pipes and instrumentation (kg).

- Insulation: the layer of insulation covering the pressure vessel (m^3).

- Cover: a polymer protection mantle surrounding the insulation (m^2).

Furthermore, the factory where the storage tank is produced and the assembly process itself must be taken into account. For each component the principal quantity is computed from the actual storage tank specifications. The storage tank is assumed to have rounded tank heads [45] while the top and bottom of the insulation layer are planar.

As a reference for modeling the production of a 2 m^3 hot water storage tank is selected. The subprocesses present are divided among the main storage tank components, the storage tank factory, the energy use during assembly and a remaining fraction, e.g. wood used for packaging. The inventories of the main components are scaled using their principal quantities as listed above. The storage tank factory is assumed to be replaced after the production of 50 000 tanks as is done in the reference process. All other records, including energy use, are scaled using the total storage tank steel mass. The storage tank is assumed to have a service life of 20 years.

For the domestic hot water tank, a similar method is used. Here, the reference process represents a 0.6 m^3 domestic hot water tank and all components are rescaled as stated above to the values for the 0.2 m^3 storage tank as used in the simulations. In addition to the above, the domestic hot water tank includes an immersed coil heat exchanger for which the mass is computed from its geometry.

Condensing gas boiler

For the condensing gas boiler, an approach similar to the heat pump was followed. The available Ecoinvent unit-process has a total mass of 143 kg so the inputs are scaled using the mass for a modulating, condensing gas boiler of 77 kg obtained from manufacturer data [154].

Waste treatment

Treatment of waste streams is taken into account for the main heating system components: the space heating storage tank if present, the domestic hot water tank and the heat pump or gas boiler. Only waste treatment of the main materials is taken into account and default Ecoinvent processes are selected to model them. Details are presented in appendix B. Furthermore, all systems are assumed to be transported 50 km by lorry to a disassembly site.

Special attention is paid to the heat pump refrigerant waste treatment as it has a potentially large effect on global warming. The refrigerant R410a which is used in most modern heat pumps has a global warming potential (GWP) of 1725 kg CO_2 eq./kg [69]. 80% of the refrigerant is assumed to be recycled when the heat pump is decommissioned. The remaining 20% is assumed to escape to the atmosphere. In Ecoinvent refrigerant release into the atmosphere is modeled as the emission of R134a. As the R134a has a GWP of 1300 kg CO_2 eq./kg the R410a emissions into the atmosphere are scaled by a factor 1725/1300 to obtain the equivalent R134a emission (the mass of refrigerant released into the atmosphere).

6.4.6 Life cycle impact assessment method

Udo de Haes et al. [179] defined four areas of protection, properties of a physical nature which have an intrinsic value that must be protected: human health, the natural environment, natural resources and the man-made environment. Specific societal or economic values can be attributed to all areas. The purpose of a life-cycle impact assessment (LCIA) method is to relate the inventory of emissions

and resources to these areas of protection. Although several impact assessment methods are available in the literature [62], in this work the ReCiPe method [78] will be used exclusively. ReCiPe was chosen as it is currently the most complete method, and offers a harmonized calculation method for endpoint indicators, e.g. the areas of protection, as well as midpoint indicators. Furthermore it allows a single score value to be computed, which allows comparison of different systems, scoring differently in individual impact categories.

ReCiPe considers 18 midpoint indicators and 3 endpoint indicators as schematically presented in figure 6.6. The endpoint indicators correspond directly to three of the four areas of protection listed above. Protection of the man-made environment is not included in the impact assessment method. The human health impact indicator is expressed in *Disability Adjusted Life Years* (DALY), and represents an estimate of the loss of life and quality of life due to disability in the world population. The ecosystems indicator is expressed in *Species · Years* representing the loss of species during a year. The resources indicator is expressed in monetary terms ($) as the marginal cost of future resource extraction.

To convert an inventory to impact indicators at the midpoint and endpoint level, LCIA methods use several models for environmental mechanisms and related assumptions. In ReCiPe, a choice between three perspectives can be made, which determines the inclusion or exclusion of some of these models:

- Individualist (I)

- Hierarchist (H)

- Egalitarian (E)

The individualist perspective computes impact on a short term time horizon (20-100 years). Only impacts that are undisputed are included, large future technological advances are assumed and the resilience of human society is assumed high. In the hierarchist perspective, a longer time frame, 100 years for some impacts to an infinite time frame for others, is assumed. The assumptions in this perspective are based on the most common policies. It is the default perspective in ReCiPe. The egalitarian perspective assumes the longest time frame for impact calculations (more than 500 years to infinite). Impacts without full scientific consensus are included and technological advances which would lower the impact are assumed small.

The conversion of impact indicators to a single score value uses a normalization and a weighting step. Normalization expresses the impact in a certain category relative to the total impact in a certain region of the world during a reference
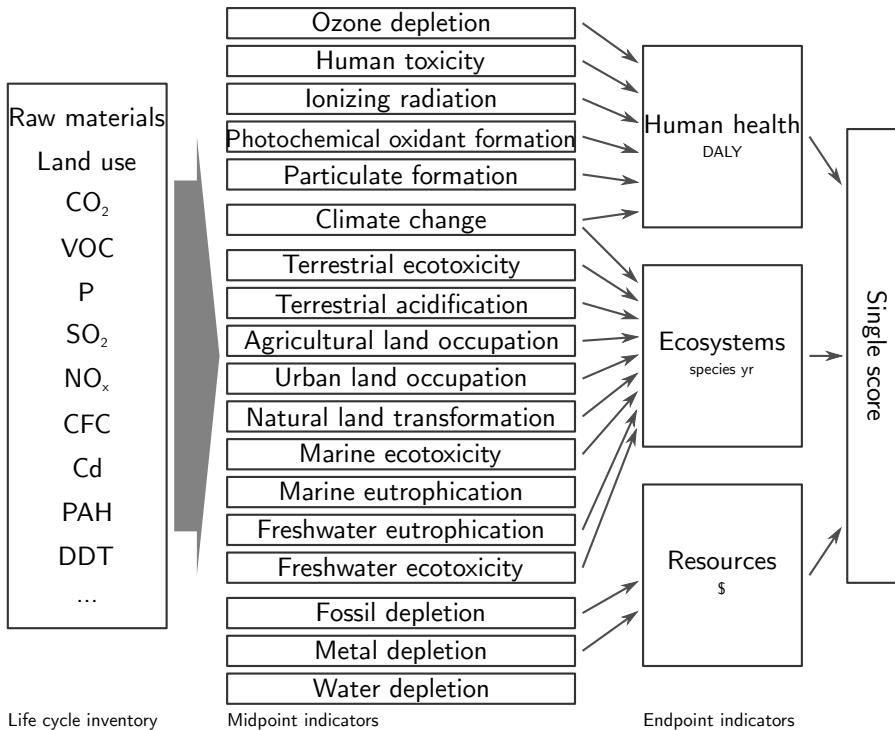
Figure 6.6: Relationship between ReCiPe midpoint and endpoint impact indicators. Adapted from [78].

year [17]. Afterwards, a single score value is obtained by computing a weighted average of the scores in different impact categories. In ReCiPe, normalization data for Europe and the entire world are available.

In this work, a hierarchist perspective with European normalization data and an average weighting set will be used as it is the most accepted and used perspective. This LCIA method is designated *ReCiPe Europe H/A*. With the average weighting dataset (A), the single score values are computed with 40%, 40% and 20% weighting for the human health, ecosystems and resources endpoint categories respectively. The main comparison of systems will be made based on the single score impact, although important midpoint indicators such as climate change and ionizing radiation will also be presented.
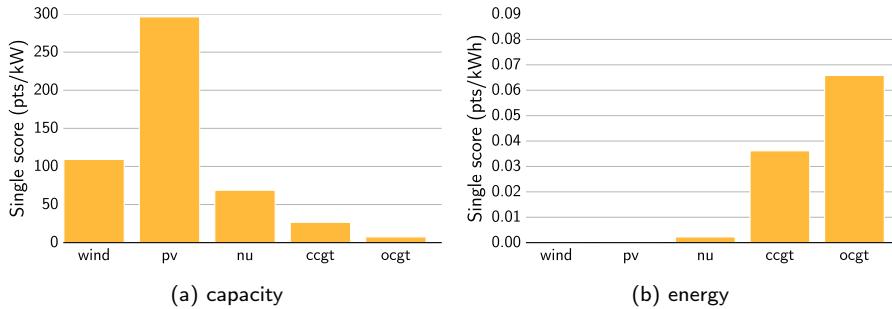
Figure 6.7: Single score data for capacity of different power plants and electricity generated by different power plants.

6.5 Space heating storage tank sizing to minimize the life-cycle impact

6.5.1 Electricity generation impact

The single score impact for electricity generated by the different power plant types under consideration are presented in figure 6.7. The results are split into a part originating from the installed power plant capacity (figure 6.7a) and a part assigned to the electricity production (figure 6.7b) as this allows the evaluation of the total impact without assumptions for the load factor in each plant type. These values are in line with values found in the literature [177].

In figure 6.8, the total single score impact of the electricity generated in Belgium is presented for the reference case, without heat pumps (*gb* scenario), and for different values of storage tank volume and control settings in the *hp* scenario. The additional impact of the extra electricity use by the 500 000 buildings with heat pumps is clearly visible as an increase of nearly 100×10^6 impact points. Differences between different heat pump scenarios seem less pronounced.

When subtracting the impacts in the *gb* scenario from the the impacts in one of the *hp* scenarios and dividing the result by the number of heat pumps, the impact attributed to the heating of a single building using a heat pump is retrieved. In figure 6.9 the single score (figure 6.9a) and midpoint climate change indicator (figure 6.9b) are presented. Overall the appearance of figure 6.9a and figure 6.9b are very similar, confirming that greenhouse gas emissions have the highest contribution to the electricity sector environmental impact.

The additional impact of electricity generated by renewable sources is zero as the installed capacity of renewables is unchanged and for these sources the full
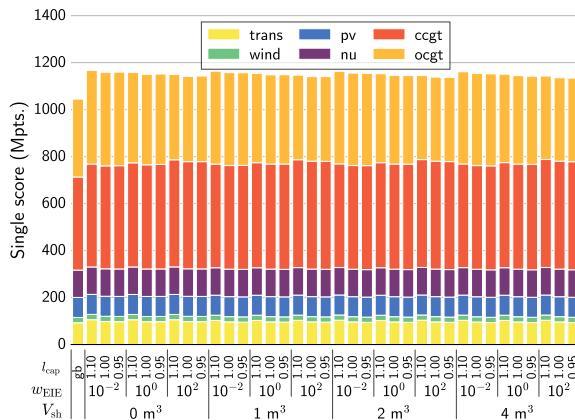
Figure 6.8: Yearly total environmental impact of the assumed electricity generation for the *gb* scenario and *hp* scenarios with varying capacity limit (l_{cap}) and environmental impact of energy use weight (w_{EIE}) control parameters and space heating storage tank size (V_{sh}).

impact is attributed to the installed capacity instead of the generated electricity. Furthermore, in all cases the residual load is always above zero meaning no curtailing of RES occurs. In the cases with a certain level of demand response to reduce the impact of electricity generation ($w_{EIE} > 10^{-2}$), a slight increase in electricity generated by nuclear power plants is observed. This results in a very small change in additional impact in the single score indicator. For the climate change midpoint indicator, this change is negligible.

For each storage tank size, a similar pattern in total impact is observed, when increasing the energy control setting, the impact is lowered. Furthermore, when tightening the overload threshold by decreasing l_{cap}, the impact is lowered further in most cases. With increasing w_{EIE}, electricity generation is shifted from OCGT plants to more efficient CCGT power plants, leading to a reduction in impact. When the overload threshold is decreased, the decrease in environmental impact is mostly caused by a reduction in required transportation capacity.

6.5.2 Heating system impact

The yearly impact of a single heating system with a heat pump lies between 11 and 17 impact points, and the associated CO_2 emissions are between 85 and 115 kg CO_2 eq. per year, depending on the space heating storage tank size (figure 6.10). The impact of a heating system with a condensing gas boiler is significantly less, only 2.5 impact points.

(a) single score

(b) climate change
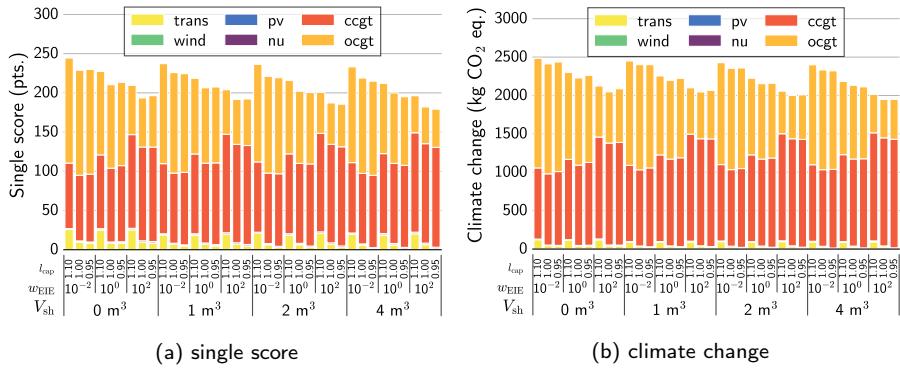
Figure 6.9: Yearly environmental impact of the additional electricity generation expressed per building for the *hp* scenarios with varying capacity limit (l_{cap}) and environmental impact of energy use weight (w_{EIE}) control parameters and space heating storage tank size (V_{sh}).

(a) single score

(b) climate change
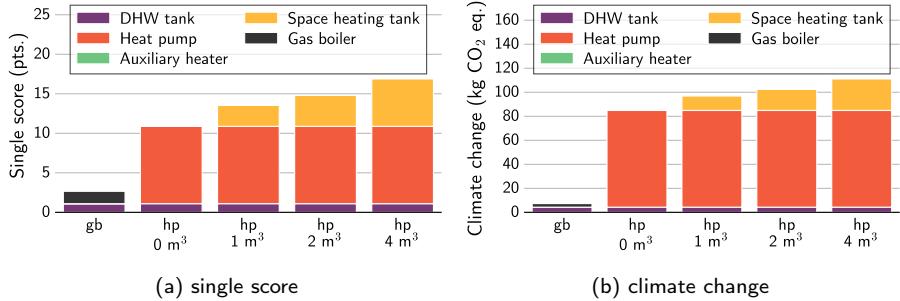
Figure 6.10: Yearly environmental impact of the heating system including heat pump and hot water storage tank in a building versus a heating system including a gas boiler. The *hp* scenario considers different storage tank sizes.

The heat pump is the main contributor to the environmental impact of the heating system, both for the endpoint single score (figure 6.10a) and the midpoint climate change (figure 6.10b) indicators. This impact is mainly caused by the refrigerant, for which the production is rather CO_2 intensive. Furthermore, during the decommissioning of the heat pump, it is assumed that part of the refrigerant, which has a large GWP, escapes to the atmosphere.

The construction and waste treatment of the space heating storage tank has the second largest environmental impact (figure 6.10). When considering the CO_2 emissions related to the storage tank, the insulation is the largest contributor, followed by the energy required during the assembly and other processes (figure 6.11b). In contrast, in the endpoint indicator, the storage tank

(a) single score

(b) climate change
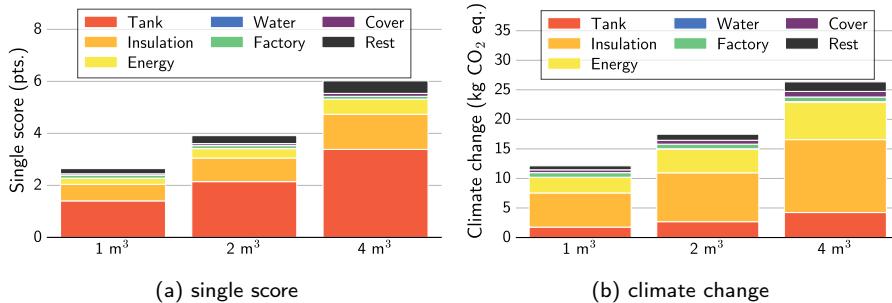
Figure 6.11: Yearly environmental impact of the hot water storage tank construction for the different investigated storage tank sizes.

pressure vessel has the largest contribution (figure 6.11a). This is caused by a large amount of iron and steel which needs to be extracted and causes a large impact in the metal depletion endpoint category.

With the results presented in chapter 3, the environmental impact of a hot water storage tank can be compared with the impact of an electrical battery system. The production of a lithium-ion battery with an initial electrical storage capacity of 1 kWh results in an environmental endpoint single score impact of 15 points and a greenhouse gas emission of 48 kg CO_2 eq. In chapter 3, the combination of a 2 m^3 hot water storage tank and an air coupled heat pump was able to discharge the equivalent of around 6 kWh electrical energy. This value is obtained by multiplying the ideal storage capacity of a 2 m^3 hot water storage tank operating between 20°C and 35°C (34.7 kWh) with the effective electrical storage capacity ratios for the 24 h simulation period (0.17-0.19) obtained in section 3.4. For lithium-ion batteries, failure after 800 - 1500 cycles is reported in the literature [53]. In the simulations described in chapter 5, the 2 m^3 storage tank performed 120 charging-discharging cycles, counted as the times the average storage tank temperature cycled between 20% and 80% of its extreme values. This results in a lithium-ion battery life time between 6.5 and 12.5 years. To obtain an electrical storage capacity of 6 kWh the yearly single score impact is between 7.2 and 13.8 points with greenhouse gas emissions between 23 and 44 kg CO_2 eq. These values are substantially higher than the values reported for the 2 m^3 hot water storage tank of around 4 points and 17 kg CO_2 eq. Nevertheless, an electrical battery has the ability to discharge electricity to the grid which makes it more versatile as it is able to reduce the fixed residual load. Furthermore, in summer when the heating demand is very low the electrical battery can still be used to shift electricity generation to less emitting power plants.

6.5.3   Total impact

Heating buildings using heat pumps and thermal energy storage tanks must be evaluated based on the the total impact which consists of the impact related to the energy use plus the impact related to the heating system construction and waste treatment. The total single score impact of heating a single building and its contributions in the areas of protection considered in the ReCiPe LCIA method are presented in figure 6.12. The reduction of impact when switching from condensing gas boilers to heat pumps is most notable. Even if heat pump owners do not take the generation and transportation of electricity into account and minimize their own cost, a reduction of around 73 points is obtained. If the control system attempts to shift the electricity demand such that more electricity is generated by more environmentally friendly power plants, a further reduction of 35 points is observed. If finally the heat pump control system attempts to reduce the peak power demand, the life-cycle impact is reduced by an extra 16 points, resulting in a total impact reduction of 124 points per building.

The addition of a hot water storage tank only marginally affects the total life-cycle impact. A maximum reduction of 12 points is obtained when a 4 m^3 storage tank is installed. If a 1 m^3 hot water storage tank is added to the system some control settings even increase the total environmental impact. In these cases, the relatively small storage tank does not significantly increase the system flexibility. However, when the storage tank is active, heat losses inevitably increase leading to an increased energy use and a small rise in environmental impact.

When analyzing the contributions of the endpoint indicators to the single score (figures 6.12a and 6.12b), the human health and resources indicator are considerably larger than the ecosystems indicator. The large human health indicator can be mainly contributed to the climate change effect, caused by CO_2 emissions either directly from the gas boiler, or indirectly from the additional electricity generation and refrigerant loss. The resources indicator has a large contribution due to the required natural gas extraction in all cases.

In figure 6.13 the single score impact, and three important midpoint indicators are presented, with contributions divided over the required additional generation and transportation capacity with respect to the *gb* scenario, the energy use (in the form of electricity or natural gas) and the heating system. It is clear that the energy use still has the largest impact for all indicators and all systems.

For the energy and capacity contributions, relative values can be obtained as these subsystems lie completely within the system boundaries. Switching from natural gas heating to a heat pump is seen to cause a 34% reduction in single

(a) main impact categories

(b) detailed impact categories
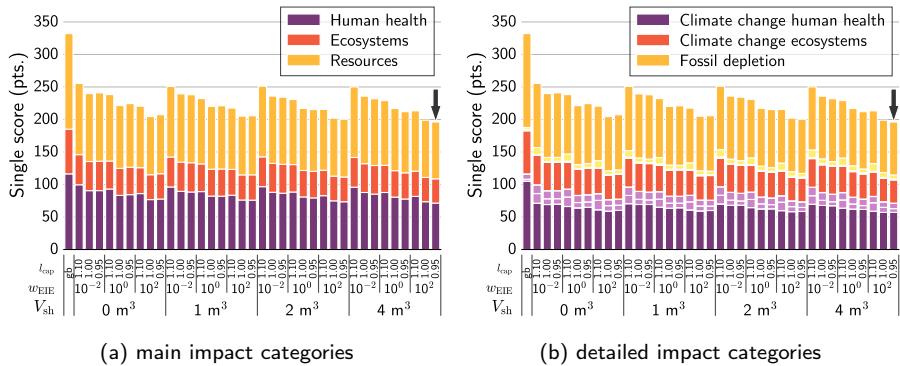
Figure 6.12: Total single score endpoint environmental impact for a single building and the contributions of different endpoint indicators to the single score for the *gb* scenario and *hp* scenarios with varying capacity limit (l_{cap}) and environmental impact of energy use weight (w_{EIE}) control parameters and space heating storage tank size (V_{sh}). On the left the added impact indicators are shown. On the right, the most contributing endpoint indicators are presented. Less contributing indicators are colored lighter and omitted in the legend. For clarity, the case with minimum impact is indicated by the arrow.

score impact when no demand response is applied. With a high energy and capacity setting a 43% reduction in impact is obtained. When a 4 m^3 storage tank is added, the reduction in single score impact related to energy use is 46% relative to the reference case using a gas boiler.

In the presented case, switching residential heating from condensing gas boilers to heat pumps results in a reduction in greenhouse gas emissions of around 1230 kg CO_2 eq. per building per year, even if the control systems do not take the electricity system needs into account. Through the use of DR, an additional saving of around 400 kg CO_2 eq. can be obtained by shifting electricity generation to more efficient power plants and reducing peak loads. The addition of a 4 m^3 space heating hot water storage tank only further reduces emissions by around 110 kg CO_2 eq. per building per year. Overall, this results in a reduction of around 1740 kg CO_2 eq. per building per year. In Belgium, total greenhouse gas emissions were around 118 Mt CO_2 eq. in the year 2014 [163]. Switching from natural gas heating to heat pump heating and applying DR with hot water storage tanks in 500 000 buildings results in a decrease in emissions of 0.87 Mt CO_2 eq. or a reduction less than 0.75%. This reduction is very small compared to the targets set by the European union or the reductions required to limit the effects of climate change (figure 6.1). Nevertheless they contribute to the goal.

The ionizing radiation indicator is observed to behave opposite to the total impact (figure 6.13c). Part of the increase in energy use is always delivered

(a) single score

(b) climate change

(c) ionizing radiation

(d) terrestrial acidification
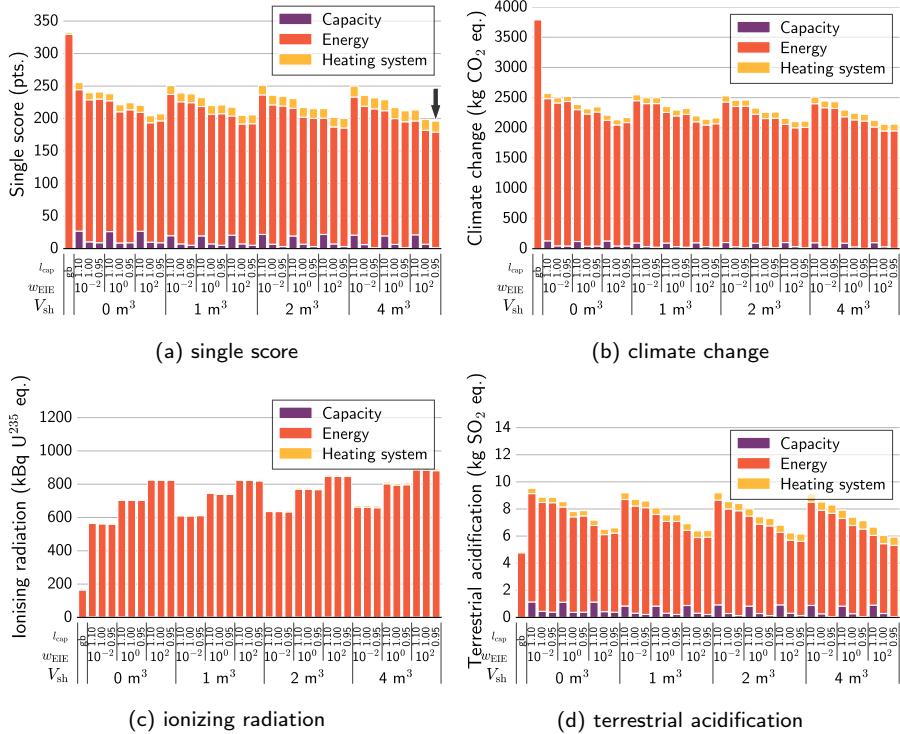
Figure 6.13: Total environmental impact of space heating using heat pumps and hot water storage tanks for demand response versus a gas boiler. The *hp* scenario considers different capacity limit (l_{cap}) and environmental impact of energy use weight (w_{EIE}) control parameters and space heating storage tank sizes (V_{sh}).

by nuclear power generation, leading to an increase in radioactive elements released to the environment. Nevertheless, the total impact of this increase is very small. Terrestrial acidification is seen to decrease when more electricity is generated by efficient power plants and when less electricity transport capacity is required (figure 6.13d). However, switching from gas boilers to heat pumps always increases acidification due to the increase in electricity generated by OCGT power plants.

6.5.4 Trade-off curves between consumer cost and environmental impact

For a building owner, the costs of being environmentally friendly are important to consider. All costs calculated in the present section are computed using Belgian electricity and natural gas tariffs as seen by building owners, including taxes, at the time of writing. This is an electricity price of 0.22 EUR/kWh from 22h to 7h and during the weekends and 0.25 EUR/kWh otherwise. A natural gas price of 0.06 EUR/kWh is used. Installation costs for the heat pump and gas boiler are obtained from [154], while costs for several storage tanks of varying sizes are retrieved from [157]. All presented cost values are yearly costs computed without a discount rate for future expenses.

With these values, and the environmental impacts of the presented scenarios computed above, trade-off curves between consumer cost and environmental impact can be generated (figure 6.14 and figure 6.15). Striking is the large difference in both cost and impact between the *gb* and the *hp* scenarios. Due to high electricity prices relative to the price of natural gas and the larger installation costs of a heat pump, switching from natural gas heating to a heat pump results in a yearly increase in costs larger than 320 EUR.

Increasing the system flexibility by adding a storage tank never incurs a decrease in costs when compared to a system with similar settings without storage tank. Even though hot water storage tanks are the cheapest option for thermal energy storage, the additional investment is too large. However, some cases with storage tank are seen to be Pareto-optimal.

The cases without storage tank and with a capacity control setting $l_{\mathrm{cap}} = 1.00$ are seen to be Pareto-efficient related to the single score impact. Most cases with a storage tank are too expensive for building owners, and similar environmental impacts can be obtained without a storage tank and different control settings. Only the cases with a 2 m^3 or 4 m^3 storage tank, an energy control setting of $w_{\mathrm{EIE}} = 10^2$ and a capacity control setting of either 1.00 or 0.95 are seen to lie on the Pareto-front (figure 6.14b). Adding a storage tank to the system always increases heat losses, as the storage tank must be kept at a relatively high temperature to be useful. The added flexibility must allow for a large enough shift in electricity generation to efficient power plants to counter the impact of the increased heat losses.

Within the *hp* scenario, a decrease in single score of 63 impact points can be obtained. However, this decrease is accompanied by an increase in costs carried by the consumer of around 265 EUR per year. Nevertheless, a large decrease in impact (55 points) can be obtained without a storage tank, by simply altering the control settings, and only increases consumer costs by 45 EUR per year.
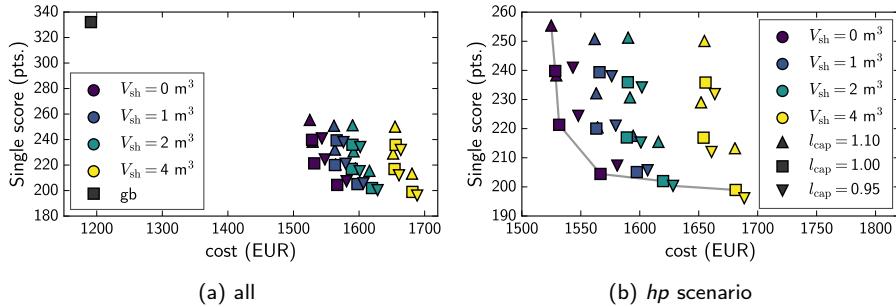
Figure 6.14: Trade-off data between yearly costs paid by the building owner and the total yearly environmental impact caused by building heating expressed as a single score impact indicator. On the left all cases, including the gas boiler scenario are shown, on the right only heat pump cases are shown. Cases on the Pareto-front are connected in gray.
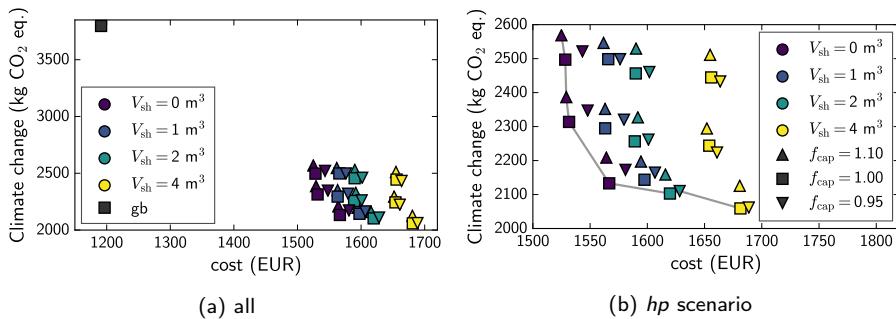
Figure 6.15: Trade-off data between yearly costs paid by the building owner and the total yearly greenhouse gas emissions caused by building heating. On the left all cases, including the gas boiler scenario are shown, on the right only heat pump cases are shown. Cases on the Pareto-front are connected in gray.

The Pareto-front related to the total greenhouse gas emissions (figure 6.15b) is similar to the single score Pareto-front. A small difference is that the case without storage tank, a high capacity control setting ($l_{cap} = 1.10$) and a medium energy control setting ($w_{EIE} = 10^0$) is also Pareto-efficient.

6.6 Conclusion

When evaluating the environmental impact of introducing heat pumps for space heating and domestic hot water production on a large scale, the potential effects on the electricity system must be taken into account. The use of demand

response and the investment in a hot water storage tank allow shifting electricity generation to more efficient power plants and reducing peak loads.

The overall environmental impact of residential heating with heat pumps is evaluated using a life-cycle assessment method and compared to the impact of a traditional gas boiler system. The introduction of a large number of heat pumps in the electricity system causes a substantial increase in electricity use and accompanying greenhouse gas emissions and environmental impact. Furthermore, the impact caused by the production of the heat pump is larger than the impact caused by gas boiler production. Nevertheless, the overall greenhouse gas emissions and environmental impact of heat pump heating is substantially lower than those of gas boiler heating even if the heat pump controllers do not take the electricity generation side into account. The application of demand response using the building thermal mass as energy storage, further reduces the impact of electricity use, and thus the total impact. The addition of a hot water storage tank to increase the thermal energy storage capacity has only a small effect on the environmental impact. The hot water storage tank mainly enables a reduction in peak load, which reduces the investments in the electricity grid and the associated environmental impact.

Overall greenhouse gas emissions are reduced from 3800 kg CO_2 eq. per building per year in case of gas boiler heating to around 2570 kg CO_2 eq. for heat pump heating without demand response. Taking the electricity system into account further reduces emissions to around 2170 kg CO_2 eq. per building per year. The introduction of a 4 m^3 hot water storage tank further lowers overall emissions to 2060 kg CO_2 eq. per building per year. In relation to the total Belgian greenhouse gas emission, this is a decrease of less than 0.75% which is very low compared to global emission targets. Nevertheless, the emissions associated with space heating and domestic hot water production in the considered set of residential buildings are substantially reduced.

In the trade-off between environmental impact and user cost, a storage tank of 1 m^3 is always suboptimal. The introduction of a storage tank in the system causes significant additional heat losses requiring a sufficiently large storage tank to make up for the additional energy use by more efficient generation and reduction in peak load.

These conclusions are of course strongly dependent on the assumptions made during the LCA. Furthermore, as the results from the integrated MPC simulation are used as inputs for the LCA, assumptions made here, for example, related to the building structure or building model, affect the LCA results.

Chapter 7

Conclusion

The use of heat pumps for residential heating applications has the potential to increase energy efficiency and reduce residential greenhouse gas emissions. However, the introduction of large numbers of heat pumps in the electricity system could disrupt the load diversity as space heating loads are ambient temperature driven and thus highly simultaneous. Flexible operation of heat pumps using the building thermal mass and a dedicated space heating hot water storage tank as thermal energy storage is proposed to mitigate this issue. Furthermore, demand response allows shifting electricity generation to more efficient power plants, further reducing the emissions associated with residential heating. When evaluating the environmental merits of such a system, the full life-cycle of the involved components with their interactions must be taken into account.

7.1   Main findings

The objective of this work was to assess the environmental impact of residential heating systems with heat pumps and hot water storage tanks in an electricity system with renewable energy sources.

In chapter 1 several research questions were posed to which in the course of this work an answer was given.

How can the total environmental impact of residential heating with heat pumps and hot water storage tanks be estimated, accounting for the effects a large scale integration of heat pumps has on the electricity system?

A life-cycle assessment of the heating system and a simplified electricity generation park is presented in chapter 6 and is used to compare emissions related to residential heating with different heating systems and to aggregate emissions of several substances and resource use into a single score impact indicator. In such an assessment it is important to take into account the effects a large scale deployment of heat pumps has on the electricity system, including the required electricity transmission and distribution capacity. The developed framework for integrated life-cycle assessment of residential heat pump heating and its effects on the electricity system was unavailable in the literature.

To model the interaction of the set of buildings and the electricity system, an integrated model predictive control simulation of a representative building and the electricity generation park is developed in chapter 5. The multi-objective model predictive control approach developed in this work is a significant step further than the analyses found in the literature which employ open-loop optimal control or do not take feedback on the electricity system into account.

The use of model predictive control is recommended over open-loop optimal control as modeling a hot water storage tank combined with a heat emission system and a heat pump in a way suitable for optimization results in a significant mismatch or underestimation of the effective storage capacity. Open-loop optimal control of heating systems including a hot water storage tank was shown to underestimate operational heating costs in chapter 4. Several optimal control formulations for a heating system including a hot water storage tank were formulated and compared whereas in the literature only temperature independent state-of-charge models were found.

The merit of different storage tank charging and discharging strategies is analyzed and discussed in chapter 3. Based on this analysis a fixed temperature charging strategy and flow modulation discharging strategy was selected as most suitable in a demand response context.

A model predictive control simulation can predict the heating costs with more accuracy as a more accurate model of the hot water storage tank can be used. In chapter 2 a hot water storage tank model suitable for use in full year building simulations, including accurate representations of three-dimensional effects, such as inflow mixing and buoyancy, is developed and experimentally validated. Furthermore, modeling attempts for immersed heat exchanger charging and storage tank heat losses were developed and compared with experimental

observations.

The above described methodology, integrating all methodological novelties, enables the estimation of the total environmental impact of residential heating with heat pumps and hot water storage tanks. To answer the remaining questions, a case study inspired by the Belgian electricity system with a large number of heat pumps and a significant amount of renewable electricity sources is performed.

What is the optimal storage tank size to minimize the total environmental impact of residential heating with heat pumps?

In a case study of an electricity system including renewable energy sources, with a large number of heat pumps participating in a demand response program to minimize the environmental impact of electricity generation, the effect of adding a storage tank of different sizes is investigated. The majority of environmental impact can be attributed to energy use. Without a hot water storage tank, the contributions to the overall impact related to the heating system production and decommissioning and the electricity transportation capacity are similar in magnitude and rather small. Adding a larger storage tank allows shifting more electricity generation from less efficient to more efficient power plants. Furthermore, a larger storage tank enables a peak electricity demand reduction, which reduces the required electricity transmission and distribution capacity. However, the environmental impact related to the storage tank itself is non-negligible and rises with storage tank size.

The addition of a small storage tank was shown to have a slight detrimental effect on the overall environmental impact due to increased heat losses. Adding a larger storage tank decreases the environmental impact of residential heating up to a storage tank size which is rather unrealistic (too large) for residential applications. Thus no optimal storage tank size was obtained or stated differently, the storage tank size which minimizes the environmental impact of residential heating with heat pumps is unrealistically large.

What is the trade-off between total environmental impact and financial cost of such a system?

Shifting residential heating from using gas boilers to heat pumps enables a significant reduction in CO_2 emissions and total environmental impact, even if the heat pump controllers do not take the electricity system into account. The thermal inertia present in the building structure and floor heating system offers a significant amount of flexibility which can be used in a demand response context for load shifting and reduction of peak demand. With a heat pump optimal control objective taking into account the environmental impact of energy use

and limiting the total demand to some extent a significant further reduction of total impact can be obtained. Adding a hot water storage tank allows for a further reduction in environmental impact, however, this further reduction is less striking.

Comparing residential heating with a heat pump or gas boiler, the former results in a significant increase in costs carried by the building owner. Currently, in Belgium, the difference between the natural gas price and the electricity price is too large for an air coupled heat pump to be cost efficient. Applying demand response to assist the electricity system through load shifting further increases building owner costs as there is no significant correlation between the price of additional electricity use and the emissions caused by its generation.

Due to the significant investment costs associated with a hot water storage tank, the overall costs significantly increase when a storage tank is installed. Adding a storage tank to a residential heating system with heat pumps does not enable cost reduction even if no demand response is applied. Heat losses from the storage tank cause a significant increase in total energy use and associated operational costs. The heat price variation resulting from the ambient temperature dependent heat pump COP and current day-night electricity tariff structures is insufficient to enable a cost reduction through adding flexibility in the form of a hot water storage tank.

On the cost-impact Pareto-curve moderately limiting the total electricity demand and applying a balance between load shifting and local cost minimization in a heat pump heating system without storage tank allows for a significant reduction in emissions and environmental impact with only a limited cost for the consumer. Based on these findings it can be concluded that the use of hot water storage tanks in a residential demand response context is not recommended. Residential buildings with floor heating systems contain sufficient thermal mass to offer flexibility for load shifting and peak load reduction to the electricity system. This enables a significant reduction of environmental impact. Naturally, these results are dependent on the assumptions made in the integrated MPC simulation and the LCA. The investment in a hot water storage tank is large, both from a financial and an environmental viewpoint, and does not result in a significant impact reduction. Probably more interesting investments are possible.

7.2   Scientific contributions

In the course of solving the different subproblems, several scientific challenges were addressed and novel models or methodologies were developed.

First, a hot water storage tank model, suitable for large time span building energy simulations was developed and validated. This model represents a step forward relative to models found in the literature, both in accuracy and applicability as it includes three-dimensional effects, such as inflow buoyancy and mixing, which are often omitted, and can be used within a range of different storage tank sizes and shapes.

Second, a methodology for comparing storage tank charging and discharging methods or strategies in a demand response context and accompanying performance indicators were developed. In the literature no similar comparison of charging and discharging strategies was found.

Third, several OCP formulations for a heating system including a heat pump and hot water storage tank were developed. Furthermore, a methodology for comparing OCP formulations in an open-loop and an MPC context was presented. Storage tank models commonly used in the literature were shown to display significant model mismatch and to underestimate heating costs when used in an open-loop OCP approach.

Fourth, a multi-objective MPC approach for the integrated system of buildings and the electricity system was developed. In contrast to studies found in the literature, this methodology employs a detailed, validated model for the hot water storage tank and includes the feedback on the electricity system.

Fifth, a framework for executing LCAs on the integrated system of buildings and the electricity system was set up. This framework is able to compute the total environmental impact of changing electricity generation unit load factors and changes in the electricity generation mix due to heat pump operation. Furthermore, an estimate of the required electricity transport capacity and the associated emissions is made, whereas in the literature, changes in the electricity system attributed to an increasing number of heat pumps are often neglected.

Finally, the applicability and solvability were proven through a case study inspired by the Belgian electricity system.

7.3   Critical reflection

In the development of the methods applied in this work, several assumptions were made. These assumptions influence the results which thus should be interpreted carefully. Furthermore, every mathematical model used in this work forms but a representation of reality and entails some uncertainty which is propagated to the results.

Although extensive attention was given to the development of the direct charging inflow mixing and buoyancy model and its validation in chapter 2, the resulting model still shows noticeable deviations from the experimental results in some cases. First, the correlations were obtained using simulations with a detailed CFD model. Although, the buoyancy and turbulence formulations in the CFD model were experimentally validated, the parametric CFD study is an extrapolation of the validated model, leading to some uncertainty. Next, the number of CFD simulations used to obtain the correlations was rather small. A larger parametric study, including other parameters could reveal different relations, an improved correlation or even require a different model structure. These uncertainties result in an uncertainty on the storage tank model which is propagated to the final results of this work. The uncertainty of the final results, resulting from the storage tank model uncertainties is difficult to assess. Nevertheless, the developed storage tank model is an improvement to models found in the literature.

During the evaluation of the effects of heat pump heating systems on the electricity system, the assumption of simultaneity of residential heating lead to the simulation of a representative building and scaling of the results to a larger number of buildings. Although overall, space heating is mainly ambient temperature driven and thus simultaneous, differences in building structure, e.g. window sizes and orientation and user behavior, influence the heat demand. The operation of heat pumps in a large set of buildings will thus not be entirely simultaneous. This has some effects on the optimal load shifting to less emitting power plants, but the largest effect is related to the peak electricity demand which, in reality, will be lower than predicted in this work. As one of the benefits of adding a hot water storage tank is that peak demands could be reduced further, the lower actual simultaneity reduces the benefits of hot water storage tanks even further.

In the model predictive control simulation, predictions of weather conditions and renewable electricity generation are required. In the present study future conditions were assumed to be known sufficiently long in advance, meaning perfect weather forecasts, at the building location, and perfect predictions of renewable generation were assumed. In reality, such forecasts are available through multiple on-line weather services and the transmission system operator dash-board. However, weather forecasts for a prediction horizon of several days are seldom accurate and never localized at a specific building location. The available predictions of renewable electricity generation are rather good, nevertheless, prediction errors do occur. These prediction errors have a detrimental effect on the operation of a real system using a model predictive control strategy. The robustness toward prediction errors was one of the reasons to choose a fixed temperature storage tank charging strategy over a variable

temperature charging strategy as presented in chapter 3. Furthermore, the presented model predictive control simulation assumes a perfect state estimation. This is possible as the building model in the system emulator is equal to the model used for optimization. Also the average storage tank temperature is assumed to be known exactly. In reality, the building model used in the control optimization will be an imperfect representation of an actual building making an exact state estimation impossible. The actual average storage tank temperature will also not be known as this would require too many temperature measurements. Techniques exist however to estimate the temperature profile in the storage tank based on the temporal evolution of a few sensors only.

The above presented imperfections will be reflected in a decrease in thermal comfort for the building occupants or an increase in costs or environmental impact. The presented values are thus upper boundaries for the actual achievable gains.

During the course of this study the impact of electricity transmission and distribution was shown to be significant. In the presented methodology, the impact related to the high voltage electricity transmission infrastructure is computed based on the residual peak electricity demand. Impact related to the medium and low voltage electricity transport infrastructure is computed based on the total peak demand. This method does not take the actual electricity grid topology or the spatial distribution of wind and photovoltaic electricity generation, fixed electricity demand and heat pumps into account. Including these would make the simulation and optimal control problem tremendously more complex, therefore this simplified approach for including emissions related to the electricity grid is used.

The evaluation of environmental impact through a life-cycle assessment further introduces uncertainty in the results. The inventory data used to model all components of the presented system is mostly derived from specific products of a few manufacturers. As production processes may differ between manufacturers, this introduces a spread of possible values. In the Ecoinvent database, a mean value for all inventory quantities is provided, often accompanied by a certain probability distribution. An estimate of the probability distribution of every substance in the total product system inventory could be computed through a Monte-Carlo analysis. Furthermore, the used impact assessment models add uncertainty to the presented midpoint and endpoint impact indicators. The added uncertainty on midpoint indicators, such as total greenhouse gas emissions is rather low, but to compute endpoint indicators several models, e.g. considering the human exposure to a substance or computing the effect on health, are used, each adding to the uncertainty. Nevertheless, the comparison of environmental impact between systems presented in this work is valuable as the uncertainties are similar for all systems.

7.4   Suggestions for future research

Although the presented direct inflow charging storage tank model is an improvement to models found in the literature, additional experiments or simulations can reduce the uncertainty on the presented model parameters and thus the model. Furthermore, expanding the model toward inflow configurations other than simple horizontal inflows is valuable. In the literature several authors show that different inflow configurations with diffusers of varying complexity can improve stratification and thus the effective storage capacity [30, 86, 88, 127]. Such inflow diffusers significantly alter the flow pattern and mixing zone, invalidating the presented correlation.

In domestic hot water storage tanks, the use of immersed heat exchangers is predominant as a strict separation of fluids is demanded and, opposed to a side arm heat exchanger, an immersed heat exchanger does not require an additional pump. A validation of the presented immersed heat exchanger charging model is thus useful, especially in the solar thermal storage field.

The investment, both financial and environmental, in the storage tank was shown to be significant. Using different types of storage tanks could reduce these costs. Buried concrete storage tanks [5, 81] can offer a significant storage volume at low costs, which could result in a more environmentally friendly and cost effective overall system. However, as pressurization of such a storage tank is very difficult, a direct inflow charging or discharging method can not be used. Unpressurized systems require the use of an immersed, mantle or side arm heat exchanger. Furthermore, as the height-diameter ratio for such a storage tank is probably incomparable to that of a storage tank located above ground, the presented models should be revalidated. To assess the benefits of such a storage tank, optimal control formulations taking into account the more mixed nature and possibly additional pumping energy requirements should be developed and evaluated.

As suggested in chapter 3, a hybrid charging strategy could be beneficial for a heating system with heat pump and storage tank. The storage tank can be charged using a minimum temperature difference strategy when the storage capacity is not critical and a fixed temperature strategy can be used when the full storage capacity is required. The implementation of such a system in an optimal control formulation however poses significant challenges. First a boolean variable is required to choose between charging method and the storage capacity should be adjusted according to this variable. Furthermore, the history of the charging strategy should be known to the optimization problem as the past charging strategy affects the current capacity. Depending on the charging strategy, the implementation of the heat pump COP also changes. As the heat

pump COP is dependent on the heat pump supply temperature, the constraint determining the heat pump power must reflect this which probably rules out the use of a quadratic constraint as presented in chapter 5. The resulting optimization will thus be a non-linear programming problem which greatly affects the computation time and the risk for local optima.

In chapter 6, the environmental impact of electricity transport was shown to be non-negligible when evaluating demand response schemes. The presented method for taking the electricity transmission and distribution networks into account is however rather simplified. In the literature, no methods were found to incorporate the infrastructure for electricity transport in a life-cycle assessment with distributed renewable generation other than using historical averages. As the transmission capacity has an effect on optimal cost scheduling [183], it is very likely that it should be taken into account in an environmental assessment. Furthermore, additional storage capacity could also supply services on a smaller scale to alleviate problems in electricity distribution networks which could lead to environmental benefits.

As was stated in section 6.4.3, in this work, the building and emission system were not included within the LCA system boundaries. This was possible as in the current analysis, different heating systems implemented in the same building are compared. However, these boundaries imply that the total environmental impact related to residential heating can not be computed, only impact differences are available. The methodology presented in chapter 6 can be valuable in the development of an LCA of the construction, use phase and end-of-life phase of the entire building. This however presents challenges for the choice of functional unit, comparison of buildings in different regions and harmonizing data sources [71].

When composing the life-cycle emissions inventory for the different components, current average values for emissions related to energy use were applied. In a future scenario where the amount of renewables is significantly higher, demand response will have a significant effect on the overall electricity mix. The impact related to the construction of for instance heat pumps and storage tanks will thus also depend on the amount of demand response in the system. This requires a different LCA approach, replacing average electricity generation records with records reflecting the effect of demand response. Furthermore, the electricity system in different regions on Earth has different requirements and will respond differently to demand response due to local differences in the potential of renewables. As production is ever globalizing, this poses additional difficulties in assessing the environmental impact of subsystems produced in different regions of the world.

Although, the use of hot water storage tanks for demand response in

residential heating with heat pumps was shown to only marginally decrease the environmental impact in the presented case study (chapter 5 and 6), this does not imply such a system has no benefits in other scenarios. As more renewable electricity sources are integrated in the electricity system, the need for flexibility rises. Thermal energy storage in the form of hot water storage tanks could play a role in such scenarios, however they will have to compete with other sources of flexibility such as battery energy storage or flexible industrial production. The methodology developed in this work can serve as a starting point for further investigating the environmental impact and optimal component sizing in future energy scenarios.

Appendix A

Demand response optimal control formulation details

In the following sections, the optimal control problem used to control the heat pumps in chapter 5 and chapter 6 is presented in full detail. For an explanation of symbols the reader is referred to the list of symbols (p. ix).

A.1 Building

The differential equations governing the building states can be written as:

$$C_{\text{in}} \frac{\mathrm{d}T_{\text{in}}}{\mathrm{d}t} = \frac{T_{\text{amb}} - T_{\text{in}}}{R_{\text{ve}}} + \frac{T_{\text{wi}} - T_{\text{in}}}{R_{\text{wi}}} + \frac{T_{\text{we}} - T_{\text{in}}}{R_{\text{w1}}} + \frac{T_{\text{fl}} - T_{\text{in}}}{R_{\text{f1}}} + \dot{Q}_{\text{in}} \quad \text{(A.1)}$$

$$C_{\text{wi}} \frac{\mathrm{d}T_{\text{wi}}}{\mathrm{d}t} = \frac{T_{\text{in}} - T_{\text{wi}}}{R_{\text{wi}}} + \dot{Q}_{\text{wi}} \quad \text{(A.2)}$$

$$C_{\text{we}} \frac{\mathrm{d}T_{\text{we}}}{\mathrm{d}t} = \frac{T_{\text{in}} - T_{\text{we}}}{R_{\text{w1}}} + \frac{T_{\text{amb}} - T_{\text{we}}}{R_{\text{w2}}} + \dot{Q}_{\text{we}} \quad \text{(A.3)}$$

$$C_{\text{fl}} \frac{\mathrm{d}T_{\text{fl}}}{\mathrm{d}t} = \frac{T_{\text{in}} - T_{\text{fl}}}{R_{\text{f1}}} + \frac{T_{\text{tr}} - T_{\text{fl}}}{R_{\text{f2}}} + \dot{Q}_{\text{fl}} \quad \text{(A.4)}$$

$$C_{\text{tr}} \frac{\mathrm{d}T_{\text{tr}}}{\mathrm{d}t} = \frac{T_{\text{fl}} - T_{\text{tr}}}{R_{\text{f2}}} + \frac{T_{\text{gnd}} - T_{\text{tr}}}{R_{\text{tr}}} + \frac{T_{\text{sh}} - T_{\text{tr}}}{R_{\text{sh}}} + \frac{T_{\text{dw}} - T_{\text{tr}}}{R_{\text{dw}}} + \frac{T_{\text{hp}} - T_{\text{tr}}}{R_{\text{hp}}}$$
$$\text{(A.5)}$$

In the optimal control problem, heat losses from the heat pump to the technical room are neglected as this requires the introduction of an additional state for the heat pump temperature with short time dynamics. In the optimal control problem, the equations are discretized with respect to time:

$$C_{\text{in}} \frac{T_{\text{in},i+1} - T_{\text{in},i}}{\Delta t} = \frac{1}{2} \frac{T_{\text{amb},i} - T_{\text{in},i}}{R_{\text{ve}}} + \frac{1}{2} \frac{T_{\text{wi},i} - T_{\text{in},i}}{R_{\text{wi}}} \tag{A.6}$$

$$+ \frac{1}{2} \frac{T_{\text{we},i} - T_{\text{in},i}}{R_{\text{w1}}} + \frac{1}{2} \frac{T_{\text{fl},i} - T_{\text{in},i}}{R_{\text{fl}}}$$

$$+ \frac{1}{2} \frac{T_{\text{amb},i+1} - T_{\text{in},i+1}}{R_{\text{ve}}} + \frac{1}{2} \frac{T_{\text{wi},i+1} - T_{\text{in},i+1}}{R_{\text{wi}}}$$

$$+ \frac{1}{2} \frac{T_{\text{we},i+1} - T_{\text{in},i+1}}{R_{\text{w1}}} + \frac{1}{2} \frac{T_{\text{fl},i+1} - T_{\text{in},i+1}}{R_{\text{fl}}} + \dot{Q}_{\text{in},i} \qquad \forall\, i$$

$$C_{\text{wi}} \frac{T_{\text{wi},i+1} - T_{\text{wi},i}}{\Delta t} = \frac{1}{2} \frac{T_{\text{in},i} - T_{\text{wi},i}}{R_{\text{wi}}} + \frac{1}{2} \frac{T_{\text{in},i+1} - T_{\text{wi},i+1}}{R_{\text{wi}}} + \dot{Q}_{\text{wi},i} \qquad \forall\, i \tag{A.7}$$

$$C_{\text{we}} \frac{T_{\text{we},i+1} - T_{\text{we},i}}{\Delta t} = \frac{1}{2} \frac{T_{\text{in},i} - T_{\text{we},i}}{R_{\text{w1}}} + \frac{1}{2} \frac{T_{\text{amb},i} - T_{\text{we},i}}{R_{\text{w2}}} \tag{A.8}$$

$$+ \frac{1}{2} \frac{T_{\text{in},i+1} - T_{\text{we},i+1}}{R_{\text{w1}}} + \frac{1}{2} \frac{T_{\text{amb},i+1} - T_{\text{we},i+1}}{R_{\text{w2}}} + \dot{Q}_{\text{we},i} \quad \forall\, i$$

$$C_{\text{fl}} \frac{T_{\text{fl},i+1} - T_{\text{fl},i}}{\Delta t} = \frac{1}{2} \frac{T_{\text{in},i} - T_{\text{fl},i}}{R_{\text{fl}}} + \frac{1}{2} \frac{T_{\text{tr},i} - T_{\text{fl},i}}{R_{\text{f2}}} \tag{A.9}$$

$$+ \frac{1}{2} \frac{T_{\text{in},i+1} - T_{\text{fl},i+1}}{R_{\text{fl}}} + \frac{1}{2} \frac{T_{\text{tr},i+1} - T_{\text{fl},i+1}}{R_{\text{f2}}} + \dot{Q}_{\text{fl},i} \qquad \forall\, i$$

$$C_{\text{tr}} \frac{T_{\text{tr},i+1} - T_{\text{tr},i}}{\Delta t} = \frac{1}{2} \frac{T_{\text{fl},i} - T_{\text{tr},i}}{R_{\text{f2}}} + \frac{1}{2} \frac{T_{\text{gnd},i} - T_{\text{tr},i}}{R_{\text{tr}}} \tag{A.10}$$

$$+ \frac{1}{2} \frac{T_{\text{sh},i} - T_{\text{tr},i}}{R_{\text{sh}}} + \frac{1}{2} \frac{T_{\text{dw},i} - T_{\text{tr},i}}{R_{\text{dw}}}$$

$$+ \frac{1}{2} \frac{T_{\text{fl},i+1} - T_{\text{tr},i+1}}{R_{\text{f2}}} + \frac{1}{2} \frac{T_{\text{gnd},i+1} - T_{\text{tr},i+1}}{R_{\text{tr}}}$$

$$+ \frac{1}{2} \frac{T_{\text{sh},i+1} - T_{\text{tr},i+1}}{R_{\text{sh}}} + \frac{1}{2} \frac{T_{\text{dw},i+1} - T_{\text{tr},i+1}}{R_{\text{dw}}} \qquad \forall\, i$$

Heat flows to the different components as a result of solar gains, internal gains and heat emission are computed as:

$$\dot{Q}_{\text{wi},i} = f_{\text{sol,wi}} S_i \frac{1}{2} \left(\dot{Q}_{\text{sol},i} + \dot{Q}_{\text{sol},i+1} \right) \qquad \forall\, i \qquad \text{(A.11)}$$

$$\dot{Q}_{\text{in},i} = f_{\text{sol,in}} S_i \frac{1}{2} \left(\dot{Q}_{\text{sol},i} + \dot{Q}_{\text{sol},i+1} \right) + \dot{Q}_{\text{gain},i} \qquad \forall\, i \qquad \text{(A.12)}$$

$$\dot{Q}_{\text{we},i} = f_{\text{sol,we}} S_i \frac{1}{2} \left(\dot{Q}_{\text{sol},i} + \dot{Q}_{\text{sol},i+1} \right) \qquad \forall\, i \qquad \text{(A.13)}$$

$$\dot{Q}_{\text{fl},i} = f_{\text{sol,fl}} S_i \frac{1}{2} \left(\dot{Q}_{\text{sol},i} + \dot{Q}_{\text{sol},i+1} \right) + \dot{Q}_{\text{em},i} \qquad \forall\, i \qquad \text{(A.14)}$$

With f_{sol} distribution factors, dividing the solar gains over the different states in accordance with [149] and S_i a solar shading control variable which is allowed to vary between 0.3 and 1.0.

The building operative temperature is linearized according to [132]:

$$T_{\text{op},i} = 0.4\, T_{\text{in},i} + 0.6 \left(0.3\, T_{\text{we},i} + 0.3\, T_{\text{wi},i} + 0.4\, T_{\text{fl},i} \right) \qquad \forall\, i \qquad \text{(A.15)}$$

Thermal discomfort costs are computed as:

$$\text{discomfort costs}_i = p_{\text{d}} \left(\Delta T_{\text{d,cold},i} + \Delta T_{\text{d,warm},i} \right) \frac{\Delta t}{3600} \qquad \forall\, i \qquad \text{(A.16)}$$

$$\Delta T_{\text{d,cold},i} \geq T_{\text{op},i}^{\min} - T_{\text{op},i} \qquad \forall\, i$$

$$\Delta T_{\text{d,cold},i} \geq 0 \qquad \forall\, i$$

$$\Delta T_{\text{d,warm},i} \geq T_{\text{op},i} - T_{\text{op},i}^{\max} \qquad \forall\, i$$

$$\Delta T_{\text{d,warm},i} \geq 0 \qquad \forall\, i$$

A.2 Heating system

The heat pump can supply heat for space heating or for domestic hot water production at three temperature levels: low temperature (lt), medium temperature (mt) and high temperature (ht):

$$\dot{Q}_{\text{hp,lt},i} = \dot{Q}_{\text{hp,lt,sh},i} + \dot{Q}_{\text{hp,lt,dw},i} \qquad \forall\, i \qquad \text{(A.17)}$$

$$\dot{Q}_{\text{hp,mt},i} = \dot{Q}_{\text{hp,mt,sh},i} + \dot{Q}_{\text{hp,mt,dw},i} \qquad \forall\, i \qquad \text{(A.18)}$$

$$\dot{Q}_{\text{hp,ht},i} = \dot{Q}_{\text{hp,ht,sh},i} + \dot{Q}_{\text{hp,ht,dw},i} \qquad \forall\, i \qquad \text{(A.19)}$$

$$\dot{Q}_{\text{hp,sh},i} = \dot{Q}_{\text{hp,lt,sh},i} + \dot{Q}_{\text{hp,mt,sh},i} + \dot{Q}_{\text{hp,ht,sh},i} \qquad \forall\, i \qquad \text{(A.20)}$$

$$\dot{Q}_{\text{hp,dw},i} = \dot{Q}_{\text{hp,lt,dw},i} + \dot{Q}_{\text{hp,mt,dw},i} + \dot{Q}_{\text{hp,ht,dw},i} \qquad \forall\, i \qquad \text{(A.21)}$$

The relation between heat pump power and heat flow rate is implemented as:

$$P_{\text{hp},i} = P_{\text{hp,lt},i} + P_{\text{hp,mt},i} + P_{\text{hp,ht},i} \qquad \forall\, i \qquad \text{(A.22)}$$

$$P_{\text{hp,lt},i} \geq \zeta_{\text{l,lt}}(T_{\text{amb},i})\dot{Q}_{\text{hp,lt},i} + \zeta_{\text{q,lt}}(T_{\text{amb},i})\dot{Q}_{\text{hp,lt},i}^2 \qquad \forall\, i \qquad \text{(A.23)}$$

$$P_{\text{hp,mt},i} \geq \zeta_{\text{l,mt}}(T_{\text{amb},i})\dot{Q}_{\text{hp,mt},i} + \zeta_{\text{q,mt}}(T_{\text{amb},i})\dot{Q}_{\text{hp,mt},i}^2 \qquad \forall\, i \qquad \text{(A.24)}$$

$$P_{\text{hp,ht},i} \geq \zeta_{\text{l,ht}}(T_{\text{amb},i})\dot{Q}_{\text{hp,ht},i} + \zeta_{\text{q,ht}}(T_{\text{amb},i})\dot{Q}_{\text{hp,ht},i}^2 \qquad \forall\, i \qquad \text{(A.25)}$$

The auxiliary domestic hot water heater is assumed to have an efficiency of 100%:

$$P_{\text{aux},i} = \dot{Q}_{\text{aux},i} \qquad \forall\, i \qquad \text{(A.26)}$$

The space heating storage tank state is computed from:

$$C_{\text{sh}}\frac{T_{\text{sh},i+1} - T_{\text{sh},i}}{\Delta t} = \frac{1}{2}\frac{T_{\text{tr},i} - T_{\text{sh},i}}{R_{\text{sh}}} + \frac{1}{2}\frac{T_{\text{tr},i+1} - T_{\text{sh},i+1}}{R_{\text{sh}}}$$
$$+ \dot{Q}_{\text{hp,sh},i} - \dot{Q}_{\text{em},i} \qquad \forall\, i \qquad \text{(A.27)}$$

With additional constraints:

$$\dot{Q}_{\text{hp,sh},i} \leq c\dot{m}_{\text{hp}}^{\max}(T_{\text{hp,lt}} - T_{\text{em,ret}}) \qquad \forall\, i \qquad \text{(A.28)}$$

$$\dot{Q}_{\text{em},i} \leq \varepsilon_{\text{em}}^{\text{nom}}c\dot{m}_{\text{em}}^{\max}(T_{\text{hp,lt}} - T_{\text{fl},i}) \qquad \forall\, i \qquad \text{(A.29)}$$

$$T_{\text{sh},i} \leq T_{\text{hp,lt}} \qquad \forall\, i \qquad \text{(A.30)}$$

$$T_{\text{sh},i} \geq T_{\text{em,ret}} \qquad \forall\, i \qquad \text{(A.31)}$$

The domestic water storage tank states are computed from:

$$C_{\text{dw,lt}}\frac{T_{\text{dw,lt},i+1} - T_{\text{dw,lt},i}}{\Delta t} = \frac{1}{2}\frac{T_{\text{dw,lt},i} - T_{\text{tr},i}}{R_{\text{dw}}}$$

$$+ \frac{1}{2} \frac{T_{\mathrm{dw,lt},i+1} - T_{\mathrm{tr},i+1}}{R_{\mathrm{dw}}} \tag{A.32}$$

$$+ \dot{Q}_{\mathrm{hp,lt,dw},i} - \dot{Q}_{\mathrm{dw,lt},i} \qquad \forall\, i$$

$$C_{\mathrm{dw,mt}} \frac{\Delta T_{\mathrm{dw,mt},i+1} - \Delta T_{\mathrm{dw,mt},i}}{\Delta t} = -\frac{1}{2} \frac{\Delta T_{\mathrm{dw,mt},i}}{R_{\mathrm{dw}}} - \frac{1}{2} \frac{\Delta T_{\mathrm{dw,mt},i+1}}{R_{\mathrm{dw}}} \tag{A.33}$$

$$+ \dot{Q}_{\mathrm{hp,mt,dw},i} - \dot{Q}_{\mathrm{dw,mt},i} \qquad \forall\, i$$

$$C_{\mathrm{dw,ht}} \frac{\Delta T_{\mathrm{dw,ht},i+1} - \Delta T_{\mathrm{dw,ht},i}}{\Delta t} = -\frac{1}{2} \frac{\Delta T_{\mathrm{dw,ht},i}}{R_{\mathrm{dw}}} - \frac{1}{2} \frac{\Delta T_{\mathrm{dw,ht},i+1}}{R_{\mathrm{dw}}} \tag{A.34}$$

$$+ \dot{Q}_{\mathrm{hp,ht,dw},i} - \dot{Q}_{\mathrm{dw,ht},i} \qquad \forall\, i$$

$$C_{\mathrm{dw,vht}} \frac{\Delta T_{\mathrm{dw,vht},i+1} - \Delta T_{\mathrm{dw,vht},i}}{\Delta t} = -\frac{1}{2} \frac{\Delta T_{\mathrm{dw,vht},i}}{R_{\mathrm{dw}}} - \frac{1}{2} \frac{\Delta T_{\mathrm{dw,vht},i+1}}{R_{\mathrm{dw}}}$$
$$\tag{A.35}$$

$$+ \dot{Q}_{\mathrm{aux},i} - \dot{Q}_{\mathrm{dw,vht},i} \qquad \forall\, i$$

With additional constraints:

$$T_{\mathrm{dw},i} = T_{\mathrm{dw,lt},i} + \Delta T_{\mathrm{dw,mt},i} + \Delta T_{\mathrm{dw,ht},i} + \Delta T_{\mathrm{dw,vht},i} \qquad \forall\, i \tag{A.36}$$

$$\dot{Q}_{\mathrm{dw},i} = \dot{Q}_{\mathrm{dw,lt},i} + \dot{Q}_{\mathrm{dw,mt},i} + \dot{Q}_{\mathrm{dw,ht},i} + \dot{Q}_{\mathrm{dw,vht},i} \qquad \forall\, i \tag{A.37}$$

$$\dot{Q}_{\mathrm{dw},i} = c\dot{m}_{\mathrm{dw},i} \left(T_{\mathrm{dw,dem}} - T_{\mathrm{mains}} \right) \qquad \forall\, i \tag{A.38}$$

$$\dot{Q}_{\mathrm{hp,dw,lt},i} \leq c\dot{m}_{\mathrm{hp}}^{\max} \left(T_{\mathrm{hp,lt}} - T_{\mathrm{dw,lt},i} \right) \qquad \forall\, i \tag{A.39}$$

$$\dot{Q}_{\mathrm{hp,dw,lt},i} \leq c\dot{m}_{\mathrm{hp}}^{\max} \left(T_{\mathrm{hp,lt}} - T_{\mathrm{dw,lt},i+1} \right) \qquad \forall\, i \tag{A.40}$$

$$T_{\mathrm{dw,lt},i} \leq T_{\mathrm{hp,lt}} \qquad \forall\, i \tag{A.41}$$

$$\dot{Q}_{\mathrm{hp,dw,mt},i} \leq c\dot{m}_{\mathrm{hp}}^{\max} \left(T_{\mathrm{hp,mt}} - T_{\mathrm{hp,lt}} - \Delta T_{\mathrm{dw,mt},i} \right) \qquad \forall\, i \tag{A.42}$$

$$\dot{Q}_{\mathrm{hp,dw,mt},i} \leq c\dot{m}_{\mathrm{hp}}^{\max} \left(T_{\mathrm{hp,mt}} - T_{\mathrm{hp,lt}} - \Delta T_{\mathrm{dw,mt},i+1} \right) \qquad \forall\, i \tag{A.43}$$

$$\Delta T_{\mathrm{dw,mt},i} \leq T_{\mathrm{hp,mt}} - T_{\mathrm{hp,lt}} \qquad \forall\, i \tag{A.44}$$

$$\dot{Q}_{\mathrm{hp,dw,ht},i} \leq c\dot{m}_{\mathrm{hp}}^{\max} \left(T_{\mathrm{hp,ht}} - T_{\mathrm{hp,mt}} - \Delta T_{\mathrm{dw,ht},i} \right) \qquad \forall\, i \tag{A.45}$$

$$\dot{Q}_{\mathrm{hp,dw,ht},i} \leq c\dot{m}_{\mathrm{hp}}^{\max} \left(T_{\mathrm{hp,ht}} - T_{\mathrm{hp,mt}} - \Delta T_{\mathrm{dw,ht},i+1} \right) \qquad \forall\, i \tag{A.46}$$

$$\Delta T_{\mathrm{dw,ht},i} \leq T_{\mathrm{hp,ht}} - T_{\mathrm{hp,mt}} \qquad \forall\, i \qquad \text{(A.47)}$$

$$\Delta T_{\mathrm{dw,vht},i} \leq T_{\mathrm{dw},i}^{\max} - T_{\mathrm{hp,ht}} \qquad \forall\, i \qquad \text{(A.48)}$$

$$T_{\mathrm{dw},i} \geq T_{\mathrm{dw},i}^{\min} \qquad \forall\, i \qquad \text{(A.49)}$$

A.3 Electricity generation

Supply and demand of electricity must be equal at all times. With M the number of buildings this results in:

$$M P_{\mathrm{hp},i} + M P_{\mathrm{aux},i} + P_{\mathrm{fixed},i} = P_{\mathrm{wind},i} + P_{\mathrm{pv},i} + P_{\mathrm{base},i} + P_{\mathrm{peak},i} \qquad \forall\, i \ \text{(A.50)}$$

Renewables and base load generation have a limited capacity. For the renewables the maximum power is time dependent:

$$P_{\mathrm{wind},i} \leq P_{\mathrm{wind},i}^{\max} \qquad \forall\, i \qquad \text{(A.51)}$$

$$P_{\mathrm{pv},i} \leq P_{\mathrm{pv},i}^{\max} \qquad \forall\, i \qquad \text{(A.52)}$$

$$P_{\mathrm{base},i} \leq P_{\mathrm{base}}^{\max} \qquad \forall\, i \qquad \text{(A.53)}$$

Base load generation has a limited ramping rate:

$$\frac{P_{\mathrm{base},i} - P_{\mathrm{base},i+1}}{\Delta t} \leq \dot{P}_{\mathrm{base}}^{\max} \qquad \forall\, i \qquad \text{(A.54)}$$

$$\frac{P_{\mathrm{base},i} - P_{\mathrm{base},i+1}}{\Delta t} \geq -\dot{P}_{\mathrm{base}}^{\max} \qquad \forall\, i \qquad \text{(A.55)}$$

The overload power is subject to:

$$P_{\mathrm{overload},i} + l_{\mathrm{cap}} P_{\mathrm{fixed}}^{\max} \geq P_{\mathrm{wind},i} + P_{\mathrm{pv},i} + P_{\mathrm{base},i} + P_{\mathrm{peak},i} \qquad \text{(A.56)}$$

A.4 Objective

The multi-criterion objective is written as:

$$\text{minimize} \quad \sum_{i} p_{\mathrm{el},i}(P_{\mathrm{hp},i} + P_{\mathrm{aux},i}) \frac{\Delta t}{3600 \times 10^3} \qquad \text{(A.57)}$$

$$+ \sum_i \sum_j w_{\text{EIE}}\, p^j_{\text{impact,ene}} P^j_i \frac{\Delta t}{3600 \times 10^3}$$

$$+ \sum_i\, p_{\text{cap}} \left(P_{\text{overload},i}\right)^2 \frac{\Delta t}{3600 \times 10^6}$$

$$+ \sum_i \text{discomfort costs}_i$$

with j an index running over all power plants.

Appendix B

Life-cycle assessment unit-processes

For reference, all unit-processes used in the heating system life-cycle assessment are presented in this Appendix. All processes were taken from the Ecoinvent version 3 database [191].

B.1   Electricity generation

Electricity generation records for different power plants were inspected and the global records were split in parts related to the generated electrical energy and parts related to the installed capacity.

- Wind power generation onshore:
  Electricity, high voltage BE| electricity production, wind, 1-3 MW turbine

  – capacity: all
  – energy: none

- Wind power generation offshore:
  Electricity, high voltage BE| electricity production, wind, 1-3 MW turbine, offshore

  – capacity: all
  – energy: none

- Photovoltaic power generation:
  Electricity, low voltage BE| electricity production, photovoltaic, 3 kWp slanted-roof installation, multi-Si, panel, mounted

  - capacity: all
  - energy: none

- Nuclear power generation:
  Electricity, high voltage BE| electricity production, nuclear, pressure water reactor

  - capacity: Nuclear power plant, pressure water reactor 1000 MW GLO
  - energy: rest

- Combined cycle gas turbine power generation:
  Electricity, high voltage TW| electricity production, natural gas, combined cycle power plant

  - capacity: Gas power plant, combined cycle, 400 MW electrical GLO
  - energy: rest

- Open cycle gas turbine power generation:
  Electricity, high voltage RoW| electricity production, natural gas, 10 MW

  - capacity: Gas turbine, 10 MW electrical GLO
  - energy: rest

B.2   Electricity transport

The following unit-processes were used to model the impact of electricity transport at different voltage levels:

- High voltage (> 20 kV):
  Transmission network, electricity, high voltage GLO

- Medium voltage (≤ 20 kV, ≥ 1 kV):
  Transmission network, electricity, medium voltage GLO

- Low voltage (< 1 kV):
  Distribution network, electricity, low voltage GLO

As the functional unit of the above processes is 1 km of line or cable, the distances are computed by scaling the distance of cables and lines in the current Belgian electricity grid [170] with the ratio of computed maximum power and actual generation capacity [52]:

$$D_{>20 \text{ kV}} = 8584 \text{ km} \frac{P_{\text{residual}}^{\text{max}}}{14574 \text{ MW}} \tag{B.1}$$

$$D_{1-20 \text{ kV}} = 75742 \text{ km} \frac{P_{\text{demand}}^{\text{max}}}{14574 \text{ MW}} \tag{B.2}$$

$$D_{<1 \text{ kV}} = 159200 \text{ km} \frac{P_{\text{demand}}^{\text{max}}}{14574 \text{ MW}} \tag{B.3}$$

In accordance with [98], emissions of dinitrogen monoxide and ozone were added to the high voltage transport process and emissions and resource use of sulfur hexafluoride were added to the medium and high voltage transport processes. The emissions per kWh as stated in the default records are scaled with the average electricity grid load factor and a grid infrastructure lifetime of 40 years is assumed:

- High voltage (> 20 kV):
  Emission to air of Dinitrogen monoxide
  $$5 \times 10^{-6} \text{ kg/kWh} \; \frac{78000 \text{ GWh/year} \cdot 40 \text{ year}}{14574 \text{ MW}}$$

  Emission to air of Ozone
  $$4.15772755243 \times 10^{-6} \text{ kg/kWh} \; \frac{78000 \text{ GWh/year} \cdot 40 \text{ year}}{14574 \text{ MW}}$$

- Medium voltage (≤ 20 kV, ≥ 1 kV):
  Production of Sulfur hexafluoride, liquid GLO
  $$1.13 \times 10^{-7} \text{ kg/kWh} \; \frac{78000 \text{ GWh/year} \cdot 40 \text{ year}}{14574 \text{ MW}}$$

  Emission to air of Sulfur hexafluoride
  $$1.13 \times 10^{-7} \text{ kg/kWh} \; \frac{78000 \text{ GWh/year} \cdot 40 \text{ year}}{14574 \text{ MW}}$$

- Low voltage (< 1 kV):
  Production of Sulfur hexafluoride, liquid GLO
  $$6.27 \times 10^{-9} \text{ kg/kWh} \; \frac{78000 \text{ GWh/year} \cdot 40 \text{ year}}{14574 \text{ MW}}$$

  Emission to air of Sulfur hexafluoride
  $$6.27 \times 10^{-9} \text{ kg/kWh} \; \frac{78000 \text{ GWh/year} \cdot 40 \text{ year}}{14574 \text{ MW}}$$

B.3   Heating system

For the heat pump, auxiliary domestic hot water heater and gas boiler, the following unit-processes were used. Inputs and emissions were scaled to obtain a total system mass consistent with manufacturer data for the systems assumed in the simulations. For the heat pump, the refrigerant mass retrieved from product data sheets was used. The refrigerant specified in the production data sheets was R410a, which is a common refrigerant in commercial heat pumps. However, the life-cycle inventory of this refrigerant is not available in the Ecoinvent database. Therefore it is modeled as the same mass of R134a refrigerant for which data is available. The difference in global warming potential between these refrigerants is taken into account and described in section B.5.

- Air source heat pump:
     Heat pump, brine-water, 10 kW RoW| production

  – Refrigerant:
       Refrigerant R134a GLO

- Resitance heater:
     Auxiliary heating unit, electric, 5 kW RoW| production

- Gas boiler:
     Gas boiler GLO

Transportation of the heating system components from the factory to the building site and from the building to the disposal facility is modeled with the Transport, freight, lorry, unspecified GLO unit-process.

B.4   Storage tank

For the space heating and domestic hot water storage tanks, detailed unit-processes were constructed starting from a reference process. The sub-processes from this reference process were categorized along the main storage tank components. For each sub-process the quantity used in the reference process is scaled using the estimated quantity for the storage tank of a given size under consideration. The used reference process and sub-processes for the space heating storage tank and domestic hot water storage tank are:

- Space heating storage tank:
     Heat storage, 2000 l RoW| production

- Pressure vessel:
    Steel, chromium steel 18/8, hot rolled GLO
    Steel, low-alloyed, hot rolled GLO
    Welding, gas, steel GLO

- Insulation:
    Waste mineral wool GLO
    Glass wool mat GLO
- Cover:
    Alkyd paint, white, without solvent, in 60% solution state GLO
- Factory:
    Hot water tank factory GLO
- Water:
    Tap water, at user Europe without Switzerland
- Electricity/Heat: All processes categorized under Electricity/Heat
- Rest: All remaining processes

- Domestic hot water tank:
    Hot water tank, 600 l RoW| production

    - Pressure vessel:
        Steel, chromium steel 18/8, hot rolled GLO
        Steel, low-alloyed, hot rolled GLO
        Welding, gas, steel GLO

    - Insulation:
        Waste mineral wool GLO
        Glass wool mat GLO
    - Cover:
        Alkyd paint, white, without solvent, in 60% solution state GLO
    - Factory:
        Hot water tank factory GLO
    - Water:
        Tap water, at user Europe without Switzerland
    - Electricity/Heat: All processes categorized under Electricity/Heat
    - Rest: All remaining processes

Transportation of the storage tank from the factory to the building site and from the building to the disposal facility is modeled with the Transport, freight, lorry, unspecified GLO unit-process.

B.5 Waste treatment

Waste treatment of the main heating system components and the storage tank is taken into account. Therefore, materials used in the different components are categorized to a limited set of material categories for which waste treatment processes are available in ecoinvent. The materials under consideration for waste treatment and the used unit-processes are:

- Copper:
    Scrap copper GLO

- Steel and iron:
    Steel and iron (waste treatment) GLO| recycling of steel and iron

- Aluminum:
    Aluminium (waste treatment) GLO| recycling of aluminium

- Oil:
    Waste mineral oil GLO

- PVC:
    Waste polyvinylchloride GLO

- Polyurethane:
    Waste polyurethane GLO

- Polyethylene:
    Waste polyethylene GLO

- Mineral wool:
    Waste mineral wool GLO

- Cardboard:
    Waste paperboard GLO

- Wood:
    Waste wood, untreated GLO

During the waste treatment of the heat pump, 20% of the refrigerant is assumed to be lost to the environment. The available process for R134a emission (Ethane, 1,1,1,2-tetrafluoro-, HFC-134a; high. pop) is therefore scaled using the global warming potentials of R134a (1300 kg CO_2 eq./kg) and R410a (1725 kg CO_2 eq./kg) [69] which is a common refrigerant in commercial heat pumps. The remaining 80% of refrigerant is assumed to be recycled.

Bibliography

[1]   Adams, W. *The future of sustainability: Re-thinking Environment and Development in the Twenty-first Century.* Tech. rep. IUCN, 2006.

[2]   Afram, A. and Janabi-Sharifi, F. "Theory and applications of HVAC control systems – A review of model predictive control (MPC)". In: *Building and Environment* 72 (2014), pp. 343–355.

[3]   Ahmad, M. W., Eftekhari, M., Steffen, T., and Danjuma, A. M. "Investigating the performance of a combined solar system with heat pump for houses". In: *Energy and Buildings* 63 (2013), pp. 138–146.

[4]   Allgöwer, F., Findeisen, R., and Nagy, Z. K. "Nonlinear model predictive control". In: *Journal of the Chinese Institute of Chemical Engineers* 35.3 (2004), pp. 299–315.

[5]   Alva, G., Liu, L., Huang, X., and Fang, G. "Thermal energy storage materials and systems for solar energy applications". In: *Renewable and Sustainable Energy Reviews* 68 (2017), pp. 693–706.

[6]   El-Amin, M. F., Sun, S., and Salam, A. "Simulation of buoyancy-induced turbulent flow from a hot horizontal jet". In: *Journal of Hydrodynamics* 26.1 (2014), pp. 104–113.

[7]   Amor, M. B., Gaudreault, C., Pineau, P.-O., and Samson, R. "Implications of integrating electricity supply dynamics into life cycle assessment: A case study of renewable distributed generation". In: *Renewable Energy* 69 (2014), pp. 410–419.

[8]   Arslan, M. and Igci, A. A. "Thermal performance of a vertical solar hot water storage tank with a mantle heat exchanger depending on the discharging operation parameters". In: *Solar Energy* 116 (2015), pp. 184–204.

[9]   Arteconi, A., Hewitt, N. J., and Polonara, F. "State of the art of thermal storage for demand-side management". In: *Applied Energy* 93 (2012), pp. 371–389.

[10] Arteconi, A., Hewitt, N. J., and Polonara, F. "Domestic demand-side management (DSM): Role of heat pumps and thermal energy storage (TES) systems". In: *Applied Thermal Engineering* 51.1-2 (2013), pp. 155–165.

[11] Arteconi, A., Patteeuw, D., Bruninx, K., Delarue, E., D'haeseleer, W., and Helsen, L. "Active demand response with electric heating systems: Impact of market penetration". In: *Applied Energy* 177 (2016), pp. 636–648.

[12] Arvesen, A., Hauan, I. B., Bolsøy, B. M., and Hertwich, E. G. "Life cycle assessment of transport of electricity via different voltage levels: A case study for Nord-Trøndelag county in Norway". In: *Applied Energy* 157 (2015), pp. 144–151.

[13] Asdrubali, F., Baldinelli, G., D'Alessandro, F., and Scrucca, F. "Life cycle assessment of electricity production from renewable energies: Review and results harmonization". In: *Renewable and Sustainable Energy Reviews* 42 (2015), pp. 1113–1122.

[14] Atilgan, B. and Azapagic, A. "An integrated life cycle sustainability assessment of electricity generation in Turkey". In: *Energy Policy* 93 (2016), pp. 168–186.

[15] Baek, S. M., Nam, J. H., Hong, H., and Kim, C. J. "Effect of brine flow rate on the performance of a spiral-jacketed thermal storage tank used for SDHW systems: A computational fluid dynamics study". In: *Applied Thermal Engineering* 31.14-15 (2011), pp. 2716–2725.

[16] Bejan, A. and Kraus, A. D. *Heat Transfer Handbook*. Wiley, 2003.

[17] Benini, L., Mancini, L., Sala, S., Schau, E., Manfredi, S., and Pant, R. *Normalisation method and data for Environmental Footprints*. Tech. rep. European Commision Joint Research Centre, 2014.

[18] Bianchini, G., Casini, M., Vicino, A., and Zarrilli, D. "Demand-response in building heating systems: A Model Predictive Control approach". In: *Applied Energy* 168 (2016), pp. 159–170.

[19] Blom, I., Itard, L., and Meijer, A. "LCA-based environmental assessment of the use and maintenance of heating and ventilation systems in Dutch dwellings". In: *Building and Environment* 45.11 (2010), pp. 2362–2372.

[20] Boden, T., Marland, G., and Andres., R. *Global, Regional, and National Fossil-Fuel CO2 Emissions*. Tech. rep. Oak Ridge, Tenn., U.S.A.: Carbon Dioxide Information Analysis Center, Oak Ridge National Laboratory, U.S. Department of Energy, 2011.

[21] Boetcher, S. K. S., Kulacki, F. A., and Davidson, J. H. "Negatively Buoyant Plume Flow in a Baffled Heat Exchanger". In: *Journal of Solar Energy Engineering-Transactions of the ASME* 132.3 (2010), pp. 1–7.

[22] Boetcher, S. K. S., Kulacki, F. A., and Davidson, J. H. "Use of a Shroud and Baffle to Improve Natural Convection to Immersed Heat Exchangers". In: *Journal of Solar Energy Engineering-Transactions of the ASME* 134.1 (2012).

[23] Boyd, S. and Vandenberghe, L. *Convex Optimization.* Cambridge University Press, 2004.

[24] Brown, N. M. and Lai, F. C. "Enhanced thermal stratification in a liquid storage tank with a porous manifold". In: *Solar Energy* 85.7 (2011), pp. 1409–1417.

[25] Brundtland, G. H. *Our Common Future: Report of the World Commission on Environment and Development.* Tech. rep. World Commission on Environment and Development, 1987.

[26] Cadafalch, J., Carbonell, D., Consul, R., and Ruiz, R. "Modelling of storage tanks with immersed heat exchangers". In: *Solar Energy* 112 (2015), pp. 154–162.

[27] Camacho, E. F. and Bordons, C. *Model Predictive control.* Springer-Verlag, 2007.

[28] Campos Celador, A., Odriozola, M., and Sala, J. M. "Implications of the modelling of stratified hot water storage tanks in the simulation of CHP plants". In: *Energy Conversion and Management* 52.8-9 (2011), pp. 3018–3026.

[29] Carvalho, A. D., Mendrinos, D., and De Almeida, A. T. "Ground source heat pump carbon emissions and primary energy reduction potential for heating in buildings in Europe—results of a case study in Portugal". In: *Renewable and Sustainable Energy Reviews* 45 (2015), pp. 755–768.

[30] Castell, A., Medrano, M., Solé, C., and Cabeza, L. F. "Dimensionless numbers used to characterize stratification in water tanks for discharging at low flow rates". In: *Renewable Energy* 35.10 (2010), pp. 2192–2199.

[31] Chung, J. D., Cho, S. H., Tae, C. S., and Yoo, H. "The effect of diffuser configuration on thermal stratification in a rectangular storage tank". In: *Renewable Energy* 33.10 (2008), pp. 2236–2245.

[32] Ciais, P., Sabine, C., Bala, G., Bopp, L., Brovkin, V., Canadell, J., Chhabra, A., DeFries, R., Galloway, J., Heimann, M., Jones, C., Quéré, C. L., Myneni, R., Piao, S., and Thornton, P. "Carbon and Other Biogeochemical Cycles". In: *Climate Change 2013 - The Physical Science Basis.* 2013. Chap. 6, pp. 465–570.

[33] Collins, M., Knutti, R., Arblaster, J., Dufresne, J.-L., Fichefet, T., Friedlingstein, P., Gao, X., Gutowski, W. J., Johns, T., Krinner, G., Shongwe, M., Tebaldi, C., Weaver, A. J., and Wehner, M. "Long-term Climate Change: Projections, Commitments and Irreversibility". In: *Climate Change 2013: The Physical Science Basis. Contribution of Working Group I to the Fifth Assessment Report of the Intergovernmental Panel on Climate Change.* 2013, pp. 1029–1136.

[34] Cooper, S. J., Hammond, G. P., McManus, M. C., and Rogers, J. G. "Impact on energy requirements and emissions of heat pumps and micro-cogenerators participating in demand side management". In: *Applied Thermal Engineering* 71.2 (2014), pp. 872–881.

[35] Crespo Del Granado, P., Pang, Z., and Wallace, S. W. "Synergy of smart grids and hybrid distributed generation on the value of energy storage". In: *Applied Energy* 170 (2016), pp. 476–488.

[36] Cruickshank, C. A. and Harrison, S. J. "Heat loss characteristics for a typical solar domestic hot water storage". In: *Energy and Buildings* 42.10 (2010), pp. 1703–1710.

[37] Cruickshank, C. A. "Evaluation of a Stratified Multi-tank Thermal Storage For Solar Heating Applications." PhD Thesis. Queen's University, 2009, p. 302.

[38] Cyx, W., Renders, N., Van Holm, M., and Verbeke, S. *IEE TABULA - Typology Approach for Building Stock Energy Assessment.* Tech. rep. 2011.

[39] Dahl Knudsen, M. and Petersen, S. "Demand response potential of model predictive control of space heating based on price and carbon dioxide intensity signals". In: *Energy and Buildings* 125 (2016), pp. 196–204.

[40] Daikin Europe N.V. *Heating technical data - ERLQ-CV3.* Tech. rep. 2013.

[41] Dar, U. I., Sartori, I., Georges, L., and Novakovic, V. "Advanced control of heat pumps for improved flexibility of Net-ZEB towards the grid". In: *Energy and Buildings* 69 (2014), pp. 74–84.

[42] De Coninck, R., Baetens, R., Saelens, D., Woyte, A., and Helsen, L. "Rule-based demand-side management of domestic hot water production with heat pumps in zero energy neighbourhoods". In: *Journal of Building Performance Simulation* 7 (2014), pp. 271–288.

[43] De Vlieger, P., Van Kenhove, E., Janssens, A., and Laverge, J. "Dynamic Thermal Modeling og Legionella Pneumophila Proliferation in Domestic Hot Water Systems". In: *14th Conference of International Building Performance Simulation Association.* 2015, pp. 1563–1568.

[44] DeForest, N., Mendes, G., Stadler, M., Feng, W., Lai, J., and Marnay, C. "Optimal deployment of thermal energy storage under diverse economic and climate conditions". In: *Applied Energy* 119 (2014), pp. 488–496.

[45] *DIN 28011 Gewolbte Boden-Klopperform*. 1993.

[46] Dincer, I. "On thermal energy storage systems and applications in buildings". In: *Energy and Buildings* 34.4 (2002), pp. 377–388.

[47] Dincer, I. and Rosen, M. A. *Thermal energy storage: systems and applications*. Wiley, 2010.

[48] Dittus, F. and Boelter, L. "Heat transfer in automobile radiators of the tubular type". In: *International Communications in Heat and Mass Transfer* 12.1 (1985), pp. 3–22.

[49] Drück, H. *MULTIPORT Store - Model for TRNSYS*. Pfaffenwaldring 6, 70550 Stuttgart, Germany, 2006.

[50] Eames, P. C. and Norton, B. "The effect of tank geometry on thermally stratified sensible heat storage subject to low Reynolds number flows". In: *International Journal of Heat and Mass Transfer* 41.14 (1998), pp. 2131–2142.

[51] Elia N.V. *Grid data*. 2013. URL: http://www.elia.be/en/grid-data (consulted on 01/01/2015).

[52] Elia N.V. *Grid data*. 2015. URL: http://www.elia.be/nl/grid-data (consulted on 10/25/2016).

[53] Eom, S.-W., Kim, M.-K., Kim, I.-J., Moon, S.-I., Sun, Y.-K., and Kim, H.-S. "Life prediction and reliability assessment of lithium secondary batteries". In: *Journal of Power Sources* 174.2 (2007), pp. 954–958.

[54] European Commission. *A policy framework for climate and energy in the period from 2020 to 2030*. Tech. rep. 2014.

[55] European Commission. *Energy 2020. A strategy for competitive, sustainable and secure energy*. Tech. rep. 2010.

[56] European Commission. *Energy Roadmap 2050*. Tech. rep. 2011.

[57] European Commission. *Energy Sources, Production Costs and Performance of Technologies for power generation, Heating and transport*. Tech. rep. 2008.

[58] European Commission. *Europe 2020: a strategy for smart, sustainable and inclusive growth*. Tech. rep. 2010.

[59] European Commission. *Eurostat*. URL: http://ec.europa.eu/eurostat (consulted on 01/01/2016).

[60] European Commission. *Proposal for a Directive of the European parliament and of the council amending Directive 2010/31/EU on the energy performance of buildings*. Tech. rep. 2016.

[61] European Commission - Directorate General for Energy and Transport. *Materials used for manufacturing solar domestic hot water systems and comments on their reliability*. Tech. rep. 2004.

[62] European Commission - Joint Research Centre - Institute for Environment and Sustainability. *International Reference Life Cycle Data System (ILCD) Handbook : Analysing of existing Environmental Impact Assessment methodologies for use in Life Cycle Assessment*. 2010, p. 115.

[63] Eynard, J., Grieu, S., and Polit, M. "Predictive control and thermal energy storage for optimizing a multi-energy district boiler". In: *Journal of Process Control* 22.7 (2012), pp. 1246–1255.

[64] Fan, L.-N. "Turbulent Buoyant Jets Into Stratified or Flowing Ambient Fluids". PhD Thesis. California Institute of Technology, 1967, pp. 45–48.

[65] Fang, T. and Lahdelma, R. "Optimization of combined heat and power production with heat storage based on sliding time window method". In: *Applied Energy* 162 (2016), pp. 723–732.

[66] Farooq, A. A., Afram, A., Schulz, N., and Janabi-Sharifi, F. "Grey-box modeling of a low pressure electric boiler for domestic hot water system". In: *Applied Thermal Engineering* 84 (2015), pp. 257–267.

[67] Finnveden, G. and Moberg, Å. "Environmental systems analysis tools – an overview". In: *Journal of Cleaner Production* 13.12 (2005), pp. 1165–1173.

[68] Fitzgerald, N., Foley, A. M., and McKeogh, E. "Integrating wind power using intelligent electric water heating". In: *Energy* 48.1 (2012), pp. 135–143.

[69] Forster, P., Ramaswamy, V., Artaxo, P., Berntsen, T., Betts, R., Fahey, D., Haywood, J., Lean, J., Lowe, D., Myhre, G., Nganga, J., Prinn, R., Raga, G., Schulz, M., and Van Dorland, R. "Changes in Atmospheric Constituents and in Radiative Forcing". In: *Climate Change 2007: The Physical Science Basis. Contribution of Working Group I to the Fourth Assessment Report of the Intergovernmental Panel on Climate Change*. Cambridge University Press, 2007, pp. 129–234.

[70] Fragaki, A., Andersen, A. N., and Toke, D. "Exploration of economical sizing of gas engine and thermal store for combined heat and power plants in the UK". In: *Energy* 33.11 (2008), pp. 1659–1670.

[71] Frischknecht, R. *IEA EBC Annex Proposal : Assessing life cycle related environmental impacts caused by buildings Preamble*. Tech. rep. IEA-EBC, 2016.

[72] Furbo, S., Vejen, N. K., and Shah, L. J. "Thermal Performance of a Large Low Flow Solar Heating System With a Highly Thermally Stratified Tank". In: *Journal of Solar Energy Engineering* 127.1 (2005), p. 15.

[73] Fux, S. F., Benz, M. J., and Guzzella, L. "Economic and environmental aspects of the component sizing for a stand-alone building energy system: A case study". In: *Renewable Energy* 55 (2013), pp. 438–447.

[74] Gang, L. and Xuefei, Z. "Thermal energy storage system integration forms for a sustainable future". In: *Renewable and Sustainable Energy Reviews* 62 (2016), pp. 736–757.

[75] García-Gusano, D., Garraín, D., and Dufour, J. "Prospective life cycle assessment of the Spanish electricity production". In: *Renewable and Sustainable Energy Reviews* (2016).

[76] Gasque, M., González-Altozano, P., Maurer, D., Moncho-Esteve, I. J., Gutiérrez-Colomer, R. P., Palau-Salvador, G., and García-Marí, E. "Study of the influence of inner lining material on thermal stratification in a hot water storage tank". In: *Applied Thermal Engineering* 75 (2015), pp. 344–356.

[77] Geering, H. P. *Optimal Control with Engineering Applications.* Springer, 2007.

[78] Goedkoop, M. and Huijbregts, M. *ReCiPe 2008.* Tech. rep. 2013.

[79] González-Altozano, P., Gasque, M., Ibáñez, F., and Gutiérrez-Colomer, R. P. "New methodology for the characterisation of thermal performance in a hot water storage tank during charging". In: *Applied Thermal Engineering* 84 (2015), pp. 196–205.

[80] Greening, B. and Azapagic, A. "Domestic heat pumps: Life cycle environmental impacts and potential implications for the UK". In: *Energy* 39.1 (2012), pp. 205–217.

[81] Guadalfajara, M., Lozano, M., and Serra, L. "Analysis of Large Thermal Energy Storage for Solar District Heating". In: *Proceedings of the Eurotherm seminar 99 Conference, Lleida, Spain - Advances in thermal energy storage 01-089.* 2014.

[82] Haeseldonckx, D., Peeters, L., Helsen, L., and D'haeseleer, W. "The impact of thermal storage on the operational behaviour of residential CHP facilities and the overall CO2 emissions". In: *Renewable and Sustainable Energy Reviews* 11.6 (2007), pp. 1227–1243.

[83] Hahne, E. and Chen, Y. "Numerical study of flow and heat transfer characteristics in hot water stores". In: *Solar Energy* 64.1-3 (1998), pp. 9–18.

[84]   Haller, M. Y., Cruickshank, C. A., Streicher, W., Harrison, S. J., Andersen, E., and Furbo, S. "Methods to determine stratification efficiency of thermal energy storage processes - Review and theoretical comparison". In: *Solar Energy* 83.10 (2009), pp. 1847–1860.

[85]   Haller, M. Y., Yazdanshenas, E., Andersen, E., Bales, C., Streicher, W., and Furbo, S. "A method to determine stratification efficiency of thermal energy storage processes independently from storage heat losses". In: *Solar Energy* 84.6 (2010), pp. 997–1007.

[86]   Han, Y. M., Wang, R. Z., and Dai, Y. J. "Thermal stratification within the water tank". In: *Renewable and Sustainable Energy Reviews* 13.5 (2009), pp. 1014–1026.

[87]   Hedegaard, K., Mathiesen, B. V., Lund, H., and Heiselberg, P. "Wind power integration using individual heat pumps – Analysis of different heat storage options". In: *Energy* 47.1 (2012), pp. 284–293.

[88]   Hegazy, A. A. and Diab, M. R. "Performance of an improved design for storage-type domestic electrical water-heaters". In: *Applied Energy* 71.4 (2002), pp. 287–306.

[89]   Henze, G. P., Felsmann, C., and Knabe, G. "Evaluation of optimal control for active and passive building thermal storage". In: *International Journal of Thermal Sciences* 43.2 (2004), pp. 173–183.

[90]   Hewitt, N. J. "Heat pumps and energy storage - The challenges of implementation". In: *Applied Energy* 89.1 (2012), pp. 37–44.

[91]   Ievers, S. and Lin, W. "Numerical simulation of three-dimensional flow dynamics in a hot water storage tank". In: *Applied Energy* 86.12 (2009), pp. 2604–2614.

[92]   International Organization for Standardization (ISO). *ISO 14040 - Environmental management - Life Cycle Assessment - Principles and Framework*. 2006.

[93]   IPCC. *Climate change 2014 Synthesis Report Contribution of Working Groups I, II and III to the Fifth Assessment Report of the Intergovernmental Panel on Climate Change*. Tech. rep. 2014.

[94]   IPCC. *Climate Change 2014 Synthesis Report Summary Chapter for Policymakers*. Tech. rep. 2014.

[95]   IPCC. *Emissions Scenarios. Summary for Policymakers*. Tech. rep. 2000.

[96]   IPCC. *Summary for Policymakers. In: Climate Change 2013: The Physical Science Basis. Contribution of Working Group I to the Fifth Assessment Report of the Intergovernmental Panel on Climate Change*. Tech. rep. 2013, pp. 1–29.

[97]   ISSO Kennisinstituut voor installatietechniek. *ISSO-49 Kwaliteitseisen vloer-en wandverwarming en vloer- en wandkoeling*. 2004.

[98]   Itten, R., Frischknecht, R., Stucki, M., Scherrer, P., and Psi, I. "Life Cycle Inventories of Electricity Mixes and Grid". In: *Paul Scherrer Institut (PSI)* June (2014), pp. 1–229.

[99]   Jiménez Cisneros, B. E., Fischer, T., Barros, R., Dokken, D., Mach, K., Bilir, T., Chatterjee, M., Ebi, K., Estrada, Y., Genova, R., Girma, B., Kissel, E., Levy, A., and MacCracken, S. "Freshwater Resources". In: *Climate Change 2014: Mitigation of Climate Change*. 2014. Chap. 3, pp. 229–269.

[100]   Jones, C., Gilbert, P., Raugei, M., Mander, S., and Leccisi, E. "An approach to prospective consequential life cycle assessment and net energy analysis of distributed electricity generation". In: *Energy Policy* 100 (2017), pp. 350–358.

[101]   Jordan, U. and Furbo, S. "Thermal stratification in small solar domestic storage tanks caused by draw-offs". In: *Solar Energy* 78.2 (2005), pp. 291–300.

[102]   Kaloudis, E., Grigoriadis, D. G. E., Papanicolaou, E., and Panidis, T. "Large eddy simulation of thermocline flow phenomena and mixing during discharging of an initially homogeneous or stratified storage tank". In: *European Journal of Mechanics, B/Fluids* 48 (2014), pp. 94–114.

[103]   Keeling, C. D., Piper, S. C., Bacastow, R. B., Wahlen, M., Whorf, T. P., Heimann, M., and Meijer, H. A. "Atmospheric CO2 and CO2 Exchange with the Terrestrial Biosphere and Oceans from 1978 to 2000: Observations and Carbon Cycle Implications". In: *A History of Atmospheric CO2 and Its Effects on Plants, Animals, and Ecosystems*. New York, NY: Springer New York, 2005, pp. 83–113.

[104]   Kelly, J. A., Fu, M., and Clinch, J. P. "Residential home heating: The potential for air source heat pump technologies as an alternative to solid and liquid fuels". In: *Energy Policy* 98 (2016), pp. 431–442.

[105]   Kepplinger, P., Huber, G., and Petrasch, J. "Autonomous optimal control for demand side management with resistive domestic hot water heaters using linear optimization". In: *Energy and Buildings* 100 (2015), pp. 50–55.

[106]   Kepplinger, P., Huber, G., and Petrasch, J. "Field testing of demand side management via autonomous optimal control of a domestic hot water heater". In: *Energy and Buildings* 127 (2016), pp. 730–735.

[107]   Kitamura, K., Mitsuishi, A., Suzuki, T., and Kimura, F. "Fluid flow and heat transfer of natural convection induced around a vertical row of heated horizontal cylinders". In: *International Journal of Heat and Mass Transfer* 92 (2016), pp. 414–429.

[108]   Klein, S. A., Beckman, W. A., Mitchell, J. W., Duffie, J., Duffie, N., Freeman, T., Mitchell, J., Braun, J., Evans, B., Kummer, J., Urban, R., Fiksel, A., Thornton, J., Blair, N., Williams, P., Bradley, D., McDowell, T., Kummert, M., Arias, D., and Duffy, M. *TRNSYS 17 a TRaN sient SYstem Simulation program.* Madison, USA, 2010.

[109]   Kleinbach, E. M., Beckman, W. A., and Klein, S. A. "Performance study of one-dimensional models for stratified thermal storage tanks". In: *Solar Energy* 50.2 (1993), pp. 155–166.

[110]   Knudsen, S. and Furbo, S. "Thermal stratification in vertical mantle heat-exchangers with application to solar domestic hot-water systems". In: *Applied Energy* 78.3 (2004), pp. 257–272.

[111]   Kopanos, G. M., Georgiadis, M. C., and Pistikopoulos, E. N. "Energy production planning of a network of micro combined heat and power generators". In: *Applied Energy* 102 (2013), pp. 1522–1534.

[112]   Kreuder, L. and Spataru, C. "Assessing demand response with heat pumps for efficient grid operation in smart grids". In: *Sustainable Cities and Society* 19 (2015), pp. 136–143.

[113]   Kreuzinger, T., Bitzer, M., and Marquardt, W. "State estimation of a stratified storage tank". In: *Control Engineering Practice* 16.3 (2008), pp. 308–320.

[114]   Kriett, P. O. and Salani, M. "Optimal control of a residential microgrid". In: *Energy* 42.1 (2012), pp. 321–330.

[115]   Kulacki, F. A., Davidson, J. H., and Hebert, M. "On the effectiveness of baffles in indirect solar storage systems". In: *Journal of Solar Energy Engineering-Transactions of the ASME* 129.4 (2007), pp. 494–498.

[116]   Lélé, S. M. "Sustainable development: A critical review". In: *World Development* 19.6 (1991), pp. 607–621.

[117]   Leonard, B. P. "A stable and accurate convective modelling procedure based on quadratic upstream interpolation". In: *Computer Methods in Applied Mechanics and Engineering* 19.1 (1979), pp. 59–98.

[118]   Li, S., Joe, J., Hu, J., and Karava, P. "System identification and model-predictive control of office buildings with integrated photovoltaic-thermal collectors, radiant floor heating and active thermal storage". In: *Solar Energy* 113 (2015), pp. 139–157.

[119] Lim, T. H., De Kleine, R. D., and Keoleian, G. A. "Energy use and carbon reduction potentials from residential ground source heat pumps considering spatial and economic barriers". In: *Energy and Buildings* 128 (2016), pp. 287–304.

[120] Longuski, J. M., Guzmán, J. J., and Prussing, J. E. "Optimal Control Theory". In: *Optimal control with aerospace applications.* Springer, 2013. Chap. 2, pp. 19–38.

[121] Mehleri, E. D., Sarimveis, H., Markatos, N. C., and Papageorgiou, L. G. "Optimal design and operation of distributed energy systems: Application to Greek residential sector". In: *Renewable Energy* 51 (2013), pp. 331–342.

[122] Menon, R. P., Paolone, M., çois Maréchal, F., and Maréchal, F. "Study of optimal design of polygeneration systems in optimal control strategies". In: *Energy* 55 (2013), pp. 134–141.

[123] Modelica Association. *Modelica.* 2016. URL: www . modelica . org (consulted on 01/25/2017).

[124] Mohan, G., Kumar, U., Pokhrel, M. K., and Martin, A. "A novel solar thermal polygeneration system for sustainable production of cooling, clean water and domestic hot water in United Arab Emirates: Dynamic simulation and economic evaluation". In: *Applied Energy* 167 (2016), pp. 173–188.

[125] Myhre, G., Shindell, D., Bréon, F.-M., Collins, W., Fuglestvedt, J., Huang, J., Koch, D., Lamarque, J.-F., Lee, D., Mendoza, B., Nakajima, T., Robock, A., Stephens, G., Takemura, T., and Zhang, H. "Anthropogenic and Natural Radiative Forcing". In: *Climate Change 2013 - The Physical Science Basis.* 2013. Chap. 8, pp. 659–740.

[126] Navarro-Espinosa, A. and Mancarella, P. "Probabilistic modeling and assessment of the impact of electric heat pumps on low voltage distribution networks". In: *Applied Energy* 127 (2014), pp. 249–266.

[127] Nelson, J. E. B., Balakrishnan, A. R., and Srinivasa Murthy, S. "Experiments on stratified chilled-water tanks: Expériences menées avec des reservoirs d'accumulation d'eau glacée à stratification". In: *International Journal of Refrigeration* 22.3 (1999), pp. 216–234.

[128] Nelson, J. E. B., Balakrishnan, A. R., and Srinivasa Murthy, S. "Transient Analysis of Energy Storage in a Thermally Stratified Water Tank". In: *International Journal of Energy Research* 22.January (1998), pp. 867–883.

[129] Nitkiewicz, A. and Sekret, R. "Comparison of LCA results of low temperature heat plant using electric heat pump, absorption heat pump and gas-fired boiler". In: *Energy Conversion and Management* 87 (2014), pp. 647–652.

[130] Nizami, D. J., Lightstone, M. F., Harrison, S. J., and Cruickshank, C. A. "Negative buoyant plume model for solar domestic hot water tank systems incorporating a vertical inlet". In: *Solar Energy* 87.1 (2013), pp. 53–63.

[131] Njoku, H. O., Ekechukwu, O. V., and Onyegegbu, S. O. "Analysis of stratified thermal storage systems: An overview". In: *Heat and Mass Transfer* 50 (2014), pp. 1017–1030.

[132] Owen, M. S., ed. *ASHRAE Handbook of Fundamentals.* ASHRAE, 2009.

[133] Pagliarini, G. and Rainieri, S. "Modeling of a thermal energy storage system coupled with combined heat and power generation for the heating requirements of a University Campus". In: *Applied Thermal Engineering* 30.10 (2010), pp. 1255–1261.

[134] Palacios, E., Admiraal, D. M., Marcos, J. D., and Izquierdo, M. "Experimental analysis of solar thermal storage in a water tank with open side inlets". In: *Applied Energy* 89.1 (2012), pp. 401–412.

[135] Pastrone, D. and Casalino, L. "Modeling and Optimization in Space Engineering". In: *Modeling and Optimization in Space Engineering.* 2013. Chap. Practical, pp. 343–362.

[136] Patteeuw, D., Bruninx, K., Arteconi, A., Delarue, E., D'haeseleer, W., and Helsen, L. "Integrated modeling of active demand response with electric heating systems coupled to thermal energy storage systems". In: *Applied Energy* 151 (2015), pp. 306–319.

[137] Patteeuw, D. and Helsen, L. "Residential buildings with heat pumps, a verified bottom-up model for demand side management studies". In: *9th International Conference on System Simulation in Buildings.* 2014, pp. 1–19.

[138] Patteeuw, D., Henze, G. P., and Helsen, L. "Comparison of load shifting incentives for low-energy buildings with heat pumps to attain grid flexibility benefits". In: *Applied Energy* 167 (2016), pp. 80–92.

[139] Patteeuw, D., Reynders, G., Bruninx, K., Protopapadaki, C., Delarue, E., D'haeseleer, W., Saelens, D., and Helsen, L. "CO2-abatement cost of residential heat pumps with active demand response: Demand- and supply-side effects". In: *Applied Energy* 156 (2015), pp. 490–501.

[140] Peeters, L., Dear, R. de, Hensen, J., D'haeseleer, W., Dear, R. de, Hensen, J., and D'haeseleer, W. "Thermal comfort in residential buildings: Comfort values and scales for building energy simulation". In: *Applied Energy* 86.5 (2009), pp. 772–780.

[141] Pehnt, M., Oeser, M., and Swider, D. J. "Consequential environmental system analysis of expected offshore wind electricity production in Germany". In: *Energy* 33.5 (2008), pp. 747–759.

[142] Petrović, S. N. and Karlsson, K. B. "Residential heat pumps in the future Danish energy system". In: *Energy* 114 (2016), pp. 787–797.

[143] Pichler, M. F., Arnitz, A., Brychta, M., Heinz, A., and Rieberer, R. "Small Scale PV-Power – On Site Use Maximization through Smart Heat Pump Control". In: *International Journal of Contemporary Energy* 2.1 (2016), pp. 22–30.

[144] Pinel, P., Cruickshank, C. A., Beausoleil-Morrison, I., and Wills, A. "A review of available methods for seasonal storage of solar thermal energy in residential applications". In: *Renewable and Sustainable Energy Reviews* 15.7 (2011), pp. 3341–3359.

[145] Porter, J. R., Xie, L., Challinor, A. J., Cochrane, K., Howden, S. M., Iqbal, M. M., Lobell, D. B., and Travasso, M. I. "Food security and food production systems". In: *Climate Change 2014: Impacts, Adaptation, and Vulnerability*. 2014. Chap. 7, pp. 485–533.

[146] Rathgeber, C., Hiebler, S., Lävemann, E., Dolado, P., Lazaro, A., Gasia, J., Gracia, A. de, Miró, L., Cabeza, L. F., König-Haagen, A., Brüggemann, D., Campos-Celador, Á., Franquet, E., Fumey, B., Dannemand, M., Badenhop, T., Diriken, J., Nielsen, J. E., and Hauer, A. "IEA SHC Task 42 / ECES Annex 29 – A Simple Tool for the Economic Evaluation of Thermal Energy Storages". In: *Energy Procedia* 91 (2016), pp. 197–206.

[147] Ren, H., Gao, W., and Ruan, Y. "Optimal sizing for residential CHP system". In: *Applied Thermal Engineering* 28.5-6 (2008), pp. 514–523.

[148] Reynders, G. "Quantifying the impact of building design on the potential of structural strorage for active demand response in residential buildings". PhD thesis. KU Leuven, Belgium, 2015.

[149] Reynders, G., Diriken, J., and Saelens, D. "Quality of grey-box models and identified parameters as function of the accuracy of input and observation signals". In: *Energy and Buildings* 82 (2014), pp. 263–274.

[150] Rhys, J. *Cumulative Carbon Emissions and Climate Change : Has the Economics of Climate Policies Lost Contact with the Physics?* Oxford Institute for Energy Studies, 2011.

[151] Rodríguez-Hidalgo, M. C., Rodríguez-Aumente, P. A., Lecuona, A., Legrand, M., and Ventas, R. "Domestic hot water consumption vs. solar thermal energy storage: The optimum size of the storage tank". In: *Applied Energy* 97 (2012), pp. 897–906.

[152] Rosen, M. A. "The exergy of stratified thermal energy storages". In: *Solar Energy* 71.3 (2001), pp. 173–185.

[153] Rosen, M. A., Tang, R., and Dincer, I. "Effect of stratification on energy and exergy capacities in thermal storage systems". In: *International Journal of Energy Research* 28.2 (2004), pp. 177–193.

[154] Rotex. *Prijzen en specificaties*. 2013.

[155] Roux, C., Schalbart, P., Assoumou, E., and Peuportier, B. "Integrating climate change and energy mix scenarios in LCA of buildings and districts". In: *Applied Energy* 184 (2016), pp. 619–629.

[156] Schibuola, L., Scarpa, M., and Tambani, C. "Demand response management by means of heat pumps controlled via real time pricing". In: *Energy and Buildings* 90 (2015), pp. 15–28.

[157] Schindler + Hofmann GmbH. *Kamdi24*. URL: https://www.kamdi24.de/schindler-hofmann-pufferspeicher (consulted on 11/14/2016).

[158] Schmidt, J. H., Merciai, S., Thrane, M., and Dalgaard, R. *Inventory of country specific electricity in LCA - consequential and attributional scenarios. Methodology report v2*. Tech. rep. Aalborg: 2.-0 LCA consultants, 2011.

[159] Shah, L. J., Andersen, E., and Furbo, S. "Theoretical and experimental investigations of inlet stratifiers for solar storage tanks". In: *Applied Thermal Engineering* 25.14-15 (2005), pp. 2086–2099.

[160] Shah, L. J. and Furbo, S. "Correlation of experimental and theoretical heat transfer in mantle tanks used in low flow {SDHW} systems". In: *Solar Energy* 64.4-6 (1998), pp. 245–256.

[161] Shin, M.-S., Kim, H.-S., Jang, D.-S., Lee, S.-N., Lee, Y.-S., and Yoon, H.-G. "Numerical and experimental study on the design of a stratified thermal storage system". In: *Applied Thermal Engineering* 24.1 (2004), pp. 17–27.

[162] Spur, R., Fiala, D., Nevrala, D., and Probert, D. "Performances of modern domestic hot-water stores". In: *Applied Energy* 83.8 (2006), pp. 893–910.

[163] Statista. *Belgium: total annual greenhouse gas emissions 2005-2014*. URL: https://www.statista.com/statistics/411381/total-annual-greenhouse-gas-emissions-in-belgium/ (consulted on 02/09/2017).

[164] Steen, D., Stadler, M., Cardoso, G., Groissböck, M., DeForest, N., and Marnay, C. "Modeling of thermal storage systems in MILP distributed energy resource models". In: *Applied Energy* 137 (2015), pp. 782–792.

[165] Steinert, P., Göppert, S., and Platzer, B. "Transient calculation of charge and discharge cycles in thermally stratified energy storages". In: *Solar Energy* 97 (2013), pp. 505–516.

[166] Strbac, G. "Demand side management: Benefits and challenges". In: *Energy Policy* 36.12 (2008), pp. 4419–4426.

[167]   Streckiené, G., Martinaitis, V., Andersen, A. N., Katz, J., Streckiene, G., Martinaitis, V., Andersen, A. N., and Katz, J. "Feasibility of CHP-plants with thermal stores in the German spot market". In: *Applied Energy* 86.11 (2009), pp. 2308–2316.

[168]   Su, Y. and Davidson, J. H. "Discharge of thermal storage tanks via immersed baffled heat exchangers: Numerical model of flow and temperature fields". In: *Journal of Solar Energy Engineering-Transactions of the ASME* 130.2 (2008), p. 021016.

[169]   Su, Y. and Davidson, J. H. "Transient natural convection heat transfer correlations for tube bundles immersed in a thermal storage". In: *Journal of Solar Energy Engineering-Transactions of the ASME* 129.2 (2007), pp. 210–214.

[170]   Synergrid. *Technische gegevens voor de transmissie- en distributienetten elektriciteit in België.* 2015. URL: http://www.synergrid.be/index.cfm?PageID=18029 (consulted on 10/25/2016).

[171]   Thür, A., Calabrese, T., Hauer, N., and Streicher, W. "Smart Grid and PV driven Heat Pump as Thermal Battery in Small Buildings for optimized Electricity Consumption". In: *11th ISES Eurosun Conference.* 2016.

[172]   Thür, A., Calabrese, T., Hauer, N., and Streicher, W. "Wärmepumpe und Photovoltaik mit Wasserspeicher und Betonkernaktivierung als thermische Batterie". In: *Otti Symposium Photovoltaische Solarenergie.* 2017.

[173]   Toyoshima, M. and Okawa, S. "An effect of a horizontal buoyant jet on the temperature distribution inside a hot water storage tank". In: *International Journal of Heat and Fluid Flow* 44 (2013), pp. 403–413.

[174]   Treyer, K. and Bauer, C. "The environmental footprint of UAE's electricity sector: Combining life cycle assessment and scenario modeling". In: *Renewable and Sustainable Energy Reviews* 55 (2016), pp. 1234–1247.

[175]   Tsuji, T. and Nagano, Y. "Velocity and temperature measurements in a natural convection boundary layer along a vertical flat plate". In: *Experimental Thermal and Fluid Science* 2.2 (1989), pp. 208–215.

[176]   Turconi, R., O'Dwyer, C., Flynn, D., and Astrup, T. "Emissions from cycling of thermal power plants in electricity systems with high penetration of wind power: Life cycle assessment for Ireland". In: *Applied Energy* 131 (2014), pp. 1–8.

[177]   Turconi, R., Boldrin, A., and Astrup, T. "Life cycle assessment (LCA) of electricity generation technologies: Overview, comparability and limitations". In: *Renewable and Sustainable Energy Reviews* 28 (2013), pp. 555–565.

[178] Turconi, R., Tonini, D., Nielsen, C. F., Simonsen, C. G., and Astrup, T. "Environmental impacts of future low-carbon electricity systems: Detailed life cycle assessment of a Danish case study". In: *Applied Energy* 132 (2014), pp. 66–73.

[179] Udo de Haes, H. A., Jolliet, O., Finnveden, G., Hauschild, M., Krewit, W., and Muller-Wenk, R. "Best Available Practice Regarding Impact Categories and Category Indicators in Life Cycle Impact Assessment". In: *International Journal of Life Cycle Assessment* 4.2 (1999), pp. 167–174.

[180] United Nations. *Transforming our world: The 2030 agenda for sustainable development.* Tech. rep. United Nations General Assembly, 2015.

[181] Van Berkel, J. "Mixing in thermally stratified energy stores". In: *Solar Energy* 58.4 (1996), pp. 203–211.

[182] Van Berkel, J., Rindt, C. C. M., and Steenhoven, a. a. V. "Thermocline dynamics in a thermally stratified store". In: *International Journal of Heat and Fluid Flow* 45 (2002), pp. 343–356.

[183] Van Den Bergh, K. "Impact of energy and climate policies on electricity generation - Analysis based on large-scale unit commitment modeling". Phd. KU Leuven, 2016.

[184] Vanhoudt, D., Geysen, D., Claessens, B., Leemans, F., Jespers, L., and Van Bael, J. "An actively controlled residential heat pump: Potential on peak shaving and maximization of self-consumption of renewable energy". In: *Renewable Energy* 63 (2014), pp. 531–543.

[185] Vasallo, M. J. and Bravo, J. M. "A MPC approach for optimal generation scheduling in CSP plants". In: *Applied Energy* 165 (2016), pp. 357–370.

[186] Vuuren, D. P. van, Elzen, M. J. G. den, Lucas, P. L., Eickhout, B., Strengers, B. J., Ruijven, B. van, Wonink, S., and Houdt, R. van. "Stabilizing greenhouse gas concentrations at low levels: an assessment of reduction strategies and costs". In: *Climatic Change* 81.2 (2007), pp. 119–159.

[187] Wächter, A. and Biegler, L. T. "On the Implementation of a Primal-Dual Interior Point Filter Line Search Algorithm for Large-Scale Nonlinear Programming". In: *Mathematical Programming* 106(1) (2006), pp. 25–57.

[188] Waite, M. and Modi, V. "Potential for increased wind-generated electricity utilization using heat pumps in urban areas". In: *Applied Energy* 135 (2014), pp. 634–642.

[189] Walmsley, M. R. W., Atkins, M. J., and Riley, J. "Thermocline management of stratified tanks for heat storage". In: *Chemical Engineering Transactions* 18 (2009), pp. 231–236.

[190] Warren, P. "A review of demand-side management policy in the UK". In: *Renewable and Sustainable Energy Reviews* 29 (2014), pp. 941–951.

[191] Weidema, B., Bauer, C., Hischier, R., Mutel, C., Nemecek, T., Reinhard, J., Vadenbo, C., and Wernet, G. *The ecoinvent database: Overview and methodology, Data quality guideline for the ecoinvent database version 3.* Tech. rep. 2013.

[192] Weisser, D. "A guide to life-cycle greenhouse gas (GHG) emissions from electric supply technologies". In: *Energy* 32.9 (2007), pp. 1543–1559.

[193] Wetter, M. *Modelica Buildings Library.* 2012. URL: `simulationresearch.lbl.gov/modelica`.

[194] Wolfram, P., Wiedmann, T., and Diesendorf, M. "Carbon footprint scenarios for renewable electricity in Australia". In: *Journal of Cleaner Production* 124 (2016), pp. 236–245.

[195] Wood, R., Al-Muslahi, S., O'Callaghan, P., and Probert, S. "Thermally stratified hot water storage systems". In: *Applied Energy* 9.3 (1981), pp. 231–242.

[196] World Resources Institute. *CAIT Climate Data Explorer.* Tech. rep. Washington DC: World Resources Institute, 2015.

[197] Yoo, H., Kim, C.-J., and Kim, C. W. "Approximate analytical solutions for stratified thermal storage under variable inlet temperature". In: *Solar Energy* 66.1 (1999), pp. 47–56.

[198] Zachár, A., Farkas, I., and Szlivka, F. "Numerical analyses of the impact of plates for thermal stratification inside a storage tank with upper and lower inlet flows". In: *Solar Energy* 74.4 (2003), pp. 287–302.

[199] Zhang, N., Lu, X., McElroy, M. B., Nielsen, C. P., Chen, X., Deng, Y., and Kang, C. "Reducing curtailment of wind electricity in China by employing electric boilers for heat and pumped hydro for energy storage". In: *Applied Energy* 184 (2016), pp. 987–994.

[200] Zhang, S. and Niu, J. "Two performance indices of TES apparatus: Comparison of MPCM slurry vs. stratified water storage tank". In: *Energy and Buildings* 127 (2016), pp. 512–520.

[201] Zhang, Y., Wang, X., Zhuo, S., and Zhang, Y. "Pre-feasibility of building cooling heating and power system with thermal energy storage considering energy supply–demand mismatch". In: *Applied Energy* 167 (2016), pp. 125–134.

[202] Zhao, Y., Lu, Y., Yan, C., and Wang, S. "MPC-based optimal scheduling of grid-connected low energy buildings with thermal energy storages". In: *Energy and Buildings* 86 (2015), pp. 415–426.

Curriculum Vitae

Brecht Baeten
Born on October 14, 1984 in Genk

Dreesstraat 64
3660 Opglabbeek, Belgium
brecht.baeten@gmail.com

Experience

2011-current: KU Leuven
Research: PhD, Residential heating using heat pumps and hot water storage tanks. Tank sizing to minimize environmental impact in a renewable energy context.
Education: Teacher of the course "Fluïdummechnica" for the bachelor in engineering technology program at the technology campus Diepenbeek.

2008-2011: Hansen Transmissions Int.
Validation engineer.

Education

2002-2008: UGent
Burgerlijk Werktuigkundig-Elektrotechnisch ingenieur, optie mechanische constructie en productie (Master of Mechanical engineering).

1998-2002: Sint-Augustinus instituut Bree
Wetenschappen-Wiskunde (Sciences-Mathematics).

List of publications

Articles in internationally reviewed academic journals

Baeten, B., Confrey, T., Pecue, S., Rogiers, F., and Helsen, L. "A validated model for mixing and buoyancy in stratified hot water storage tanks for use in building energy simulations". In: *Applied Energy* 172 (2016), pp. 217–229.

Baeten, B., Rogiers, F., and Helsen, L. "Reduction of heat pump induced peak electricity use and required generation capacity through thermal energy storage and demand response". In: *Applied Energy* 195 (2017), pp. 184–195

Articles in international conference proceedings

Baeten, B., Rogiers, F., and Helsen, L. "Energy cost reduction by optimal control of ideal sensible thermal energy storage in domestic space heating". In: *Proceedings of the Eurotherm seminar 99 Conference, Lleida, Spain - Advances in thermal energy storage 01-045.* 2014

Baeten, B., Rogiers, F., Patteeuw, D., and Helsen, L. "Comparison of optimal control formulations for stratified sensible thermal energy storage in space heating applications". In: *Proceedings of the IEA-ECES-Greenstock Conference, Bejing, China.* 2015